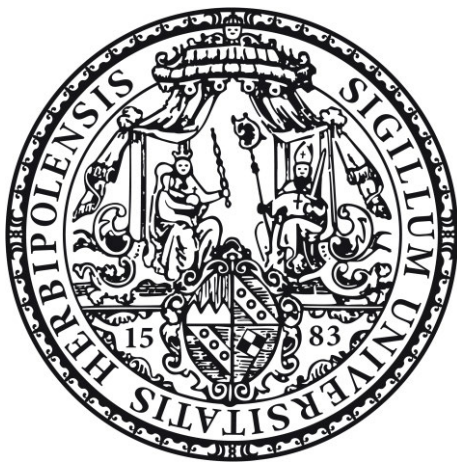


INVESTIGATION OF DICARBA-CLOSEO-DODECABORANE AS A SUBSTITUENT ON THREE-COORDINATE BORON AND AS AN ACCEPTOR IN A PYRENE-DONOR-ACCEPTOR SYSTEM



Dissertation zur Erlangung des naturwissenschaftlichen Doktorgrades der
Julius-Maximilians-Universität Würzburg

vorgelegt von

Johannes Heinrich Krebs

aus Würzburg

Würzburg, 2022

Eingereicht bei der Fakultät für Chemie und Pharmazie am:

Gutachter der schriftlichen Arbeit

1. Gutachter: Prof. Dr. Dr. h.c. Todd B. Marder
2. Gutachter: Prof. Dr. Qing Ye

Prüfer des öffentlichen Promotionskolloquiums

1. Prüfer: Prof. Dr. Dr. h.c. Todd B. Marder
2. Prüfer: Prof. Dr. Qing Ye
3. Prüfer: Prof. Dr. Florian Beuerle

Datum des öffentlichen Promotionskolloquiums am:

Doktorurkunde ausgehändigt am:

Pessimism of the Intellect, Optimism of the Will

„My mind is pessimistic, but my will is optimistic. Whatever the situation, I imagine the worst that could happen in order to summon up all my reserves and will power to overcome every obstacle.“

Antonio Gramsci

Die Experimente zur vorliegenden Arbeit wurden in der Zeit von November 2017 bis July 2022 am
Institut für Anorganische Chemie der Julius-Maximilians-Universität Würzburg unter der Aufsicht von
Prof. Dr. Dr. h. c. Todd B. Marder durchgeführt.

Affidavit

I hereby confirm that my thesis entitled “Investigation of Dicarba-*clos*o-dodecaborane as a Substituent on Three-coordinate Boron and as an Acceptor in a Pyrene-Donor-Acceptor System” is the result of my own work. I did not receive any help or support from commercial consultants. All sources and/or materials applied are listed and specified in the thesis.

Furthermore, I confirm that this thesis has not yet been submitted as part of another examination process neither in identical nor in similar form.

Würzburg,

Eidesstattliche Erklärung

Hiermit erkläre ich an Eides statt, die Dissertation „Investigation of Dicarba-*clos*o-dodecaborane as a Substituent on Three-coordinate Boron and as an Acceptor in a Pyrene-Donor-Acceptor System“ eigenständig, d.h. insbesondere selbstständig und ohne Hilfe eines kommerziellen Promotionspartners angefertigt und keine anderen als die von mir angegebenen Quellen und Hilfsmittel verwendet zu haben.

Ich erkläre außerdem, dass die Dissertation weder in gleicher noch in ähnlicher Form bereits in einem anderen Prüfungsverfahren vorgelegen hat.

Würzburg,

Acknowledgment

Acknowledgment

First of all, I would like to thank **Prof. Dr. Dr. h. c. Todd B. Marder** for the opportunity to do my PhD in your group, our second family. I am thankful for the trust and freedom gave me in following my research and perusing my curiosity and interests. This gave me a broad set of skills, preparing me for the challenges to come. Your ways to approach things as well as your high ethical standards will stick with me forever.

Next, I want to thank **Prof. Dr. Maik Finze** for the generous supply of starting material necessary for all my research as well as access to their equipment, without which, some of my projects would be just half as interesting.

Thanks to **Prof. Dr. Holger Braunschweig** and **Dr. Ivo Krummenacher** for the contributions in writhing the papers and especially, measuring and evaluating the cyclic voltammetry experiments in all my chapters. Thanks to **Dr. Krzysztof Radacki** for his help whenever I had a problem in the X-Ray lab or with the cluster. Thanks to **Alena Häfner, Sonja Fuchs** and **Dr. Arumugam Jayaraman** for your cooperation and help in the second paper.

Thanks to **Prof. Dr. Zhenyang Lin** and **Dr. Xueying Guo** for the insanely fast calculations that helped completing the second paper.

Thanks to **Prof. Dr. Alan Welch** for giving his thoughts on my very first paper. It meant a lot.

Most importantly, I want to thank the whole Marder family. This colorful arrangement of people was never boring, and I will miss all the serious and especially the bogus discussion we had. Thanks to **Dr. Alexandra Friedrich** for solving crystals, teaching crystallography and in general being helpful during my whole thesis. Especially, for the opportunity to visit three different synchrotrons, those were my personal highlights during my time in this group. Thank you, **Dr. Stephan Wagner** for keeping the GC-MS systems running and planning the new building for the Inorganic Institute, which is a nice place to work at. Thanks to **Christoph Mahler** for measuring a HRMS samples and enjoyable lunch breaks. Special Thanks to **Sabine Lorenzen** for suppling me with starting materials and being a pleasant person to work with. You were missed during our lunch breaks at the end of my time. Thanks to **Hildegard Holzinger** for ordering all our supplies and chemicals.

Thanks to **Dr. Florian Rauch** for guidance, and open ear and the, at times, ridiculous rants that made up a big part of this group. You are my ideal chemist; “You may not like it, but *this is what peak performance looks like*”. Thanks to **Dr. Julia Merz** for her constant support regarding pyrenes and for bringing Loki to our group. Thanks to **Robert Ricker** for being one of my longest friends that I made studying chemistry. You are one of the most curious, straightforward, and helpful persons I know.

Acknowledgment

Never change! Thanks to **Dr. Sarina Berger** and **Dr. Jan Maier** each in their own way for their work in the group and together with Robert for memorable board game nights in the “AK Board Games”. **Dr. Florian Kerner**, **Dr. Matthias Ferger**, **Dr. Jörn Nitsch**, **Dr. Jiang He**, **Dr. Zhu Wu**, **Dr. Xiaolei Zhang** and **Dr. Goutam Kumar Kole** for helpful discussions in the lab and broader discussions over a beer after work.

Thanks also to my interns **Lisa Brändler**, **Christian Schmidle**, **Martin Luff**, **Yelyzaveta Yatsenko**, **Julie Borel**, and **Eduard Glok** for the work you have done, your help was much appreciated.

Thanks also to **Dr. Rüdiger Bertermann**, **Marie-Luise Schäfer**, and **Laura Wolz** in the NMR department for measuring many of my samples and keeping the machines running. Also, many thanks to **Liselotte Michels** and **Sabine Timmroth** for the elemental analysis measurements, **Gertrud Wunderling** for keeping our kitchen in good shape, **Alfred Schertzer** and **Stephan Kooper** for argon and dry ice supply, the glass blowers **Berthold Fertig** and **Bernhard Werner** and the workshop team **Alois Ruf**, **Wolfgang Obert**, **Frank Förtsch**, **Michael Ramold**, and **Manfred Reinhart**. I also want to thank **Bianca Putz**, **Stefanie Ziegler**, **Birgit Zepke** and especially **Eva Wittenberg**, **Maria Eckhardt** and **Cornelia Walter** for the tons of organizational work you have done for our group and the whole institute.

Nicht zuletzt möchte ich meiner Familie danken. Ohne ihre Unterstützung wäre nichts von dem hier möglich gewesen. **Erna**, deine Unterstützung von klein auf und in jeder Lebenslage bedeutet mir sehr viel. Wir haben viel erlebt und ich habe viel gelernt. Mit deinem Tatendrang und Einsatz in so vielen Bereichen bist du mir ein strahlendes Vorbild. **Dieter** und **Gertrud** unsere Diskussionen über Gott und die Welt haben aus mir (hoffentlich) einen kritisch denkenden Menschen gemacht, der Dinge hinterfragt und seine eigenen Schlüsse zieht. Ich weiß, dass ich mich immer auf euch verlassen kann. **Kristina**, großartige Schwester und großartiger Mensch im Allgemeinen, du hast einen klasse moralischen Kompass, Einfühlungsvermögen und, auch wenn es stressig ist, Durchhaltevermögen. Ich freue mich auf viele weitere kleine Ausflüge und Familien treffen.

Vielen Dank auch an **Eva**, als meine Freundin stehest du mir jetzt schon fast mein halbes Leben bei, tolerierst meine Eigenheiten und erlebst mit mir alles was das Leben so zu bieten hat. Mit dir kann ich zur Ruhe kommen, lachen und entspannen. Auch deiner Familie bin ich dankbar mich so herzlich aufgenommen zu haben.

List of Publications

The publications listed below are reproduced in this dissertation. The table itemizes at which position in this work the papers have been reproduced. The publication in Chapter 1 is published under a creative common license (CC BY 4.0). The manuscript in Chapter 2 is submitted or close to submission at time of this work and as such, the respective contributions can be found attached to the chapter. The results in chapter 3 are soon to be submitted to a peer reviewed journal, and as such, are already presented in a similar format.

Publication	Position
<u>J. Krebs, M. Haehnel, I. Krummenacher, A. Friedrich, H. Braunschweig, M. Finze, L. Ji, T. B. Marder, <i>Chem. Eur. J.</i> 2021, 27, 8159–8167.</u> DOI: 10.1002/chem.202100938	Chapter 1
<u>Johannes Krebs, Alena Häfner, Sonja Fuchs, Xueying Guo, Dr. Florian Rauch, Dr. Antonius Eichhorn, Dr. Ivo Krummenacher, Dr. Alexandra Friedrich, Prof. Dr. Lei Ji, Prof. Dr. Maik Finze, Prof. Dr. Zhenyang Lin, Prof. Dr. Holger Braunschweig, Prof. Dr. Todd B. Marder</u>	Chapter 2

Further publications:

W. Ming, X. Liu, A. Friedrich, J. Krebs, Y. P. Budiman, M. Huang, T. B. Marder, *Green Chem.* **2020**, 22, 2184–2190. DOI: 10.1039/D0GC00346H

W. Ming, X. Liu, A. Friedrich, J. Krebs, T. B. Marder, *Org. Lett.* **2020**, 22, 365–370. DOI: 10.1021/acs.orglett.9b03773

A. K. Narsaria, F. Rauch, J. Krebs, P. Endres, A. Friedrich, I. Krummenacher, H. Braunschweig, M. Finze, J. Nitsch, F. M. Bickelhaupt, T. B. Marder, *Adv. Funct. Mater.* **2020**, 30, 2002064. DOI: 10.1002/adfm.202002064

F. Rauch, J. Krebs, J. Gunther, A. Friedrich, M. Hahnel, I. Krummenacher, H. Braunschweig, M. Finze, T. B. Marder, *Chem. Eur. J.* **2020**, 26, 10626–10633. DOI: 10.1002/chem.202002348

M. Ferger, S. M. Berger, F. Rauch, M. Schonitz, J. Ruhe, J. Krebs, A. Friedrich, T. B. Marder, *Chem. Eur. J.* **2021**, 27, 9094–9101. DOI: 10.1002/chem.202100632

J. He, F. Rauch, A. Friedrich, J. Krebs, I. Krummenacher, R. Bertermann, J. Nitsch, H. Braunschweig, M. Finze, T. B. Marder, *Angew. Chem. Int. Ed.* **2021**, 60, 4833–4840. DOI: 10.1002/anie.202013692

M. Huang, Z. Wu, J. Krebs, A. Friedrich, X. Luo, S. A. Westcott, U. Radius, T. B. Marder, *Chem. Eur. J.* **2021**, 27, 8149–8158. DOI: 10.1002/chem.202100342

List of Publications

X. Jia, J. Nitsch, Z. Wu, A. Friedrich, J. Krebs, I. Krummenacher, F. Fantuzzi, H. Braunschweig, M. Moos, C. Lambert, B. Engels, T. B. Marder, *Chem. Sci.* **2021**, *12*, 11864-11872. DOI: 10.1039/d1sc02409d

M. Huang, J. Hu, S. Shi, A. Friedrich, J. Krebs, S. A. Westcott, U. Radius, T. B. Marder, *Chem. Eur. J.* **2022**, *28*, e202200480. DOI: 10.1002/chem.202200480

List of Abbreviations

List of Abbreviations

a	acceptor
abs	absorption
AIE	aggregation-induced-emission
ASAP	atmospheric solids analysis probe
calc.	calculated
CI	configuration Interaction
Cp	cyclopentadienyl
CT	charge transfer
CV	cyclic voltammetry
CW	continus wave
d	donor
dba	diibenzylideneacetone ($C_{17}H_{14}O$)
DCM	dichloromethane (CH_2Cl_2)
DFT	density functional theory
Elem. Anal.	elemental analysis
em	emission
EPR	electron paramagnetic resonance
esd	estimated standard deviations
ESI	electro-spray ionization
FLP	frustrated lewis pair
FWHM	full width at half maximum
GC-MS	gas chromatography–mass spectrometry
HEX	hexane (C_6H_{14})
HOMO	highest occupied molecular orbital
HPLC	high-performance liquid chromatography
HRMS	high resolution mass spectrometry
IRF	instrument response function
LE	locally exited
LIFDI	liquid injection field desorption ionization
LUMO	lowest unoccupied molecular orbital
mes	mesityl ($2,4,6\text{-Me}_3C_6H_2$)
MO	molecular orbital
Naph	naphthalenide ($C_{10}H_8$)

List of Abbreviations

<i>n</i> BuLi	<i>n</i> -butyllithium (C ₄ H ₉ Li)
NICS	nucleus-independent chemical shift values
NMR	nuclear magnetic resonance
<i>o</i>	<i>ortho</i>
OFET	organic field-effect transistor
OLED	organic light-emitting diode
OPV	organic photovoltaics
PAH	polycyclic aromatic hydrocarbon
pin	pinacolato ((CH ₃) ₄ C ₂ O ₂)
rt.	room temperature
SE	skeletal electron
SOMO	singly occupied molecular orbital
SPS	solvent purification system
TBAF	tetra- <i>n</i> -butylammonium fluoride ((CH ₃ CH ₂ CH ₂ CH ₂) ₄ N ⁺ F ⁻)
TCSPC	time-correlated single-photon counting
TD-DFT	time dependent density functional theory
THF	tetrahydrofuran ((CH ₂) ₄ O)
TIPS	triisopropyl silyl (C ₉ H ₂₁ Si)
TLC	thin layer chromatography
TOL	toluene (C ₇ H ₈)
UV/Vis	ultra violet/visible

Table of Contents

Table of Contents

1. Chapter 1	21
1.1 Title and Abstract	22
1.2 Introduction.....	23
1.3 Results and Discussion	24
1.3.1 Synthesis, stability, and characterization	24
1.3.2 Electrochemistry.....	25
1.3.3 Chemical Reduction.....	25
1.3.4 EPR spectroscopy.....	26
1.3.5 Single-crystal structure analysis	26
1.3.6 Photophysical properties.....	30
1.3.7 DFT and TD-DFT studies.....	31
1.4 Conclusions.....	34
1.5 References.....	35
1.6 Author contributions and agreement	40
2. Chapter 2	43
2.1 Title and Abstract	44
2.2 Introduction.....	45
2.3 Results and Discussion	46
2.3.1 Synthesis and observation.....	46
2.3.2 Molecular geometries before and after the rearrangement	49
2.3.3 Quantum chemical transition state calculations.....	52
2.3.4 Photophysical properties and TD-DFT calculations	54
2.3.5 Electrochemical properties.....	60
2.4 Conclusion	61
2.5 References.....	62
2.6 Author contributions and agreement	65
3. Chapter 3	73
3.1 Title and Abstract	73
3.2 Introduction.....	74
3.1 Results and Discussion	76
3.1.1 Synthesis and observation.....	76
3.1.2 Structural characterization	77
3.1.3 Photophysical properties.....	80

Table of Contents

3.1.4	DFT and TD-DFT calculations	82
3.1.5	Electrochemical properties.....	84
3.2	Conclusion	85
3.3	References.....	86
4.	Summary/Zusammenfassung	90
4.1	Summary of Chapter 1	90
4.2	Summary of Chapter 2	92
4.3	Summary of Chapter 3	95
4.4	Zusammenfassung Chapter 1.....	98
4.5	Zusammenfassung Chapter 2.....	100
4.6	Zusammenfassung Chapter 3.....	103
5.	Experimental	106
5.1	Supporting Information Chapter 1	106
5.1.1	General experimental details	106
5.1.2	Synthetic procedures.....	109
5.1.3	EPR measurement	113
5.1.4	Single-crystal X-ray diffraction.....	114
5.1.5	Electrochemistry.....	118
5.1.6	Photophysical properties.....	119
5.1.7	TD-DFT calculations	121
5.1.8	References	128
5.2	Supporting Information Chapter 2	129
5.2.1	General experimental details	129
5.2.2	Synthetic procedures.....	132
5.2.3	Single-crystal X-ray diffraction.....	141
5.2.4	Geometry tables	144
5.2.5	Photophysical data	148
5.2.6	Cyclic voltammetry	151
5.2.7	DFT and TD-DFT results	152
5.2.8	References	180
5.3	Supporting Information Chapter 3	181
5.3.1	General experimental details	181
5.3.2	Synthetic procedures.....	183
5.3.3	Single-crystal X-ray diffraction.....	200
5.3.4	Photophysical data	202

Table of Contents

5.3.5	DFT and TD-DFT results	205
5.3.6	References	210

Table of Contents

Chapter 1

1. CHAPTER 1

Chapter 1 was published in a peer-reviewed journal and is used in this partial cumulative thesis. Minor changes were made to the original to conform to the general format of this thesis.

1.1 Title and Abstract

Synthesis and Structure of an *o*-Carboranyl-substituted Three-coordinate Borane Radical Anion

Johannes Krebs^a, Martin Haehnel^a, Dr. Ivo Krummenacher^a, Dr. Alexandra Friedrich^a, Prof. Dr. Holger Braunschweig^a, Prof. Dr. Maik Finze^a, Prof. Dr. Lei Ji^b, Prof. Dr. Todd B. Marder^{a*}

^{a)} Institute for Inorganic Chemistry and Institute for Sustainable Chemistry & Catalysis with Boron, Julius-Maximilians-Universität Würzburg, Am Hubland, 97074 Würzburg (Germany)

^{b)} Frontiers Science Center for Flexible Electronics (FSCFE) & Shaanxi Institute of Flexible Electronics (SIFE), Northwestern Polytechnical University, 127 West Youyi Road, 710072 Xi'an (China)

*

Keywords

Carborane; charge transfer; radical; three-coordinate boron; Wade's rules

Abstract

Bis(1-(4-tolyl)-carboran-2-yl)-(4-tolyl)-borane [(1-(4-MeC₆H₄)-*clos*o-1,2-C₂B₁₀H₉-2-)₂(4-MeC₆H₄)B] (**1.1**), a new bis(*o*-carboranyl)-(R)-borane was synthesised by lithiation of the *o*-carboranyl precursor and subsequent salt metathesis reaction with (4-tolyl)BBr₂. Cyclic voltammetry experiments on **1.1** show multiple distinct reduction events with a one-electron first reduction. In a selective reduction experiment the corresponding paramagnetic radical anion **1.1**^{•-} was isolated and characterized. Single-crystal structure analyses allow an in-depth comparison of **1.1**, **1.1**^{•-}, their calculated geometries, and the S₁ excited state of **1.1**. Photophysical studies of **1.1** show a charge transfer (CT) emission with low quantum yield in solution but a strong increase in the solid state. TD-DFT calculations were used to identify transition-relevant orbitals.

1.2 Introduction

Three-coordinate boron-containing π -conjugated molecules are of considerable interest. Boron, with its empty p_z orbital, is a strong acceptor, influencing the LUMO energy level, thereby tuning the HOMO-LUMO gap.^[1–11] Three-coordinate boron has applications in linear^[8,12–32] and non-linear optics,^[33–43] bioimaging,^[45–56] sensors,^[57–61] frustrated Lewis pairs (FLPs),^[62–63] and OLEDs.^[64,65]

Dicarba-*closo*-dodecaboranes are a different class of boron-based compounds that increasingly gain recognition in materials^[66–71] and pharmaceutical fields.^[72–76] They are unique building blocks in optoelectronic materials with high thermal stability due to their 3-dimensional aromaticity.^[77–83] The *ortho*-isomer is a rotation-dependent π -acceptor, accepting electron density into its C1–C2 σ^* -anti-bonding orbital, often leading to aggregation-induced emission (AIE).^[84–98] Both aspects provide opportunities for novel material design. Close-range conjugation of a carboranyl moiety to a 3-coordinate boron has rarely been studied. Examples include *o*-carboranyl-substituted boron dihalides or acids for use in materials^[79,99–101] and more recent, crystallographic studies of C-isopropyl-*o*-carborane-organoboron derivatives with solid state geometries similar to 3-coordinate boranes.^[102] *o*-Carboranes substituted with C-benzodiazaborolyl donor moieties were examined by photophysical, electrochemical, and spectroelectrochemical methods showing large Stokes shifts due to a substituent-to-cage charge transfer (CT) transition.^[8,103–105] Analogues of triarylboranes were synthesised using the BMes₂ moiety as substituent and their spectro- and electrochemical properties were studied.^[106] Recently, 9-borafluorene analogues of carborane-fused “boroles” resulted in strong Lewis acidity while eliminating the rotational freedom of *ortho*-carborane.^[107,108] A variety of B–N type borylated carboranes were reported featuring a strong interaction between boron and nitrogen.^[109–114]

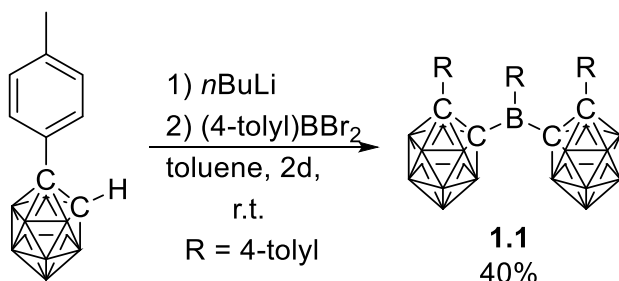
The elasticity of the C1–C2 bond of *o*-carborane (1.629(6) Å) was studied in the presence of bulky substituents^[115–117] (1.712(7) to 2.156(4) Å) and as a function of the C1–C2 σ^* -anti-bonding orbital population by donating groups at C1 and C2 (1.723(2) to (2.065(7) Å).^[118–127] The interest in electrochemical reduction^[105,128–132] to populate this anti-bonding orbital has led to its application in reversible electrochemical uranium capture.^[133] According to Wade’s rules, such an increase of skeletal electrons (SE) results in a transition from a 2n+2 *closo*- towards a 2n+4 *nido*-structure.^[134,135] Reports of rare 2n+3 SE structures have always sparked curiosity throughout the cluster community.^[136–148] The 2n+3 *closo-nido* cluster intermediates of *o*-carboranes offer a structural comparison with calculated S₁ CT excited state geometries as shown by Weber and Fox *et al.*^[104,147,149] Reduction of *o*-carboranes results in a 2n+3 SE system and typically requires a conjugated π -system to stabilize the resulting radical.^[150–153] Few such crystal structures have been reported, all of which are dianionic^[144,147] or double bonded,^[146] resulting in diamagnetism. However, Weber and Fox *et al.* showed by a natural population analysis that the phenylene bridge in [1,4-(1-Ph-*closo*-1,2-C₂B₁₀H₁₀-2-)₂C₆H₄]²⁻ is virtually neutral and, as such, the clusters can be considered to be two independent radicals.^[147] However, to the best of our knowledge, no crystallographic characterization of a paramagnetic *o*-carboranyl monoanion has been reported. Herein, we report the synthesis and characterization of a new bis(*o*-carboranyl)borane. The stabilizing effect of a 3-coordinate borane enabled the isolation and crystallographic study of its paramagnetic monoanion. Similarities between the geometry of the 2n+3 SE *o*-carboranyl radical anion and the optimized geometry of the S₁ state of the neutral system help to understand the charge transfer mechanism and validate calculations thereof. Additionally, the

combination of 3-coordinate boron and *o*-carborane in a single molecule reveals the relative acceptor strengths.

1.3 Results and Discussion

1.3.1 Synthesis, stability, and characterization

Bis(1-(4-tolyl)-carboran-2-yl)-(4-tolyl)-borane (**1.1**) was chosen since the carboranyl moieties with their low steric demand enable free rotation at the $C_{\text{cluster}}-\text{B}_{\text{borane}}$ bonds and the 2-fold substitution offers an intramolecular comparison on reduction or excitation. Lithiation of 1-(4-tolyl)-*o*-carborane^[110] and subsequent salt metathesis with dibromo(*p*-tolyl)borane in toluene gave **1.1** in 40% yield (Scheme 1.1).



Scheme 1.1. Synthesis of 3-coordinate bis(1-(4-tolyl)-carboran-2-yl)-(4-tolyl)-borane (**1.1**).

The yield of the reaction increased by a factor of 2 at room temperature for 2 days for step 2, compared to an overnight reaction at 80 °C. Compound **1.1** is unstable towards nucleophiles and decomposes in a solution in air within seconds. In the solid state, especially single crystals of a few hundred μm, decomposition takes up to 3 days under ambient conditions. Decomposition in the presence of moisture leads to 1-(4-tolyl)-1,2-dicarba-*clos*o-dodecarborane and 4-tolylboronic acid according to NMR spectroscopy and GC-MS.

Compound **1.1** was characterized by elemental analysis, HRMS, and NMR spectroscopy. The 3-coordinate ¹¹B NMR signal of **1.1** at 71.5 ppm is weak and broad (see Supporting Information). The downfield shift of the ¹¹B NMR signals of the B_{cluster} atoms of **1.1** compared to the precursor were used to monitor reaction progress.

1.3.2 Electrochemistry

Redox potentials of **1.1** were measured by cyclic voltammetry in CH_2Cl_2 (Figure 1.1) showing a partially reversible one-electron reduction at $E_{1/2} = -1.35 \text{ V}$ (vs. Fc/Fc^+), very similar to that of the related **1-Ph-2-(Mes)₂B-*creso*-1,2-C₂B₁₀H₁₀** ($E_{1/2}$ in the range of -1.31 to -1.39 V).^[106] The second reduction at $E_{pc} = -1.63 \text{ V}$ is clearly irreversible as shown by the dashed-line scan in Figure 1.1, as is the third reduction at $E_{pc} = -1.87 \text{ V}$, which shows a corresponding oxidation peak at $E_{pa} = -1.57 \text{ V}$.

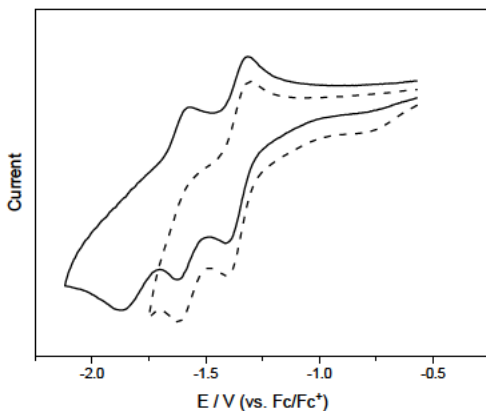
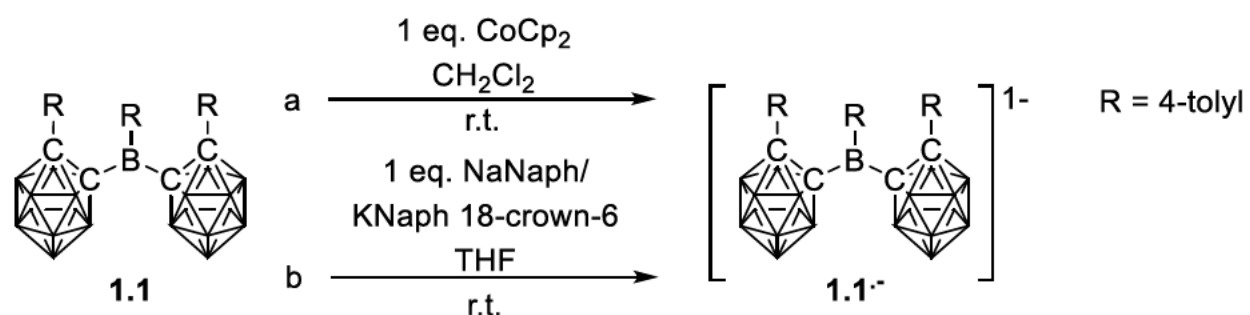


Figure 1.1. Cyclic voltammograms of **1.1** in $\text{CH}_2\text{Cl}_2/0.1 \text{ M } [\text{nBu}_4\text{N}][\text{PF}_6]$ with a scan rate 250 mVs^{-1} . Both scans were normalized.

1.3.3 Chemical Reduction

Several reduction protocols were employed to isolate the reduced form of **1.1** and a controlled and thus selective first reduction was achieved with Cp_2Co in CH_2Cl_2 ($E^0 = -1.33 \text{ V}$ vs. Fc/Fc^+). The reduction product $\text{CoCp}_2^+ \mathbf{1.1}^{1-}$ was precipitated from CH_2Cl_2 with hexane at $-30 \text{ }^\circ\text{C}$ (Scheme 1.2a). Reductions were also carried out in THF with elemental sodium, sodium naphthalenide (NaNaph), or potassium naphthalenide crown ether ($\text{K}(18\text{-crown-6})\text{Naph}$) (Scheme 1.2b). A color change from pale yellow to deep blue was observed upon addition of up to 1.0 equiv of each reducing agent, which is attributed to the monoanion $\mathbf{1.1}^{1-}$ (Scheme 1.2).



Scheme 1.2. Reduction of **1.1**.

All attempts to isolate the higher reduction products were unsuccessful, which seems to be in line with the observed irreversibility of the respective electrochemical reduction events.

1.3.4 EPR spectroscopy

The X-band (9.85 GHz) EPR spectrum of **1.1^{•-}** in THF (Figure 1.2) shows a broad single line of 1.4 mT width, centered close to the free electron g value $g_i = 2.0023$. The lack of resolved hyperfine couplings, even at low temperatures, points to significant delocalization of the unpaired electron spin density over one or both clusters as has been observed and simulated for *o*-carborane-centered radicals.^[130,154]

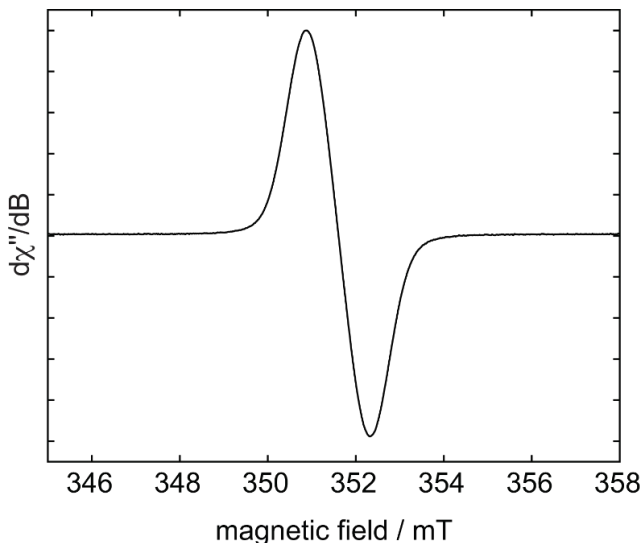


Figure 1.2. Experimental CW X-band (9.85 GHz) EPR spectrum of **1.1^{•-}** in THF at room temperature. Isotropic g value = 2.0026 and peak-to-peak linewidth = 1.4 mT.

1.3.5 Single-crystal structure analysis

Single crystals of **1.1** suitable for X-ray diffraction were grown from a saturated toluene solution at $-30\text{ }^{\circ}\text{C}$, and crystals of **Na⁺1.1^{•-}**, **CoCp₂⁺1.1^{•-}**, and **{K[18]crown-6·(THF)₂}⁺1.1^{•-}** were grown by hexane diffusion into saturated THF solutions at $-30\text{ }^{\circ}\text{C}$. The crystal structure of **{K[18]crown-6·(THF)₂}⁺1.1^{•-}** is of high quality, while those of **Na⁺1.1^{•-}** and **CoCp₂⁺1.1^{•-}** are of poorer quality and thus, are presented as confirmation of the monoanions in the Supporting Information, only. For consistency, the *o*-carboranyl moiety with the C₂_{cluster}—C₁_{cluster}—B1—C₁_{toloyl} dihedral angle closest to 90° with respect to the 3-coordinate borane plane is labeled **a**, which is important for comparisons due to the interaction between the p_z-orbital of B1 and the C1—C2 σ*-anti-bonding orbital of *o*-carborane. A comparison of the neutral and reduced structures and their respective calculated geometries and the calculated geometry of the S₁ state of **1.1** are listed in Table 1.1 and in the text as (experimental(esd)/calculated Å).

Table 1.1. Selected bond lengths [Å] and angles [°] of **1.1** and $\{\text{K}[18]\text{crown-6}\cdot(\text{THF})_2\}^+\text{1.1}^-$ from experiment, optimized structures (Calc.), and optimized structure of the S_1 state of **1.1** (S_1 -Calc.).

Compound	1.1	1.1 Calc.^a	1.1 S_1-Calc.^a	$\{\text{K}[18]\text{crown-6}\cdot(\text{THF})_2\}^+\text{1.1}^-$	1.1^- Calc. ^a
B1–C1	1.553(3)	1.551	1.573	1.575(3)	1.577
B1–C1a	1.608(3)	1.610	1.522	1.521(3)	1.528
B1–C1b	1.626(2)	1.605	1.601	1.616(3)	1.618
C1a–C2a	1.726(2)	1.708	2.171	2.311(3)	2.284
C1b–C2b	1.761(2)	1.758	1.694	1.732(3)	1.748
C2a–C3a	1.507(2)	1.503	1.483	1.477(3)	1.475
C2b–C3b	1.502(2)	1.499	1.504	1.504(3)	1.501
∠ C1–B1–C1a	118.4(1)	117.8	113.2	118.6(2)	119.1
∠ C1–B1–C1b	120.2(1)	119.7	119.7	118.6(2)	118.4
∠ C1a–B1–C1b	121.2(1)	122.4	127.0	122.2(2)	122.5
Sum ∠ C–B1–C	359.8(3)	359.9	359.9	359.7(6)	360.0
∠ C2a–C1a–B1–C1 ^b	62.4(2)	65.1	73.6	94.4(2)	85.8
∠ C2b–C1b–B1–C1 ^b	−44.0(2)	−43.3	−31.5	54.9(3)	46.0

^a B3LYP/6-31G*. ^b Angles with respect to the 3-coordinate borane plane.

The two *o*-carboranyl moieties in **1.1** adopt a *transoid* conformation with dihedral angles C2a–C1a–B1–C1 (62.4(2)/65.1°) and C2b–C1b–B1–C1 (−44.0(2)/−43.3°) (Figure 1.3, right). The *o*-carboranyl moiety **a** has a greater overlap of C1–C2 σ- and B1-p_z orbitals. The 3-coordinate boron atom has a nearly ideal trigonal planar configuration, with the sum of the C–B–C angles being 359.8(3)/359.9°. The B1–C1 bond length to the tolyl-moiety (1.553(3)/1.551 Å) is as expected (avg B(3)–Ar bond = 1.556 Å).^[155] The B1–C1b (1.626(2)/1.605 Å) bond is significantly longer than the B1–C1a (1.608(3)/1.610 Å) bond in the solid state, while this difference is not present in the computed bond lengths. The C1b–C2b (1.761(2)/1.758 Å) bond is longer by ca. 0.035 Å (calc. 0.050 Å) than the C1a–C2a (1.726(2) Å/1.708 Å) bond both in the solid state and the computed molecule. Bond lengthening is observed for bonds involving tolyl groups with the smaller dihedral angle (C2b–C1b–B1–C1), which are nearly parallel with an angle of 12.47(5)° between plane normals and an intramolecular π-stacking interaction with interplanar distances of 3.1532(18) and 3.3724(19) Å.

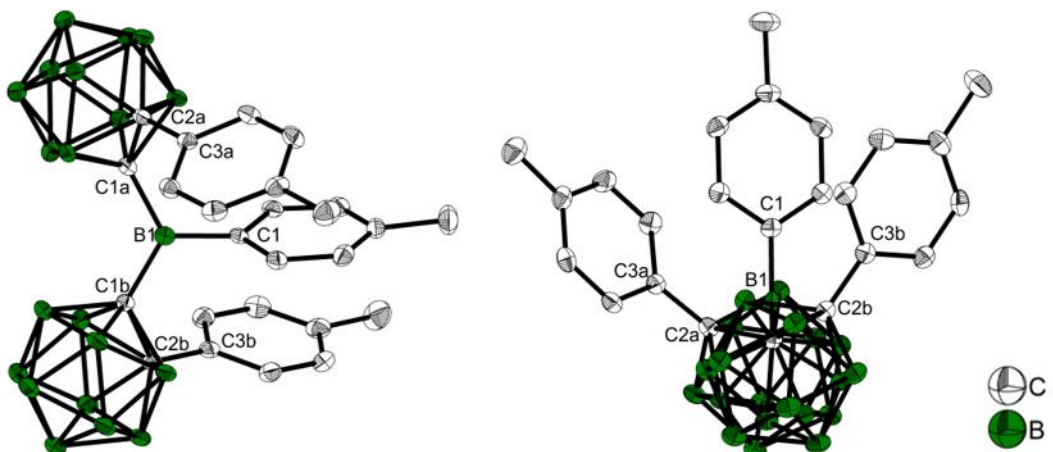


Figure 1.3. Molecular structure of **1.1** in the solid state at 100 K. H atoms are omitted for clarity. Thermal ellipsoids are drawn at 50% probability. Left, view perpendicular to the 3-coordinate boron plane; right, view along C1b–B1–C1a.

In the structure of the monoanion **1.1⁻** (Figure 1.4), both carboranyls are rotated such that the C-tolyl groups lie on the same side of the 3-coordinate boron plane, whereas in the neutral compound one lies above and one below this plane. Similar to **1.1**, the configuration of the 3-coordinate boron atom in **1.1⁻** is trigonal planar with the sum of the C–B–C angles being 359.7(6)/360°, with slightly larger angles between the carboranes C1a–B1–C1b. However, the dihedral angle C2a–C1a–B1–C1 (94.4(2)/85.8°) is close to 90°, while C2b–C1b–B1–C1 (54.9(3)/46.0°) is smaller. In comparison to neutral **1.1**, the crystal structure of the paramagnetic monoanion **1.1⁻** shows a large increase of the carborane C1a–C2a bond length by almost 0.6 Å resulting in bond cleavage (C1a–C2a = 1.726(2)/1.708 Å in **1.1**; C1a–C2a = 2.311(3)/2.284 Å in **1.1⁻**, Table 1.1). This reduction-induced cage opening is only observed in moiety **a**, and it is present in all 3 monoanion structures with different cations (Figures 1.4 and 5, Tables 1.1 and 5.1.2).

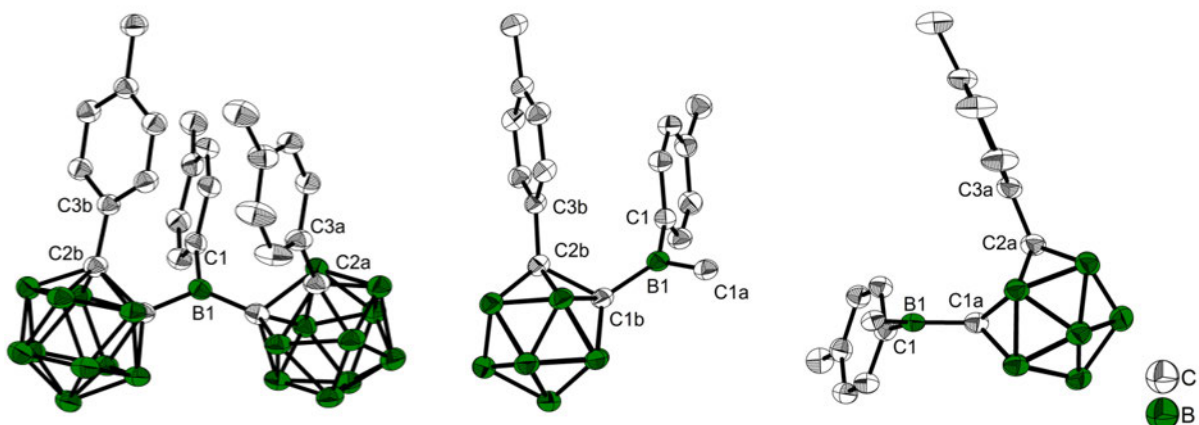


Figure 1.4. Molecular structure of $\{\text{K}[18]\text{crown-6-(THF)}\}^+ \cdot \text{1.1}^-$ in the solid state at 100 K. H atoms, solvent molecules, and cations are omitted for clarity. Thermal ellipsoids are drawn at 50% probability. Left, view of the full molecule; middle, view perpendicular to the C1b–C2b bond with (p-tolyl)carborane **a** omitted for clarity; right, view perpendicular to the C1a–C2a bond with (p-tolyl)carborane **b** omitted for clarity.

A similar elongation of the C1–C2 bond in the carborane cage upon reduction was proposed by Weber, Fox and co-workers from theoretical computations on the monoanion geometries of C-diazaborolyl-*o*-carboranes and was attributed to the location of the negative charge in the cage.^[104] The bonds adjacent to C1a–C2a are also affected by the reduction, with a significant contraction of the B1–C1a (1.521(3)/1.528 Å) bond by ca. –0.09 Å compared to $d(B1\text{--}C1a/C1b)$ of both carboranyl moieties in 1.1, and to a smaller contraction (–0.03 Å) of the C2a–C3a (1.477(3)/1.475 Å) bond, which connects the tolyl moiety to carboranyl a. Radical anion 1.1[–] exhibits a small lengthening (+0.022 Å) of $d(B1\text{--}C1)$ (1.575(3)/1.577 Å). The population of the π -character B1–C1a LUMO orbital (see calculations) increases its bond order explaining the contraction and the tendency towards a 90° dihedral angle. The C1a–C2a σ^* -anti-bonding orbital is also populated, lengthening the C1a–C2a bond. In contrast to the significant changes in the carboranyl moiety a, only small changes are observed for the carboranyl moiety b upon reduction, i.e., the C1b–C2b (1.732(3)/1.448 Å) cluster bond is slightly shorter by 0.03 Å in 1.1[–] than in 1.1, as is the B1–C1b (1.616(3)/1.618 Å) bond by 0.01 Å, while $d(C2b\text{--}C3b)$ (1.504(3)/1.501 Å) remains the same within 3 esd's. The slightly shorter bonds may be due to the absence of π -stacking interactions between tolyl groups in 1.1[–] and, hence, not to the reduction process itself. This observation suggests that the *o*-carboranyl moiety b plays no role in stabilizing the additional negative charge.

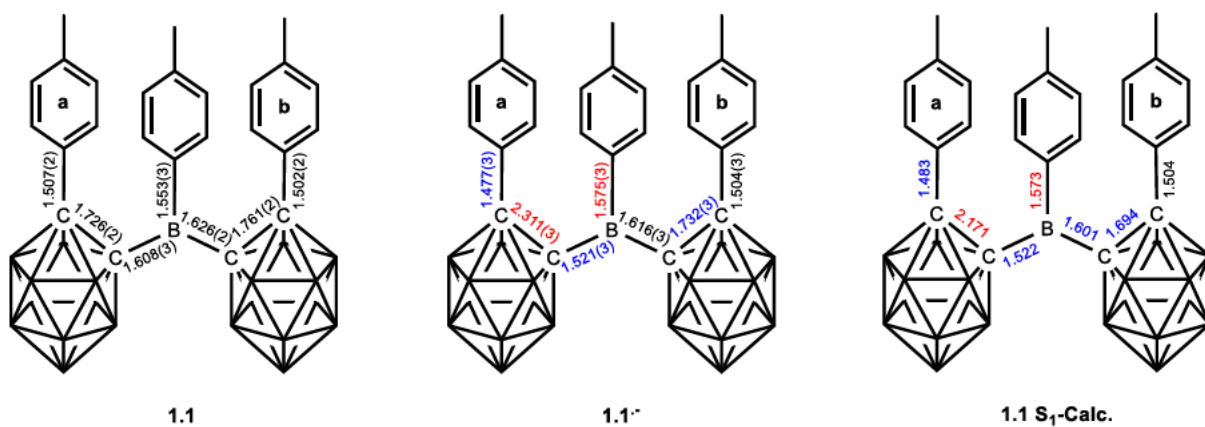


Figure 1.5. Bond lengths in 1.1, 1.1[–] and the optimized S₁ state of 1.1. Red: increase in bond length, blue: decrease in bond length.

The optimized geometry of the excited S₁ state of shows 1.1 a strong resemblance to that of the radical anion 1.1[–] (Figure 1.5). A similarity of the S₁ excited-state and the monoanion geometries was proposed by Weber, Fox, and co-workers for the C-diazaborolyl-*o*-carborane from computations.^[104] Again, the *o*-carboranyl group b and the 3-coordinate B-bound tolyl moiety of 1.1[–] are very similar to the neutral compound 1.1. However, the parameters for the carboranyl moiety a show strong resemblance to the structure of 1.1[–]. The bond contraction of B1–C1a (1.522 Å), as well as the bond elongation of C1a–C2a (2.284 Å) in the S₁ state agree well with the structural changes observed for 1.1[–]. The C2a–C3a (1.483 Å) bond is also significantly shorter than $d(C2b\text{--}C3b)$ (1.504 Å). These similarities suggest comparable geometrical reorganizations during reduction and the CT process after excitation.

1.3.6 Photophysical properties

Photophysical data for **1.1** are listed in Table 1.2. The lowest energy absorption maximum of **1.1** shows almost no dependence on solvent polarity (toluene 376 nm, CH_2Cl_2 381 nm) and is weakly allowed ($\epsilon = 1800 \text{ M}^{-1}\text{cm}^{-1}$) (Figure 1.6). The excitation spectrum in the solid state exhibits a strong bathochromic shift (420 nm) of the lowest energy absorption maximum compared to that in solution. The emission band is strongly red shifted (561 nm as solid, 566 nm in CH_2Cl_2 , 585 nm in toluene) compared to the absorption with large apparent Stokes shifts (6000 cm^{-1} as solid, 8600 cm^{-1} in CH_2Cl_2 , 9500 cm^{-1} in toluene), indicating a significant geometry change in the excited state, typical of carborane chromophores.^[103]

The emission maxima show a weak hypsochromic shift due to the direction change of the dipole moment from the ground to the excited state. The calculated orbital overlap parameter (Λ) of 0.42 at the CAM-B3LYP level of theory suggests a CT from the initial excitation at the tolyl moiety to the *o*-carborane cage (see TD-DFT calculations).^[156,157] Quantum yields in solution were too low to be determined reliably, with decomposition visible in the absorption spectrum after extended measurements, but in the solid state, the quantum yield is 0.19, a behavior typical of carborane chromophores.^[69,84,95]

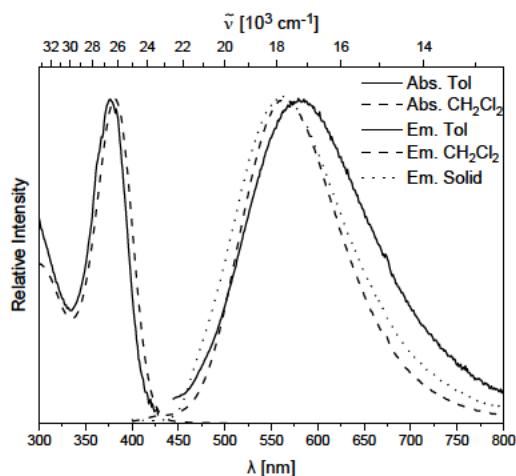


Figure 1.6. Absorption (<450 nm) and emission (>450 nm, excited at lowest energy absorption maximum) spectra of **1.1** in toluene (solid line), CH_2Cl_2 (dashed line) and solid state (dotted line).

Table 1.2. Photophysical data for compounds **1.1** and **1.1^{•-}**.

Compound	solvent	λ_{abs} [nm]	ϵ [M ⁻¹ cm ⁻¹]	λ_{em} [nm]	Apparent Stokes Shift [cm ⁻¹]	τ [ns]	Φ_F
1.1	toluene	376		585	9500	— ^a	— ^a
1.1	CH ₂ Cl ₂	381	1800	566	8600	— ^a	— ^a
1.1	Solid	420 ^b		561	6000	14.0	0.19
CoCp ₂ ^{+1.1^{•-}}	CH ₂ Cl ₂	591					
{K[18]crown-6-(THF) ₂ } ^{+1.1^{•-}}	THF	615					

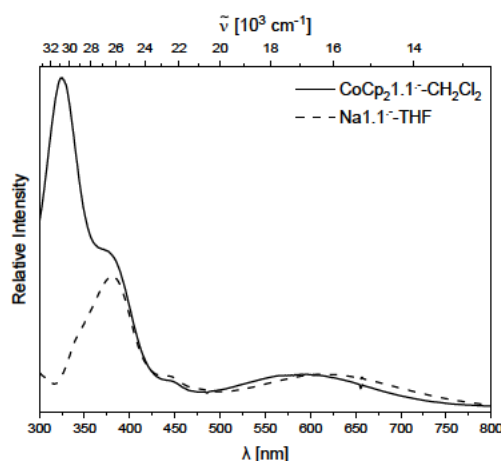
^a Could not be determined reliably.^b Calculated from excitation spectrum (see 5.1.1).**Figure 1.7.** Absorption spectra of CoCp₂^{+1.1^{•-} (solid line) in CH₂Cl₂ and {K[18]crown-6-(THF)₂}^{+1.1^{•-} in THF (dashed line).}}

Figure 1.7 displays the UV/Vis spectra of **1.1^{•-}** in CH₂Cl₂ and THF, which are nearly identical, apart from a strong band at 323 nm, which can be ascribed to the cobaltocinium counter ion^[158] featuring a broad band in the low-energy region (591 nm in CH₂Cl₂, 615 nm in THF).

1.3.7 DFT and TD-DFT studies

Optimized ground state structures were calculated at the B3LYP/6-31G* level of theory in the gas phase starting from the solid state molecular geometries.^[103,106] For **1.1**, the HOMO is located on the tolyl moiety at the 3-coordinate boron and on the carboranyl-bound tolyl moiety **b** (Figure 1.8). All occupied orbitals down to HOMO-4 are located on tolyl groups. The LUMO is located mostly on the 3-coordinate boron with p_z-character and participation of the carborane C1-C2 σ*-MO's depending on the respective dihedral overlap. In solution, with freely rotating carboranyl moieties, the first reduction, observed in the CV, should most likely take place at the 3-coordinate boron p_z orbital followed by a geometrical reorganization of one of the carborane cages, as has been described before.^[104] To gain insight into the photophysical properties of **1.1**, TD-DFT calculations were carried out using the Coulomb attenuated functional CAM-B3LYP/6-31G*, which usually gives a better

description of CT systems compared to B3LYP.^[159] The $S_1 \leftarrow S_0$ transition largely resembles a HOMO-LUMO transition at 3.71 eV ($\lambda = 334$ nm) that exhibits a relatively low oscillator strength of $f = 0.102$ (Table 1.3). The use of the orbital overlap parameter Λ ($0 \leq \Lambda \leq 1$, where 0 and 1 correspond to no and complete overlap, respectively) offers a method to quantify the spatial overlap of transition orbitals.^[156] With a relatively high separation given by $\Lambda = 0.42$ together with the observed spectrum, the first transition can be categorized as CT. The simulated data are in good agreement with the UV/Vis spectrum (see 5.1 Supporting Information Chapter 1).

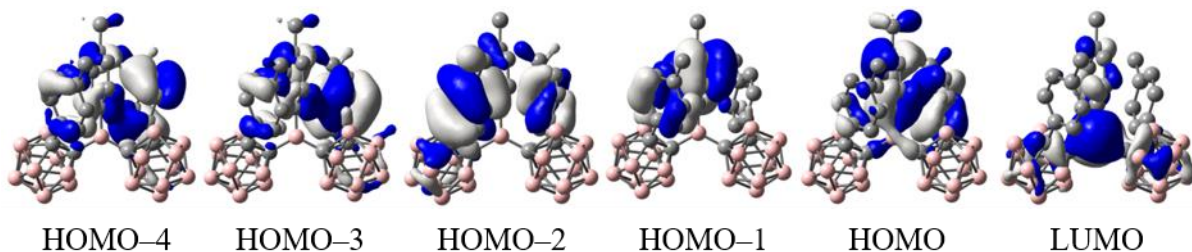
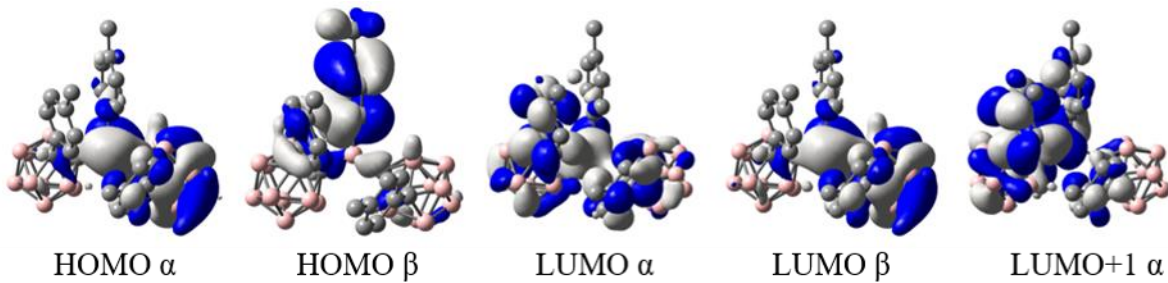


Figure 1.8. Frontier orbitals of **1.1**.

Table 1.3. TD-DFT calculated transitions (toluene) of **1.1** (CAM-B3LYP/6-31G*).

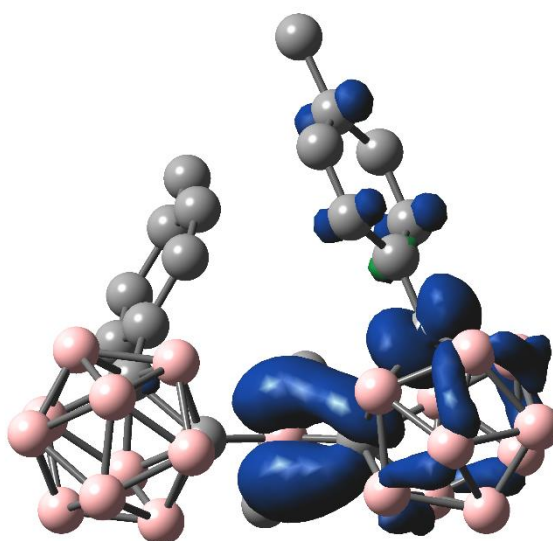
FC-S _n	E[eV] (E[nm])	f	Contribution > 10%	Λ
S ₁	3.71 (334)	0.102	HOMO → LUMO (86%)	0.42
S ₂	4.27 (290)	0.004	H-2 → LUMO (12%) H-1 → LUMO (76%)	0.33
S ₃	4.53 (274)	0.013	H-2 → LUMO (82%) H-1 → LUMO (13%)	0.32
S ₄	4.61 (269)	0.014	H-4 → LUMO (11%) H-3 → LUMO (73%)	0.36
S ₅	4.96 (250)	0.006	H-4 → LUMO (76%) H-3 → LUMO (10%)	0.30

For **1.1^{•-}**, the HOMO α (SOMO) is mainly delocalized over the carboranyl moiety **a** (C1–C2 σ^* -anti-bonding orbital) with some contribution from the aligned 3-coordinate boron atom p_z -orbital. The LUMO α is spread over the carboranyl moiety **b**, the *o*-carborane-bound tolyl moieties **a** and **b**, and the 3-coordinate boron (Figure 1.9). The $S_1 \leftarrow S_0$ transition between these two MO's has LE character ($\Lambda = 0.68$) and a small energy gap of 2.08 eV ($\lambda = 595.9$ nm) with an oscillator strength of 0.1301 (Table 1.4), agreeing nicely with the absorption spectrum (see Supporting Information). Given the participation of the carboranyl moiety **b** in the first transition, alternating carborane radicals seem plausible. A continuous delocalization between both appears to be inhibited by the energy necessary to reorganize both carboranyl moieties simultaneously.

**Figure 1.9.** Frontier orbitals of $\mathbf{1.1}^{\bullet-}$.**Table 1.4.** TD-DFT calculated transitions (gas phase) of $\mathbf{1.1}^{\bullet-}$ (B3LYP/6-31G*).

FC-S _n	E[eV] (E[nm])	f	Contribution > 10%	Δ
S ₁	2.08 (596)	0.1301	HOMO α \rightarrow LUMO α (92%)	0.68
S ₂	2.35 (528)	0.0054	HOMO α \rightarrow L+1 α (93%)	0.54
S ₃	2.79 (443)	0.0014	HOMO α \rightarrow L+2 α (71%) HOMO α \rightarrow L+3 α (27%)	0.50
S ₄	2.88 (430)	0.003	HOMO α \rightarrow L+2 α (27%) HOMO α \rightarrow L+3 α (71%)	0.68
S ₅	3.13 (396)	0.0042	HOMO α \rightarrow L+4 α (35%) HOMO β \rightarrow LUMO β (46%)	0.54

The spin density map of $\mathbf{1.1}^{\bullet-}$ at the B3LYP/6-31G* level of theory reveals a distribution of 57% on the carborane cage **a**, 37% on B1 and 5% on the carboranyl-bound tolyl **a** (Figure 1.10). This distribution underlines the significant delocalization of the negative charge between B1, C1a, and C2a and provides confirmation of the hypothesis derived from the crystal structure, suggesting that *o*-carborane is a stronger acceptor than the borane unit, confirming previous reports.^[106]

**Figure 1.10.** Spin density map of $\mathbf{1.1}^{\bullet-}$ at B3LYP/6-31G* level of theory (ISO value = 0.0025).

1.4 Conclusions

We report the synthesis and properties of an unusual bis(*o*-carboranyl) substituted 3-coordinate borane [$(1-(4-\text{MeC}_6\text{H}_4)-\text{closo-}1,2-\text{C}_2\text{B}_{10}\text{H}_9-2-)_2(4-\text{MeC}_6\text{H}_4)\text{B}$] (**1.1**). Cyclic voltammetry studies revealed a partially reversible one-electron first reduction, and the resulting radical anion **1.1^{•-}** was isolated using different reduction protocols. EPR spectroscopy confirmed the paramagnetic nature of the anion and the involvement of the *o*-carboranyls in the delocalization of the unpaired electron spin. The solid-state structure of the radical anion revealed major contributions of B1 and one of the *o*-carboranyl moieties to the delocalization of the extra electron, with negligible change of bond distances within the second *o*-carboranyl moiety. The perpendicular orientation of the reduced *o*-carborane fragment facilitates optimal overlap between the 3-coordinate boron p_z-orbital and the C1–C2 σ*-anti-bonding orbital leading to a shorter B1–C1a and longer C1a–C2a bond. Strong similarities between the 2n+3 SE *o*-carborane structure of the radical anion **1.1^{•-}** and the optimized structure of the S₁ state of **1.1** confirm predictions regarding geometrical reorganization in the CT process. The photophysical studies show a CT emission with a large Stokes shift of up to 9500 cm⁻¹. Like other known carborane dyads, **1.1** has a small quantum yield in solution with a strong increase in the solid state ($\Phi_F = 19\%$). Upon reduction, a broad low energy absorption appears at ca. 600 nm. The experimental observations are in good agreement with the calculations at the B3LYP/6-31G* level of theory.

1.5 References

- [1] N. S. Hosmane, *Boron science. New technologies and applications*, CRC Press, Boca Raton, FL, **2012**.
- [2] N. S. Hosmane, R. Eagling, *Handbook of boron science with applications in organometallics, catalysis, materials and medicine*, World Scientific, New Jersey, **2019**.
- [3] C. D. Entwistle, T. B. Marder, *Angew. Chem. Int. Ed.* **2002**, *41*, 2927–2931; *Angew. Chem.* **2002**, *114*, 3051.
- [4] C. D. Entwistle, T. B. Marder, *Chem. Mater.* **2004**, *16*, 4574–4585.
- [5] S. Yamaguchi, A. Wakamiya, *Pure Appl. Chem.* **2006**, *78*, 1413–1424.
- [6] F. Jäkle, *Coord. Chem. Rev.* **2006**, *250*, 1107–1121.
- [7] R. Stahl, C. Lambert, C. Kaiser, R. Wortmann, R. Jakober, *Chem. Eur. J.* **2006**, *12*, 2358–2370.
- [8] L. Weber, D. Eickhoff, T. B. Marder, M. A. Fox, P. J. Low, A. D. Dwyer, D. J. Tozer, S. Schwedler, A. Brockhinke, H.-G. Stammler, B. Neumann, *Chem. Eur. J.* **2012**, *18*, 1369–1382.
- [9] L. Ji, S. Griesbeck, T. B. Marder, *Chem. Sci.* **2017**, *8*, 846–863.
- [10] S.-Y. Li, Z.-B. Sun, C.-H. Zhao, *Inorg. Chem.* **2017**, *56*, 8705–8717.
- [11] E. von Grotthuss, A. John, T. Kaese, M. Wagner, *Asian J. Org. Chem.* **2018**, *7*, 37–53.
- [12] N. Matsumi, K. Naka, Y. Chujo, *J. Am. Chem. Soc.* **1998**, *120*, 5112–5113.
- [13] S. Yamaguchi, S. Akiyama, K. Tamao, *J. Am. Chem. Soc.* **2000**, *122*, 6335–6336.
- [14] W.-L. Jia, D. Song, S. Wang, *J. Org. Chem.* **2003**, *68*, 701–705.
- [15] A. Wakamiya, T. Ide, S. Yamaguchi, *J. Am. Chem. Soc.* **2005**, *127*, 14859–14866.
- [16] I. Yamaguchi, B.-J. Choi, T.-A. Koizumi, K. Kubota, T. Yamamoto, *Macromolecules* **2007**, *40*, 438–443.
- [17] U. Megerle, F. Selmaier, C. Lambert, E. Riedle, S. Lochbrunner, *Phys. Chem. Chem. Phys.* **2008**, *10*, 6245–6251.
- [18] L. Weber, V. Werner, M. A. Fox, T. B. Marder, S. Schwedler, A. Brockhinke, H.-G. Stammler, B. Neumann, *Dalton Trans.* **2009**, 2823–2831.
- [19] E. Januszewski, A. Lorbach, R. Grewal, M. Bolte, J. W. Bats, H.-W. Lerner, M. Wagner, *Chem. Eur. J.* **2011**, *17*, 12696–12705.
- [20] Z. Zhou, A. Wakamiya, T. Kushida, S. Yamaguchi, *J. Am. Chem. Soc.* **2012**, *134*, 4529–4532.
- [21] C. Reus, S. Weidlich, M. Bolte, H.-W. Lerner, M. Wagner, *J. Am. Chem. Soc.* **2013**, *135*, 12892–12907.
- [22] J. Yoshino, Y. Nakamura, S. Kunitomo, N. Hayashi, H. Higuchi, *Tetrahedron Lett.* **2013**, *54*, 2817–2820.
- [23] A. Ito, K. Kawanishi, E. Sakuda, N. Kitamura, *Chem. Eur. J.* **2014**, *20*, 3940–3953.
- [24] X. Yin, J. Chen, R. A. Lalancette, T. B. Marder, F. Jäkle, *Angew. Chem. Int. Ed.* **2014**, *53*, 9761–9765; *Angew. Chem.* **2014**, *37*, 9919–9923.
- [25] Z. Zhang, R. M. Edkins, J. Nitsch, K. Fucke, A. Eichhorn, A. Steffen, Y. Wang, T. B. Marder, *Chem. Eur. J.* **2015**, *21*, 177–190.
- [26] J. Merz, J. Fink, A. Friedrich, I. Krummenacher, H. H. Al Mamari, S. Lorenzen, M. Haehnel, A. Eichhorn, M. Moos, M. Holzapfel, H. Braunschweig, C. Lambert, A. Steffen, L. Ji, T. B. Marder, *Chem. Eur. J.* **2017**, *23*, 13164–13180.
- [27] J. He, F. Rauch, A. Friedrich, D. Sieh, T. Ribbeck, I. Krummenacher, H. Braunschweig, M. Finze, T. B. Marder, *Chem. Eur. J.* **2019**, *25*, 13777–13784.
- [28] X. Jia, J. Nitsch, L. Ji, Z. Wu, A. Friedrich, F. Kerner, M. Moos, C. Lambert, T. B. Marder, *Chem. Eur. J.* **2019**, *25*, 10845–10857.
- [29] J. Merz, A. Steffen, J. Nitsch, J. Fink, C. B. Schürger, A. Friedrich, I. Krummenacher, H. Braunschweig, M. Moos, D. Mims, C. Lambert, T. B. Marder, *Chem. Sci.* **2019**, *10*, 7516–7534.
- [30] F. Rauch, P. Endres, A. Friedrich, D. Sieh, M. Hänel, I. Krummenacher, H. Braunschweig, M. Finze, L. Ji, T. B. Marder, *Chem. Eur. J.* **2020**, *26*, 12951–12963.
- [31] F. Rauch, S. Fuchs, A. Friedrich, D. Sieh, I. Krummenacher, H. Braunschweig, M. Finze, T. B. Marder, *Chem. Eur. J.* **2020**, *26*, 12794–12808.

Chapter 1

- [32] Z. Wu, J. Nitsch, J. Schuster, A. Friedrich, K. Edkins, M. Loebnitz, F. Dinkelbach, V. Stepanenko, F. Würthner, C. M. Marian, L. Ji, T. B. Marder, *Angew. Chem. Int. Ed.* **2020**, *39*, 17137–17144; *Angew. Chem.* **2020**, *39*, 17285–17292.
- [33] Z. Yuan, N. J. Taylor, T. B. Marder, I. D. Williams, S. K. Kurtz, L.-T. Cheng, *J. Chem. Soc., Chem. Commun.* **1990**, *23*, 1489–1492.
- [34] Z. Yuan, N. J. Taylor, Y. Sun, T. B. Marder, I. D. Williams, C. Lap-Tak, *J. Organomet. Chem.* **1993**, *449*, 27–37.
- [35] Z. Yuan, N. J. Taylor, R. Ramachandran, T. B. Marder, *Appl. Organometal. Chem.* **1996**, *10*, 305–316.
- [36] Z.-Q. Liu, Q. Fang, D. Wang, G. Xue, W.-T. Yu, Z.-S. Shao, M.-H. Jiang, *Chem. Commun.* **2002**, 2900–2901.
- [37] Z.-Q. Liu, Q. Fang, D. Wang, D.-X. Cao, G. Xue, W.-T. Yu, H. Lei, *Chem. Eur. J.* **2003**, *9*, 5074–5084.
- [38] M. Chariot, L. Porrès, C. D. Entwistle, A. Beeby, T. B. Marder, M. Blanchard-Desce, *Phys. Chem. Chem. Phys.* **2005**, *7*, 600–606.
- [39] Z. Yuan, C. D. Entwistle, J. C. Collings, D. Albesa-Jové, A. S. Batsanov, J. A. K. Howard, N. J. Taylor, H. M. Kaiser, D. E. Kaufmann, S.-Y. Poon, W.-Y. Wong, C. Jardin, S. Fathallah, A. Boucekkine, J.-F. Halet, T. B. Marder, *Chem. Eur. J.* **2006**, *12*, 2758–2771.
- [40] J. C. Collings, S.-Y. Poon, C. Le Droumaguet, M. Charlot, C. Katan, L.-O. Pålsson, A. Beeby, J. A. Mosely, H. M. Kaiser, D. Kaufmann, W.-Y. Wong, M. Blanchard-Desce, T. B. Marder, *Chem. Eur. J.* **2009**, *15*, 198–208.
- [41] C. D. Entwistle, J. C. Collings, A. Steffen, L.-O. Pålsson, A. Beeby, D. Albesa-Jové, J. M. Burke, A. S. Batsanov, J. A. K. Howard, J. A. Mosely, S.-Y. Poon, W.-Y. Wong, F. Ibersiene, S. Fathallah, A. Boucekkine, J.-F. Halet, T. B. Marder, *J. Mater. Chem.* **2009**, *19*, 7532–7544.
- [42] L. Ji, R. M. Edkins, L. J. Sewell, A. Beeby, A. S. Batsanov, K. Fucke, M. Drafz, J. A. K. Howard, O. Moutounet, F. Ibersiene, A. Boucekkine, E. Furet, Z. Liu, J.-F. Halet, C. Katan, T. B. Marder, *Chem. Eur. J.* **2014**, *20*, 13618–13639.
- [43] P. Chen, A. S. Marshall, S.-H. Chi, X. Yin, J. W. Perry, F. Jäkle, *Chem. Eur. J.* **2015**, *21*, 18237–18247.
- [44] X. Li, X. Guo, L. Cao, Z. Xun, S. Wang, S. Li, Y. Li, G. Yang, *Angew. Chem. Int. Ed.* **2014**, *53*, 7809–7813; *Angew. Chem.* **2014**, *30*, 7943–7947.
- [45] J. Liu, X. Guo, R. Hu, J. Xu, S. Wang, S. Li, Y. Li, G. Yang, *Anal. Chem.* **2015**, *87*, 3694–3698.
- [46] B. Chen, G. Feng, B. He, C. Goh, S. Xu, G. Ramos-Ortiz, L. Aparicio-Ixta, J. Zhou, L. Ng, Z. Zhao, B. Liu, B. Z. Tang, *Small* **2016**, *12*, 782–792.
- [47] S. Griesbeck, Z. Zhang, M. Gutmann, T. Lühmann, R. M. Edkins, G. Clermont, A. N. Lazar, M. Haehnel, K. Edkins, A. Eichhorn, M. Blanchard-Desce, L. Meinel, T. B. Marder, *Chem. Eur. J.* **2016**, *22*, 14701–14706.
- [48] J. Liu, X. Guo, R. Hu, X. Liu, S. Wang, S. Li, Y. Li, G. Yang, *Anal. Chem.* **2016**, *88*, 1052–1057.
- [49] J. Liu, S. Zhang, C. Zhang, J. Dong, C. Shen, J. Zhu, H. Xu, M. Fu, G. Yang, X. Zhang, *Chem. Commun.* **2017**, *53*, 11476–11479.
- [50] S. Pagidi, N. K. Kalluvettukuzhy, P. Thilagar, *Langmuir* **2018**, *34*, 8170–8177.
- [51] S. Griesbeck, M. Ferger, C. Czernetzi, C. Wang, R. Bertermann, A. Friedrich, M. Haehnel, D. Sieh, M. Taki, S. Yamaguchi, T. B. Marder, *Chem. Eur. J.* **2019**, *25*, 7679–7688.
- [52] S. Griesbeck, E. Michail, F. Rauch, H. Ogasawara, C. Wang, Y. Sato, R. M. Edkins, Z. Zhang, M. Taki, C. Lambert, S. Yamaguchi, T. B. Marder, *Chem. Eur. J.* **2019**, *25*, 13164–13175.
- [53] S. Griesbeck, E. Michail, C. Wang, H. Ogasawara, S. Lorenzen, L. Gerstner, T. Zang, J. Nitsch, Y. Sato, R. Bertermann, M. Taki, C. Lambert, S. Yamaguchi, T. B. Marder, *Chem. Sci.* **2019**, *10*, 5405–5422.
- [54] J. Liu, K. Cheng, C. Yang, J. Zhu, C. Shen, X. Zhang, X. Liu, G. Yang, *Anal. Chem.* **2019**, *91*, 6340–6344.
- [55] J. Liu, S. Zhang, B. Zhao, C. Shen, X. Zhang, G. Yang, *Biosens. Bioelectron.* **2019**, *142*, 111497.
- [56] J. Dong, C. Zhang, B. Zhao, X. Zhang, Z. Leng, J. Liu, *Dyes and Pigments* **2020**, *174*, 108077.
- [57] S. Yamaguchi, S. Akiyama, K. Tamao, *J. Am. Chem. Soc.* **2001**, *123*, 11372–11375.
- [58] K. Parab, K. Venkatasubbaiah, F. Jäkle, *J. Am. Chem. Soc.* **2006**, *128*, 12879–12885.

Chapter 1

- [59] M. Elbing, G. C. Bazan, *Angew. Chem. Int. Ed.* **2008**, *47*, 834–838; *Angew. Chem.* **2008**, *5*, 846–850.
- [60] T. W. Hudnall, C.-W. Chiu, F. P. Gabbaï, *Acc. Chem. Res.* **2009**, *42*, 388–397.
- [61] K. C. Song, H. Kim, K. M. Lee, Y. S. Lee, Y. Do, M. H. Lee, *Dalton Trans.* **2013**, *42*, 2351–2354.
- [62] G. C. Welch, R. R. San Juan, J. D. Masuda, D. W. Stephan, *Science* **2006**, *314*, 1124–1126.
- [63] D. W. Stephan, G. Erker, *Angew. Chem. Int. Ed.* **2015**, *54*, 6400–6441; *Angew. Chem.* **2015**, *22*, 6498–6541.
- [64] Y. Shirota, *J. Mater. Chem.* **2000**, *10*, 1–25.
- [65] A. Wakamiya, K. Mori, S. Yamaguchi, *Angew. Chem. Int. Ed.* **2007**, *46*, 4273–4276; *Angew. Chem.* **2007**, *23*, 4351–4354.
- [66] R. N. Grimes, *Carboranes*, Academic Press, New York, **2016**.
- [67] J. Mei, N. L. C. Leung, R. T. K. Kwok, J. W. Y. Lam, B. Z. Tang, *Chem. Rev.* **2015**, *115*, 11718–11940.
- [68] R. Núñez, M. Tarrés, A. Ferrer-Ugalde, F. F. de Biani, F. Teixidor, *Chem. Rev.* **2016**, *116*, 14307–14378.
- [69] J. Ochi, K. Tanaka, Y. Chujo, *Angew. Chem. Int. Ed.* **2020**, *25*, 9841–9855; *Angew. Chem.* **2020**, *25*, 9925–9939.
- [70] V. I. Bregadze, *Chem. Rev.* **1992**, *92*, 209–223.
- [71] B. P. Dash, R. Satapathy, J. A. Maguire, N. S. Hosmane, *New J. Chem.* **2011**, *35*, 1955–1972.
- [72] I. B. Sivaev, V. I. Bregadze, *Eur. J. Inorg. Chem.* **2009**, *2009*, 1433–1450.
- [73] M. Scholz, E. Hey-Hawkins, *Chem. Rev.* **2011**, *111*, 7035–7062.
- [74] F. Issa, M. Kassiou, L. M. Rendina, *Chem. Rev.* **2011**, *111*, 5701–5722.
- [75] J. F. Valliant, K. J. Guenther, A. S. King, P. Morel, P. Schaffer, O. O. Sogbein, K. A. Stephenson, *Coord. Chem. Rev.* **2002**, *232*, 173–230.
- [76] A. F. Armstrong, J. F. Valliant, *Dalton Trans.* **2007**, 4240–4251.
- [77] E. Hao, B. Fabre, F. R. Fronczek, M. G. H. Vicente, *Chem. Commun.* **2007**, 4387–4389.
- [78] P. F. H. Schwab, M. D. Levin, J. Michl, *Chem. Rev.* **1999**, *99*, 1863–1934.
- [79] D. A. Brown, H. M. Colquhoun, J. A. Daniels, J. A. H. MacBride, I. R. Stephenson, K. Wade, *J. Mater. Chem.* **1992**, *2*, 793–804.
- [80] H. M. Colquhoun, P. L. Herbertson, K. Wade, I. Baxter, D. J. Williams, *Macromolecules* **1998**, *31*, 1694–1696.
- [81] E. Hao, B. Fabre, F. R. Fronczek, M. G. H. Vicente, *Chem. Mater.* **2007**, *19*, 6195–6205.
- [82] O. K. Farha, A. M. Spokoyny, K. L. Mulfort, M. F. Hawthorne, C. A. Mirkin, J. T. Hupp, *J. Am. Chem. Soc.* **2007**, *129*, 12680–12681.
- [83] M. A. Fox, K. Wade, *J. Mater. Chem.* **2002**, *12*, 1301–1306.
- [84] K. Kokado, Y. Chujo, *Macromolecules* **2009**, *42*, 1418–1420.
- [85] K. Kokado, Y. Chujo, *J. Org. Chem.* **2011**, *76*, 316–319.
- [86] K. Kokado, A. Nagai, Y. Chujo, *Tetrahedron Lett.* **2011**, *52*, 293–296.
- [87] M. Tominaga, H. Naito, Y. Morisaki, Y. Chujo, *New J. Chem.* **2014**, *38*, 5686–5690.
- [88] Y.-J. Cho, S.-Y. Kim, M. Cho, W.-S. Han, H.-J. Son, D. W. Cho, S. O. Kang, *Phys. Chem. Chem. Phys.* **2016**, *18*, 9702–9708.
- [89] X. Li, Y. Yin, H. Yan, C. Lu, *Chem. Asian J.* **2017**, *12*, 2207–2210.
- [90] K. Tanaka, K. Nishino, S. Ito, H. Yamane, K. Suenaga, K. Hashimoto, Y. Chujo, *Faraday Discuss.* **2017**, *196*, 31–42.
- [91] S.-Y. Kim, J. D. Lee, Y.-J. Cho, M. R. Son, H.-J. Son, D. W. Cho, S. O. Kang, *Phys. Chem. Chem. Phys.* **2018**, *20*, 17458–17463.
- [92] X. Wu, J. Guo, Y. Quan, W. Jia, D. Jia, Y. Chen, Z. Xie, *J. Mater. Chem. C* **2018**, *6*, 4140–4149.
- [93] H. Yan, Y. Yin, X. Li, S. Yan, C. Lu, *Chem. Asian J.* **2018**, *13*, 3155–3159.
- [94] Y.-C. Duan, Y. Gao, Y. Geng, Y. Wu, G.-G. Shan, L. Zhao, M. Zhang, Z.-M. Su, *J. Mater. Chem. C* **2019**, *7*, 2699–2709.
- [95] R. Huang, H. Liu, K. Liu, G. Wang, Q. Liu, Z. Wang, T. Liu, R. Miao, H. Peng, Y. Fang, *Anal. Chem.* **2019**, *91*, 14451–14457.
- [96] J. Jiao, J.-X. Kang, Y. Ma, Q. Zhao, H. Li, J. Zhang, X. Chen, *Front. Chem.* **2019**, *7*, 768.

- [97] Y. Nie, H. Zhang, J. Miao, Y. Wang, Y. Li, D. Tu, H. Yan, G. Sun, X. Jiang, *Inorg. Chem. Commun.* **2019**, *106*, 1–5.
- [98] X. Wu, J. Guo, Y. Lv, D. Jia, J. Zhao, H. Shan, X. Jin, Y. Ma, *Mater. Chem. Front.* **2020**, *4*, 257–267.
- [99] B. M. Mikhailov, A. Shagova, *Russ. Chem. Bull.* **1972**, *21*, 1187.
- [100] Y. Z. Voloshin, S. Y. Erdyakov, I. G. Makarenko, E. G. Lebed, T. V. Potapova, S. V. Svidlov, Z. A. Starikova, E. V. Pol'shin, M. E. Gurskii, Y. N. Bubnov, *Russ. Chem. Bull.* **2007**, *56*, 1787–1794.
- [101] S. Y. Erdyakov, Y. Z. Voloshin, I. G. Makarenko, E. G. Lebed, T. V. Potapova, A. V. Ignatenko, A. V. Vologzhanina, M. E. Gurskii, Y. N. Bubnov, *Inorg. Chem. Commun.* **2009**, *12*, 135–139.
- [102] S. V. Svidlov, Y. Z. Voloshin, N. S. Yurgina, T. V. Potapova, A. Y. Belyy, I. V. Ananyev, Y. N. Bubnov, *Russ. Chem. Bull.* **2014**, *63*, 2343–2350.
- [103] L. Weber, J. Kahlert, R. Brockhinke, L. Böhling, A. Brockhinke, H.-G. Stammler, B. Neumann, R. A. Harder, M. A. Fox, *Chem. Eur. J.* **2012**, *18*, 8347–8357.
- [104] L. Weber, J. Kahlert, L. Böhling, A. Brockhinke, H.-G. Stammler, B. Neumann, R. A. Harder, P. J. Low, M. A. Fox, *Dalton Trans.* **2013**, *42*, 2266–2281.
- [105] L. Weber, J. Kahlert, R. Brockhinke, L. Böhling, J. Halama, A. Brockhinke, H.-G. Stammler, B. Neumann, C. Nervi, R. A. Harder, M. A. Fox, *Dalton Trans.* **2013**, *42*, 10982–10996.
- [106] J. Kahlert, L. Böhling, A. Brockhinke, H.-G. Stammler, B. Neumann, L. M. Rendina, P. J. Low, L. Weber, M. A. Fox, *Dalton Trans.* **2015**, *44*, 9766–9781.
- [107] S. Yruegas, J. Axtell, K. Kirlikovali, A. Spokoyny, C. D. Martin, *Chem. Commun.* **2019**, *55*, 2892–2895.
- [108] A. Benton, J. D. Watson, S. M. Mansell, G. M. Rosair, A. J. Welch, *J. Organomet. Chem.* **2020**, *907*, 121057.
- [109] Y. Nie, J. Miao, H. Wadeohl, H. Pritzkow, T. Oeser, W. Siebert, *Z. Anorg. Allg. Chem.* **2013**, *639*, 1188–1193.
- [110] J. L. Boone, R. J. Brotherton, L. L. Petterson, *Inorg. Chem.* **1965**, *4*, 910–912.
- [111] H. Wang, J. Zhang, Z. Lin, Z. Xie, *Organometallics* **2016**, *35*, 2579–2582.
- [112] G. Zi, H.-W. Li, Z. Xie, *Organometallics* **2002**, *21*, 3850–3855.
- [113] G. Zi, H.-W. Li, Z. Xie, *Organometallics* **2002**, *21*, 1136–1145.
- [114] Y. Nie, J. Miao, H. Pritzkow, H. Wadeohl, W. Siebert, *J. Organomet. Chem.* **2013**, *747*, 174–177.
- [115] R. Li. Thomas, A. J. Welch, *Polyhedron* **1999**, *18*, 1961.
- [116] B. W. Hutton, F. MacIntosh, D. Ellis, F. Herisse, S. A. Macgregor, D. McKay, V. Petrie-Armstrong, G. M. Rosair, D. S. Perekalin, H. Tricas, A. J. Welch, *Chem. Commun.* **2008**, 5345–5347.
- [117] G. F. Jin, J.-H. Hwang, J.-D. Lee, K.-R. Wee, I.-H. Suh, S. O. Kang, *Chem. Commun.* **2013**, *49*, 9398–9400.
- [118] L. A. Boyd, W. Clegg, R. C. B. Copley, M. G. Davidson, M. A. Fox, T. G. Hibbert, J. A. K. Howard, A. Mackinnon, R. J. Peace, K. Wade, *Dalton Trans.* **2004**, 2786–2799.
- [119] J. M. Oliva, N. L. Allan, P. V. R. Schleyer, C. Viñas, F. Teixidor, *J. Am. Chem. Soc.* **2005**, *127*, 13538–13547.
- [120] J. Li, R. Pang, Z. Li, G. Lai, X.-Q. Xiao, T. Müller, *Angew. Chem. Int. Ed.* **2019**, *58*, 1397–1401, *Angew. Chem.* **2019**, *5*, 1411–1415.
- [121] Y. Wu, J. Zhang, Z. Xie, *Chinese Chem. Lett.* **2019**, *30*, 1530–1532.
- [122] N. Mandal, A. K. Pal, P. Gain, A. Zohaib, A. Datta, *J. Am. Chem. Soc.* **2020**, *142*, 5331–5337.
- [123] J. M. Oliva, L. Serrano-Andrés, D. J. Klein, P. v. R. Schleyer, J. Michl, *Int. J. Photoenergy* **2009**, *2009*, 1–9.
- [124] J. Llop, C. Viñas, J. M. Oliva, F. Teixidor, M. A. Flores, R. Kivekas, R. Sillanpää, *J. Organomet. Chem.* **2002**, *657*, 232–238.
- [125] L. Böhling, A. Brockhinke, J. Kahlert, L. Weber, R. A. Harder, D. S. Yufit, J. A. K. Howard, J. A. H. MacBride, M. A. Fox, *Eur. J. Inorg. Chem.* **2016**, 403–412.
- [126] M. A. Fox, R. J. Peace, W. Clegg, M. R. Elsegood, K. Wade, *Polyhedron* **2009**, *28*, 2359.
- [127] R. Pang, J. Li, Z. Cui, C. Zheng, Z. Li, W. Chen, F. Qi, L. Su, X.-Q. Xiao, *Dalton Trans.* **2019**, *48*, 7242.

Chapter 1

- [128] M. A. Fox, C. Nervi, A. Crivello, A. S. Batsanov, J. A. K. Howard, K. Wade, P. J. Low, *J. Solid State Electrochem.* **2009**, *13*, 1483–1495.
- [129] K. Hosoi, S. Inagi, T. Kubo, T. Fuchigami, *Chem. Commun.* **2011**, *47*, 8632–8634.
- [130] H. Tricas, M. Colon, D. Ellis, S. A. Macgregor, D. McKay, G. M. Rosair, A. J. Welch, I. V. Glukhov, F. Rossi, F. Laschi, P. Zanello, *Dalton Trans.* **2011**, *40*, 4200–4211.
- [131] S. Inagi, K. Hosoi, T. Kubo, N. Shida, T. Fuchigami, *Electrochemistry* **2013**, *81*, 368–370.
- [132] J. R. Miller, A. R. Cook, L. Šimková, L. Pospíšil, J. Ludvík, J. Michl, *J. Phys. Chem. B* **2019**, *123*, 9668–9676.
- [133] M. Keener, C. Hunt, T. G. Carroll, V. Kampel, R. Dobrovetsky, T. W. Hayton, G. Ménard, *Nature* **2020**, *577*, 652–655.
- [134] K. Wade, *J. Chem. Soc.* **1971**, 792–793.
- [135] A. J. Welch, *Chem. Commun.* **2013**, *49*, 3615–3616.
- [136] X. Fu, H.-S. Chan, Z. Xie, *J. Am. Chem. Soc.* **2007**, *129*, 8964–8965.
- [137] J. Zhang, X. Fu, Z. Lin, Z. Xie, *Inorg. Chem.* **2015**, *54*, 1965–1973.
- [138] T. Peymann, C. B. Knobler, M. F. Hawthorne, *Chem. Commun.* **1999**, 2039–2040.
- [139] O. K. Farha, R. L. Julius, M. W. Lee, R. E. Huertas, C. B. Knobler, M. F. Hawthorne, *J. Am. Chem. Soc.* **2005**, *127*, 18243–18251.
- [140] B. T. King, B. C. Noll, A. J. McKinley, J. Michl, *J. Am. Chem. Soc.* **1996**, *118*, 10902–10903.
- [141] J. Kaleta, J. Tarábek, A. Akdag, R. Pohl, J. Michl, *Inorg. Chem.* **2012**, *51*, 10819–10824.
- [142] M. J. Ingleson, M. F. Mahon, A. S. Weller, *Chem. Commun.* **2004**, 2398–2399.
- [143] A. R. Cook, M. Valášek, A. M. Funston, P. Poliakov, J. Michl, J. R. Miller, *J. Phys. Chem. A* **2018**, *122*, 798–810.
- [144] T. D. Getman, C. B. Knobler, M. F. Hawthorne, *J. Am. Chem. Soc.* **1990**, *112*, 4593–4594.
- [145] T. D. Getman, C. B. Knobler, M. F. Hawthorne, *Inorg. Chem.* **1992**, *31*, 101–105.
- [146] K. Chui, H.-W. Li, Z. Xie, *Organometallics* **2000**, *19*, 5447–5453.
- [147] J. Kahlert, H.-G. Stammmer, B. Neumann, R. A. Harder, L. Weber, M. A. Fox, *Angew. Chem. Int. Ed.* **2014**, *53*, 3702–3705; *Angew. Chem.* **2014**, *14*, 3776–3779.
- [148] H. A. Mills, J. Martin, A. L. Rheingold, A. Spokoyny, *J. Am. Chem. Soc.* **2019**, *142*, 4586–4591.
- [149] M. A. Fox, C. Nervi, A. Crivello, P. J. Low, *Chem. Commun.* **2007**, 2372.
- [150] L. I. Zakharkin, *Pure Appl. Chem.* **1972**, *29*, 513–526.
- [151] J. H. Morris, H. J. Gysling, D. Reed, *Chem. Rev.* **1985**, *85*, 51–76.
- [152] K. A. Bilevich, L. I. Zakharkin, O. Y. Okhlobystin, *Russ. Chem. Bull.* **1965**, *14*, 1887.
- [153] K. A. Bilevich, L. I. Zakharkin, O. Y. Okhlobystin, *Russ. Chem. Bull.* **1967**, *16*, 435–437.
- [154] N. C. D. Patel, J. M. Oliva-Enrich, M. A. Fox, *Eur. J. Inorg. Chem.* **2017**, *2017*, 4568–4574.
- [155] F. H. Allen, O. Kennard, D. G. Watson, L. Brammer, A. G. Orpen, R. Taylor, *J. Chem. Soc., Perkin Trans. 2* **1987**, S1.
- [156] M. J. G. Peach, P. Benfield, T. Helgaker, D. J. Tozer, *J. Chem. Phys.* **2008**, *128*, 44118.
- [157] T. Lu, F. Chen, *J. Comput. Chem.* **2012**, *33*, 580–592.
- [158] R. Warratz, G. Peters, F. Studt, R.-H. Römer, F. Tuczek, *Inorg. Chem.* **2006**, *45*, 2531–2542.
- [159] T. Yanai, D. P. Tew, N. C. Handy, *Chem. Phys. Lett.* **2004**, *393*, 51–57.

1.6 Author contributions and agreement

Autor	A1 JK	A2 MH	A3 IK	A4 AF	A5 HB	A6 MF	A7 LJ	A8 TBM	\sum in Prozent
Synthesis and characterization	10%								5% 15%
Electrochemistry and EPR-spectroscopy				5%					5%
Single-crystal structure analysis	9%	1%			5%				15%
Photophysical properties	15%								15%
DFT and TD-DFT calculations	15%								15%
Verfassen der Veröffentlichung	16%		2%	2%					5% 25%
Korrektur der Veröffentlichung					1%	1%	1%	3%	6%
Koordination der Veröffentlichung	2%							2%	4%
Summe	67%	1%	7%	7%	1%	1%	6%	10%	100%

Chapter 1

Bl. Nr. 4, 2010 Seite 37
„Angabe Autorenschaft“
Synthesis and Structure of an o-Carboranyl-Substituted Three-Coordinate Borane Radical Anion“

J. Krebs, M. Hähnel, I. Krummenacher, A. Friedrich, H. Braunschweig, M. Finze, L. Ji, T. B. Marder, *Chem. Eur. J.* 2021, 27, 8159–8167.
DOI: 10.1002/chem.202100938

Die Mitauteoren der in dieser (teil-)kumulativen Dissertation verwendeten Manuskripte sind sowohl über die Nutzung als auch über die angegebenen Eigenanteile informiert und stimmen den zu.

Angabe Autorenschaft: Anwählen Dropdownmenü / Autorenunterschrift oder Angabe Verweis: Kontrollkästchen über Eigenschaften aktivieren!

<p>Autor/in 1 (Johannes Krebs) Hauptautor/in <input type="checkbox"/> Verweis: E-Mail hinterlegt</p> <p>Autor/in 2 (Martin Hähnel) Koautor/in <input type="checkbox"/> Verweis: E-Mail hinterlegt</p> <p>Autor/in 3 (Ivo Krummenacher) Koautor/in <input type="checkbox"/> Verweis: E-Mail hinterlegt</p>	<p>Autor/in 4 (Alexandra Frieden) Koautor/in <input type="checkbox"/> Verweis: E-Mail hinterlegt</p> <p>Autor/in 5 (Holger Braunschweig) Koautor/in <input type="checkbox"/> Verweis: E-Mail hinterlegt</p> <p>Autor/in 6 (Mark Finze) Koautor/in <input checked="" type="checkbox"/> Verweis: E-Mail hinterlegt</p>	<p>Autor/in 7 (Lei Ji) Koautor/in <input type="checkbox"/> Verweis: E-Mail hinterlegt</p> <p>Autor/in 8 (Todd Marder) Korrespondenzautor/in <input type="checkbox"/> Verweis: E-Mail hinterlegt</p> <p>Würzburg, 19.07.2022 (Datum)</p> <p>Prof. Dr. Todd B. Marder</p>
--	---	---

Chapter 1

2. CHAPTER 2

Disclaimer: The synthesis and characterizations of compounds **2.2b** and **2.3b** of the following chapter have been done by Alena Häfner and Sonja Fuchs and will be part of another Thesis. The DFT calculation presented in the “Quantum chemical transition state calculations” were done by Xueying Guo and Prof. Dr. Zhenyang Lin. The cyclic voltammetry experiments were done by Ivo Krummenacher. I do not claim any this work as my own. A detailed overview can be found in “2.6 Author contributions and agreement”.

2.1 Title and Abstract

Backbone controlled LUMO Energy induces intramolecular C–H activation in *ortho*-bis-9-borafluorene-substituted phenylene and *o*-carboranyl compounds leading to novel 9,10-diboraanthracene derivatives

Johannes Krebs,^{a†} Alena Häfner,^{a†} Sonja Fuchs,^a Xueying Guo,^b Dr. Florian Rauch,^a Dr. Antonius Eichhorn,^a Dr. Ivo Krummenacher,^a Dr. Alexandra Friedrich,^a Prof. Dr. Lei Ji,^{a,c*} Prof. Dr. Maik Finze,^a Prof. Dr. Zhenyang Lin,^{b,*} Prof. Dr. Holger Braunschweig,^{a,*} Prof. Dr. Todd B. Marder^{a,*}

^aInstitute for Inorganic Chemistry and Institute for Sustainable Chemistry & Catalysis with Boron, Julius-Maximilians-Universität Würzburg, Am Hubland, 97074 Würzburg, Germany

^bDepartment of Chemistry, Hong Kong University of Science and Technology, Clear Water Bay, Hong Kong

^cFrontiers Science Center for Flexible Electronics, Xi'an Institute of Flexible Electronics (IFE), Northwestern Polytechnical University, 127 West Youyi Road, Xi'an, Shaanxi, P.R. China

Abstract

The choice of backbone linker for two *ortho*-bis-(9-borafluorene)s has a great influence on the LUMO located at the boron centers and therefore the reactivity of the respective compounds. Herein, we report the room temperature rearrangement of 1,2-bis-(9-borafluorenyl)-*ortho*-carborane, $C_2B_{10}H_{10}\text{-}1,2\text{-}[B(C_{12}H_8)]_2$ (**[2.2a]**) featuring *o*-carborane as the inorganic three-dimensional backbone and the synthesis of 1,2-bis-(9-borafluorenyl)-benzene, $C_6H_4\text{-}1,2\text{-}[B(C_{12}H_8)]_2$ (**2.2b**) its phenylene analog. DFT calculations on the transition state for the rearrangement support an intramolecular C–H bond activation process *via* an S_EAr-like mechanism in **[2.2a]**, and predicted that the same rearrangement would take place in **2.2b**, but at elevated temperatures, which indeed proved to be the case. The rearrangement gives access to **2.3a** and **2.3b** as dibora-benzo[a]fluoroanthene isomers, a form of diboron polycyclic aromatic hydrocarbons (PAHs) that had yet to be explored. The isolated compounds **2.2b**, **2.3a** and **2.3b** were fully characterized by NMR, HRMS, cyclic voltammetry (CV), single crystal X-ray diffraction analysis and photophysical measurements, supported by DFT and TD-DFT calculations.

2.2 Introduction

For several decades, 3-coordinate boron, as a carbonium analog, has been of significant interest for use in connected π -systems as a neutral p-doping option. The trigonal planar boron and its perpendicular, vacant p-orbital lead to its use as a strong π -acceptor moiety and as a Lewis acid.^[1-4] Applications include chromophores for biological applications and electrooptical devices,^[5-10] Lewis acids for small molecule activation,^[11-16] and selective small anion sensors.^[17-20]

Specifically, boroles (**2.I**) (Figure 2.1), the isoelectronic BC₄-ring analogs of the antiaromatic cyclopentadiene cation (Cp⁺), have recently generated considerable interest due to their antiaromatic electron configuration and low HOMO-LUMO energy gap that results in unique reactivities as well as photophysical properties.^[21-27] Benzannulated 9-borfluorenes (**2.II**) offer a stabilized version of the otherwise hard to handle boroles, thus facilitating accessibility.^[28-30] Much research has been carried out to investigate the influence of the *exo*-substituent on boron,^[31-32] the fused π -system,^[28, 33] its (anti-)aromaticity,^[34-35] and the boron-centered LUMO energy.

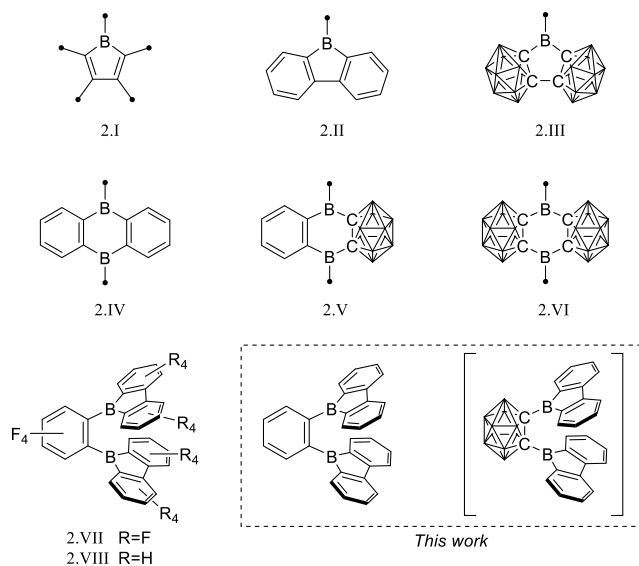


Figure 2.1. Examples of borole, 9-borafluorene, and 9,10-boraanthracene motifs, and their 3-dimensional analogs. The unlabeled cluster vertices represent BH units.

In search of increased Lewis acidity, several groups experimented with exchanging boron-bound phenylene backbone systems for C-C-substituted *ortho*-carboranes, locked in plane by both the C1 and C2 vertices. Martin *et al.* published a three dimensional analog of 9-borafluorene (**2.III**).^[36] In a subsequent study, Welch *et al.* confirmed the strong Lewis acidic behavior of such compounds.^[37] The same trend was observed for the 9,10-diboraanthracene^[38-39] motif (**2.IV**), when phenyl groups were replaced by the carborane moiety (**2.V**)^[40] resulting in Lewis superacids that show very low reduction potentials (**2.VI**).^[41]

Ortho-carborane can act as a multifunctional acceptor in charge transfer (CT) processes when connected to π -systems.^[42-45] Additionally, carborane itself has been shown to lower the LUMO energy of boranes, especially when the p_z orbital on boron aligns with the C1-C2 σ^* -anti-bonding orbital.^[46-49] A similar effect can be observed when the carborane is attached to boron via a conjugated π -system.^[48]

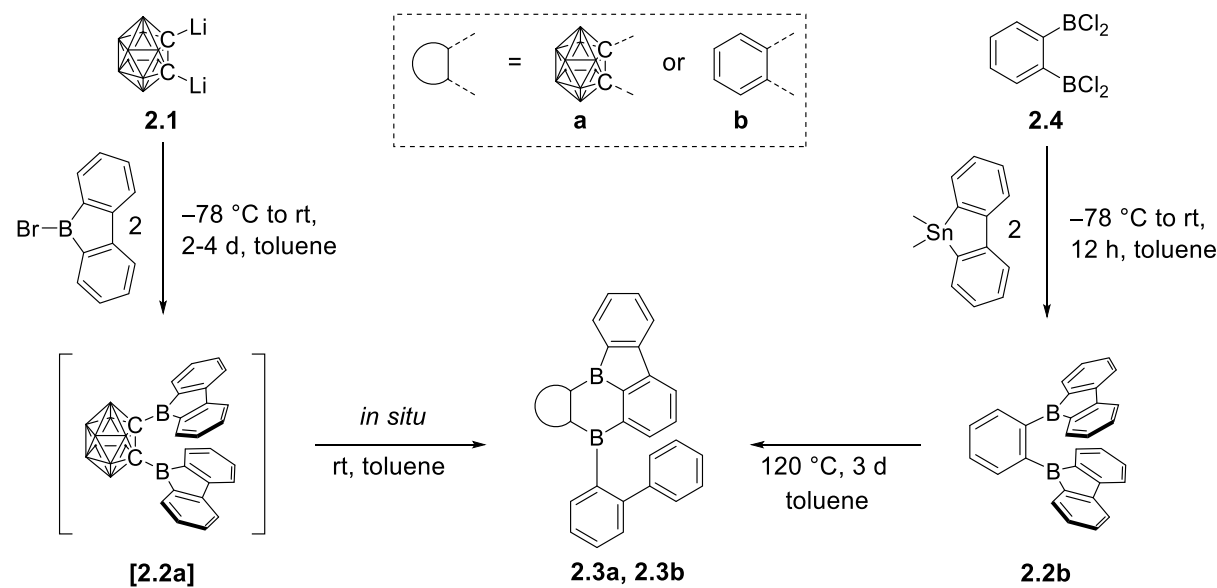
It is well-known that C-bound *ortho*-1,2-C₂B₁₀H₁₁ exerts a strong inductive electron withdrawing effect.^[50-51]

A focus on boron centers and how they interact with a proximal substituent has been prevalent in the literature starting from classical triaryl boranes and their use as bidentate Lewis acid initiators in olefin polymerization chemistry.^[52-55] In this pursuit, a perfluorinated bis-9-borafluorene (**2.VII**) further increased the Lewis acidity.^[56] Later, one-electron bonds were studied in naphthyl-, diphenyl- or methyl- bridged bis-9-borafluorenes.^[57-60]

Similar to boroles,^[22] 9-borafluorenes are known to undergo ring expansion reactions *via* insertions of heteroatoms,^[61-67] alkynes,^[68-70] and alkenes^[49] into one of the endocyclic B-C bonds. Ring opening reactions with moisture or protic solvents such as alcohols were reported for **2.VII** and the generic boroles.^[71-72] The ring-opening polymerization of 9-H-9-borafluorenes is well understood as a progression from its preferred *in situ* dimer formation to oligomeric structures utilizing the loss of antiaromaticity and ring strain as the driving force.^[73-76] In the case of the tetraarylborate anion, 9-mes₂-9-borafluorene (mes = mesityl), and its analogs, ring expansion via benzylic C-H activation of one *ortho*-methyl group on the mesityl moiety was observed when irradiated at 300 nm.^[77]

2.3 Results and Discussion

2.3.1 Synthesis and observation



Scheme 2.1. Synthesis of **2.2b**, **2.3a** and **2.3b**. The unlabeled cluster vertices represent BH units.

O-carborane has a strong stabilizing effect on the LUMO of an exo C-bound boron moiety.^[46-47, 49] With this in mind, we planned the synthesis of **[2.2a]**. We expected a geometry that would align the exo B p_z-orbitals and the C1-C2 σ*-anti-bonding *o*-carborane orbital, maximizing the effect on photophysical and electrochemical properties of 9-borafluorene. Furthermore, we planned to compare our results with those of the previously reported, fully fluorinated and backbone fluorinated bis-9-borafluorenes **2.VII** and **2.VIII**.^[56, 78]

Thus, dilithio *o*-carborane was reacted with two equivalents of 9-bromo-9-borafluorene (Scheme 2.1). To our surprise, instead of **[2.2a]**, a bright orange solid **2.3a** was isolated. Compound **2.3a** was characterized by ^1H , ^{11}B and $^{13}\text{C}\{^1\text{H}\}$ NMR spectroscopy, HRMS, and single crystal X-ray diffraction. The latter revealed that one 9-borafluorene unit is connected to the second exo boron center resulting from a C–H bond activation, forming a phenyl-*o*-carborane– B_2C_4 -subunit similar to that in **V**. The other 9-borafluorene unit undergoes a ring opening process resulting in an *ortho*-biphenyl substituent (Figure 2.3). At this point, we suspected a reaction cascade in which **[2.2a]** formed and rearranged yielding **2.3a** as a result of the reaction conditions. The low yield of 13% suggests incomplete conversion or the loss of ionic side products during filtration of the toluene suspension. Compound **2.3a** is prone to nucleophilic attack and was handled strictly under an inert atmosphere.

When **2.3a** was crystallized from toluene *via* hexane diffusion in the presence of a small amount of THF, the mono THF adduct **2.3a·THF** was isolated as single crystals suitable for X-ray diffraction (Figure 2.2). This structure suggests that B1 of the five-membered BC_4 -ring is more Lewis acidic than B2. This was confirmed by subsequent DFT-calculations, that show a larger distribution of the HOMO on B1 compared to B2, *vide infra*. The boron carbon bond lengths in **2.3a·THF** are in the expected range for a 4-coordinate, sp^3 -hybridized boron. The loss of conjugation in the π -system result in colorless crystals.

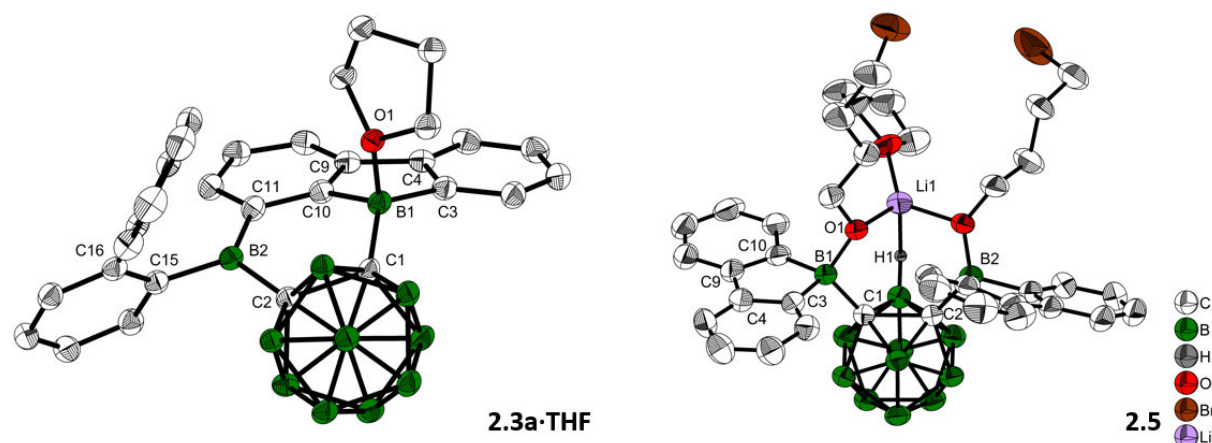
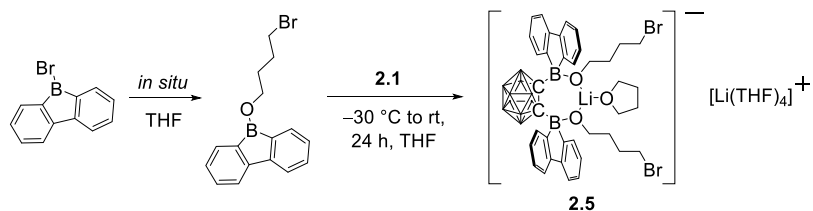


Figure 2.2. Solid state molecular structure of **2.3a·THF** and **2.5** from single-crystal X-ray diffraction at 100 K. Atomic displacement ellipsoids are drawn at the 50% probability level and solvent molecules and hydrogen atoms are omitted for clarity. For **5**, the second cation $[\text{Li}(\text{THF})_4]^+$, the minor parts of disordered THF and one of the alkyl groups are omitted for clarity. Selected bond lengths (\AA), bond angles (deg), and dihedral angles (deg): For **2.3a·THF**: C1–C2 1.717(2), B1–O1 1.624(3), B1–C1 1.624(3), B2–C2 1.603(3); B1–C1–C2–B2 0.9(2). For **2.5**: C1–C2 1.806(5), B1–C1 1.680(6), B2–C2 1.701(6), H1–Li1 2.15(4); B1–C1–C2–B2 1.1(5).

In our initial reactions, we used *n*BuLi (2.1 eq.) for *in situ* lithiation of the *o*-carborane followed by reaction with the 9-bromo-9-borafluorene at elevated temperatures. To reduce the likelihood of competing reactions, due to the high temperatures and the use of excess base, in subsequent studies dilithio *o*-carborane was isolated prior to use. From experience, we know that substitution at the second *o*-carborane carbon atom at room temperature requires extended reaction times. The observation of the rearrangement, even at room temperature, led us to investigate the transition state using quantum chemical calculations (*vide infra*). Simultaneously, to confirm the initial formation of **[2.2a]**, the reaction was monitored at lower temperatures via NMR spectroscopy. However, due to the

low solubility of the dilithium salt in toluene at or below room temperature, the results were inconclusive. Running the reaction in ether solvents, especially THF, increased the solubility of the dilithium salt significantly, but 9-bromo-9-borafluorene is known to cleave ethers^[79-80] which, in this case, led to the formation of compound **2.5**. Crystals of **2.5** were isolated and characterized using single crystal X-ray diffraction (Figure 2.2).

The structure of **2.5** shows that two equivalents of 9-bromo-9-borafluorene had already reacted with THF via ring opening to form 9-(4-bromobutoxy)-9-borafluorene, which subsequently reacted with the dilithio *o*-carborane generating two 4-coordinate boron centers without elimination of the alkoxy groups (Scheme 2.2.).



Scheme 2.2. Formation of compound **2.5**. The unlabeled cluster vertices represent BH units.

The resulting dianionic structure coordinates to one of the corresponding lithium cations via the two oxygen atoms and an hydridic cluster B-H (H1–Li1 2.15(4) Å). The tetra coordination of the boron centers B1 and B2 in compound **2.5** inhibits a subsequent rearrangement. The formation of this bis-*ortho*-substituted carborane constitutes important evidence for the *in situ* formation of **[2.2a]**. From these experiments we conclude that the rate of the rearrangement reaction is higher than the rate at which **[2.2a]** is formed.

Quantum chemical calculations suggested a higher activation barrier for the rearrangement of the analog of **[2.2a]** containing a phenylene backbone (**2.2b**) as will be discussed in detail later (*vide infra*). As a result, we synthesized **2.2b**, the electron rich analog of its fluorinated predecessors **2.VII** and **2.VIII**. Transmetallation of a stannafluorene with the known^[81] bis-(dichloroboryl)benzene (**2.4**) (Scheme 2.1) gave a bright yellow solid in an excellent yield of 79%. It is noteworthy that the product formation does not depend on the stoichiometry, as observed in an equimolar reaction. The compound was handled under an inert atmosphere and decomposes if vacuum dried from a CH₂Cl₂ solution. The ¹¹B NMR spectrum shows a broad resonance at 67.0 ppm, typical of 9-borafluorenes.^[29] Furthermore, ¹H and ¹³C{¹H} NMR spectroscopy, along with HRMS and crystal structure analysis, confirm the structure of **2.2b** (Figure 2.3).

Unfortunately, a selective route to the carborane analogue of 1,2-(BCl₂)₂-1,2-C₂B₁₀H₁₀, has not been reported. Reaction of dilithio *o*-carborane with trihaloboranes led to mixtures containing higher order substitutions.^[41] As a result, we did not attempt this route for the synthesis of **[2.2a]**.

Confirming the quantum chemical prediction, heating compound **2.2b** for three days at 120 °C in toluene led to the formation of a bright orange solid with complete conversion, according to ¹H NMR spectroscopy. Without the need for further purification, compound **2.3b** was characterized by ¹H and ¹³C{¹H} NMR spectroscopy, HRMS and single crystal X-ray diffraction. The broad ¹¹B NMR signal of **2.3b** is shifted upfield slightly from that of **2.2b** to 63.9 ppm, and only one signal was detected despite the lower symmetry. The rearrangement of **2.2b** is identical, in principle, to the one observed for **[2.2a]**,

in this case resulting in a diboraanthracene-like subunit. UV irradiation for 4 h in a C₆H₆ solution at room temperature did not lead to rearrangement.

2.3.2 Molecular geometries before and after the rearrangement

Solid state molecular structures of **2.2b**, **2.3a** and **2.3b** are shown in Figure 2.3. The optimized structures of **2.2b**, **2.3a** and **2.3b** at the ωB97X-D/6-31G(d,p) level of theory in the gas phase fit the crystal structures nicely (Table 2.1). As compound **[2.2a]** could not be isolated, the DFT-optimized structure was used for comparisons (Figure 2.3).

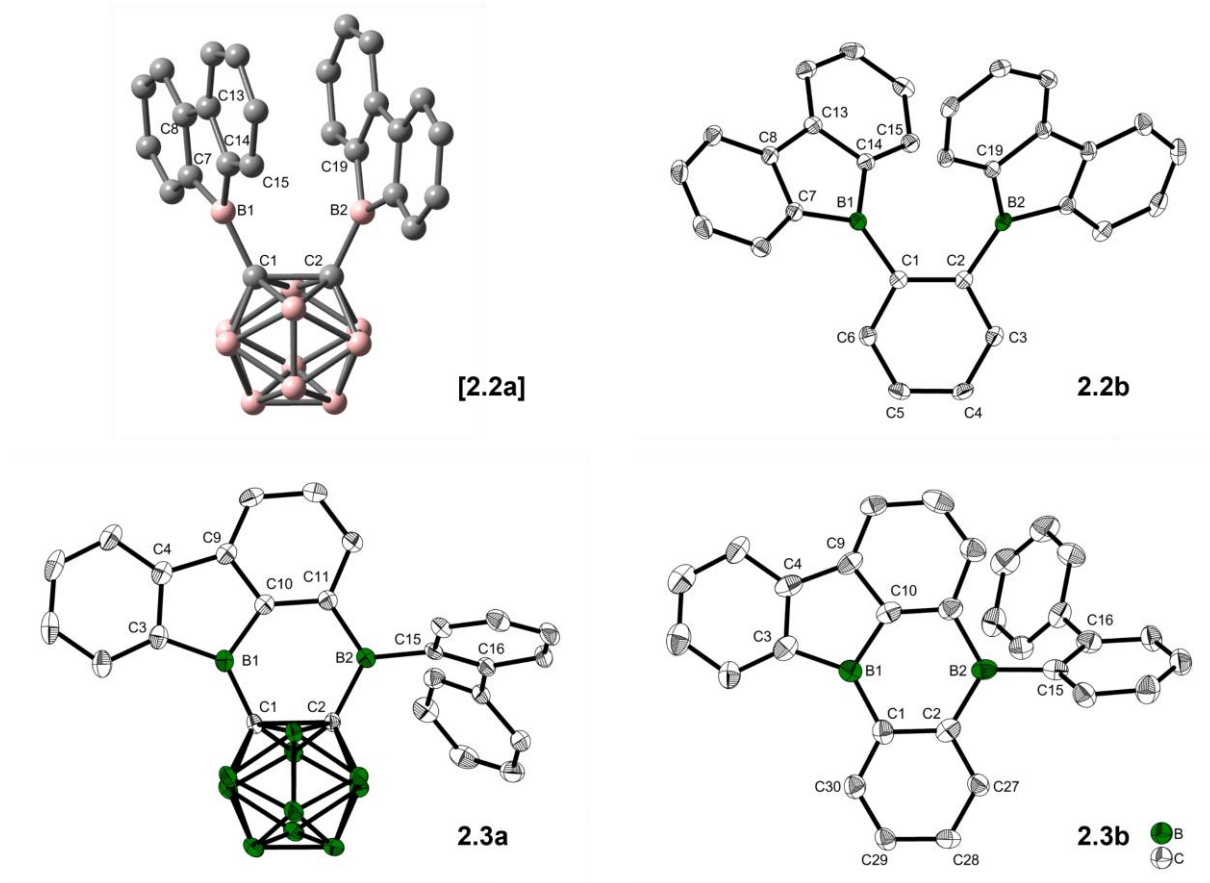


Figure 2.3. Optimized structure of **[2.2a]** at the ωB97X-D/6-31G(d,p) level of theory in the gas phase (B = red, C = grey). Solid-state molecular structures of **2.2b**, **2.3a** and **2.3b** from single-crystal X-ray diffraction at 100 K. Atomic displacement ellipsoids are drawn at the 50% probability level and hydrogen atoms are omitted for clarity. For **2.3b**, only one of four symmetry-independent molecules is shown, and solvent molecules are omitted for clarity.

Crystals suitable for X-ray analysis of **2.2b** were grown from toluene. Although not crystallographically identical, both 9-borafluorenes in the molecule have similar relevant structural parameters within the range of error. The 3-coordinate boron atoms B1 and B2 each form one B–C bond (B1–C1 1.554(2) Å and B2–C2 1.551(2) Å) to the phenylene-backbone, which may be slightly shorter than those in 9-phenyl-9-borafluorene (1.573(9)/1.58(1) Å), although the large errors in the latter values do not allow a definitive conclusion.^[82] In the solid state, the 9-borafluorenes and the backbone planes are twisted at dihedral angles of 43.6(2)° (C14–B1–C1–C2) and 39.2(2)° (C1–C2–B2–C19), respectively, while the

dihedral angle between both 9-borafluorene substituents ($B_1-C_1-C_2-B_2$) is $13.2(2)^\circ$. The two 9-borafluorene substituents repel each other slightly, resulting in a $B_1-C_1-C_2$ angle of $124.9(1)^\circ$ and $B_2-C_2-C_1 = 123.6(1)^\circ$. A deformation is visible in the phenylene backbone with the C_1-C_2 bond ($1.426(2)$ Å) being the longest and C_4-C_5 ($1.386(2)$ Å), on the opposite side of the phenylene ring, being the shortest bond. The $B\cdots B$ distance in **2b** ($3.186(2)$ Å) is longer in comparison to the unfused perfluoroaryldiborane $C_6F_4-1,2-[B(C_6F_5)_2]_2$ (3.138 Å)^[53] and its perfluoro-bis-9-borafluorenyl analog $C_6F_4-1,2-[B(C_{12}F_8)]_2$ (**2.VII**) (3.056 Å).^[56] The distance between atoms B_2 and C_{15} that are involved in the bond formation towards the rearranged compound **2.3b** is $3.252(2)$ Å.

Table 2.1. Selected bond lengths [Å], distances [Å], and angles [°] of **2.2a**, **2.2b**, **2.3a** and **2.3b** in the crystal structures and optimized structures at the ω B97X-D/6-31G(d,p) level of theory.

	[2.2a] calc. ^[a]	2.2b crystal	2.2b calc. ^[a]		2.3a crystal	2.3a calc.	2.3b crystal ^[c]	2.3b calc.
C_1-C_2	1.674	1.426(2)	1.420	C_1-C_2	1.718(2)	1.693	1.43(2) ^[c]	1.429
$C_1-C_6 /$ C_2-C_3	-	1.402(2) 1.405(2)	1.402	$B_1-C_1-C_2$	114.4(1)	114.3	117.2(5) ^[c]	117.2
$C_5-C_6 /$ C_3-C_4	-	1.388(2) 1.389(2)	1.393	$B_2-C_2-C_1$	118.5(1)	118.8	122.9(5) ^[c]	122.7
C_4-C_5	-	1.386(2)	1.393	$C_1-B_1-C_{10}$ $C_{10}-B_1-C_3$ $C_3-B_1-C_1$	119.5(1) 105.5(1) 135.0(1)	119.9 105.1 134.9	117.9(5) ^[c] 103.5(5) ^[c] 138.6(5) ^[c]	118.5 103.3 138.2
B_1-C_1 ^[b]	1.600	1.554(2) 1.551(2)	1.556	$\Sigma C-B_1-C$	360.0(3)	359.9	360.0(15) ^[c]	360.0
$B_1\cdots B_2$	3.054	3.186(2)	3.083	$\Sigma C-B_2-C$	358.8(3)	359.4	360.0(15) ^[c]	359.9
$B_2\cdots C_{15}$ ^[b]	3.487	3.252(2) 3.354(2)	3.231	$B_1-C_1-C_2-B_2$	2.6(2)	3.6	3.0(7) ^[c]	2.7
$C_2-C_1-B_1,$ $C_1-C_2-B_2$	115.6	124.9(1) 123.6(1)	122.1	$C_2-B_2-C_{15}-C_{16}$	82.4(1)	79.4	59.3(6) ^[c]	63.3
$B_1-C_1-C_2-B_2$	6.3	13.2(2)	9.4					
$C_2-C_1-B_1-C_{14}$ ^[b]	59.5	43.6(1) 39.2(1)	43.5					

[a] The optimized structures of **2.2a** and **2.2b** have a C_2 axis and therefore equivalent 9-borafluorene moieties.

[b] Values are given for both crystallographically independent 9-borafluorene moieties for the crystal structures of **2.2b**.

[c] Four symmetry-independent molecules are present in the crystal structure of **2.3b** and the mean value are shown here. The separate values can be found in the Supporting Information.

Crystals suitable for X-ray analysis of **2.3a** were grown from toluene *via* hexane diffusion. The B_1C_3 plane of this rearranged product, while not perfectly trigonal ($C_1-B_1-C_{10} = 119.5(1)^\circ$, $C_{10}-B_1-C_3 = 105.5(1)^\circ$, $C_3-B_1-C_1 = 135.0(1)^\circ$), is planar with the sum of angles being $360.0(1)^\circ$. All of the $C-B_2-C$ angles are close to 120° , with the sum being $358.8(1)^\circ$ in the solid state, only slightly deviating from planarity. In comparison to the carborane-phenyl analog of 9,10-diboraanthracene **2.V** ($C-C = 1.675(7)$ Å)^[40] and the carborane-carborane analog of 9,10-diboraanthracene **2.VI** ($1.667(3)$ Å)^[41], the C_1-C_2 carborane bond in **2.3a** is significantly elongated ($1.718(2)$ Å). The extended 9-borafluorene system is nearly planar with internal dihedral angles close to 0° or 180° ($B_1-C_1-C_2-B_2 = 2.6(2)^\circ$, $C_2-C_1-B_1-C_3 = 176.1(1)^\circ$). The *ortho*-biphenyl group is rotated close to a perpendicular orientation ($C_2-B_2-C_{15}-C_{16} = 82.4(1)^\circ$) with respect to the boron-containing π -system.

Chapter 2

Crystals suitable for X-ray analysis of **2.3b** were grown from toluene *via* pentane diffusion. The unit cell contains four symmetry-independent molecules. Due to a low bond precision and a large bond length variation between symmetry-independent molecules (see Table 5.2.3 in the Supporting Information) a detailed discussion of experimental B–C and C–C bond length differences is not possible. However, the bond angles and dihedrals are of sufficient accuracy and vary only slightly between the symmetry-independent molecules, which allows a thorough discussion. Similar to **2.3a**, the angles surrounding the boron center B1 show a strong distortion from perfect trigonal geometry ($C10\text{--}B1\text{--}C3 = 102.4(5) - 104.0(5)^\circ$, $C1\text{--}B1\text{--}C10 = 116.9(5) - 118.8(5)^\circ$, $C1\text{--}B1\text{--}C3 = (137.5(5) - 140.6(5)^\circ)$ with the sum of angles being $360.0(15)^\circ$). The second boron center B2 is perfectly trigonal planar with each C–B–C angle 120° within 3 esd's and the sum of angles being $360.0(15)^\circ$. The former backbone shows a similar average bond length for C1–C2 (ca. $1.43(2)$ Å) as in compound **2.2b** ($1.426(2)$ Å). The biphenyl group bonded to B2 is rotated by $58.2(6) - 60.7(6)^\circ$ with respect to the boron containing π -system in all four symmetry-independent molecules. The crystal structure of **2.3b** has a π -system with the structure of a di-borabenz[a]fluoroanthene.

A comparison of the optimized starting geometries at the ω B97X-D/6-31G(d,p) level of theory (Table 2.1) reveals some relevant differences between **[2.2a]** and **2.2b**, that can be seen in the C(1)–C(2) bond lengths of 1.674 Å and 1.420 Å, respectively, and in the B(1)–C(1) bond lengths, of 1.600 Å and 1.556 Å, respectively. The differences are a direct result of the different backbones and are in their expected range. In general, this should result in a greater distance between the 9-borafluorenyl substituents for the *o*-carborane backbone. However, an attraction in **[2.2a]** between the two moieties can be observed in the B1–C1–C2 angle (115.6°), while signs of steric repulsion (122.1°), consistent with the crystal structure, can be observed in **2.2b**, compared to the ideal 120° angle expected for both phenylene and carboranyl backbones. Both compounds show similar B1–B2 distances (3.054 Å (**[2.2a]**) and 3.083 Å (**2.2b**)) in their optimized geometries which, for **2.2b**, is a significant deviation from the solid-state structure ($3.186(2)$ Å). This could be a result packing effects in the crystalline state and the calculation being in the gas phase. The dihedral angles between the backbone C–C bond and the 9-borafluorene described by C(2)–C(1)–B(1)–C(14) are relevant for possible interactions with the backbone. For **2.2b**, a twist of 43.5° is observed, while **[2.2a]**, shows a larger angle of 59.5° . The difference in these angles also results in a longer B2···C15 distance for **[2.2a]** (3.487 Å) compared to **2.2b** (3.231 Å), where the new bond is formed in the rearrangement.

2.3.3 Quantum chemical transition state calculations

DFT calculations were carried out using different DFT functionals (ω B97X-D, M062X, and B3LYP-D3(BJ)) to provide further insight into the rearrangement processes of **[2.2a]** and **2.2b** with a focus on the differences observed for the carboranyl and phenyl backbones. More information on the calculated geometries can be found in the Supporting Information (Tables 5.2.2 – 5.2.4).

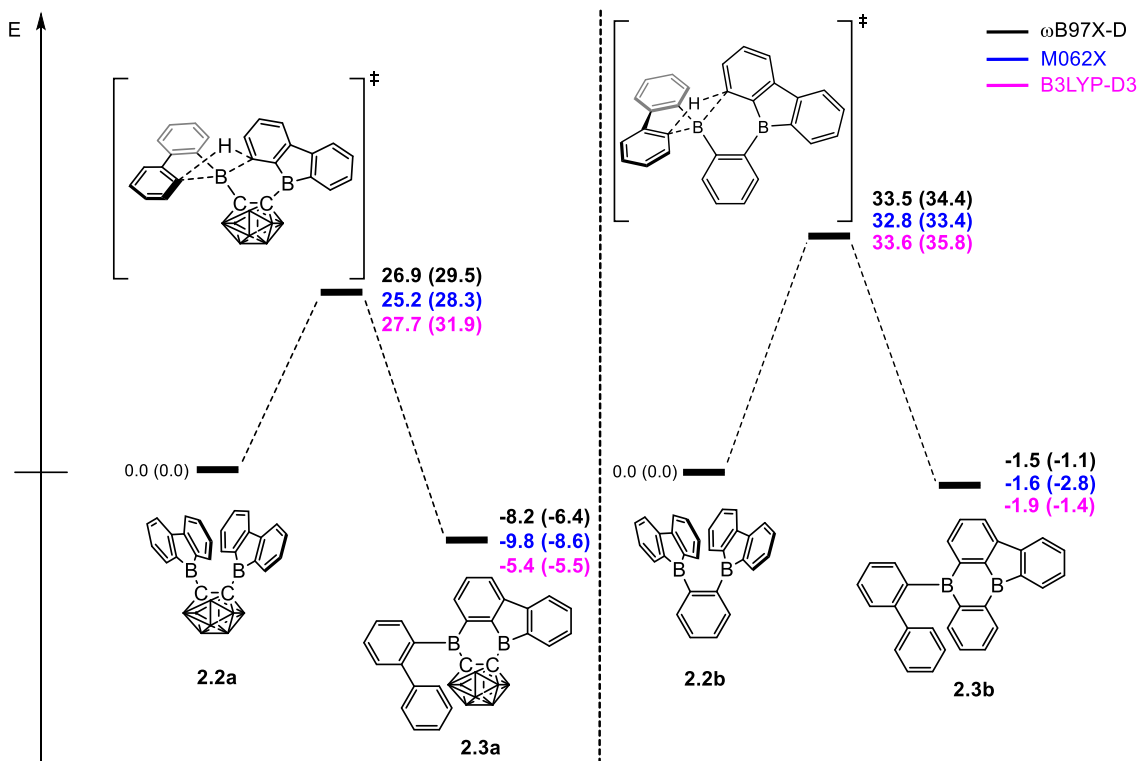


Figure 2.4. Energy profiles calculated for the re-arrangement processes for **[2.2a]** (left) and **2.2b** (right). The relative Gibbs free energies and electronic energies (in parenthesis) are given in kcal/mol. The unlabeled cluster vertices represent BH units.

Figure 2.4 shows that the resulting energy profiles calculated with these functionals are very similar. In both cases, the rearrangement follows the path of an electrophilic aromatic substitution. The rearrangement starts with the bis-9-borafluorenyl *ortho*-substituted species which offer boron-centered LUMOs and aromatic electron density in proximity. The calculated rearrangement transition state structures involve C–H bond activation *via* an S_EAr-like mechanism, resembling a concerted electrophilic aromatic substitution process having a Wheland-like transition state (Figures 2.4 and 2.5). After the proton shift and the associated BC₄-ring opening, the arene σ -complex evolves to form a new planar system having a biphenyl substituent.

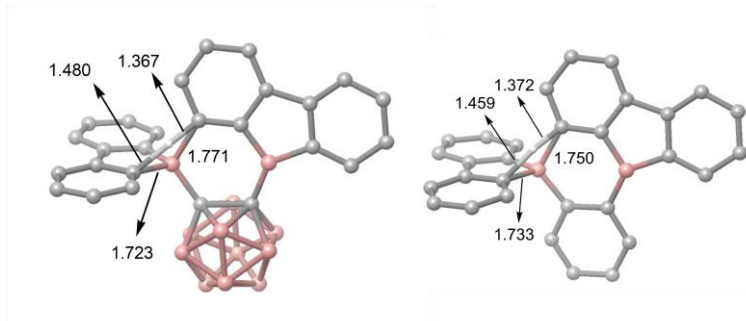


Figure 2.5. The two calculated transition state structures at the ω B97X-D level of theory for the rearrangement processes shown in Figure 2.4 involving C–H bond activation. Bond lengths are shown in Å.

The energy barriers calculated for the rearrangement of **[2.2a]** are within the range 25.2–27.7 kcal/mol, a result that is reasonable considering a reaction time of 48 h or more. The activation barrier for the rearrangement process of **2.2b** is ca. 7 kcal/mol higher, confirming our experimental observation that **2.2b** is kinetically much more stable than **[2.2a]**. Furthermore, the calculations correctly predicted the rearrangement at elevated temperatures. The significantly lower barrier for the rearrangement of **[2.2a]** is associated with a relatively higher exothermicity of the rearrangement, consistent with the notion that a C-connected *o*-carboranyl group is highly electron-withdrawing, which facilitates the C–H bond activation process. This effect can be seen in the stabilized LUMO energy of **[2.2a]** (Figure 2.6). The small energy difference between **2.2b** and **2.3b** suggests a possible equilibrium that was not observed experimentally. In contrast, **2.3a** is thermodynamically significantly more stable than **[2.2a]**.

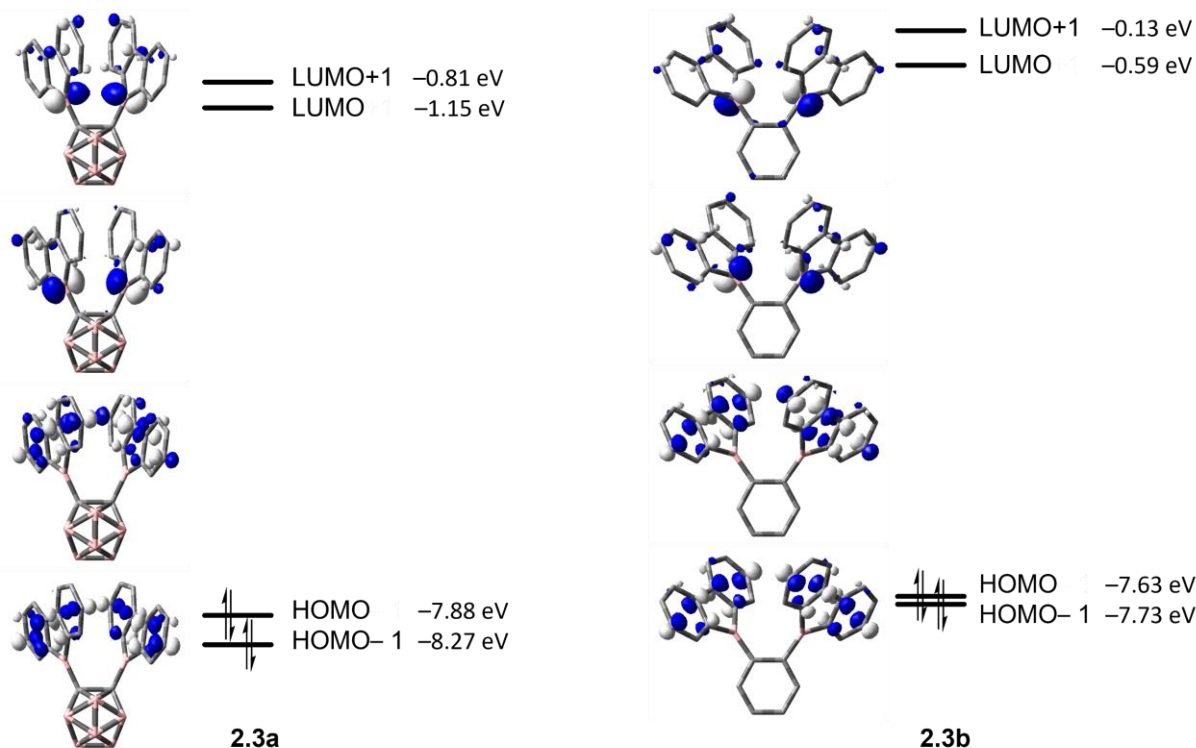


Figure 2.6. HOMO–1, HOMO, LUMO and LUMO+1 energies calculated at the ω B97X-D/6-31G(d,p) level of theory for **[2.2a]** and **2.2b** (isovalue: $\pm 0.06 [e \text{ } \text{a}_0^{-3}]^{1/2}$).

2.3.4 Photophysical properties and TD-DFT calculations

The photophysical properties of compounds **2.2b**, **2.3a** and **2.3b** were investigated, and observations rationalized *via* complementary DFT and TD-DFT calculations. The photophysical data is summarized in Table 2.2. The ground state structures were first optimized in gas phase starting from their crystal structures at the B3LYP/6-31+G(d,p) level of theory. As previous studies have shown the need for range-separated hybrid functionals in CT transitions, TD-DFT calculations were done CAM-B3LYP functionals with and without a hexane solvent spheres (Supporting Information).^[31, 83-84] We determined the degree of CT character by calculating the orbital overlap parameter Λ for the transitions (Table 2.3 and 5.2 Supporting Information Chapter 2).

Table 2.2. Photophysical data of compounds **2.2b**, **2.3a** and **2.3b**.

Compound	Solvent	λ_{abs} [nm]	λ_{em} [nm] ^[a]	apparent Stokes shift [cm ⁻¹]	τ [ns]	Φ
2.2b	solid	440 ^[b]	540	4200	125.8	0.49
2.3a	hexane	438, 377, ^[c] 323, 299	568	520	100 ^[d]	0.13 ^[d]
	toluene	450, 372, ^[c] 325, 295	592	5300	50 ^[d]	0.12 ^[d]
2.3b	CH ₂ Cl ₂	451, ^[c] 327, 301	596	5400	38.5 ^[d]	0.12 ^[d]
	solid	499 ^[b]	604	3500	44	0.19
	hexane	450, 380, 350, 320,	548, 580	4000, 5000	84.4 (86.2%) ^[d] 128.7 (13.8%) ^[d]	0.07 ^[d]
	toluene	460, 380, 352, 324,	598	5000	48.5 (86.2%) ^[d] 132.4 (13.8%) ^[d]	0.07 ^[d]
	solid	450, ^[b] 500 ^[b, c]	583	5100, 2800	33.1 (19.2%) 85.8 (79.4%)	0.11

[a] Excited at the respective $\lambda_{\text{abs},\text{max}}$ of the S₁ ← S₀ transition. [b] Calculated from excitation spectrum (see Supporting Information). [c] Approximate values due to the lack of clear maximum. [d] Low reliability due to visible decomposition.

Compound **2.2b** showed rapid decomposition in solution, so providing reliable data was only possible from solid-state experiments. The excitation and emission spectra of **2.2b**, **2.3a** and **2.3b** are depicted in Figure 2.7. For **2.2b**, we observe a broad absorption reaching 500 nm with its maximum at 440 nm and an emission maximum at 540 nm. Both emission and excitation maxima are in the range of previously reported non-donor-functionalized 9-borafluorene derivatives ($\lambda_{\text{abs}} \approx 400$ nm, $\lambda_{\text{em}} \approx 510$ nm).^[28] Similar to other 9-borafluorene compounds,^[31-33, 85-86] **2.2b** exhibits a very long fluorescence lifetime ($\tau_F = 126$ ns), suggesting a small transition dipole moment. The quantum yield ($\Phi_F = 0.49$) is comparatively high for borafluorenes, and is the highest quantum yield reported for a borafluorenes in the solid state.

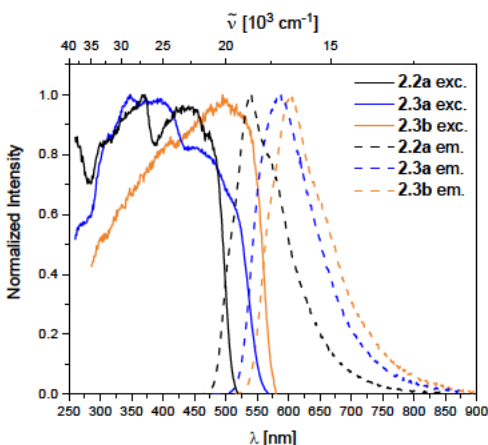


Figure 2.7. Normalized excitation and emission spectra of the compounds 2.2a (black), 2.3a (blue), and 2.3b (orange) in the solid state.

In comparison to our previous results,^[31] this suggests a weakly allowed localized excitation (LE) transition on the borafluorene moieties. This is supported by TD-DFT calculations carried out at the CAM-B3LYP/6-31+G(d,p) level of theory in the gas phase. The lowest energy $S_1 \leftarrow S_0$ and $S_2 \leftarrow S_0$ transitions exhibit very low oscillator strengths and can be classified as weakly allowed transitions (Table 2.3). HOMO and HOMO-1, as well as LUMO and LUMO+1 are situated on the borafluorene moieties with only minor contributions from the phenylene moiety (Figure 2.9).

Photophysical properties of 2.3a and 2.3b in the solid state show a significant resemblance to those of 2.2b, with a broad excitation to ca. 500 nm and emissions at 604 and 583 nm for 2.3a and 2.3b, respectively. Unlike 2.2b, the rearranged compounds exhibit significantly lower quantum yields of $\Phi_F = 0.19$ and 0.11 for 2.3a and 2.3b, respectively.

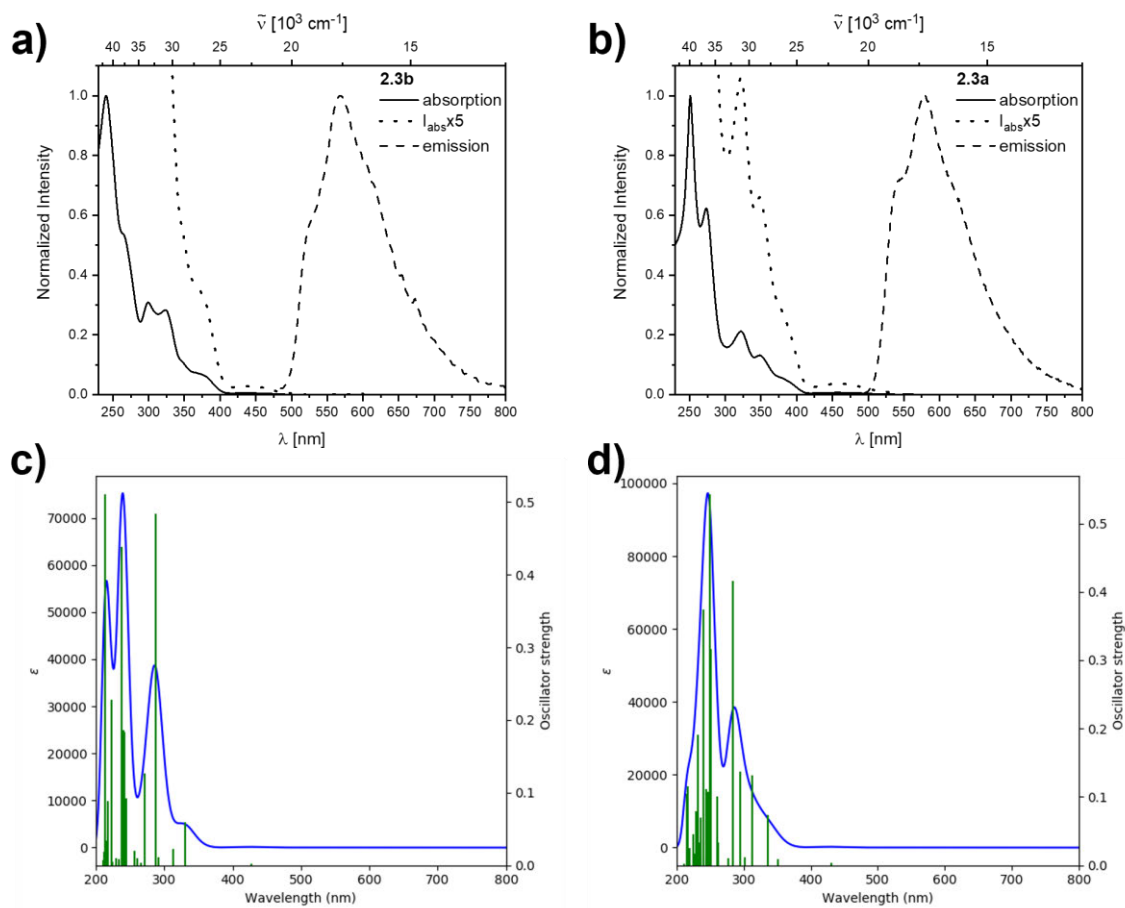


Figure 2.8. Normalized absorption and emission spectra of the rearranged compounds **2.3a** (a)) and **2.3b** (b)) in hexane. The dotted lines are blowups shown to visualize the lowest energy transitions. Simulated spectra calculated at the CAM-B3LYP/6-31+G(d,p) level of theory in a hexane solvent model for **2.3a** (c)) and **2.3b** (d)).

Similar to, but slower than for compound **2.2b**, rapid decomposition of compounds **2.3a** and **2.3b** was observed, and extinction coefficients could not be determined reliably. The photophysical properties of the rearranged compounds **2.3a** and **2.3b** in solution retain their 9-borafluorene-like transitions (Figure 2.8). Both compounds show very weak transitions in hexane at 438 and 450 nm, respectively. TD-DFT calculations at the CAM-B3LYP/6-31+G(d,p) confirm weakly allowed transitions in this energy region with low transition dipole moments and, generally, give a good fit to the experimental spectra (Figure 2.8).

For **2.3a** and **2.3b**, the lowest energy transition has a strong resemblance to that in typical 9-borafluorenes in the orbital distribution across the π -system (Figure 2.9 and Table 2.3). With the resemblance to benzo[a]fluoranthene, the additional boron center and the resulting loss in symmetry, the rearranged compounds **2.3a** and **2.3b** show slightly higher transition dipole moments and an increase in CT character ($\Delta \leq 0.6$). Interestingly, the calculated 9-borafluorene-like HOMO appears as HOMO-1 in the carborane-containing compound **2.3a**. Thus in **2.3a**, there is a significant stabilization of the 9-borafluorene-like HOMO-1 due to the strong -I inductive effect of the *o*-carborane.^[50-51] This inductive effect is known to stabilize connected 3-coordinate boranes and adjacent π -systems.^[46, 87-90] This stabilization can also be observed for the LUMO and LUMO+1, but is weaker for the biphenyl HOMO due to its unfavorable out of plane rotation. For **2.3b**, the higher energy of the comparable

orbital (HOMO) can also be explained by the increase in PAH-HOMO energies with increasing number of aromatic carbon atoms in the system.^[91-94]

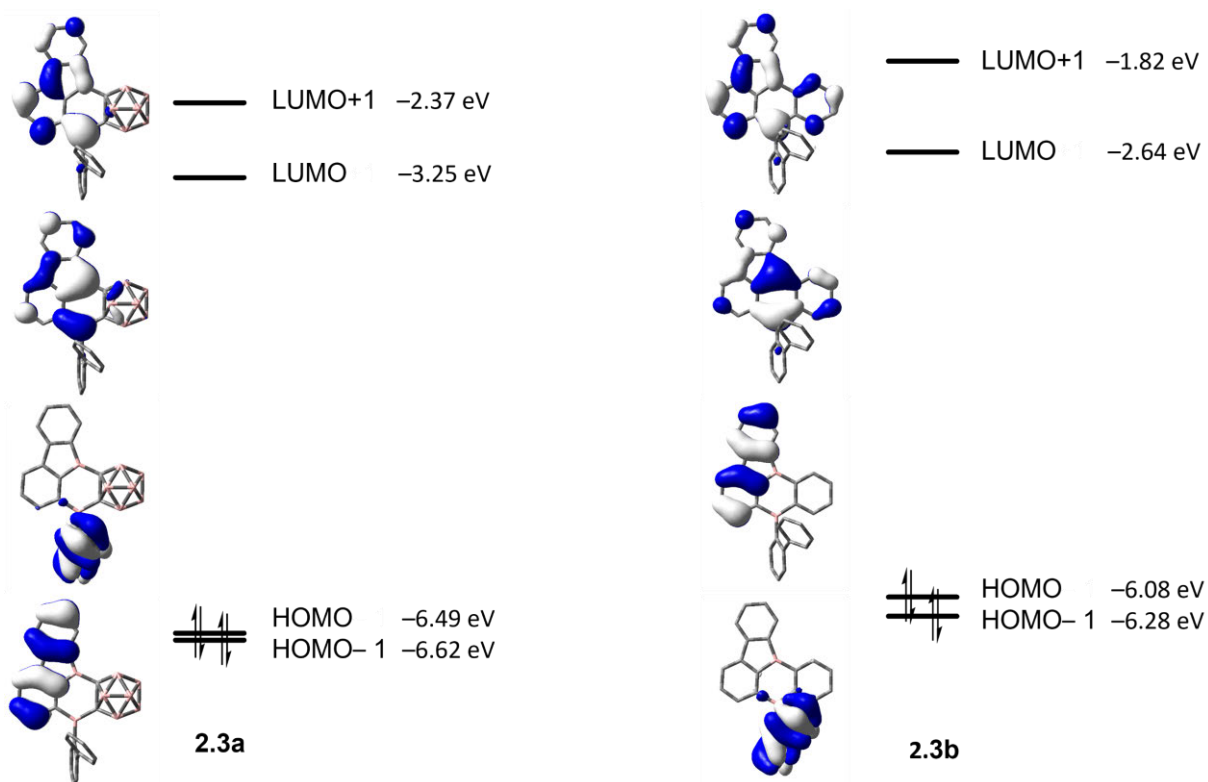


Figure 2.9. HOMO–1, HOMO, LUMO and LUMO+1 energies calculated at the CAM-B3LYP/6-31+G(d,p) level of theory for **2.3a** and **2.3b** (isovalue: $\pm 0.03 [e \text{ } a_0^{-3}]^{1/2}$).

Chapter 2

Table 2.3. Lowest energy transitions with a 9-borafluorene character calculated at the CAM-B3LYP/6-31+G(d,p) level of theory for **2.2b** in the gas phase and for **2.3a** and **2.3b** in n-hexane.

Compound	State	E [eV]	λ [nm]	f	Symmetry	Major contributions	Λ
2.2b	$S_1 \leftarrow S_0$	3.07	403.46	0.0016	A	HOMO \rightarrow LUMO (66%) H-1 \rightarrow L+1 (30%)	0.61
	$S_2 \leftarrow S_0$	3.10	400.57	0.0001	A	H-1 \rightarrow LUMO (62%) HOMO \rightarrow L+1 (35%)	0.61
	$S_3 \leftarrow S_0$	3.97	312.68	0.1529	A	H-2 \rightarrow LUMO (83%)	0.61
2.3a	$S_1 \leftarrow S_0$	2.90	427.41	0.0021	A	H-1 \rightarrow LUMO (68%) HOMO \rightarrow LUMO (25%)	0.51
	$S_2 \leftarrow S_0$	3.75	330.81	0.059	A	HOMO \rightarrow LUMO (52%) H-1 \rightarrow LUMO (16%) HOMO \rightarrow L+1 (12%)	0.41
	$S_5 \leftarrow S_0$	4.32	286.97	0.4836	Singlet-A	H-4 \rightarrow LUMO (39%) H-1 \rightarrow L+1 (30%) HOMO \rightarrow L+1 (10%)	0.63
2.3b	$S_{15} \leftarrow S_0$	5.23	236.85	0.4388	Singlet-A	H-7 \rightarrow LUMO (13%) H-6 \rightarrow LUMO (11%) H-4 \rightarrow L+1 (35%)	0.62
	$S_1 \leftarrow S_0$	2.88	430.44	0.0031	A	HOMO \rightarrow LUMO (91%)	0.51
	$S_2 \leftarrow S_0$	3.53	350.79	0.0091	A	H-2 \rightarrow LUMO (89%)	0.60
2.3b	$S_3 \leftarrow S_0$	3.69	335.95	0.0738	A	H-1 \rightarrow LUMO (62%) H-3 \rightarrow LUMO (16%)	0.34
	$S_7 \leftarrow S_0$	4.37	283.97	0.4162	Singlet-A	H-6 \rightarrow LUMO (32%) H-4 \rightarrow LUMO (14%) HOMO \rightarrow L+1 (21%)	0.62
	$S_{12} \leftarrow S_0$	4.98	249.08	0.5429	Singlet-A	H-8 \rightarrow LUMO (10%) H-2 \rightarrow L+1 (39%) H-1 \rightarrow L+1 (12%)	0.55

Both **2.3a** and **2.3b** exhibit yellow to orange, low energy emissions at 568 and 580 nm in hexane, respectively, showing a broad vibrational progression that is lost in solvents of higher polarity for **2.3a**. For **2.3a**, a bathochromic shift in the emission, depending on the solvent polarity, is observed from 568 nm in hexane to 596 nm in dichloromethane (Figure 2.10).

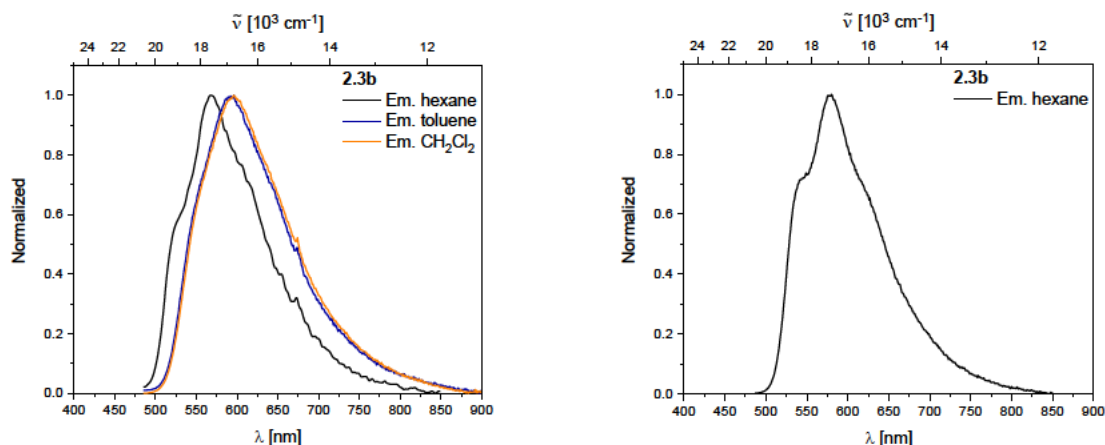


Figure 2.10. Left: Emission spectra of 2.3a in hexane (black), toluene (blue), and CH_2Cl_2 (orange). Right: Emission spectra of 2.3b in hexane.

Decomposition was observed in solution for both rearranged compounds and should be kept in mind regarding the reliability of quantitative measurements. Both compounds show long lifetimes of ca. 100 ns in hexane with low quantum yields ($\Phi_F = 0.13$ (2.3a) and 0.07 (2.3b)) indicating weakly allowed transitions (Table 2.2).

Furthermore, we were interested in the BC_4 -ring antiaromaticity of both compounds. Calculations of out of plane nucleus-independent chemical shift values (NICS(1)_{zz}) at the B3LYP/6-31+G(d,p) level of theory show higher values for 2.3a, being 26.4 and 24.5 for 2.3a and 2.3b, respectively. The NICS(1)_{zz} values are in the range of other reported benzannulated boroles that have been reported.^[31]

2.3.5 Electrochemical properties

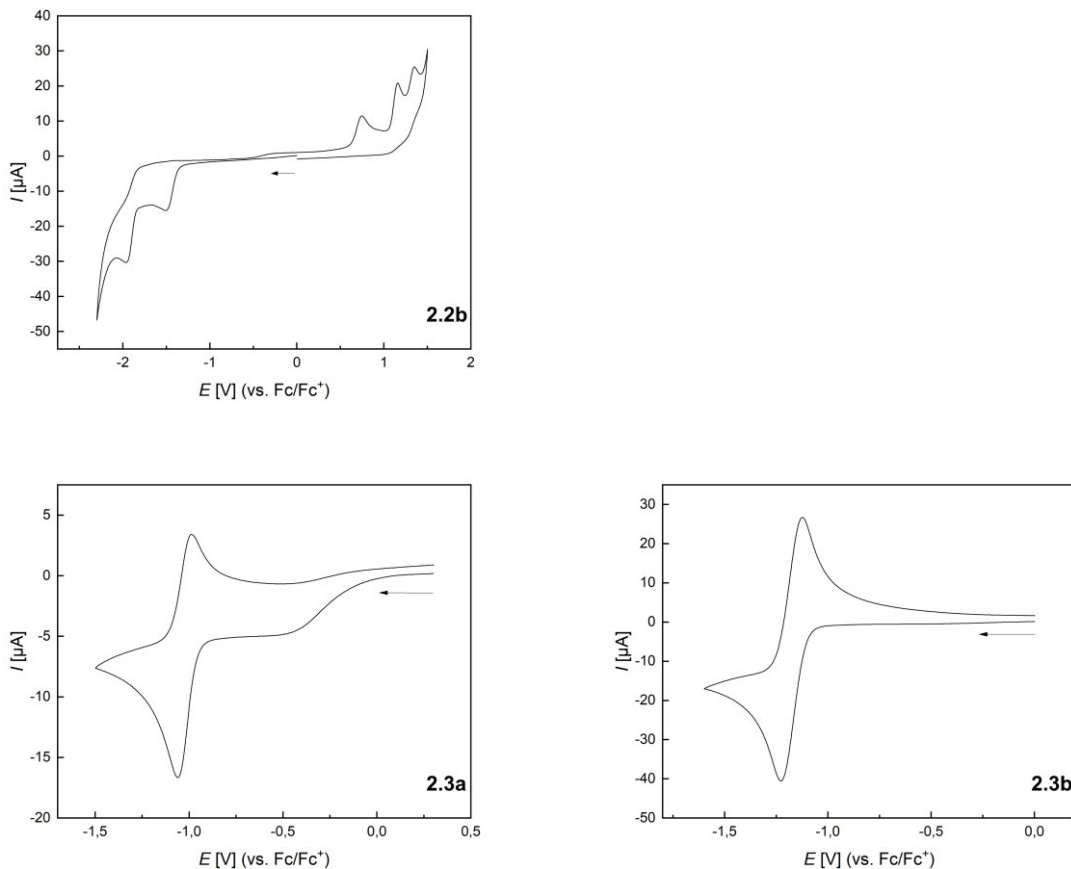


Figure 2.11. Normalized cyclic voltammograms of **2.2b**, **2.3a** and **2.3b** as solutions in CH_2Cl_2 at room temperature; supporting electrolyte, ($[n\text{Bu}_4\text{N}][\text{PF}_6]$) (0.1 mol L^{-1}); scan rate, 200 mV s^{-1} ; vs Fc/Fc^+ . Additional information can be found in the supporting information.

Table 2.4. Reduction and oxidation potentials of **2.2b**, **2.3a** and **2.3b**.

	1 st red. [V]	2 nd red. [V]	1 st ox. [V]
2a	$E_{pc} = -1.50$	$E_{pc} = -1.96$	$E_{pa} = 0.98$
3a	$E_{1/2} = -1.17$	$E_{pc} = -1.85$	-
3b	$E_{1/2}^{[a]} = -1.03$	$E_{pc} = -2.14$	$E_{pa} = 0.84$

[a] Partially reversible reduction

The cyclic voltammogram of **2.2b** shows an irreversible reduction at $E_{pc} = -1.5 \text{ V}$ and a second irreversible reduction at $E_{pc} = -1.96 \text{ V}$ (Figure 2.11 and Table 2.4). The presence of two borafluorenyl groups is clearly reflected in the first reduction potential, which is significantly lower than that in other 9-borafluorenes.^[32] However, the reduction potentials are in good agreement with related 1,8-naphthalenediyl- and methylene-bridged bisboranes from the groups of Gabbaï and Wagner.^[57-58, 60] In addition, the observation of two clearly spaced reduction processes suggests a communication between the two boron centers and the possible formation of a one-electron B–B bond.^[57-60]

Compounds **2.3a** and **2.3b** exhibit even lower, at least partially reversible, first reduction potentials at $E_{1/2} = -1.03$ and $E_{1/2} = -1.17$ V, respectively, in agreement with their calculated lower LUMO energies (see Figure 2.9). Moreover, the effect of the carborane unit in stabilizing the LUMO is clearly visible.

Both the extended π -system, which resembles that of benzo[a]fluoranthene, and the presence of two boron atoms in **2.3a** and **2.3b**, explain their lower reduction potentials compared to those in 9,10-diboraanthracenes^[38] and related all-carbon PAHs.^[95] A more apt comparison, especially for **2.3b**, are the doubly boron-doped PAHs reported by Würthner *et al.*, which also show exceptionally low reduction potentials of up to $E_{1/2} = -1.07$ V.^[96] Comparison with the doubly carborane-fused and π -electron poor variants of 9,10-diboraanthracene (**2.VI**) reported by Ye and co-workers with reduction potentials as low as $E_{pc} = -0.75$ V further underscores the LUMO-lowering effect of carboranes even without the participation of their C1–C2 σ^* anti bonding orbitals.^[41]

2.4 Conclusion

While attempting the synthesis of 1,2-bis-9-borafluorenyl-*o*-carborane (**[2.2a]**), using *ortho*-carborane as a three-dimensional backbone to lower the boron based LUMO energies in 9-borafluorenes, we observed an intramolecular rearrangement at room temperature. Investigation of the transition state using DFT calculations showed that the rearrangement follows an S_EAr-like mechanism that is enabled by a low lying LUMO, the targeted feature of compound **[2.2a]**. The same calculations for a phenyl-backbone predict a significantly higher energy barrier for such a rearrangement. As a result, we were able to synthesize and characterize 1,2-bis-9-borafluorenylbenzene (**2.2b**), the phenylene analog of **[2.2a]** and **VII**, following a tin-boron exchange route. The crystal structure of **2.2b** analysis shows the two 9-borafluorene units in a face-to-face arrangement with a dihedral angle of 43.5° with respect to the phenylene backbone. In solution, communication between the two boron centers was observed in the CV measurement. Reliable photophysical data were obtained from the solid state, showing typical 9-borafluorene properties and a high quantum yield with respect to comparable compounds. After confirming the predicted rearrangement in compound **2.2b**, products **2.3a** and **2.3b** were isolated and fully characterized. The single crystal structures show very similar structural motifs that differ by the phenylene-/o-carboranyl ring, and therefore the size of the π -system and inductive effects of the cluster. Isomers of this diborane motif have been suggested for use in organic light-emitting devices.^[97] Our photophysical studies show weak absorption bands at ca. 450 nm and yellow emissions at ca. 590 nm. TD-DFT calculations and experimental observations agree with a 9-borafluorene-like transition character. A strong electron affinity was observed for **2.3a** and **2.3b** with reduction potentials of $E_{1/2} = -1.03$ and $E_{1/2} = -1.17$ V, respectively. In general, the reactivity shown herein offers a pathway to BC₄B-six membered ring-containing PAHs for phenyl and especially carborane-containing systems. In principle, following the bis-*ortho* substitution motif, other tri-aryl substituents that offer a β -CH unit might rearrange in a similar fashion.

2.5 References

- [1] C. D. Entwistle, T. B. Marder, *Angew. Chem. Int. Ed.* **2002**, *41*, 2927–2931.
- [2] C. D. Entwistle, T. B. Marder, *Chem. Mater.* **2004**, *16*, 4574–4585.
- [3] S. Yamaguchi, A. Wakamiya, *Pure Appl. Chem.* **2006**, *78*, 1413–1424.
- [4] F. Jäkle, *Coord. Chem. Rev.* **2006**, *250*, 1107–1121.
- [5] S. K. Mellerup, S. Wang, *Trends Chem.* **2019**, *1*, 77–89.
- [6] M. Godumala, S. Choi, M. J. Cho, D. H. Choi, *J. Mater. Chem. C* **2019**, *7*, 2172–2198.
- [7] E. von Grotthuss, A. John, T. Kaese, M. Wagner, *Asian J. Org. Chem.* **2018**, *7*, 37–53.
- [8] L. Ji, S. Griesbeck, T. B. Marder, *Chem. Sci.* **2017**, *8*, 846–863.
- [9] S. Agnoli, M. Favaro, *J. Mater. Chem. A* **2016**, *4*, 5002–5025.
- [10] A. Wakamiya, S. Yamaguchi, *Bull. Chem. Soc. Jpn.* **2015**, *88*, 1357–1377.
- [11] Y. Su, R. Kinjo, *Chem. Soc. Rev.* **2019**, *48*, 3613–3659.
- [12] Y. Wang, W. Chen, Z. Lu, Z. H. Li, H. Wang, *Angew. Chem. Int. Ed.* **2013**, *52*, 7496–7499.
- [13] Q. Yin, Y. Soltani, R. L. Melen, M. Oestreich, *Organometallics* **2017**, *36*, 2381–2384.
- [14] A. Dasgupta, K. Stefkova, R. Babaahmadi, B. F. Yates, N. J. Buurma, A. Ariafard, E. Richards, R. L. Melen, *J. Am. Chem. Soc.* **2021**, *143*, 4451–4464.
- [15] S. Rendler, M. Oestreich, *Angew. Chem. Int. Ed.* **2008**, *47*, 5997–6000.
- [16] A. Corma, H. García, *Chem. Rev.* **2003**, *103*, 4307–4366.
- [17] C. R. Wade, A. E. J. Brooms Grove, S. Aldridge, F. P. Gabbaï, *Chem. Rev.* **2010**, *110*, 3958–3984.
- [18] S. Yamaguchi, S. Akiyama, K. Tamao, *J. Am. Chem. Soc.* **2001**, *123*, 11372–11375.
- [19] K. Parab, K. Venkatasubbaiah, F. Jäkle, *J. Am. Chem. Soc.* **2006**, *128*, 12879–12885.
- [20] T. W. Hudnall, C.-W. Chiu, F. P. Gabbaï, *Acc. Chem. Res.* **2009**, *42*, 388–397.
- [21] B. Su, R. Kinjo, *Synthesis* **2017**, *49*, 2985–3034.
- [22] J. H. Barnard, S. Yruegas, K. Huang, C. D. Martin, *Chem. Commun.* **2016**, *52*, 9985–9991.
- [23] H. Braunschweig, I. Krummenacher, J. Wahler, in *Adv. Organomet. Chem.*, Vol. 61 (Ed.: M. J. F. Anthony F. Hill), Elsevier, Amsterdam, **2013**, pp. 1–53.
- [24] H. Braunschweig, T. Kupfer, *Chem. Commun.* **2011**, *47*, 10903.
- [25] A. Steffen, R. M. Ward, W. D. Jones, T. B. Marder, *Coord. Chem. Rev.* **2010**, *254*, 1950–1976.
- [26] A. P. Sadimenko, in *Adv. Heterocycl. Chem.*, Vol. 79 (Ed.: A. R. Katritzky), Academic Press, Amsterdam, **2001**, pp. 115–197.
- [27] W. Zhang, B. Zhang, D. Yu, G. He, *Sci. Bull.* **2017**, *62*, 899–900.
- [28] J. He, F. Rauch, M. Finze, T. B. Marder, *Chem. Sci.* **2020**, *12*, 128–147.
- [29] X. Su, T. A. Bartholome, J. R. Tidwell, A. Pujol, S. Yruegas, J. J. Martinez, C. D. Martin, *Chem. Rev.* **2021**, *121*, 4147–4192.
- [30] R. Köster, G. Benedikt, *Angew. Chem. Int. Ed.* **1963**, *2*, 323–324.
- [31] F. Rauch, S. Fuchs, A. Friedrich, D. Sieh, I. Krummenacher, H. Braunschweig, M. Finze, T. B. Marder, *Chem. Eur. J.* **2020**, *26*, 12794–12808.
- [32] M. F. Smith, S. J. Cassidy, I. A. Adams, M. Vasiliu, D. L. Gerlach, D. A. Dixon, P. A. Rupar, *Organometallics* **2016**, *35*, 3182–3191.
- [33] J. He, F. Rauch, A. Friedrich, J. Krebs, I. Krummenacher, R. Bertermann, J. Nitsch, H. Braunschweig, M. Finze, T. B. Marder, *Angew. Chem. Int. Ed.* **2021**, *60*, 4833–4840.
- [34] A. Iida, A. Sekioka, S. Yamaguchi, *Chem. Sci.* **2012**, *3*, 1461.
- [35] A. Iida, S. Yamaguchi, *J. Am. Chem. Soc.* **2011**, *133*, 6952–6955.
- [36] S. Yruegas, J. C. Axtell, K. O. Kirlikovali, A. M. Spokoyny, C. D. Martin, *Chem. Commun.* **2019**, *55*, 2892–2895.
- [37] A. Benton, J. D. Watson, S. M. Mansell, G. M. Rosair, A. J. Welch, *J. Organomet. Chem.* **2020**, *907*, 121057.
- [38] C. Reus, S. Weidlich, M. Bolte, H. W. Lerner, M. Wagner, *J. Am. Chem. Soc.* **2013**, *135*, 12892–12907.
- [39] E. Januszewski, A. Lorbach, R. Grewal, M. Bolte, J. W. Bats, H.-W. Lerner, M. Wagner, *Chem. Eur. J.* **2011**, *17*, 12696–12705.

Chapter 2

- [40] Y. Nie, J. Miao, H. Wadeppohl, H. Pritzkow, T. Oeser, W. Siebert, *Z. Anorg. Allg. Chem.* **2013**, *639*, 1188–1193.
- [41] C. Zhang, J. Wang, W. Su, Z. Lin, Q. Ye, *J. Am. Chem. Soc.* **2021**, *143*, 8552–8558.
- [42] L. Ji, S. Riese, A. Schmiedel, M. Holzapfel, M. Fest, J. Nitsch, B. F. E. Curchod, A. Friedrich, L. Wu, H. H. Al Mamari, S. Hammer, J. Pflaum, M. A. Fox, D. J. Tozer, M. Finze, C. Lambert, T. B. Marder, *Chem. Sci.* **2022**, *13*, 5205–5219.
- [43] K.-R. Wee, Y.-J. Cho, J. K. Song, S. O. Kang, *Angew. Chem. Int. Ed.* **2013**, *52*, 9682–9685.
- [44] R. Núñez, M. Tarrés, A. Ferrer-Ugalde, F. F. d. Biani, F. Teixidor, *Chem. Rev.* **2016**, *116*, 14307–14378.
- [45] J. Ochi, K. Tanaka, Y. Chujo, *Angew. Chem. Int. Ed.* **2020**, *59*, 9841–9855.
- [46] J. Krebs, M. Haehnel, I. Krummenacher, A. Friedrich, H. Braunschweig, M. Finze, L. Ji, T. B. Marder, *Chem. Eur. J.* **2021**, *27*, 8159–8167.
- [47] J. Kahlert, L. Böhling, A. Brockhinke, H.-G. Stammier, B. Neumann, L. M. Rendina, P. J. Low, L. Weber, M. A. Fox, *Dalton Trans.* **2015**, *44*, 9766–9781.
- [48] J. O. Huh, H. Kim, K. M. Lee, Y. S. Lee, Y. Do, M. H. Lee, *Chem. Commun.* **2010**, *46*, 1138–1140.
- [49] T. Bischof, X. Guo, I. Krummenacher, L. Beßler, Z. Lin, M. Finze, H. Braunschweig, *Chem. Sci.* **2022**.
- [50] M. F. Hawthorne, R. G. Adler, *J. Am. Chem. Soc.* **1970**, *92*, 6174–6182.
- [51] M. F. Hawthorne, T. E. Berry, P. A. Wegner, *J. Am. Chem. Soc.* **1965**, *87*, 4746–4750.
- [52] K. Köhler, W. E. Piers, A. P. Jarvis, S. Xin, Y. Feng, A. M. Bravakis, S. Collins, W. Clegg, G. P. A. Yap, T. B. Marder, *Organometallics* **1998**, *17*, 3557–3566.
- [53] V. C. Williams, W. E. Piers, W. Clegg, M. R. J. Elsegood, S. Collins, T. B. Marder, *J. Am. Chem. Soc.* **1999**, *121*, 3244–3245.
- [54] V. C. Williams, C. Y. Dai, Z. M. Li, S. Collins, W. E. Piers, W. Clegg, M. R. J. Elsegood, T. B. Marder, *Angew. Chem. Int. Ed.* **1999**, *38*, 3695–3698.
- [55] V. C. Williams, G. J. Irvine, W. E. Piers, Z. M. Li, S. Collins, W. Clegg, M. R. J. Elsegood, T. B. Marder, *Organometallics* **2000**, *19*, 1619–1621.
- [56] P. A. Chase, L. D. Henderson, W. E. Piers, M. Parvez, W. Clegg, M. R. J. Elsegood, *Organometallics* **2005**, *25*, 349–357.
- [57] A. Hübner, T. Kaese, M. Diefenbach, B. Endeward, M. Bolte, H. W. Lerner, M. C. Holthausen, M. Wagner, *J. Am. Chem. Soc.* **2015**, *137*, 3705–3714.
- [58] J. D. Hoefelmeyer, F. P. Gabbaï, *J. Am. Chem. Soc.* **2000**, *122*, 9054–9055.
- [59] S. Biswas, I. M. Oppel, H. F. Bettinger, *Inorg. Chem.* **2010**, *49*, 4499–4506.
- [60] A. Hübner, A. M. Diehl, M. Diefenbach, B. Endeward, M. Bolte, H.-W. Lerner, M. C. Holthausen, M. Wagner, *Angew. Chem. Int. Ed.* **2014**, *53*, 4832–4835.
- [61] W. Yang, K. E. Krantz, D. A. Dickie, A. Molino, D. J. D. Wilson, R. J. Gilliard, *Angew. Chem. Int. Ed.* **2020**, *59*, 3971–3975.
- [62] W. Zhang, G. Li, L. Xu, Y. Zhuo, W. Wan, N. Yan, G. He, *Chem. Sci.* **2018**, *9*, 4444–4450.
- [63] S. Yruegas, J. J. Martinez, C. D. Martin, *Chem. Commun.* **2018**, *54*, 6808–6811.
- [64] K. R. Bluer, L. E. Laperriere, A. Pujol, S. Yruegas, V. A. K. Adiraju, C. D. Martin, *Organometallics* **2018**, *37*, 2917–2927.
- [65] H. F. Bettinger, M. Müller, *J. Phys. Org. Chem.* **2015**, *28*, 97–103.
- [66] M. Müller, C. Maichle-Mössmer, H. F. Bettinger, *Angew. Chem. Int. Ed.* **2014**, *53*, 9380–9383.
- [67] S. Biswas, C. Maichle-Mössmer, H. F. Bettinger, *Chem. Commun.* **2012**, *48*, 4564.
- [68] T. Tsukada, Y. Shoji, K. Takenouchi, H. Taka, T. Fukushima, *Chem. Commun.* **2022**, *58*, 4973–4976.
- [69] J. Kashida, Y. Shoji, T. Fukushima, *Asian J. Chem.* **2019**, *14*, 1879–1885.
- [70] Y. Shoji, N. Tanaka, S. Muranaka, N. Shigeno, H. Sugiyama, K. Takenouchi, F. Hajjaj, T. Fukushima, *Nat. Commun.* **2016**, *7*, 12704.
- [71] S. P. Lewis, J. Chai, S. Collins, T. J. J. Sciarone, L. D. Henderson, C. Fan, M. Parvez, W. E. Piers, *Organometallics* **2009**, *28*, 249–263.

Chapter 2

- [72] Z. Zhang, R. M. Edkins, M. Haehnel, M. Wehner, A. Eichhorn, L. Mailänder, M. Meier, J. Brand, F. Brede, K. Müller-Buschbaum, H. Braunschweig, T. B. Marder, *Chem. Sci.* **2015**, *6*, 5922–5927.
- [73] A. Hübner, Z. W. Qu, U. Englert, M. Bolte, H. W. Lerner, M. C. Holthausen, M. Wagner, *J. Am. Chem. Soc.* **2011**, *133*, 4596–4609.
- [74] H. Zhu, Z.-W. Qu, *J. Comput. Chem.* **2014**, *35*, 1107–1110.
- [75] A. Hübner, M. Diefenbach, M. Bolte, H.-W. Lerner, M. C. Holthausen, M. Wagner, *Angew. Chem. Int. Ed.* **2012**, *51*, 12514–12518.
- [76] A. Hübner, A. M. Diehl, M. Bolte, H.-W. Lerner, M. Wagner, *Organometallics* **2013**, *32*, 6827–6833.
- [77] J. Radtke, S. K. Mellerup, M. Bolte, H.-W. Lerner, S. Wang, M. Wagner, *Org. Lett.* **2018**, *20*, 3966–3970.
- [78] H. Budy, S. E. Prey, C. D. Buch, M. Bolte, H. W. Lerner, M. Wagner, *Chem. Commun.* **2021**, *58*, 254–257.
- [79] J. B. Heilmann, Y. Qin, F. Jäkle, H.-W. Lerner, M. Wagner, *Inorg. Chim. Acta* **2006**, *359*, 4802–4806.
- [80] H. C. Brown, Y. Yamamoto, *J. Am. Chem. Soc.* **1971**, *93*, 2796–2798.
- [81] D. Kaufmann, *Chem. Ber.* **1987**, *120*, 901–905.
- [82] L. Kaufmann, H. Vitze, M. Bolte, H.-W. Lerner, M. Wagner, *Organometallics* **2008**, *27*, 6215–6221.
- [83] M. J. Peach, P. Benfield, T. Helgaker, D. J. Tozer, *J. Chem. Phys.* **2008**, *128*, 044118.
- [84] T. Yanai, D. P. Tew, N. C. Handy, *Chem. Phys. Lett.* **2004**, *393*, 51–57.
- [85] X. Chen, G. Meng, G. Liao, F. Rauch, J. He, A. Friedrich, T. B. Marder, N. Wang, P. Chen, S. Wang, X. Yin, *Chem. Eur. J.* **2021**, *27*, 6274–6282.
- [86] S. J. Cassidy, I. Brettell-Adams, L. E. McNamara, M. F. Smith, M. Bautista, H. Cao, M. Vasiliu, D. L. Gerlach, F. Qu, N. I. Hammer, D. A. Dixon, P. A. Rupar, *Organometallics* **2018**, *37*, 3732–3741.
- [87] Y. Morisaki, M. Tominaga, T. Ochiai, Y. Chujo, *Chem. Asian J.* **2014**, *9*, 1247–1251.
- [88] Y. Morisaki, M. Tominaga, Y. Chujo, *Chem. Eur. J.* **2012**, *18*, 11251–11257.
- [89] V. I. Bregadze, *Chem. Rev.* **2002**, *92*, 209–223.
- [90] K. Nishino, K. Hashimoto, K. Tanaka, Y. Morisaki, Y. Chujo, *Tetrahedron Lett.* **2016**, *57*, 2025–2028.
- [91] Y. Xu, Q. Chu, D. Chen, A. Fuentes, *Front. Mech. Eng.* **2021**, *7*.
- [92] D. Chen, H. Wang, *Proc. Combust. Inst.* **2019**, *37*, 953–959.
- [93] E. M. Adkins, J. A. Giaccai, J. H. Miller, *Proc. Combust. Inst.* **2017**, *36*, 957–964.
- [94] J. H. Miller, J. D. Herdman, C. D. O. Green, E. M. Webster, *Proc. Combust. Inst.* **2013**, *34*, 3669–3675.
- [95] A. John, M. Bolte, H. W. Lerner, M. Wagner, *Angew. Chem. Int. Ed.* **2017**, *56*, 5588–5592.
- [96] J. M. Farrell, C. Mütsel, D. Bialas, M. Rudolf, K. Menekse, A.-M. Krause, M. Stolte, F. Würthner, *J. Am. Chem. Soc.* **2019**, *141*, 9096–9104.
- [97] D. Tang, C. Li, Z. Zhang, F. Wang, CN111377956, Jiangsu Sunera Technology Co., Ltd., China, 2020.

2.6 Author contributions and agreement

Detailierte Darstellung der Anteile an der Veröffentlichung (in %) Angabe Autoren/innen (ggf. Haupt- / Ko- / korrespondierende/r Autor/in) mit Vorname Nachname (Initialen)														
Autor	JK	AH	SF	XG	FR	AE	IK	AF	LJ	MF	ZL	HB	TBM	\sum in Prozent
Synthesis and characterization	12%	15%	2%							1%				30%
Electrochemistry								2%						2%
Single-crystal structure analysis	5%		2%			1%			2%					10%
Photophysical properties	5%					3%								8%
Transition state calculations (DFT)							5%							5%
TD-DFT calculations (+DFT)	9%													9%
Verfassen der Veröffentlichung	17%	4%												21%
Korrektur der Veröffentlichung	3%				1%		1%		1%	1%				12%
Koordination der Veröffentlichung	2%												1%	3%
Summe	50%	22%	4%	5%	4%	1%	3%	3%	2%	1%	1%	1%	3%	100%

Chapter 2

Aklärung zur Autorenschaft
"Backbone controlled LUMO Energy induces intramolecular C–H activation in *ortho*-bis-9-borafluorene-substituted phenyl and o-carboranyl compounds leading to novel 9,10-diboranthracene derivatives"

Johannes Krebs, Alena Häfner, Sonja Fuchs, Xueying Guo, Dr. Florian Rauch, Dr. Antonius Eichhorn, Dr. Ivo Krummenacher, Dr. Alexandra Friedrich, Prof. Dr. Lei Ji, Prof. Dr. Maik Finze, Prof. Dr. Zhenyang Lin, Prof. Dr. Holger Braunschweig, Prof. Dr. Todd B. Marder.
DOI:

Die Mitauteuren der in dieser (teil-)kumulativen Dissertation verwendeten Manuskripte sind sowohl über die Nutzung als auch über die angegebenen Eigenanteile informiert und stimmen dem zu.

Angabe Autorenschaft: Anwählen Dropdowmmenü / Autorenunterschrift oder Angabe Verweis: Kontrollkästchen über Eigenschaften aktivieren!

Autor/in 3 (Sonja Fuchs)

Koautor/in

Verweis: E-Mail hinterlegt

Autor/in 2 (Alena Häfner)

Hauptautor/in

Verweis: E-Mail hinterlegt

Autor/in 1 (Johannes Krebs)

Hauptautor/in

Verweis: E-Mail hinterlegt

Autor/in 6 (Antonius Eichhorn)

Koautor/in

Verweis: E-Mail hinterlegt

Autor/in 5 (Florian Rauch)

Koautor/in

Verweis: E-Mail hinterlegt

Autor/in 4 (Xueying Guo)

Koautor/in

Verweis: E-Mail hinterlegt

Autor/in 8 (Ivo Krummenacher)

Koautor/in

Verweis: E-Mail hinterlegt

Autor/in 8 (Alexandra Friedrich)

Koautor/in

Verweis: E-Mail hinterlegt

Chapter 2

7.14	<p>Autor/in 1 (Lei Ji)</p> <p>Korrespondenzautor/in</p> <p><input type="checkbox"/> Verweis; E-Mail hinterlegt</p> <p>[Redacted]</p>	<p>Autor/in 2 (Mark Finze)</p> <p>Koautor/in</p> <p><input checked="" type="checkbox"/> Verweis; E-Mail hinterlegt</p> <p>[Redacted]</p>	<p>Autor/in 3 (Zhenyang Lin)</p> <p>Korrespondenzautor/in</p> <p><input checked="" type="checkbox"/> Verweis; E-Mail hinterlegt</p> <p>[Redacted]</p>	<p>Autor/in 4 (Holger Braunschweig)</p> <p>Korrespondenzautor/in</p> <p><input type="checkbox"/> Verweis; E-Mail hinterlegt</p> <p>[Redacted]</p>	<p>Autor/in 5 (Todd B. Marder)</p> <p>Korrespondenzautor/in</p> <p><input type="checkbox"/> Verweis; E-Mail hinterlegt</p> <p>[Redacted]</p>	<p>Würzburg, 19.07.2022</p> <p>(Datum)</p> <p>Prof. Dr. Todd B. Marder</p>
------	--	--	---	---	--	--

Chapter 2

3. CHAPTER 3

3.1 Title and Abstract

Synthesis, Photophysical and Electronic Properties of a D- π -A julolidine-like Pyrenyl-*o*-Carborane

Johannes Krebs,^a Lisa Bändler,^a Dr. Ivo Krummenacher,^a Dr. Alexandra Friedrich,^a Prof. Dr. Basile F. E. Curchod,^b Prof. Dr. Maik Finze,^a Prof. Dr. Todd B. Marder^{a*}

^aInstitute for Inorganic Chemistry and Institute for Sustainable Chemistry & Catalysis with Boron, Julius-Maximilians-Universität Würzburg, Am Hubland, 97074 Würzburg, Germany

^bUniversity of Bristol, Bristol BS8 1TH, United Kingdom

Abstract: We synthesized 2-(1-1,2-Dicarbadodecaboranyl(12))-6,6,12,12-tetramethyl-7,8,11,12-tetrahydro-6H,10H-phenaleno[1,9-fg]pyrido[3,2,1-ij]quinoline (**3.4**) a julolidine-like pyrenyl-*o*-carborane, with pyrene substituted at the 2,7-positions on the HOMO/LUMO nodal plane, continuing our research. Using solid state molecular structures, photophysical data, cyclic voltammetry, DFT and TD-DFT calculations we compare *o*-carborane and the B(mes)₂ (mes = 2,4,6-Me₃C₆H₂) as acceptor groups and confirm the julolidine-like donor strength. With the well understood pyrene frontier orbitals as a method of measuring donor and acceptor strength, we compare *o*-carborane and B(mes)₂ as acceptors, and examine the role of the julolidine-like moiety on pyrene.

3.2 Introduction

Pyrene as one of the most studied and best understood polycyclic aromatic hydrocarbons (PAH), is a popular widely employed luminophore due to its long-lived singlet excited states and tendency for excimer and exciplex formation.^[1] Its versatility can be seen in the diverse field of applications. A popular example is its use in optical materials for the use in organic light emitting diodes (OLEDs), organic field-effect transistors (OFETs), and organic photovoltaic cells (OPVs).^[1-4] It has also been used as linker in metal organic frameworks (MOF)^[5-7] and covalent organic frameworks (COFs).^[8-9] Pyrene containing materials are also applicable in sensors sensitive to temperature,^[10] pressure,^[11-12] pH,^[13] and the detection of small molecules^[14-17] and metal ions.^[18] They have also been employed in series of biological systems and in combination with biomolecules.^[19] As such, pyrenes were investigated for their interactions in macromolecules and lipids oligonucleotides,^[20-31] and nucleic acids, especially DNA.^[29-30, 32-45] In cells, pyrene was used to detect reactive oxygen species (ROS).^[46-49]

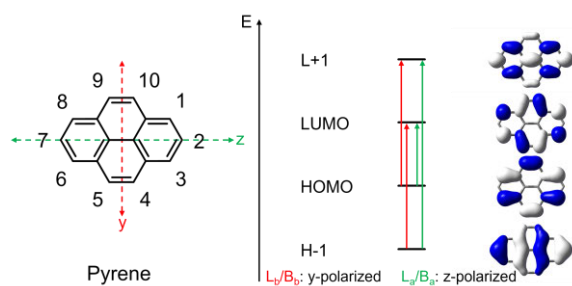


Figure 3.1. Atom numbering system in pyrene, typical electronic transitions colored regarding their polarization along a Cartesian coordinate system, and its frontier orbitals.

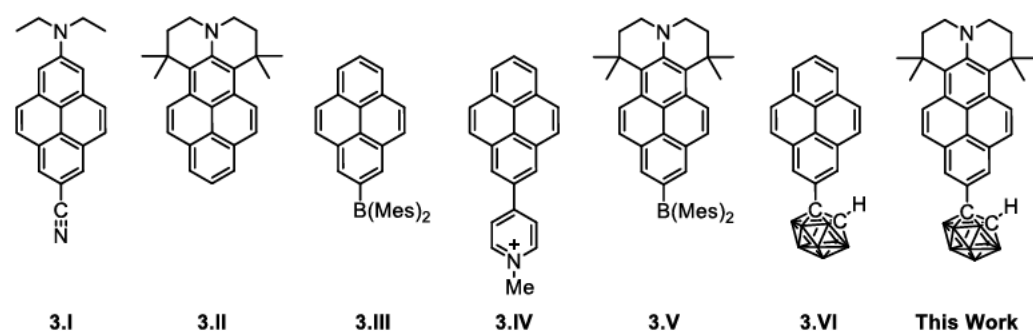
Functionalization of pyrene typically follows from its frontier molecular orbitals (Figure 3.1). With its highest occupied molecular orbital (HOMO) and lowest occupied molecular orbital (LUMO) having major contributions at 1,3,6 and 8, these positions react readily *via* electrophilic substitution.^[1, 50-56] Substitution at the equivalent 4,5,9- and 10-positions, referred to as K-region, takes advantages of their alkene-like nature using alkene selective reagents.^[56-59] Substitutions at the remaining 2- and 7-positions, that lie along the nodal plane of the HOMO and LUMO, were problematic, but became readily accessible *via* regioselective Ir-catalyzed C–H borylation.^[50-51, 56, 60-61] Pyrene derivatives substituted at the 2- or 2,7-positions are of great interest for chromophores as they often possess long fluorescence lifetimes.^[50]

The photophysical transitions observed in the pyrene are a result of its high symmetry. The lowest energy transition $S_1 \leftarrow S_0$ was identified as a configuration interaction (CI) between $\text{HOMO-1} \rightarrow \text{LUMO}$ and $\text{HOMO} \rightarrow \text{LUMO+1}$ and is referred to as L_b following the Platt nomenclature.^[50] It is polarized in the “y” direction (Figure 3.1). As the respective transition dipole moments \mathbf{M} cancel each other out, this transition is dipole forbidden ($\epsilon = 510 \text{ M}^{-1} \text{ cm}^{-1}$).^[50] The $\text{HOMO} \rightarrow \text{LUMO}$ transition $S_2 \leftarrow S_0$, referred to L_a , is polarized along the long “z” axis and is allowed ($\epsilon = 55000 \text{ M}^{-1} \text{ cm}^{-1}$).^[62] The $S_3 \leftarrow S_0$ transition, again polarized along the short “y” axis, however, enhances the effect of the respective dipole moments \mathbf{M} (B_b) making it an allowed transition ($\epsilon = 54000 \text{ M}^{-1} \text{ cm}^{-1}$). The long axis “z” polarized transition (B_a) from $S_4 \leftarrow S_0$ is also allowed ($\epsilon = 88000 \text{ M}^{-1} \text{ cm}^{-1}$).^[63-65]

In the case of substitution at the 2,7-positions, the nodal plane in the HOMO and LUMO of pyrene results no overlap with donors and acceptors. However, HOMO-1 and LUMO+1 have a major

contribution from the 2,7-positions and therefore will interact.^[50] Depending on the donor or acceptor strength, calculations show that it is possible to destabilize the HOMO-1 above HOMO and stabilize the LUMO+1 below LUMO.^[62] This can effectively result in a lower HOMO-LUMO gap. Our experiments have shown for donors, that a diethylamino donor in 3.I (Scheme 3.1) is already enough for this orbital swap to occur^[66] but is even more pronounced for the tetramethyl-julolidine-like^[67-71] pyrene 3.II.^[62] It was also reported for 2,7-Bis(dianisylamino)pyrene by Ito *et al.*^[72]

For acceptors we observed in 3.I, a lowered LUMO-LUMO+1 gap showing that the CN group is not quite strong enough as an acceptor.^[66] For the B(mes)₂ group in 3.III the calculations showed that one group is strong enough for the LUMO-LUMO+1 swap to occur.^[50, 73] In a more recent study on 3.IV, we could show that a single methylated pyridinyl group has an acceptor strength strong enough to clearly stabilize the pyrene like LUMO+1 below the LUMO.^[32] In 3.V, the combination of julolidine-like and B(mes)₂ moieties results in an orbital “shuffling” with an orbital swap for the HOMOs and the LUMOs simultaneously resulting in a charge-transfer character S₁ states and large apparent Stokes shifts into the green region.^[62, 74]

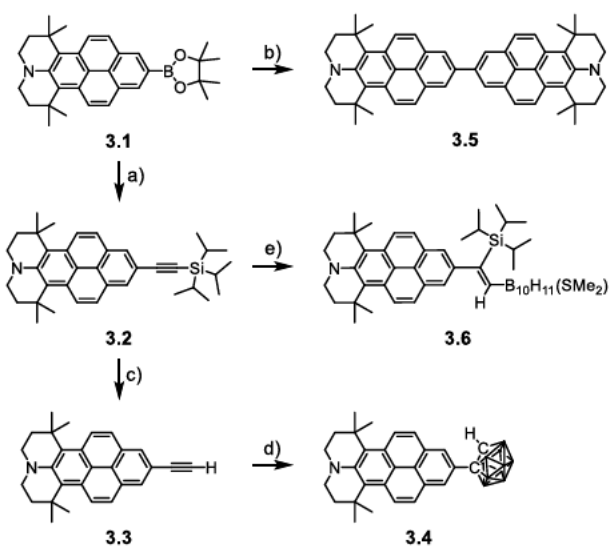


Scheme 3.1. Related known compounds. The unlabeled cluster vertices represent BH units.

The carborane cluster 1,2-dicarbadodecaborane(12) (*o*-carborane) has seen a surge in recent years in its use as substituent on PAH's.^[75-76] In monoaryl-substituted compounds, the *o*-carborane moiety is able to rotate almost freely around its exo-C_{Carboranyl}–C_{Aryl} bond, with calculated barriers of ca. 1.4 kJ Mol⁻¹.^[75, 77] In discussions of optimized geometries and solid state molecular structures, the dihedral angle ψ with respect to the aromatic plane and the *o*-carborane C1–C2 bond is an important parameter controlling the *o*-carborane and π -system interaction. At $\psi = 90^\circ$ the C1–C2 bond is perpendicular to the aromatic plane facilitating conjugation between the arylene π -system and the *o*-carborane LUMO, namely the C1–C2 antibonding (σ^*) orbital, comparable to hyperconjugation.^[75, 78-80] With the coexistence of aromatic local excitation (LE) ($\psi = 0$) and *o*-carborane charge transfer (CT) ($\psi = 90$) excited states, this ability to act as a rotation dependent acceptor can result in dual emission.^[77, 81-90] *O*-carboranes are also known to influence connected systems with their strong π -inductive effect, stabilizing the frontier orbitals.^[91-93] We and others studied the coexisting LE and CT excited states can be connected by a low energy potential barrier and yet show very different geometries and orbital distributions.^[77, 87-88, 94-96] In 1-(pyrenyl-2'-yl)-*o*-carborane (3.VI), we were able to simulate and experimentally confirm a thermodynamical equilibrium between the LE and CT excited states by determining the relevant interconversion rates.^[77] Apart from 3.VI, pyrenyl-*o*-carboranes have already received considerable attention as chromophores and show potential applications in photocatalysis.^[85-86, 88, 97-98]

3.1 Results and Discussion

3.1.1 Synthesis and observation



Scheme 3.2. Synthesis of compounds 3.4 and 3.6 and byproduct 3.5. a) I-C≡C-TIPS (1.1 equiv), Pd(dba)₂ (10 mol %), Cs₂CO₃ (1.1 equiv), rt, methanol, 20 h, 45%; b) Compound 3.5 was isolated as byproduct in reaction a) due to trace oxygen, 3%. c) TBAF (5 equiv), rt, THF, 1 h, 82%; d) $B_{10}H_{12}(SMe_2)_2$ (1.5 equiv), AgOAc (10 mol %), 100 °C, toluene, 2 d, 36%; e) $B_{10}H_{12}(SMe_2)_2$ (1.5 equiv), AgOAc (10 mol %), 100 °C, toluene, 2 d, 62%. The unlabeled cluster vertices represent BH units.

The synthesis of compound 3.4 and its intermediates are summarized in Scheme 3.2. Compound 3.1 was obtained following the known iridium-catalyzed regioselective 2-borylation of pyrene followed by amination and the formation of the julolidine-like moiety and the subsequent iridium-catalyzed C-H borylation at the 7-position, as described previously.^[51, 60, 62] It is worth noting that the julolidine-like moiety on pyrene is prone to react with silica under UV irradiation and solutions thereof show decomposition in contact with air. In a palladium-catalyzed cross-coupling reaction with (iodoethyl)triisopropylsilane, 3.2 was synthesized in good yields.^[99] This reaction, however, also led to the formation of homo-coupled compound 3.5 as a side product in low yields due to trace oxygen. Following established methods, 3.2 was deprotected giving compound 3.3 in excellent yields. The deprotected alkyne 3.3 was reacted with *arachno*- $B_{10}H_{12}(SMe_2)_2$ in an one-step silver(I)-catalyzed process, as described by Toppino *et al.*, yielding 3.4.^[100] The analogous reaction starting from the TIPS-protected alkyne 3.3 did not result in the desired *o*-dicarba-*c*₂*o*-dodecacarborane, but in the B-H *trans*-insertion and rearrangement product 3.6, a *nido* borane that still contains an SMe₂ group. This process has been previously described as a 1,2-silyl group migration on the alkyne (terminal C to internal C) in related reactions.^[101-102] Compound 3.6 is stable enough that workup *via* column chromatography in the dark was feasible.

3.1.2 Structural characterization

Compounds **3.2**, **3.4**, **3.5** and **3.6** were investigated by single-crystal X-ray diffraction; selected bond lengths and angles are listed in Table 3.1 and the structures are shown in Figure 3.2. For comparison, Table 3.1 lists parameters of related molecules from previous studies.

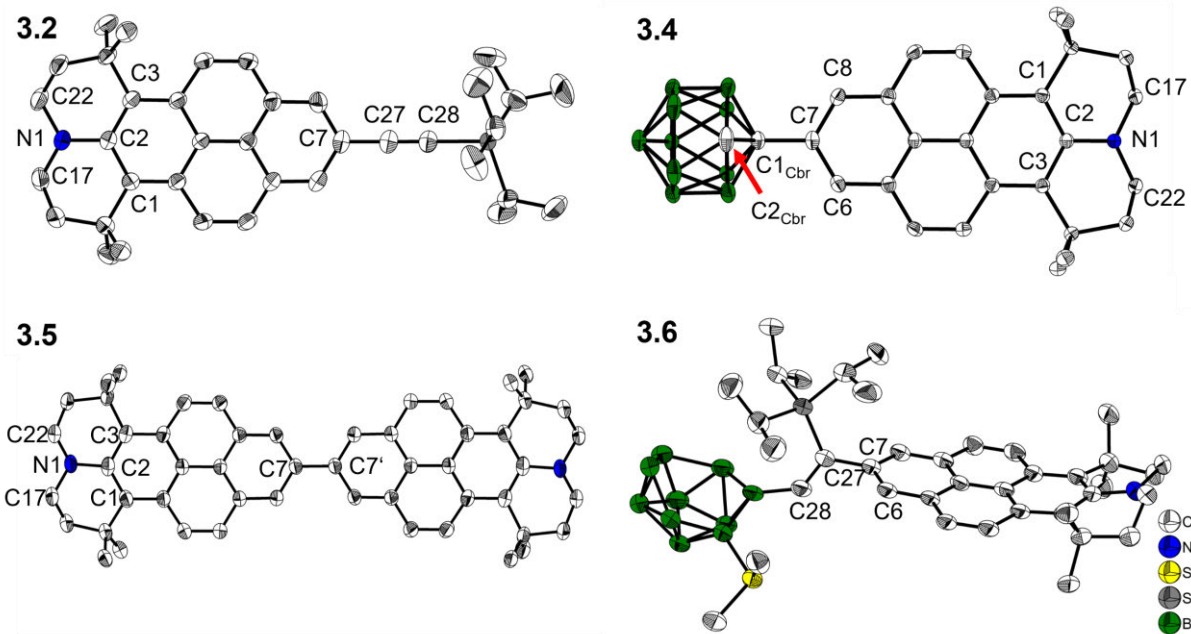


Figure 3.2. Solid state molecular structure of **3.2**, **3.4**, **3.5** and **3.6** from single-crystal X-ray diffraction at 100 K. Atomic displacement ellipsoids are drawn at the 50% probability level. Hydrogen atoms and, for **3.5** and **3.6**, solvent molecules are omitted for clarity.

Table 3.1. Selected bond lengths [Å] and angles [°] of **3.2**, **3.4**, **3.5**, **3.6**, **3.II**, **3.V** and **3.VI**.

	3.2	3.4	3.5	3.6	3.II ^[62]	3.V ^[62]	3.VI ^[77]
N1–C2	1.399(2)	1.381(2)	1.410(8)	1.399(5)	1.404(3)	1.391(3)	
C7–C27 (sp ₂ -sp)		1.441(2)		1.489(5)		(sp ₂ -sp ₂)	
C27–C28 (sp-sp)		1.201(2)		1.345(5)		(sp ₂ -sp ₂)	
C1_{cbr}–C2_{cbr}			1.660(2)				1.646(5) 1.641(7) 1.638(6) 1.647(7)
C1_{cbr}–C7			1.509(2)				1.502(5) 1.504(7) 1.498(5) 1.506(6)
C7–C7'				1.497(3)			
Σ₄ CNC	351.0(4)	355.6(6)	349.4(8)	352.4(5)	350.7(5)	355.7(6)	
C1–C2–N1–C17	22.2(2)		21.1(8)	20.7(5)	17.2(3)	11.2(3)	
C3–C2–N1–C22	13.0(2)	12.2(2)	15.0(8)	10.7(5)	19.8(3)	14.8(3)	
C6–C7–C1_{cbr}–C2_{cbr}			93.13(9)				33.5(5) 30.6(6) 24.2(6) 39.9(6)
C6–C7–C27–C28				84.0(5)			

As demonstrated previously, the exceptionally strong julolidine-type donor moiety has a significant influence on attached π -systems.^[62] The degree of donor electron density delocalization in the aromatic system can be seen in the N1–C2 bond length. As a result, a slight trend towards shorter bond lengths can be observed going from the donor- π -donor system **3.5** (1.410(8) Å) and donor- π systems **3.2**, **3.6** and **3.II** (1.399(2), 1.399(5) and 1.404(3) Å) to the donor- π -acceptor systems **3.4** and **3.V** (1.381(2) and 1.391(3) Å), albeit that many of these bond lengths overlap within 3 esd's. In all julolidine-type moieties the nitrogen atom adopts a pyramidal geometry visible in the CNC angle sum that is lower than 360°. Additionally, both alkyl substituents on N are tilted below the pyrene plane visible in torsion angles at C1–C2–N1–C17 and C3–C2–N1–C22 between 12 and 22° (Figure 5.3.2 and 5.3.3).

For *o*-carborane as an acceptor in **3.4**, and in the four independent molecules present in the unit cell of **3.VI**, we observe essentially no difference in the carborane C1–C2 bond lengths (1.660(2) and 1.638(6) – 1.647(7) Å, respectively) and the bond lengths between the pyrene and the carborane moiety (1.509(2) and 1.498(5) – 1.506(6) Å, respectively) within 3 esd's. These parameters are usually indicative of electron density delocalization from the arene to the carborane moiety in the form of C1_{cbr}–C7 bond shortening and C1_{cbr}–C2_{cbr} bond elongation. For **3.4**, we observe a small elongation compared to the typical *o*-carboranyl C1_{cbr}–C2_{cbr} bond length of 1.624(8) Å.^[103] In **3.4**, the torsion angle at C6–C7–C1_{cbr}–C2_{cbr} is 93.13(9)° but considering the mirror plane that runs perpendicular to the lengths of pyrene intersects atoms C1_{cbr} and C2_{cbr}, the real ψ angle is 90° and deviates due to an angle between the *o*-carborane moiety and the pyrene plane at 6.7°. This should give an optimal overlap

between the pyrene π -system and the C1–C2 σ^* -anti-bonding orbital. For **3.VI**, however, torsion angles between 24.2(6) and 39.9(6) Å were observed inhibiting a similar interaction in the solid state.

A crystal of the rearranged product **3.6** was obtained and the structure is shown in Figure 3.2. The newly formed C=C double bond is almost perpendicular to the pyrene plane due to the high steric demand of the TIPS-group α - to the aromatic system. The *nido*-decaborane species is coordinated by one of the initial two dimethylsulfide molecules.

Of the four obtained crystal structures only **3.2** and **3.4** show a packing that could allow π -stacking (Figure 3.3). In **3.2**, the molecules adopt a sandwich herring-bone packing with the TIPS-groups facing the pyrene surface of the adjacent molecule. Two molecules between two herring-bone progression face each as dimers in opposite direction with a π – π -distance of 3.62 Å (Figure 3.3a and Figure 5.3.1). In the crystal structure of **3.4**, the molecules stack in rows centered on the mirror plane forming sheets with a short *o*-carborane C–H \cdots π distance of 2.35 Å. This distance is quite similar to an alkyne C–H \cdots π interactions in ethynylbenzenes due to the comparable *o*-carborane and alkyne pK_A values.^[104] The two pyrenes have only a small overlap area and the shortest distance between the π -systems is located at the N with 3.96 Å.

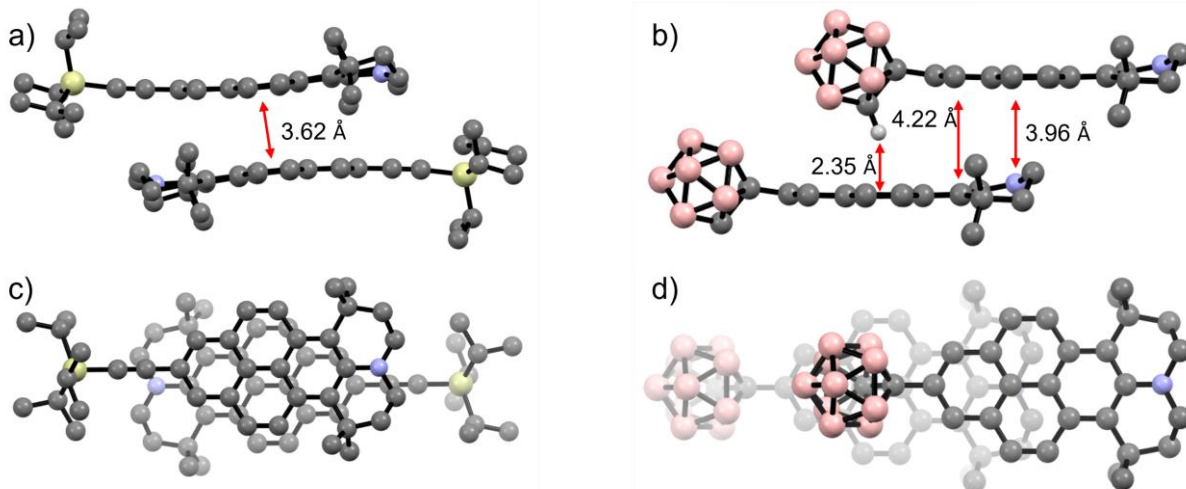


Figure 3.3. Stacking of the molecules of **3.2** (side a), top c)) and **3.4** (side a), top d)) in the solid state. Elements: B = red; C = gray, N = blue; Si = yellow. Hydrogen atoms are omitted for clarity.

3.1.3 Photophysical properties

We previously explored the photophysical and electronic properties of 3.I, 3.V and 3.VI and found that the amino group in 3.II and V was a strong enough π -donor to raise the pyrene HOMO–1 orbital, which has a significant contribution from C2 and C7, above the normal pyrene HOMO, which has a nodal plane through C2 and C7.^[50, 62] Likewise, an Et₂N moiety in 3.I had a similar effect.^[66]

We also employed 3.VI as model to study the thermodynamic equilibrium between LE and CT states resulting in dual emission. In this, and in other examples, the carborane moiety can act as a rotation-dependent acceptor making use of the *o*-carborane C1–C2 σ^* orbital. We were interested in enhancing the CT character in 3.VI by adding a strong donor at the opposite, 7-position of the pyrene moiety.

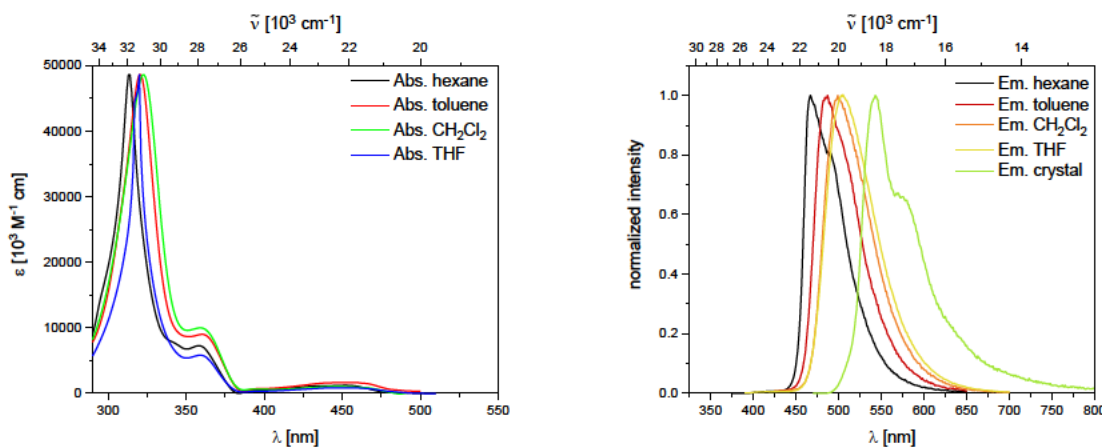


Figure 3.4. Normalized absorption (left) and emission (right) spectra compound 3.4 in solvents of different polarity and in the crystalline solid state. Extinction coefficient given for toluene.

The absorption spectrum of compound 3.4 resembles spectra of the 2,7-D- π -A-pyrenes published previously, including 3.II and 3.V.^[62] The lowest energy absorption $S_1 \leftarrow S_0$ at 450 nm is weak ($\epsilon = \text{ca. } 1600 \text{ M}^{-1} \text{ cm}^{-1}$ in toluene) and can be attributed to the short-axis-polarized and transition-dipole-forbidden L_b band (Figure 3.4, Table 3.2).^[50, 63-64] As observed previously, a strong donor results in an enhancement of this broadened L_b band while the *o*-carborane acceptor, as in 3.VI, would result in an absorption spectrum with pyrene character, again providing a good example that donors destabilize the HOMO–1 significantly whereas acceptors, studied thus far, stabilize the LUMO+1 to a lesser extent. Compared to pyrene and 3.VI, compound 3.4 shows a strong bathochromic shift in the absorption spectrum. The solvent polarity has a very small effect on the lowest L_b and the allowed L_a ($\sim 360 \text{ nm}$) transition and a significant effect on the strongest band ($\sim 325 \text{ nm}$) assigned to an overlap of the B_a and B_b bands.

Compound 3.4 shows a blue to green emission depending on the solvent (Figure 3.4). The emission maxima display a bathochromic shift with increasing solvent polarity. Apart from the emission in hexane, no vibration bands are observed in solution. In contrast to compound 3.VI, compound 3.4 does not show dual emission at any concentration, at either low or higher temperatures, in different solvents or in the solid state. The broad nature and solvatochromism does suggest a degree of charge transfer character, but the small apparent Stokes shift is an argument against this observation. In the crystalline solid state, a yellow-orange emission can be observed that could be the result of a CT due to the favorable Ψ angle of 90° (Figure 3.2). Since the distance between the pyrenes and the overlap

area lie outside the range (3.4–3.7 Å and 40–80%, respectively)^[105–106] that would typically result in excimer formation in the crystalline state, we expect a monomer emission.

The highest quantum yield in solution was observed in hexane ($\Phi = 0.35$) which is very similar to that in the solid state. Similarities in hexane and the solid state due to aggregates in hexane were ruled out as the solubility in hexane at room temperature was acceptable and different concentrations (10^{-5} – 10^{-6} mol L⁻¹) had no effect on the emission spectra.

In general, the emission properties of compound **3.4** show a slightly stronger bathochromic shift compared to **3.V** in the solid state as well as in all solvents that were in common.^[62] A significant difference was observed in the quantum yields. Compound **3.4**, with *o*-carborane as an acceptor shows a value that is 50% lower in hexane solution, compared to acceptor moieties Bpin and B(mes)₂. Yet, in contrast to these compounds, does maintain its reasonably high quantum yield in the solid state, a typical characteristic in *o*-carborane-aromatic chromophores.^[75–76, 107]

Table 3.2. Photophysical data for **3.4**.

Solvent	λ_{abs} [nm] (ϵ [10^3 M ⁻¹ cm ⁻¹])	λ_{em} [nm] ^[a]	apparent Stokes shift [cm ⁻¹]	τ [ns]	Φ
solid	495 ^[b]	543, 573	1700	8.1 (31%) 15.7 (69%)	0.35
hexane	453, 360, 314	467, 487	700	11.2 (29%) 17.0 (71%)	0.35
toluene	454 (1.6), 361 (9), 321 (48)	485	2300	7.7 (17%) 13.3 (83%)	0.29
CH ₂ Cl ₂	448, 359, 323	499	2300	5.8 (17%) 9.4 (83%)	0.13
THF	451, 360, 320	505	2400	8.1 (31%) 15.7 (69%)	0.21

[a] Excited at the respective $\lambda_{\text{abs},\text{max}}$ of the S₁ ← S₀ transition. [b] Calculated from excitation spectrum (see Supporting Information).

3.1.4 DFT and TD-DFT calculations

As a follow up study to our earlier results on 2,7-D- π -A-pyrenes we used comparable parameters for our DFT calculations. The ground-state structures were first optimized in the gas-phase at the B3LYP/6-31g(d) level of theory and, in line with our previous studies, we then used range-separated hybrid functionals that are necessary to obtain a reliable picture of the nature and relative energetic ordering of the excited states in pyrenes.^[50, 62] We have thus used the CAM-B3LYP (6-31g(d,p)) functional for the subsequent TD-DFT calculations (Table 3.4).

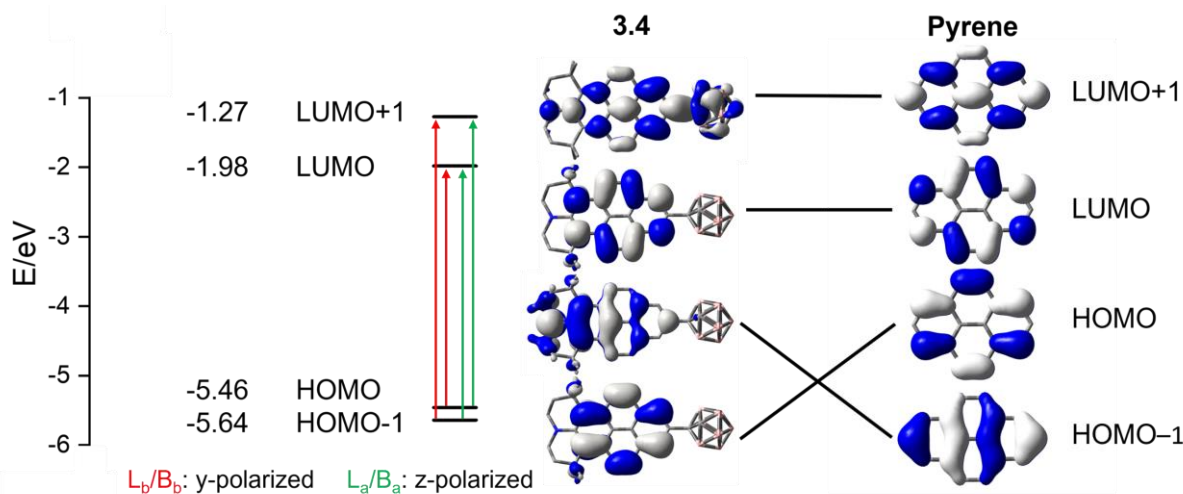


Figure 3.5. Molecular orbital diagram for **3.4** (B3LYP 6-31g(d,p)) including the transitions involved in the four experimentally observed major absorptions L_b/B_b (short-axis y-polarized) and L_a/B_a (long-axis z-polarized). The depicted orbitals follow the calculated energetic order and to the right are given the equivalent orbitals in pyrene.

Figure 3.5 shows the relevant four key frontier molecular orbitals and their major absorptions L_b/B_b (short-axis y-polarized) and L_a/B_a (long-axis z-polarized). As expected, the julolidine-like donor group results in a significant destabilization of the pyrene HOMO–1 orbital resulting in a switch of the order of the orbitals. *O*-carborane as an acceptor did stabilize the LUMO, and more pronounced the LUMO+1 orbital energies when compared with the D-pyrene **3.II**, but not to the extent that previously has been calculated for the D-A pyrene compound **3.V**, which indicated an orbital switch of the LUMO and the LUMO+1.

For comparison, Table 3.3 shows the HOMO–1, HOMO, LUMO and LUMO+1 energies and together with their similarity to pyrene orbital ordering. While $B(\text{mes})_2$ in **3.V** lowers LUMO+1 by 1.19 eV, dropping it below the LUMO of **II** which is unchanged in energy, *o*-carborane in **3.4** lowers both the LUMO+1 (by 0.69 eV) and LUMO (by 0.37 eV), leaving their energetic ordering unchanged. Thus, while the empty boron p-orbital on $B(\text{mes})_2$ significantly stabilizes LUMO+1 with which it can conjugate, there is no inductive effect on the LUMO. In contrast, there is a weaker, if any, conjugation between the LUMO+1 of the julolidine-like pyrene, and the *o*-carborane C1–C2 σ^* orbital in the ground state, but a significant –I inductive effect of the carborane on both LUMO and LUMO+1 of the julolidine-like pyrene. Likewise, while the $B(\text{mes})_2$ group has very little effect on the julolidine-like pyrene HOMO and HOMO–1, stabilizing them by only 0.05 and 0.02 eV, respectively, the *o*-carborane substituent stabilizes the julolidine-like pyrene HOMO and HOMO–1, by 0.29 and 0.37 eV, respectively.

In summary, from comparison there could be a small “conjugative” effect of the *o*-carborane C1–C2 σ^* orbital in **3.4** on the pyrene like LUMO+1, in addition to the $-I$ inductive effect, which is apparent for all four frontier orbitals.

Table 3.3. Calculated orbital energies at the B3LYP/6-31G(d,p) level of theory of **3.4** and the known compounds **3.II**, **3.V**, and **3.VI**. The related orbitals in unsubstituted pyrene are shown in parentheses.

orbital	3.II	3.V	3.VI	3.4
L+1	−0.58 (L+1)	−1.61 (LUMO)	−1.62 (L+1)	−1.27 (L+1)
LUMO	−1.61 (LUMO)	−1.77 (L+1)	−2.23 (LUMO)	−1.98 (LUMO)
HOMO	−5.17 (H−1)	−5.22 (H−1)	−6.02 (HOMO)	−5.46 (H−1)
H−1	−5.27 (HOMO)	−5.29 (HOMO)	−6.86 (H−1)	−5.64 (HOMO)

O-carborane appears to influence π -systems with its strong $-I$ inductive effect, largely independent of its rotational position. Even the most favorable position when C1–C2 is arranged perpendicular to the connected pi system, the Frank-Condon timescale of transitions permits a cluster rearrangement (bond elongation) facilitating optimal acceptor abilities. In situations and timescales that allow for geometric relaxation like rearrangements in the excited state, for example in **3.VI**, or in the case of reductions, carborane can act as an acceptor in a different way, visible in the characteristic C1–C2 bond elongation.

Table 3.4. TD-DFT results (CAM-B3LYP/6-31G(d,p)) for the observed major absorption bands of **3.4**.

State	E [eV] (λ [nm])	f	Major contributions	Symmetry
$S_1 \leftarrow S_0$	3.37 (368)	0.0427	HOMO \rightarrow LUMO (83%) H−1 \rightarrow L+1 (12%)	y (L_b)
$S_2 \leftarrow S_0$	3.73 (332)	0.2587	H−1 \rightarrow LUMO (81%) HOMO \rightarrow L+1 (16%)	z (L_a)
$S_3 \leftarrow S_0$	4.35 (285)	0.1239	H−1 \rightarrow L+1 (70%) H−2 \rightarrow LUMO (11%) HOMO \rightarrow LUMO (11%)	y (B_b)
$S_4 \leftarrow S_0$	4.64 (267)	1.8442	HOMO \rightarrow L+1 (74%) H−1 \rightarrow LUMO (18%)	z (B_a)

In contrast to pyrene and **3.V**, the donor acceptor pyrene **3.4** does not show a 50:50 (HOMO \rightarrow LUMO:HOMO−1 \rightarrow LUMO+1) weighted configuration interaction for its L_b $S_1 \leftarrow S_0$ absorption but a 83:17 ratio for this transition (Table 3.4). There is a strong resemblance to the D-pyrene compound **3.II** which, shows the same energetic ordering of the four frontier orbital and ratio in the electronic transitions. In line with the experimental photophysical data, the lowest energy transition (L_b) is weakly allowed with a calculated oscillator strength of $f = 0.0427$ due to the interaction with the z-polarized HOMO−1 \rightarrow LUMO+1 transition. With little participation of the *o*-carborane, the transitions involve mostly the N-donor lone pair and pyrene π -orbitals (Figure 3.5 and Table 3.4).

3.1.5 Electrochemical properties

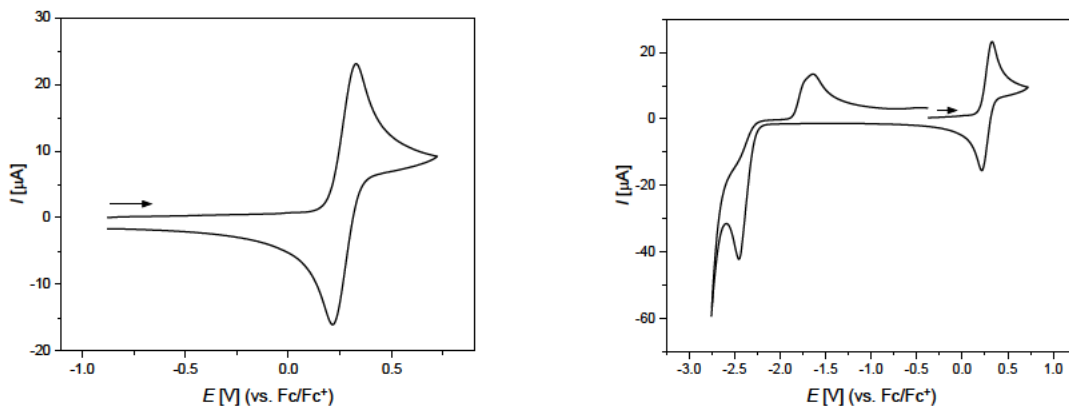


Figure 3.6. Normalized cyclic voltammograms of 3.4 as a solution in CH_2Cl_2 at room temperature; supporting electrolyte, ($[n\text{Bu}_4\text{N}][\text{PF}_6]$ (0.1 mol L⁻¹); scan rate, 200 mV s⁻¹; vs Fc/Fc^+ .

The cyclic voltammogram of 3.4 shows a reversible oxidation $E_{1/2[\text{ox}]} = 0.27$ V and an irreversible reduction at $E_{\text{pc}} = -2.45$ V (Figure 3.6, Table 3.5). The oxidation potentials of 3.4, 3.II and 3.V, all bearing the julolidine-like moiety, are nearly identical. The reduction potentials of 3.4 and 3.V are in a similar region while the B(mes)₂ moiety gives a reversible, and the *o*-carboranyl moiety an irreversible reduction. The irreversible reduction is an indication of a follow up reaction of the radical anion of 3.4. Unfortunately, there are no electrochemical properties reported for 3.VI.

Table 3.5. Cyclic voltammetry results for compounds 3.4 and 3.II measured in $\text{CH}_2\text{Cl}_2/0.1$ M $[n\text{Bu}_4\text{N}][\text{PF}_6]$, and of 3.V in THF/0.1 M $[n\text{Bu}_4\text{N}][\text{PF}_6]$ relative to the Fc/Fc^+ couple.

compound	$E_{1/2[\text{red}]}$ [V]	$E_{1/2[\text{ox}]}$ [V]
3.4	-2.45 (E_{pc})	0.27
3.II ^[62]	-	0.20
3.V ^[62]	-2.51	0.29

DFT calculations of the optimized geometry of the radical anion of 3.4 at the UB3LYP 6-31g(d,p) level of theory gave a local minimum with a *o*-carborane C1–C2 of ca. 1.67 Å and a SOMO very similar to the LUMO of 3.4 (Figure 3.5). From previous experience and due to the irreversible nature of the reduction we suspected a rearrangement of the *o*-carborane moiety expressed in a C1–C2 bond elongation. Indeed, DFT calculations scanning optimized geometries with expanding C1–C2 bond lengths, show a local minimum for the closed cluster, that we obtained initially, and a global minimum for the opened cluster (Figure 3.7). In future calculations, the obtained result needs to be confirmed by reversing the scan direction. The SOMO distribution changes from a pyrene-LUMO-like to *o*-carborane centered SOMO with a residual distribution on pyrene that resembles the pyrene LUMO+1, especially regarding the participation of the pyrene 2- and 7-positions. This is an interesting adiabatic change of electronic character of the anion of 3.4 in the ground state. The relocation of the electronic charge to the *o*-carborane, after the initial reduction, could explain the observed irreversible reduction. In Chapter 1, we describe the radical anion crystal structure of a *o*-carborane compound as an analogue to the S₁–

state, here, this could be an indication of an energetically favorable *o*-carborane centered CT excited state that coexists like in **3.VI**.^[77, 108]

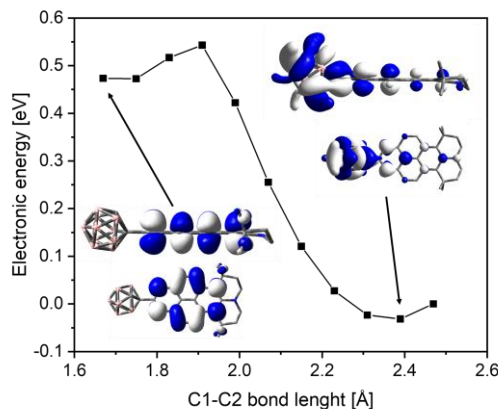


Figure 3.7. Analysis of the ground state potential energy of the radical anion of **3.4** at the UB3LYP 6-31g(d,p) level of theory. Different minima of the ground state potential energy are given by the black squares as a function of the C1–C2 bond length. The SOMO distribution at chosen points along the scan are each shown from two perspectives. Calculated single-point energies match the scan energies.

3.2 Conclusion

Following our earlier studies on julolidine-like and *o*-carboranyl pyrenes we synthesized compound **3.4**. From our synthesis we were able to isolate several interesting compounds of which **3.2** offers a multitude of functionalization's due to its terminal alkyne group. Structures of **3.2**, **3.4**, **3.5** and **3.6** were obtained by single-crystal X-ray diffraction and were compared to related previously published compounds. Compound **3.4** had one of the shortest C–N bonds indicating of a strong donor- π -conjugation and a perpendicular orientation of the *o*-carborane to the pyrene plane. Photophysical studies showed absorption properties similar to the reference molecules and a bathochromic shift of the emission. The julolidine-like donor moiety was identified to have the strongest qualitative effect on the absorption and emission spectra. Theoretical studies using DFT calculations allowed for a comparison of the HOMO-1, HOMO, LUMO and LUMO+1 orbital ordering in **3.4**, **3.II**, **3.V**, and **3.VI**, with respect to the unsubstituted pyrene. TD-DFT calculations were used to rationalize and compare the photophysical properties of **3.4** with previous results. The *o*-carborane moiety appears to influence the pyrene π -system mainly *via* its $-I$ inductive effect, largely independent of its rotational position. In the case of **3.VI**, it was shown that the long excited state lifetime allows rotation of the carborane C1–C2 bond into a position perpendicular to the attached pyrene π -system, permitting a cluster rearrangement (C–C bond elongation) facilitating the optimal acceptor ability in *o*-carborane and resulting in CT from pyrene to the carborane. As discussed in Chapter 1, in the case of a 1-electron reduction process, C1–C2 bond elongation is observed, as was calculated for the CT state of **3.VI** and related species. In the case of our new compound **3.4**, investigation of the anion *via* DFT calculations revealed an energetically favorable *o*-carborane located SOMO. This, together with the observed CT character, visible in a small bathochromic shift in the emission in solvents of increasing polarity, indicates a similar exited state dynamic for **3.4** as it was reported for **3.VI**. Further computational work is required to fully understand the nature of the excited state.

3.3 References

- [1] T. M. Figueira-Duarte, K. Müllen, *Chem. Rev.* **2011**, *111*, 7260–7314.
- [2] F. Dumur, *Eur. Polym. J.* **2020**, *126*, 109564.
- [3] K. Kalyanasundaram, J. Thomas, *J. Am. Chem. Soc.* **1977**, *99*, 2039–2044.
- [4] W.-L. Jia, T. M c Cormick, Q.-D. Liu, H. Fukutani, M. Motala, R.-Y. Wang, Y. Tao, S. Wang, *J. Mater. Chem.* **2004**, *14*, 3344–3350.
- [5] M. Eddaoudi, J. Kim, N. Rosi, D. Vodak, J. Wachter, M. O'Keeffe, O. M. Yaghi, *Science* **2002**, *295*, 469–472.
- [6] N. L. Rosi, J. Kim, M. Eddaoudi, B. Chen, M. O'Keeffe, O. M. Yaghi, *J. Am. Chem. Soc.* **2005**, *127*, 1504–1518.
- [7] C. A. Williams, A. J. Blake, C. Wilson, P. Hubberstey, M. Schröder, *Cryst. Growth Des.* **2008**, *8*, 911–922.
- [8] T. Sick, J. M. Rotter, S. Reuter, S. Kandambeth, N. N. Bach, M. Döblinger, J. Merz, T. Clark, T. B. Marder, T. Bein, D. D. Medina, *J. Am. Chem. Soc.* **2019**, *141*, 12570–12581.
- [9] S. Ghosh, Y. Tsutsui, K. Suzuki, H. Kaji, K. Honjo, T. Uemura, S. Seki, *Mol. Syst. Des. Eng.* **2019**, *4*, 325–331.
- [10] J. B. Birks, M. D. Lumb, I. H. Munro, B. H. Flowers, *Proc. Math. Phys. Eng. Sci.* **1964**, *280*, 289–297.
- [11] R. H. Templer, S. J. Castle, A. R. Curran, G. Rumbles, D. R. Klug, *Faraday Discuss.* **1999**, *111*, 41–53.
- [12] B. J. Basu, N. Vasantharajan, C. Raju, *Sens. Actuators B Chem.* **2009**, *138*, 283–288.
- [13] M. R. Pokhrel, S. H. Bossmann, *J. Phys. Chem. B* **2000**, *104*, 2215–2223.
- [14] A. Ueno, I. Suzuki, T. Osa, *Anal. Chem.* **1990**, *62*, 2461–2466.
- [15] H. Ikeda, M. Nakamura, N. Ise, N. Oguma, A. Nakamura, T. Ikeda, F. Toda, A. Ueno, *J. Am. Chem. Soc.* **1996**, *118*, 10980–10988.
- [16] Y. Fujiwara, Y. Amao, *Sens. Actuators B Chem.* **2003**, *89*, 58–61.
- [17] T. Aoyagi, H. Ikeda, A. Ueno, *Bull. Chem. Soc. Jpn.* **2001**, *74*, 157–164.
- [18] V. Merz, J. Merz, M. Kirchner, J. Lenhart, T. B. Marder, A. Krueger, *Chem. Eur. J.* **2021**, *27*, 8118–8126.
- [19] K. Ayyavoo, P. Velusamy, *New J. Chem.* **2021**, *45*, 10997–11017.
- [20] F. M. Winnik, *Chem. Rev.* **1993**, *93*, 587–614.
- [21] F. M. Winnik, M. A. Winnik, S. Tazuke, *J. Phys. Chem.* **1987**, *91*, 594–597.
- [22] J. Duhamel, *Langmuir* **2012**, *28*, 6527–6538.
- [23] T. Zhang, Scott D. Taylor, M. Palmer, J. Duhamel, *Biophys. J.* **2016**, *111*, 1267–1277.
- [24] M. Fowler, J. Duhamel, X. P. Qiu, E. Korchagina, F. M. Winnik, *J. Polym. Sci. B Polym. Phys.* **2018**, *56*, 308–318.
- [25] D. Kim, R. Amos, M. Gauthier, J. Duhamel, *Langmuir* **2018**, *34*, 8611–8621.
- [26] D. Sahoo, V. Narayanaswami, C. M. Kay, R. O. Ryan, *Biochemistry* **2000**, *39*, 6594–6601.
- [27] P. Somerharju, *Chem. Phys. Lipids* **2002**, *116*, 57–74.
- [28] N. I. Zahid, L. Ji, M. F. Khyasudeen, A. Friedrich, R. Hashim, T. B. Marder, O. K. Abou-Zied, *Langmuir* **2019**, *35*, 9584–9592.
- [29] M. E. Østergaard, P. J. Hrdlicka, *Chem. Soc. Rev.* **2011**, *40*, 5771–5788.
- [30] C. Wu, C. Wang, L. Yan, C. J. Yang, *J. Biomed. Nanotechnol.* **2009**, *5*, 495–504.
- [31] Ž. Ban, Z. Karačić, S. Tomić, H. Amini, T. B. Marder, I. Piantanida, *Molecules* **2021**, *26*.
- [32] G. K. Kole, J. Merz, A. Amar, B. Fontaine, A. Boucekkine, J. Nitsch, S. Lorenzen, A. Friedrich, I. Krummenacher, M. Košćak, H. Braunschweig, I. Piantanida, J.-F. Halet, K. Müller-Buschbaum, T. B. Marder, *Chem. Eur. J.* **2021**, *27*, 2837–2853.
- [33] K. Yamana, H. Zako, K. Asazuma, R. Iwase, H. Nakano, A. Murakami, *Angew. Chem. Int. Ed.* **2001**, *40*, 1104–1106.
- [34] V. A. Korshun, D. A. Stetsenko, M. J. Gait, *J. Chem. Soc., Perkin trans. 1* **2002**, 1092–1104.

- [35] E. Kostenko, M. Dobrikov, D. Pyshnyi, V. Petyuk, N. Komarova, V. Vlassov, M. Zenkova, *Nucleic Acids Res.* **2001**, *29*, 3611–3620.
- [36] A. Mahara, R. Iwase, T. Sakamoto, K. Yamana, T. Yamaoka, A. Murakami, *Angew. Chem. Int. Ed.* **2002**, *41*, 3648–3650.
- [37] I. V. Astakhova, D. Lindegaard, V. A. Korshun, J. Wengel, *Chem. Commun.* **2010**, *46*, 8362–8364.
- [38] U. B. Christensen, E. B. Pedersen, *Nucleic Acids Res.* **2002**, *30*, 4918–4925.
- [39] V. V. Filichev, E. B. Pedersen, *Org. Biomol. Chem.* **2003**, *1*, 100–103.
- [40] K. Gröger, D. Baretic, I. Piantanida, M. Marjanović, M. Kralj, M. Grabar, S. Tomić, C. Schmuck, *Org. Biomol. Chem.* **2011**, *9*, 198–209.
- [41] I. V. Astakhova, A. D. Malakhov, I. A. Stepanova, A. V. Ustinov, S. L. Bondarev, A. S. Paramonov, V. A. Korshun, *Bioconjugate Chem.* **2007**, *18*, 1972–1980.
- [42] L. Hernandez-Folgado, C. Schmuck, S. Tomić, I. Piantanida, *Bioorg. Med. Chem. Lett.* **2008**, *18*, 2977–2981.
- [43] L. Hernandez-Folgado, D. Baretic, I. Piantanida, M. Marjanović, M. Kralj, T. Rehm, C. Schmuck, *Chem. Eur. J.* **2010**, *16*, 3036–3056.
- [44] J. Wu, Y. Zou, C. Li, W. Sicking, I. Piantanida, T. Yi, C. Schmuck, *J. Am. Chem. Soc.* **2012**, *134*, 1958–1961.
- [45] F. Ma, W.-j. Liu, Q. Zhang, C.-y. Zhang, *Chem. Commun.* **2017**, *53*, 10596–10599.
- [46] W. M. Vaughn, G. Weber, *Biochemistry* **1970**, *9*, 464–473.
- [47] O. Oter, A. C. Ribou, *J. Fluoresc.* **2009**, *19*, 389–397.
- [48] M. J. Wawi, A. Bijoux, N. Inguimbert, C. Mahler, S. Wagner, T. B. Marder, A.-C. Ribou, *Chem. Bio. Chem.* **2021**, *22*, 1676–1685.
- [49] M. J. Wawi, C. Mahler, N. Inguimbert, T. B. Marder, A.-C. Ribou, *Free Radic. Res.* **2022**, 1–15.
- [50] A. G. Crawford, A. D. Dwyer, Z. Liu, A. Steffen, A. Beeby, L.-O. Pålsson, D. J. Tozer, T. B. Marder, *J. Am. Chem. Soc.* **2011**, *133*, 13349–13362.
- [51] D. N. Coventry, A. S. Batsanov, A. E. Goeta, J. A. Howard, T. B. Marder, R. N. Perutz, *Chem. Commun.* **2005**, 2172–2174.
- [52] M. Ottonelli, M. Piccardo, D. Duce, S. Thea, G. Dellepiane, *J. Phys. Chem. A* **2012**, *116*, 611–630.
- [53] H. Ju, K. Wang, J. Zhang, H. Geng, Z. Liu, G. Zhang, Y. Zhao, D. Zhang, *Chem. Mater.* **2017**, *29*, 3580–3588.
- [54] J. M. Casas-Solvas, J. D. Howgego, A. P. Davis, *Org. Biomol. Chem.* **2014**, *12*, 212–232.
- [55] X. Feng, J.-Y. Hu, C. Redshaw, T. Yamato, *Chem. Eur. J.* **2016**, *22*, 11898–11916.
- [56] Q. Lu, G. K. Kole, A. Friedrich, K. Müller-Buschbaum, Z. Liu, X. Yu, T. B. Marder, *J. Org. Chem.* **2020**, *85*, 4256–4266.
- [57] J. Merz, M. Dietz, Y. Vonhausen, F. Wober, A. Friedrich, D. Sieh, I. Krummenacher, H. Braunschweig, M. Moos, M. Holzapfel, C. Lambert, T. B. Marder, *Chem. Eur. J.* **2020**, *26*, 438–453.
- [58] L. Zöphel, V. Enkelmann, K. Müllen, *Org. Lett.* **2013**, *15*, 804–807.
- [59] L. Zöphel, D. Beckmann, V. Enkelmann, D. Chercka, R. Rieger, K. Müllen, *Chem. Commun.* **2011**, *47*, 6960.
- [60] A. G. Crawford, Z. Liu, I. A. Mkhaldid, M. H. Thibault, N. Schwarz, G. Alcaraz, A. Steffen, J. C. Collings, A. S. Batsanov, J. A. Howard, T. B. Marder, *Chem. Eur. J.* **2012**, *18*, 5022–5035.
- [61] A. S. Batsanov, J. A. K. Howard, D. Albesa-Jové, J. C. Collings, Z. Liu, I. A. I. Mkhaldid, M.-H. Thibault, T. B. Marder, *Cryst. Growth Des.* **2012**, *12*, 2794–2802.
- [62] J. Merz, J. Fink, A. Friedrich, I. Krummenacher, H. H. Al Mamari, S. Lorenzen, M. Haehnel, A. Eichhorn, M. Moos, M. Holzapfel, H. Braunschweig, C. Lambert, A. Steffen, L. Ji, T. B. Marder, *Chem. Eur. J.* **2017**, *23*, 13164–13180.
- [63] E. W. Thulstrup, J. W. Downing, J. Michl, *Chem. Phys.* **1977**, *23*, 307–319.
- [64] F. W. Langkilde, E. W. Thulstrup, J. Michl, *J. Chem. Phys.* **1983**, *78*, 3372–3381.
- [65] C. Lambert, J. Ehbets, D. Rausch, M. Steege, *J. Org. Chem.* **2012**, *77*, 6147–6154.
- [66] L. Ji, A. Lorbach, R. M. Edkins, T. B. Marder, *J. Org. Chem.* **2015**, *80*, 5658–5665.

- [67] Z. Zhang, R. M. Edkins, J. Nitsch, K. Fucke, A. Eichhorn, A. Steffen, Y. Wang, T. B. Marder, *Chem. Eur. J.* **2015**, *21*, 177–190.
- [68] G. Pinkus, *Ber. Dtsch. Chem. Ges.* **1892**, *25*, 2798–2806.
- [69] B. Balaganesan, S.-W. Wen, C. H. Chen, *Tetrahedron Lett.* **2003**, *44*, 145–147.
- [70] K. H. Lee, Y.-K. Kim, S.-S. Yoon, *Bull. Korean Chem. Soc.* **2012**, *33*, 3433–3436.
- [71] Z. E. X. Dance, M. J. Ahrens, A. M. Vega, A. B. Ricks, D. W. McCamant, M. A. Ratner, M. R. Wasielewski, *J. Am. Chem. Soc.* **2008**, *130*, 830–832.
- [72] R. Kurata, K. Tanaka, A. Ito, *J. Org. Chem.* **2016**, *81*, 137–145.
- [73] L. Ji, R. M. Edkins, A. Lorbach, I. Krummenacher, C. Brückner, A. Eichhorn, H. Braunschweig, B. Engels, P. J. Low, T. B. Marder, *J. Am. Chem. Soc.* **2015**, *137*, 6750–6753.
- [74] R. Kurata, A. Ito, M. Gon, K. Tanaka, Y. Chujo, *J. Org. Chem.* **2017**, *82*, 5111–5121.
- [75] R. Núñez, M. Tarrés, A. Ferrer-Ugalde, F. F. d. Biani, F. Teixidor, *Chem. Rev.* **2016**, *116*, 14307–14378.
- [76] J. Ochi, K. Tanaka, Y. Chujo, *Angew. Chem. Int. Ed.* **2020**, *59*, 9841–9855.
- [77] L. Ji, S. Riese, A. Schmiedel, M. Holzapfel, M. Fest, J. Nitsch, B. F. E. Curchod, A. Friedrich, L. Wu, H. H. Al Mamari, S. Hammer, J. Pflaum, M. A. Fox, D. J. Tozer, M. Finze, C. Lambert, T. B. Marder, *Chem. Sci.* **2022**, *13*, 5205–5219.
- [78] M. A. Fox, C. Nervi, A. Crivello, P. J. Low, *Chem. Commun.* **2007**, 2372–2374.
- [79] L. Weber, J. Kahlert, R. Brockhinke, L. Böhling, A. Brockhinke, H.-G. Stammler, B. Neumann, R. A. Harder, M. A. Fox, *Chem. Eur. J.* **2012**, *18*, 8347–8357.
- [80] L. Weber, J. Kahlert, L. Böhling, A. Brockhinke, H.-G. Stammler, B. Neumann, R. A. Harder, P. J. Low, M. A. Fox, *Dalton Trans.* **2013**, *42*, 2266–2281.
- [81] S.-Y. Kim, Y.-J. Cho, G. F. Jin, W.-S. Han, H.-J. Son, D. W. Cho, S. O. Kang, *Phys. Chem. Chem. Phys.* **2015**, *17*, 15679–15682.
- [82] J. Ochi, K. Yuhara, K. Tanaka, Y. Chujo, *Chem. Eur. J.* **2022**, *28*, e202200155.
- [83] H. So, J. H. Kim, J. H. Lee, H. Hwang, D. K. An, K. M. Lee, *Chem. Commun.* **2019**, *55*, 14518–14521.
- [84] K. Nishino, K. Tanaka, Y. Chujo, *Asian J. Org. Chem.* **2019**, *8*, 2228–2232.
- [85] X. Wu, J. Guo, J. Zhao, Y. Che, D. Jia, Y. Chen, *Dyes Pigm.* **2018**, *154*, 44–51.
- [86] K. Nishino, H. Yamamoto, K. Tanaka, Y. Chujo, *Asian J. Org. Chem.* **2017**, *6*, 1818–1822.
- [87] H. Naito, K. Nishino, Y. Morisaki, K. Tanaka, Y. Chujo, *Angew. Chem. Int. Ed.* **2017**, *56*, 254–259.
- [88] K. Nishino, H. Yamamoto, K. Tanaka, Y. Chujo, *Org. Lett.* **2016**, *18*, 4064–4067.
- [89] S. Mukherjee, P. Thilagar, *Chem. Commun.* **2016**, *52*, 1070–1093.
- [90] X. Wu, J. Guo, Y. Cao, J. Zhao, W. Jia, Y. Chen, D. Jia, *Chem. Sci.* **2018**, *9*, 5270–5277.
- [91] Y. Morisaki, M. Tominaga, T. Ochiai, Y. Chujo, *Chem. Asian J.* **2014**, *9*, 1247–1251.
- [92] Y. Morisaki, M. Tominaga, Y. Chujo, *Chem. Eur. J.* **2012**, *18*, 11251–11257.
- [93] V. I. Bregadze, *Chem. Rev.* **2002**, *92*, 209–223.
- [94] D. Tahaoğlu, H. Usta, F. Alkan, *J. Phys. Chem. A* **2022**.
- [95] K. Nishino, K. Uemura, M. Gon, K. Tanaka, Y. Chujo, *Molecules* **2017**, *22*, 2009.
- [96] K. Nishino, K. Uemura, K. Tanaka, Y. Chujo, *New J. Chem.* **2018**, *56*, 11370.
- [97] S. Kim, J. H. Lee, H. So, M. Kim, M. S. Mun, H. Hwang, M. H. Park, K. M. Lee, *Inorg. Chem. Front.* **2020**, *7*, 2949–2959.
- [98] X. Yang, B. Zhang, Y. Gao, C. Liu, G. Li, B. Rao, D. Chu, N. Yan, M. Zhang, G. He, *Adv. Sci.* **2022**, *9*, 2101652.
- [99] J.-S. Tang, M. Tian, W.-B. Sheng, C.-C. Guo, *Synth.* **2012**, *2012*, 541–546.
- [100] A. Toppino, A. R. Genady, M. E. El-Zaria, J. Reeve, F. Mostofian, J. Kent, J. F. Valliant, *Inorg. Chem.* **2013**, *52*, 8743–8749.
- [101] A. Korotvíčka, I. Šnajdr, P. Štěpnička, I. Císařová, Z. Janoušek, M. Kotora, *Eur. J. Inorg. Chem.* **2013**, *2013*, 2789–2798.
- [102] R. L. Ernest, W. Quintana, R. Rosen, P. J. Carroll, L. G. Sneddon, *Organometallics* **1987**, *6*, 80–88.

Chapter 3

- [103] A. R. Turner, H. E. Robertson, K. B. Borisenco, D. W. H. Rankin, M. A. Fox, *Dalton Trans.* **2005**, 1310–1318.
- [104] A. S. Batsanov, J. C. Collings, R. M. Ward, A. E. Goeta, L. Porrès, A. Beeby, J. A. Howard, J. W. Steed, T. B. Marder, *Cryst. Eng. Comm.* **2006**, *8*, 622–628.
- [105] Y. Ge, Y. Wen, H. Liu, T. Lu, Y. Yu, X. Zhang, B. Li, S.-T. Zhang, W. Li, B. Yang, *J. Mater. Chem. C* **2020**, *8*, 11830–11838.
- [106] J. Hoche, H.-C. Schmitt, A. Humeniuk, I. Fischer, R. Mitrić, M. I. Röhr, *Phys. Chem. Chem. Phys.* **2017**, *19*, 25002–25015.
- [107] K. Kokado, Y. Chujo, *Macromolecules* **2009**, *42*, 1418–1420.
- [108] J. Krebs, M. Haehnel, I. Krummenacher, A. Friedrich, H. Braunschweig, M. Finze, L. Ji, T. B. Marder, *Chem. Eur. J.* **2021**, *27*, 8159–8167.

4. SUMMARY/ZUSAMMENFASSUNG

4.1 Summary of Chapter 1

Chapter 1 reports the synthesis and properties of the unusual bis(*o*-carboranyl) substituted 3-coordinate borane $[(1-(4-\text{MeC}_6\text{H}_4)-\text{closo-}1,2-\text{C}_2\text{B}_{10}\text{H}_{9-2-})_2(4-\text{MeC}_6\text{H}_4)\text{B}]$ (**1.1**) (Figure 4.1.1). Cyclic voltammetry studies revealed a partially reversible one-electron reduction, and EPR spectroscopy confirmed the paramagnetic nature of the anion and the involvement of the *o*-carboranyl moieties in the delocalization of the unpaired electron. The resulting radical anion **1.1**^{•-} was isolated and crystallized using several different reduction protocols.

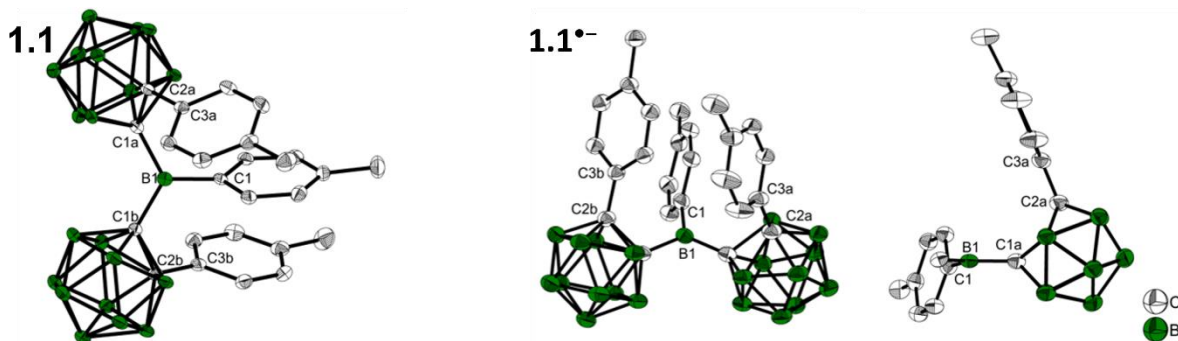


Figure 4.1.1: Left: Molecular structure of **1.1** in the solid state at 100 K. H atoms are omitted for clarity. Thermal ellipsoids are drawn at 50% probability. Middle: Molecular structure of $\{\text{K}[18]\text{crown-6}\cdot(\text{THF})_2\}^+\cdot\mathbf{1.1}^{\bullet-}$ in the solid state at 100 K. H atoms, solvent molecules, and cations are omitted for clarity. Thermal ellipsoids are drawn at 50% probability. Right: Molecular structure of $\{\text{K}[18]\text{crown-6}\cdot(\text{THF})_2\}^+\cdot\mathbf{1.1}^{\bullet-}$ viewed perpendicular to the C1a–C2a bond, with the second (*p*-tolyl)carborane moiety omitted for clarity.

The solid-state structure of the radical anion (Figure 4.1.1) revealed major contributions of the 3-coordinate boron and one of the *o*-carboranyl moieties to the delocalization of the extra electron, but only a negligible change of bond distances within the second *o*-carboranyl moiety. The perpendicular orientation of the reduced *o*-carborane fragment facilitates optimal overlap between the 3-coordinate boron p_z-orbital and the C1–C2 σ*-anti-bonding orbital leading to a shorter B1–C1a and longer C1a–C2a bond (Figure 4.1.2). Strong similarities between the 2n+3 skeletal electron *o*-carborane structure of the radical anion **1.1**^{•-} and the optimized structure of the S₁ state of **1.1** confirm predictions regarding geometrical reorganization in the CT process which involves charge transfer to the *o*-carborane moiety.

Summary

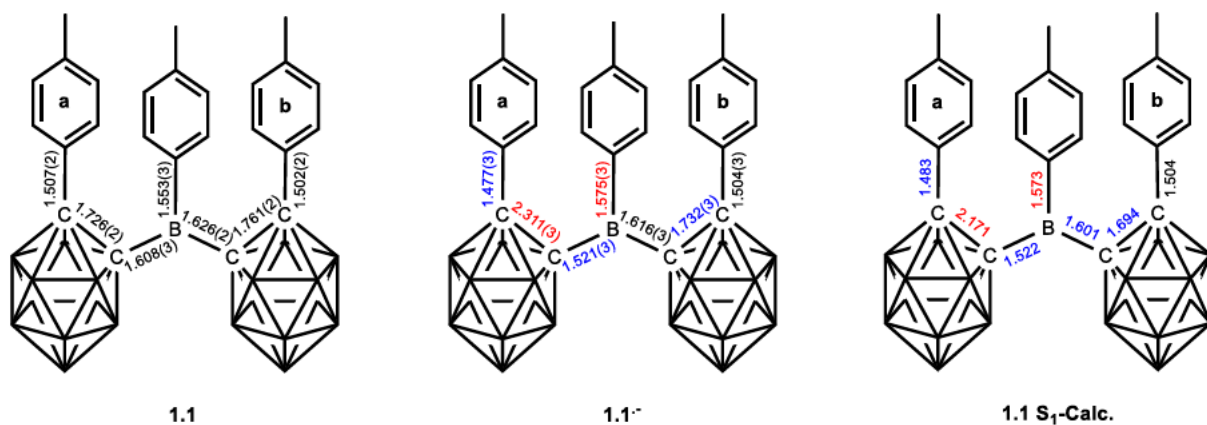


Figure 4.1.2: Bond lengths in **1.1**, **1.1^{•-}** and the optimized **S₁** state of **1.1**. Red: increase in bond length, blue: decrease in bond length.

Photophysical studies (Figure 4.1.3) show a CT emission with a large Stokes shift of up to 9500 cm^{-1} . Like other known *o*-carborane dyads, **1.1** has a low quantum yield in solution with a strong increase in the solid state ($\Phi_F = 19\%$). Upon reduction, a broad low energy absorption appears at ca. 600 nm for **1.1^{•-}**. The experimental observations are in good agreement with the respective (TD-)DFT calculations at the (CAM-)B3LYP/6-31G* level of theory for the optimized ground state geometries as well as the photophysical transitions.

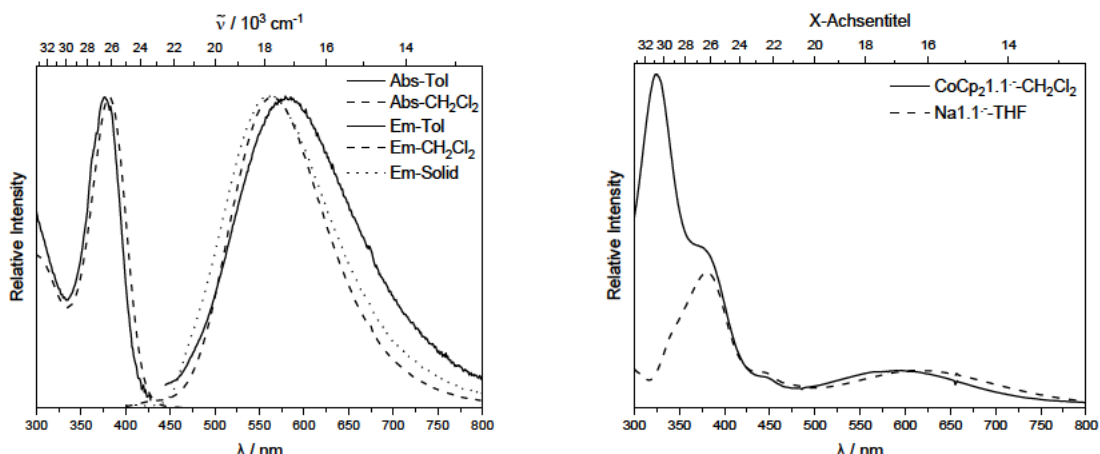
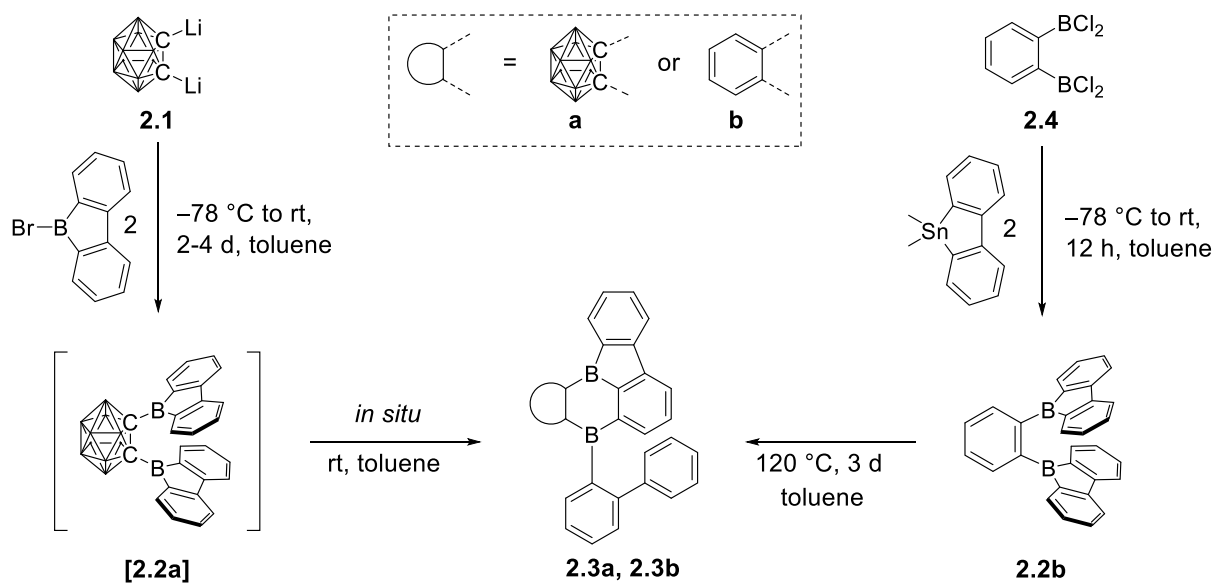


Figure 4.1.3: Left: absorption (<450 nm) and emission (>450 nm, excited at lowest energy absorption maximum) spectra of **1.1** in toluene (solid line), **CH₂Cl₂** (dashed line) and solid state (dotted line). Right: absorption spectra of **CoCp₂+1.1^{•-}** in **CH₂Cl₂** (solid line) and **[K[18]crown-6·(THF)₂]⁺1.1^{•-}** in **THF** (dashed line).

4.2 Summary of Chapter 2

Chapter 2 reports the attempted synthesis of 1,2-bis-9-borafluorenyl-*o*-carborane (**[2.2a]**), using *ortho*-carborane as a three-dimensional backbone to lower the boron centered LUMO energies in 9-borafluorenes. The synthetic approach resulted in an intramolecular rearrangement at room temperature giving compound **2.3a** (Scheme 4.2.1), the structure of which was confirmed by single-crystal X-ray diffraction. The isolation of only **2.3a** from reactions carried out under different conditions is an indication that the rate of rearrangement is greater than the rate at which **[2.2a]** is formed. A theoretical investigation of the transition state, using DFT calculations, showed that the rearrangement follows an S_EAr-like mechanism that is enabled by a low lying LUMO, the targeted feature of compound **[2.2a]**. The same calculations, for an analogous compound containing phenyl-backbone rather than the carboranyl one, predict a significantly higher barrier for the rearrangement process. As a result, it was possible to synthesize and characterize 1,2-bis-9-borafluorenylbenzene (**2.2b**), a more electron-rich analog of **[2.2a]**. As predicted by the calculations, the rearrangement also takes place at a higher temperature, for compound **2.2b**. Product **2.3b** was isolated and fully characterized.



Scheme 4.2.1. Synthesis of **2.2b**, **2.3a** and **2.3b**. The unlabeled cluster vertices represent BH units.

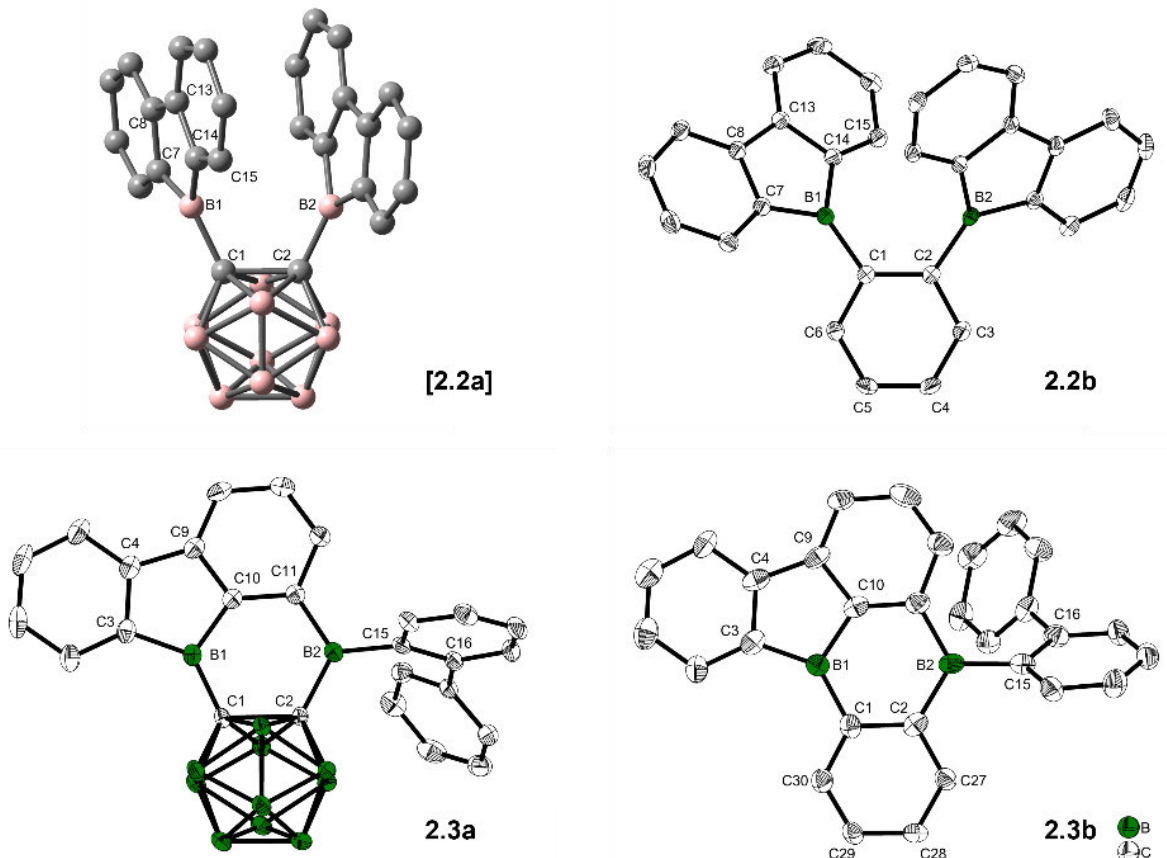


Figure 4.2.1. Optimized structure of **[2.2a]** at the ω B97X-D/6-31G(d,p) level of theory in the gas phase and solid-state molecular structures of **2.2b**, **2.3a** and **2.3b** from single-crystal X-ray diffraction at 100 K. Atomic displacement ellipsoids are drawn at the 50% probability level and hydrogen atoms are omitted for clarity. For **2.3b**, only one of four symmetry-independent molecules is shown, and solvent molecules are omitted for clarity.

The optimized structure of **[2.2a]** and the single-crystal structure of **2.2b** as well as the single-crystal structures **2.3a** and **2.3b** were compared and are shown in Figure 4.2.1. The essential difference between **[2.2a]** and **2.2b** is a longer backbone C1–C2 bond length in **[2.2a]** that should result in a longer B–B distance but is compensated by an attraction between the 9-borafluorenyl units visible in the B1–C1–C2 angles. The essential difference between **2.3a** and **2.3b** is in the one phenyl-/o-carboranyl ring and, therefore, the size of the π -system and the inductive electron withdrawing effect *via* the o-carborane cluster.

Summary

Photophysical studies show a 9-borafluorene-like transition character in the weak absorption bands at ca. 450 nm and yellow emissions at ca. 590 nm for 2.3a and 2.3b, respectively (Figure 4.2.2). This was supported by TD-DFT calculations that fit the experimental observations nicely.

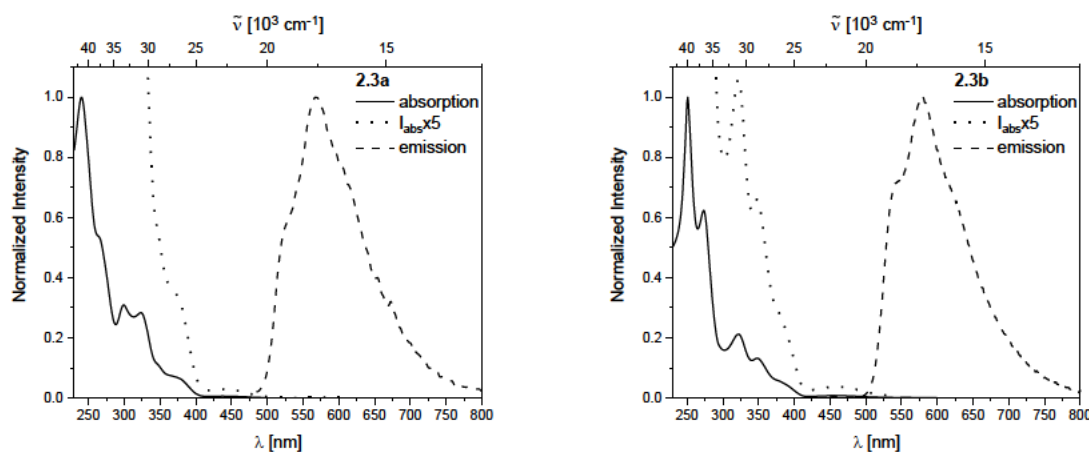
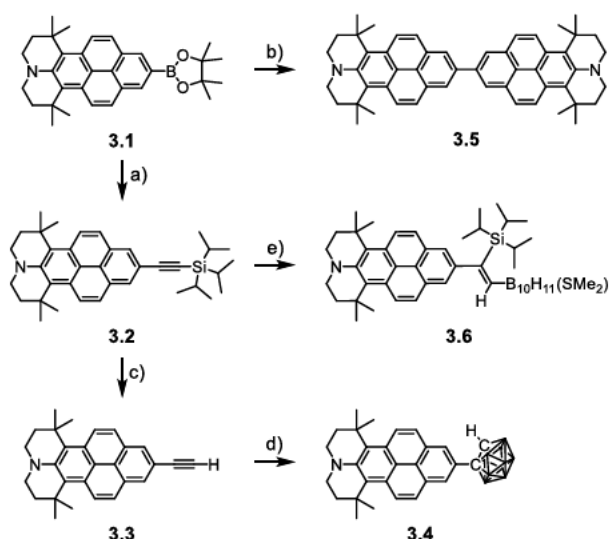


Figure 4.2.2. Normalized absorption and emission spectra of the rearranged compounds 2.3a (left) and 2.3b (right) in toluene. As a dotted line, the five times enhanced absorption is shown to visualize the weak, lowest energy transition.

A strong electron affinity was observed for 2.3a and 2.3b, with low reduction potentials of $E_{1/2} = -1.03$ and $E_{1/2} = -1.17$ V, respectively. In general, the reactivity shown herein was strongly influenced by *o*-carborane as a backbone and offers a pathway to generate BC₄B-six-membered ring-containing PAHs for both phenyl- and *o*-carboranyl-containing compounds.

4.3 Summary of Chapter 3

In Chapter 3, we were interested in generating a charge transfer (CT) transition from a strong julolidine-like donor moiety to an *o*-carborane acceptor across a pyrene bridge using the 2,7-positions of the pyrene moiety. This was based on a recent report from our group on the thermodynamic equilibrium between locally excited (LE) and CT states of the related 1-(2'-pyrenyl)-*o*-carborane compound which did not contain the strongly π -donating julolidine-like moiety. For the synthesis of the new compound, we started with the known compound 3.1 and, after 3 steps, obtained the target compound 3.4 (Scheme 4.3.1). The intermediate 3.3 offers a wide range of possibility for further functionalization due to its terminal alkyne group. Compound 3.5 was obtained as a homocoupled side product due to trace oxygen in reaction a) and was characterized crystallographically. Compound 3.6 is the result of a B–H insertion and rearrangement of the silyl group at the alkyne, and it was also characterized crystallographically.



Scheme 4.3.1. Synthesis of compounds 3.4 and 3.6 and byproduct 3.5. a) I-C \equiv C-TIPS (1.1 equiv), Pd(dba)₂ (10 mol %), Cs₂CO₃ (1.1 equiv), rt, methanol, 20 h, 45%; b) Compound 5 was isolated as byproduct in reaction a) due to trace oxygen, 3%. c) TBAF (5 equiv), rt, THF, 1 h, 82%; d) B₁₀H₁₂(SMe₂)₂ (1.5 equiv), AgOAc (10 mol %), 100 °C, toluene, 2 d, 36%; e) B₁₀H₁₂(SMe₂)₂ (1.5 equiv), AgOAc (10 mol %), 100 °C, toluene, 2 d, 62%. The unlabeled cluster vertices represent BH units.

Compounds 3.2, 3.4, 3.5 and 3.6 were investigated by single-crystal X-ray diffraction (Figure 4.3.2) and compared to similar known compounds. Noteworthy is the short C_{pyrene}–N bond, that is an indication for a strong delocalization of the lone pair to the pyrene system.

Summary

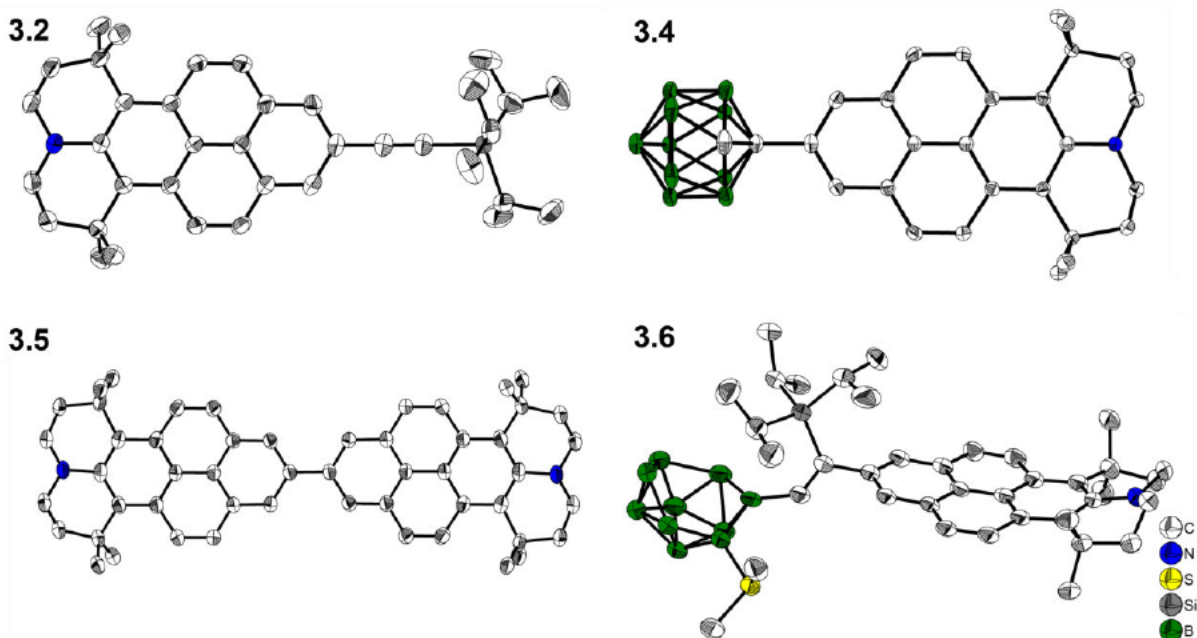


Figure 4.3.1. Solid state molecular structure of 3.2, 3.4, 3.5 and 3.6 from single-crystal X-ray diffraction at 100 K. Atomic displacement ellipsoids are drawn at the 50% probability level. Hydrogen atoms and for 3.5 and 3.6 solvent molecules are omitted for clarity.

Photophysical studies of 3.4 showed that the lowest energy absorption $S_1 \leftarrow S_0$ at 450 nm is weak ($\epsilon = \text{ca. } 1600 \text{ M}^{-1}\text{cm}^{-1}$) and can be attributed to the short-axis-polarized and transition-dipole-forbidden L_b band. Compared to pyrene, compound 3.4 shows a strong bathochromic shift in the absorption spectrum, a blue to green emission depending on the solvent, and a yellow-orange emission in the solid state (Figure 4.3.3). The emission maxima display a bathochromic shift with increasing solvent polarity. The highest quantum yield in solution was observed in hexane ($\Phi = 0.35$) which is very similar to that in the solid state.

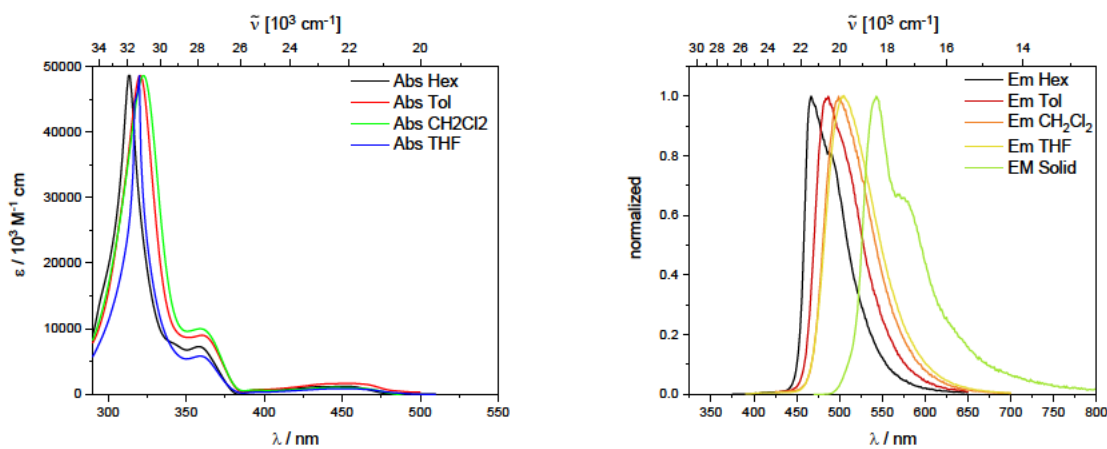


Figure 4.3.3. Normalized absorption (left) and emission (right) spectra compound 3.4. Extinction coefficient given for toluene.

As expected, the julolidine-like donor group results in a significant destabilization of the pyrene-like HOMO-1 resulting in a switch of the order of the HOMO and HOMO-1. *O*-carborane as an acceptor stabilizes the LUMO and, slightly more pronounced, the LUMO+1 when compared to known examples.

Summary

The extent of the stabilization is smaller, than that observed for $\text{B}(\text{mes})_2$ and, thus, did not result in an orbital switch of the LUMO and the LUMO+1 (Figure 4.3.2).

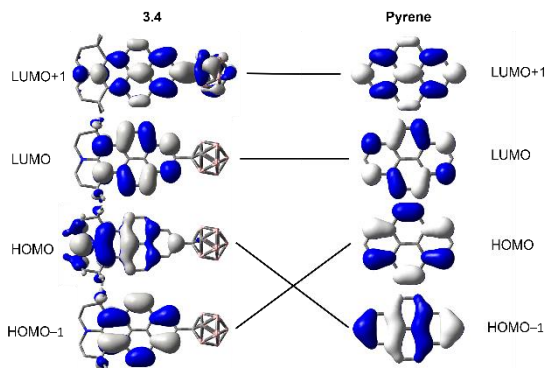


Figure 4.3.2. Molecular orbital diagram for **3.4** and pyrene. The orbitals depicted follow the calculated energetic order and are compared by their shape equivalent orbitals.

The *o*-carborane moiety appears to influence the pyrene π -system mainly *via* its $-I$ inductive effect, largely independent of its rotational position. In the case of 1-(2'-pyrenyl)-*o*-carborane, it was shown that the long excited state lifetime allows rotation of the carborane C1–C2 bond into a position perpendicular to the attached pyrene π -system, permitting a cluster rearrangement (C–C bond elongation) facilitating the optimal acceptor ability in *o*-carborane and resulting in CT from pyrene to the carborane. As discussed in Chapter 1, in the case of a 1-electron reduction process, C1–C2 bond elongation is observed, as was calculated for the CT state of 1-(2'-pyrenyl)-*o*-carborane and related species. In the case of our new compound **3.4**, while we do observe a small bathochromic shift in the emission in solvents of increasing polarity, suggesting a degree of CT character, further, ongoing computational work is required to understand fully the nature of the excited state.

4.4 Zusammenfassung Chapter 1

Kapitel 1 beschreibt die Synthese und die Eigenschaften eines ungewöhnlichen bis(*o*-Carboranyl)-substituierten, dreifach-koordinierten Borans [*(1-(4-MeC₆H₄)-closo-1,2-C₂B₁₀H₉-2-)₂(4-MeC₆H₄)B*] (**1.1**) (Abbildung 4.1.1). Zyklische Voltammetrie-Studien ergaben eine teilweise reversible Reduktion mit einem Elektron, und die EPR-Spektroskopie bestätigte die paramagnetische Natur des Anions und die Beteiligung der *o*-Carboranyl-Anteile an der Delokalisierung des ungepaarten Elektrons. Das resultierende radikalische Anion **1.1^{•-}** wurde mit verschiedenen Reduktionsprotokollen isoliert und kristallisiert.

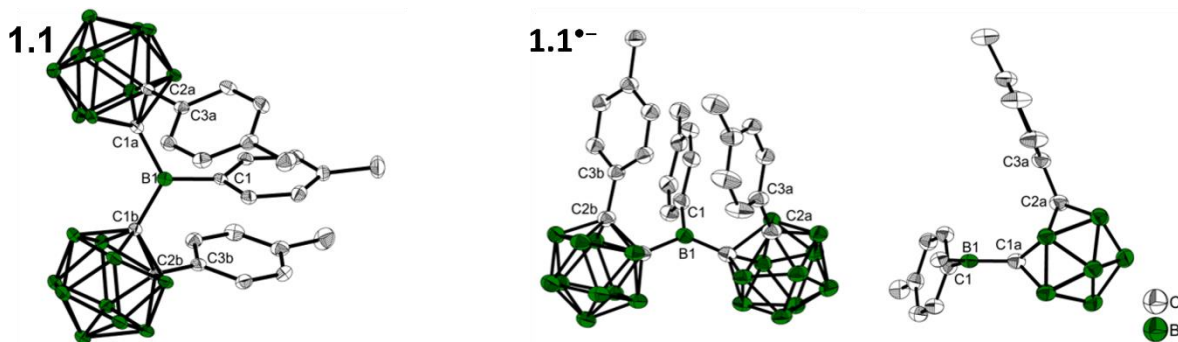


Abbildung 4.1.1: Links: Molekülstruktur von **1.1** im festen Zustand bei 100 K. Die H-Atome wurden zur besseren Übersicht weggelassen. Die thermischen Ellipsoide sind mit einer Wahrscheinlichkeit von 50% gezeichnet. Mitte: Molekülstruktur von **{K[18]crown-6·(THF)₂}⁺·1.1^{•-}** im festen Zustand bei 100 K. H-Atome, Lösungsmittelmoleküle und Kationen wurden zur besseren Übersicht weggelassen. Die thermischen Ellipsoide sind mit einer Wahrscheinlichkeit von 50 % gezeichnet. Rechts: Molekülstruktur von **{K[18]crown-6·(THF)₂}⁺·1.1^{•-}** senkrecht zur C1a–C2a-Bindung gesehen, wobei die zweite (*p*-Tolyl)carboran-Einheit zur besseren Übersicht weggelassen wurde.

Die Festkörperstruktur des radikalischen Anions (Abbildung 4.1.1) zeigt, dass das dreifach koordinierte Bor und eine der *o*-Carboranyleinheiten wesentlich zur Delokalisierung des zusätzlichen Elektrons beitragen, während sich die Bindungsabstände innerhalb der zweiten *o*-Carboranyleinheit nur unwesentlich ändern. Die senkrechte Ausrichtung des reduzierten *o*-Carboran-Fragments erleichtert eine optimale Überlappung zwischen dem pz-Orbital des dreifach koordinierten Bors und dem C1–C2 σ*-Orbital, was zu einer kürzeren B1–C1a- und einer längeren C1a–C2a-Bindung führt (Abbildung 4.1.2). Starke Ähnlichkeiten zwischen der 2n+3-Skelett-Elektronen-*o*-Carboran-Struktur des radikalischen Anions **1.1^{•-}** und der optimierten Struktur des S₁-Zustands von **1.1** bestätigen die Vorhersagen bezüglich der geometrischen Reorganisation im CT-Prozess, die einen Ladungstransfer zum *o*-Carboran-Teil beinhaltet.

Zusammenfassung

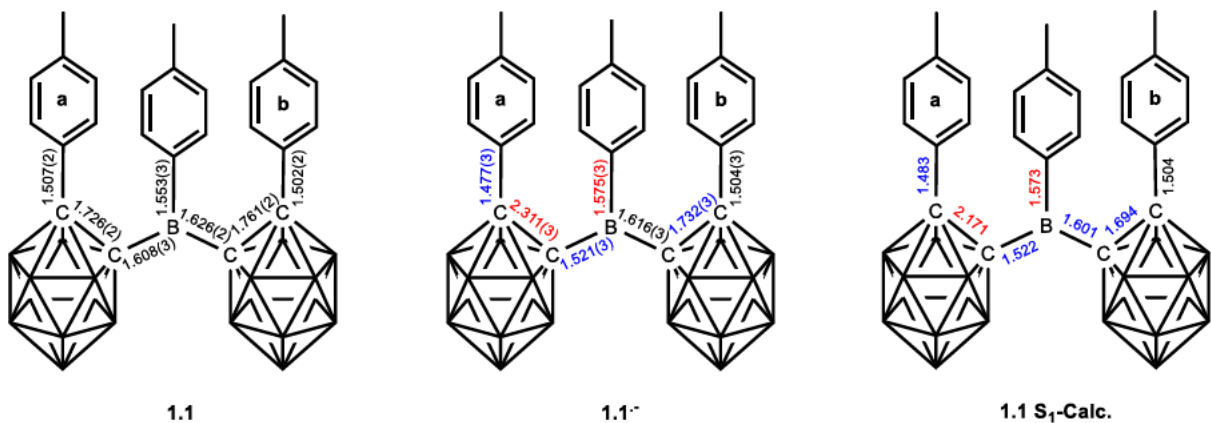


Abbildung 4.1.2: Bindungslängen in 1.1, 1.1⁻, und dem optimierten S₁-Zustand von 1.1. Rot: Zunahme der Bindungslänge, blau: Abnahme der Bindungslänge.

Photophysikalische Untersuchungen (Abbildung 4.1.3) zeigen eine CT-Emission mit einer großen Stokes-Verschiebung von bis zu 9500 cm⁻¹. Wie andere bekannte o-Carboran Verbindungen hat 1.1 in Lösung eine geringe Quantenausbeute, die im festen Zustand stark ansteigt ($\Phi_F = 19\%$). Bei der Reduktion erscheint eine breite Absorption niedriger Energie bei ca. 600 nm für 1.1⁻. Die experimentellen Beobachtungen stehen in guter Übereinstimmung mit den entsprechenden (TD-)DFT-Berechnungen auf dem (CAM-)B3LYP/6-31G*-Theorenebene für die optimierten Grundzustandsgeometrien sowie die photophysikalischen Übergänge.

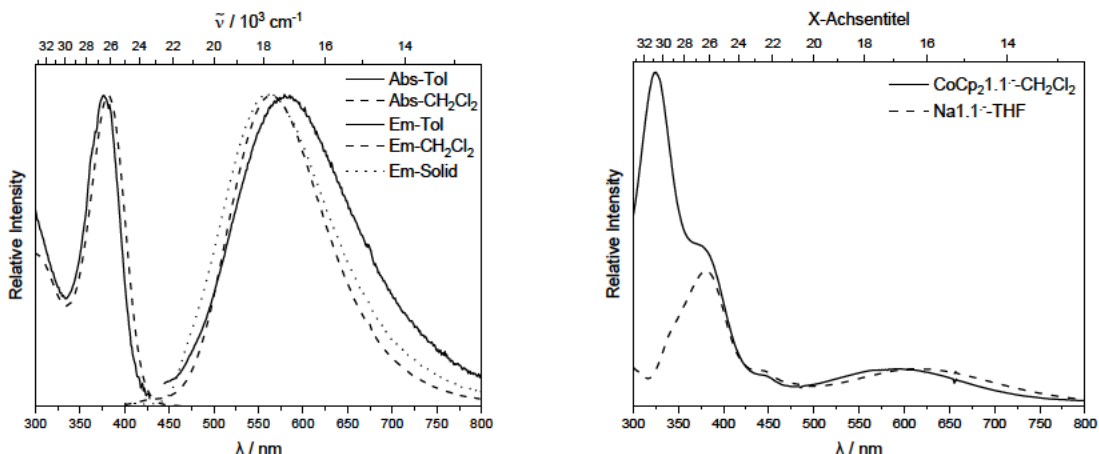
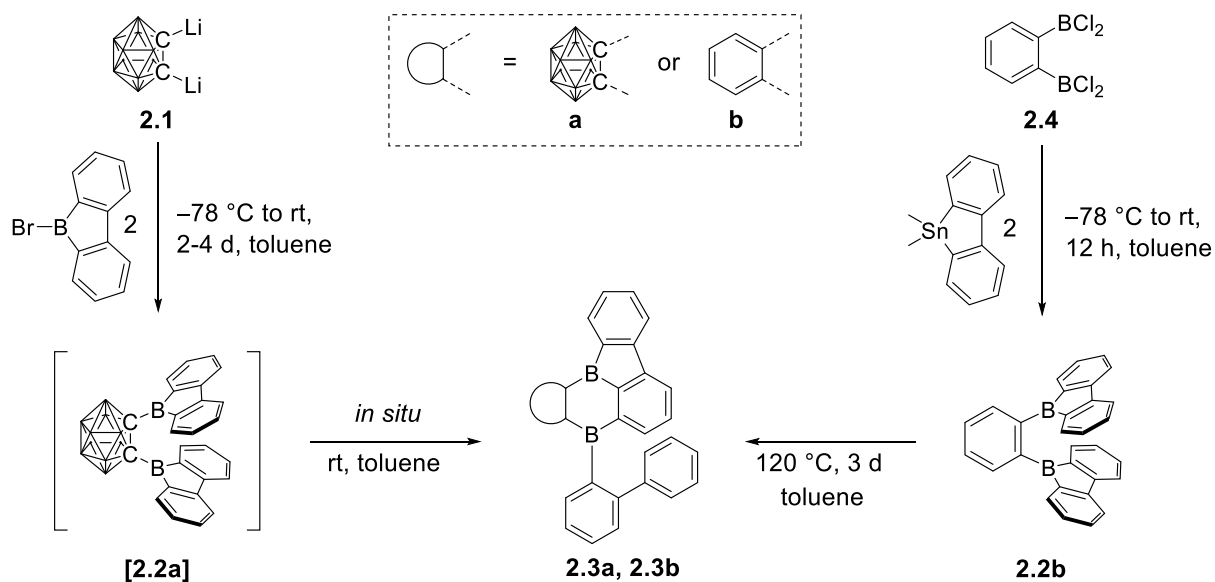


Abbildung 4.1.3: Links: Absorptions- (<450 nm) und Emissionsspektren (>450 nm, angeregt bei niedrigstem Energie-Absorptionsmaximum) von 1.1 in Toluol (durchgezogene Linie), CH₂Cl₂ (gestrichelte Linie) und im festen Zustand (gepunktete Linie). Rechts: Absorptionsspektren von CoCp₂⁺1.1⁻ (durchgezogene Linie) in CH₂Cl₂ und {K[18]crown-6·(THF)₂}⁺1.1⁻ in THF (gestrichelte Linie).

4.5 Zusammenfassung Chapter 2

Kapitel 2 handelt von der angestrebte Synthese von 1,2-Bis-9-borafluorenyl-o-carboran ([**2.2a**]) unter Verwendung von *o*-Carboran als dreidimensionales Rückgrat zur Senkung der borzentrierten LUMO-Energien in 9-Borafluoren. Der synthetische Ansatz führte zu einer intramolekularen Umlagerung bei Raumtemperatur, aus der die Verbindung **2.3a** (Schema 4.2.1) hervorging, deren Struktur durch Röntgeneinkristalldiffraktion bestätigt wurde. Die Isolierung von nur **2.3a** aus Reaktionen, die unter verschiedenen Bedingungen durchgeführt wurden, ist ein Hinweis darauf, dass die Umlagerungsgeschwindigkeit größer ist als die Geschwindigkeit, mit der [**2.2a**] gebildet wird. Eine theoretische Untersuchung des Übergangszustands mit Hilfe von DFT-Berechnungen ergab, dass die Umlagerung einem S_EAr-ähnlichen Mechanismus folgt, der durch ein tief liegendes LUMO, das Zielmerkmal der Verbindung [**2.2a**], ermöglicht wird. Dieselben Berechnungen für eine analoge Verbindung, die ein Phenyl-Rückgrat anstelle des Carboranyl-Rückgrat enthält, sagen eine deutlich höhere Barriere für den Umlagerungsprozess voraus. Infolgedessen konnte 1,2-Bis-9-borafluorenylbenzol (**2.2b**), als elektronenreicheres Analogon von [**2.2a**], synthetisiert und charakterisiert werden. Wie in den Berechnungen vorhergesagt, findet die Umlagerung auch bei der Verbindung **2.2b** bei einer höheren Temperatur statt. Das Produkt **2.3b** wurde isoliert und vollständig charakterisiert.



Schema 4.2.1. Synthese von **2.2b**, **2.3a** und **2.3b**. Die unbeschrifteten Cluster-Eckpunkte stellen BH-Einheiten dar.

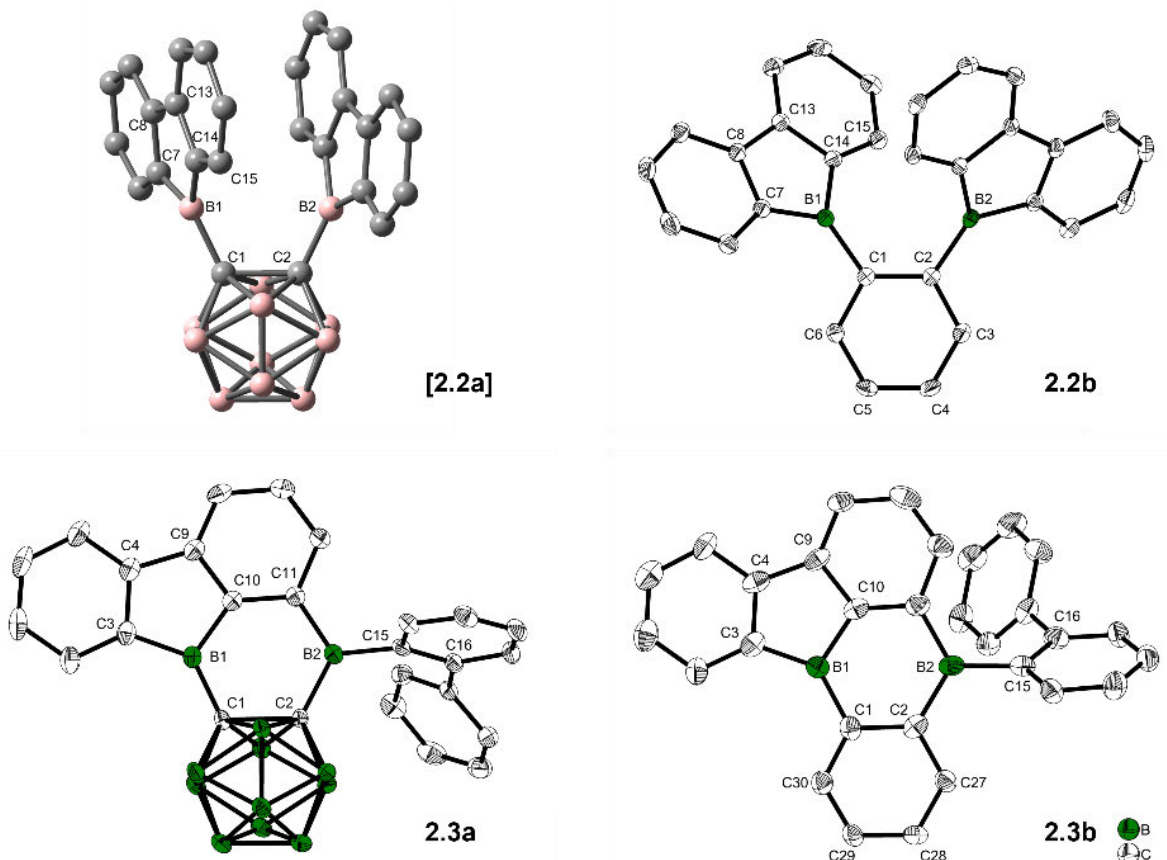


Abbildung 4.2.1. Optimierte Struktur von **[2.2a]** auf dem ω B97X-D/6-31G(d,p)-Niveau der Theorie in der Gasphase und Festkörper-Molekülstrukturen von **2.2b**, **2.3a** und **2.3b** aus der Einkristall-Röntgenbeugung bei 100 K. Die Atomverschiebungsellipsoide sind auf dem 50%-Wahrscheinlichkeitsniveau gezeichnet, und die Wasserstoffatome sind zur besseren Übersicht weggelassen worden. Für **2.3b** ist nur eines der vier symmetrieunabhängigen Moleküle dargestellt, und die Lösungsmittelmoleküle sind zur besseren Übersicht weggelassen worden.

Die optimierte Struktur von **[2.2a]** und die Einkristallstruktur von **2.2b** sowie die Einkristallstrukturen **2.3a** und **2.3b** wurden verglichen und sind in Abbildung 4.2.1 dargestellt. Der wesentliche Unterschied zwischen **[2.2a]** und **2.2b** ist eine längere C1–C2-Bindung im Rückgrat von **[2.2a]**, die zu einem größeren B–B-Abstand führen sollte, aber durch eine Anziehung zwischen den 9-Borafluoreneinheiten kompensiert wird, die in den B1–C1–C2-Winkel sichtbar ist. Der wesentliche Unterschied zwischen **2.3a** und **2.3b** besteht in dem einen Phenyl-/o-Carboranylring und damit in der Größe des π -Systems und der induktiven elektronenziehenden Wirkung über den o-Carboran-Cluster.

Zusammenfassung

Photophysikalische Untersuchungen zeigen einen 9-Borafluoren-ähnlichen Übergangscharakter in den schwachen Absorptionsbanden bei ca. 450 nm und der gelben Emission bei ca. 590 nm für 2.3a bzw. 2.3b (Abbildung 4.2.2). Dies wurde durch TD-DFT-Berechnungen bestätigt, die gut zu den experimentellen Beobachtungen passten.

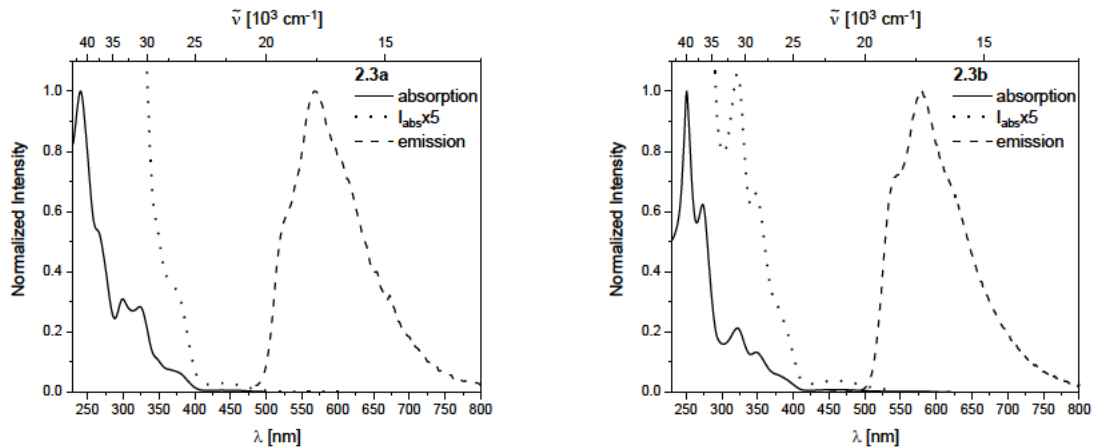
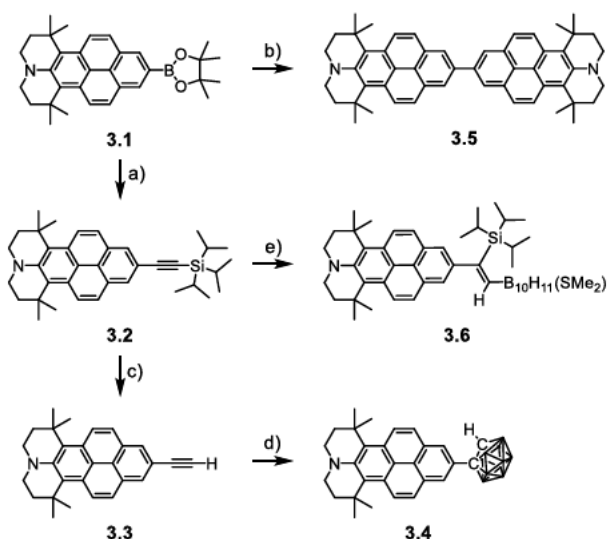


Abbildung 4.2.2. Normalisierte Absorptions- und Emissionspektren der umgelagerten Verbindungen 2.3a (links) und 2.3b (rechts) in Toluol. Als gepunktete Linie ist die fünffach erhöhte Absorption dargestellt, um den schwachen Übergang mit der niedrigsten Energie zu visualisieren

Eine starke Elektronenaffinität wurde für 2.3a und 2.3b in niedrigen Reduktionspotentialen von $E_{1/2} = -1,03$ bzw. $E_{1/2} = -1,17$ V beobachtet. Generell wurde die hier gezeigte Reaktivität stark von *o*-Carboran als Rückgrat beeinflusst und bietet einen Weg zur Erzeugung von BC₄B-Sechsring-enthaltenden PAHs sowohl für Phenyl- als auch für *o*-Carboranyl-enthaltende Verbindungen.

4.6 Zusammenfassung Chapter 3

In Kapitel 3 interessierten wir uns für die Erzeugung eines Ladungstransfer-(CT)-Übergangs von einem starken Julolidin-ähnlichen Donor zu einem *o*-Carboran Akzeptor über eine Pyren-Brücke unter Verwendung der 2,7-Stellungen des Pyrens. Grundlage hierfür war ein kürzlich erschienener Bericht unserer Gruppe über das thermodynamische Gleichgewicht zwischen lokal angeregten (LE) und CT-Zuständen der verwandten 1-(2'-Pyrenyl)-*o*-Carboran-Verbindung, die nicht den stark π -donierenden julolidinartigen Anteil enthielt. Für die Synthese der neuen Verbindung haben wir mit der bekannten Verbindung 3.1 begonnen und nach drei Schritten die Zielverbindung 3.4 erhalten (Schema 4.3.1). Das Zwischenprodukt 3.3 bietet aufgrund seiner endständigen Alkin-Gruppe ein breites Spektrum an Möglichkeiten für eine weitere Funktionalisierung. Die Verbindung 3.5 wurde als homokuppeltes Nebenprodukt aufgrund von Sauerstoffspuren in Reaktion a) erhalten und kristallographisch charakterisiert. Verbindung 3.6 ist das Ergebnis einer B-H-Insertion und Umlagerung der Silylgruppe am Alkin und wurde ebenfalls kristallographisch charakterisiert.



Schema 4.3.1. Synthese der Verbindungen 3.4 und 3.6 und des Nebenprodukts 3.5. a) I-C≡C-TIPS (1,1 Äquiv), Pd(dba)₂ (10 Mol-%), Cs₂CO₃ (1,1 Äquiv), rt, Methanol, 20 h, 45%; b) Verbindung 5 wurde als Nebenprodukt in Reaktion a) aufgrund von Sauerstoffspuren isoliert, 3%. c) TBAF (5 Äquiv), rt, THF, 1 h, 82%; d) B₁₀H₁₂(SMe₂)₂ (1,5 Äquiv), AgOAc (10 mol%), 100 °C, Toluol, 2 d, 36%; e) B₁₀H₁₂(SMe₂)₂ (1,5 Äquiv), AgOAc (10 mol%), 100 °C, Toluol, 2 d, 62%. Die nicht beschrifteten Cluster-Eckpunkte stellen BH-Einheiten dar.

Die Verbindungen 3.2, 3.4, 3.5 und 3.6 wurden mittels Einkristall-Röntgenbeugung untersucht (Abbildung 4.3.2) und mit ähnlichen bekannten Verbindungen verglichen. Bemerkenswert ist die kurze C_{Pyren}-N-Bindung, die ein Hinweis auf eine starke Delokalisierung des freien Elektronenpaares zum Pyren-System ist.

Zusammenfassung

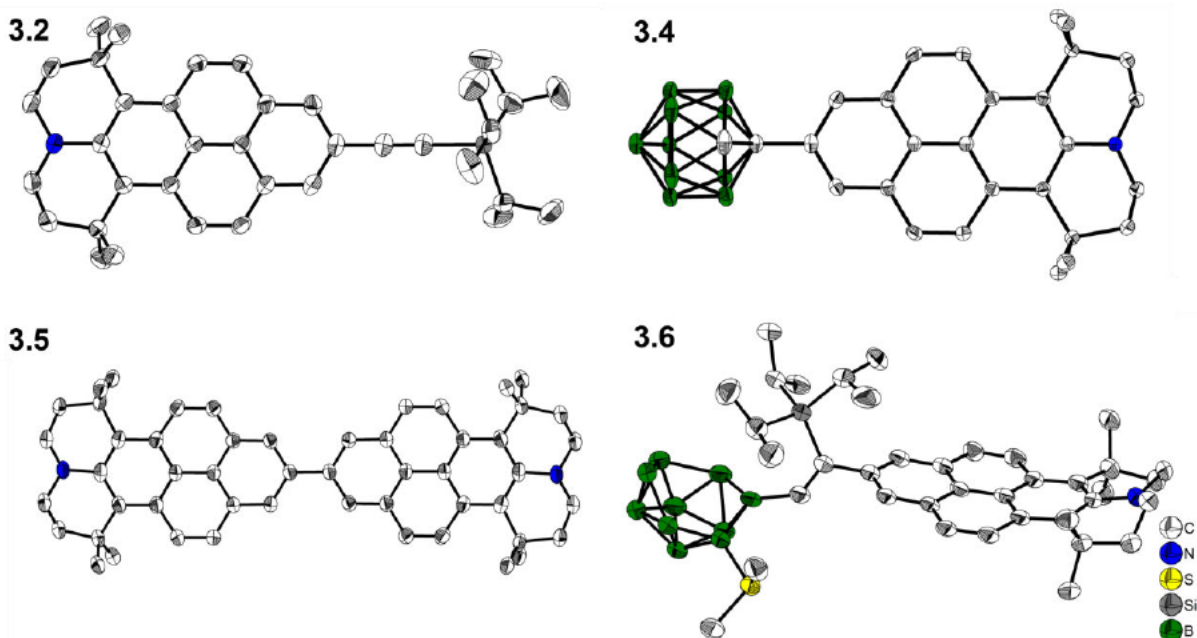


Abbildung 4.3.1. Festkörper-Molekülstruktur von 3.2, 3.4, 3.5 und 3.6 aus der Einkristall-Röntgenbeugung bei 100 K. Die Atomverschiebungsellipsoide sind auf dem 50%-Wahrscheinlichkeitsniveau gezeichnet. Die Wasserstoffatome und die Lösungsmittelmoleküle von 3.5 und 3.6 sind zur besseren Übersicht weggelassen worden.

Photophysikalische Untersuchungen von 3.4 ergaben, dass die Absorption $S_1 \leftarrow S_0$ bei 450 nm mit der niedrigsten Energie schwach ist ($\epsilon = \text{ca. } 1600 \text{ M}^{-1}\text{cm}^{-1}$) und auf die kurzachsig polarisierte und durch die Dipole verbogene L_B-Bande zurückgeführt werden kann. Im Vergleich zu Pyren zeigt die Verbindung 3.4 eine starke bathochrome Verschiebung des Absorptionsspektrums, eine blaue bis grüne Emission in Abhängigkeit vom Lösungsmittel und eine gelb-orange Emission im festen Zustand (Abbildung 4.3.3). Die Emissionsmaxima zeigen eine bathochrome Verschiebung mit zunehmender Lösungsmittelpolarität. Die höchste Quantenausbeute in Lösung wurde in Hexan beobachtet ($\Phi = 0,35$), was derjenigen im festen Zustand sehr ähnlich ist.

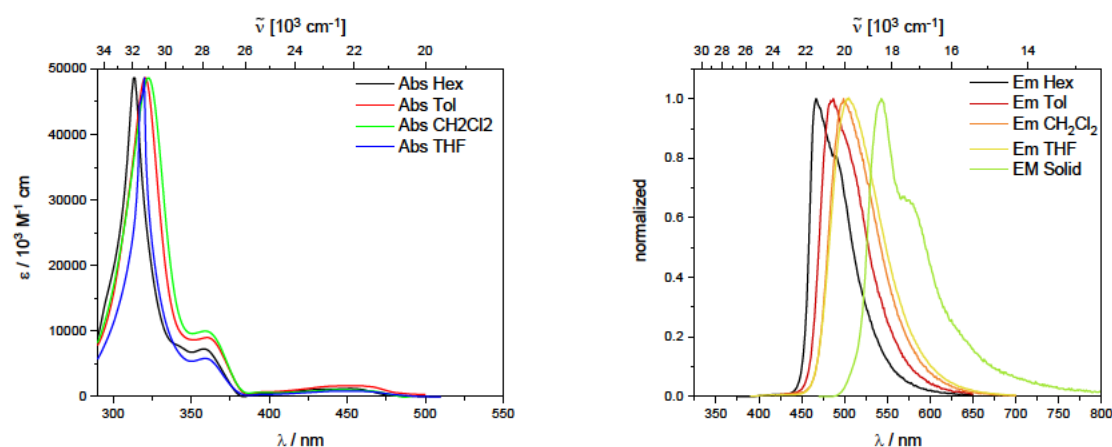


Abbildung 4.3.3. Normalisierte Absorptions- (links) und Emissionsspektren (rechts) Verbindung 3.4. Extinktionskoeffizient für Toluol.

Wie erwartet, führt die Julolidin-ähnliche Donorgruppe zu einer erheblichen Destabilisierung des pyrenähnlichen HOMO-1, was zu einem Wechsel der Reihenfolge von HOMO und HOMO-1 führt. *O*-Carboran als Akzeptor stabilisiert das LUMO und, etwas stärker ausgeprägt, das LUMO+1 im Vergleich zu bekannten Beispielen. Das Ausmaß der Stabilisierung ist geringer als bei B(mes)₂ und führte daher nicht zu einem Orbitalwechsel des LUMO und des LUMO+1 (Abbildung 4.3.2).

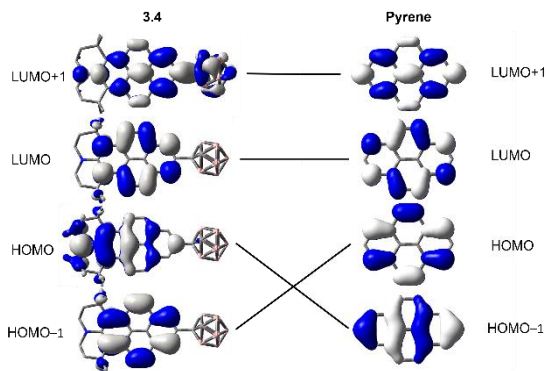


Abbildung 4.3.2. Molekulares Orbitaldiagramm für **3.4** und Pyren. Die dargestellten Orbitale folgen der berechneten energetischen Ordnung und werden anhand ihrer Ähnlichkeit verglichen.

Der *o*-Carboran-Anteil scheint das π -System des Pyrens hauptsächlich über seinen $-I$ induktiven Effekt zu beeinflussen, und zwar weitgehend unabhängig von seiner Rotationsposition. Im Fall von 1-(2'-Pyrenyl)-*o*-Carboran wurde gezeigt, dass die lange Lebensdauer des angeregten Zustands eine Rotation der C1-C2-Bindung des Carborans in eine Position senkrecht zum angehängten π -System des Pyrens ermöglicht, wodurch eine Clusterumordnung (Verlängerung der C-C-Bindung) möglich wird, die die optimale Akzeptorfähigkeit des *o*-Carborans erleichtert und zu einer CT von Pyren zum Carboran führt. Wie in Kapitel 1 erörtert, wird bei einem Reduktionsprozess mit einem Elektron eine Verlängerung der C1-C2-Bindung beobachtet, wie sie für den CT-Zustand von 1-(2'-Pyrenyl)-*o*-Carboran und verwandten Arten berechnet wurde. Im Fall unserer neuen Verbindung **3.4** beobachten wir zwar eine kleine bathochrome Verschiebung der Emission in Lösungsmitteln mit zunehmender Polarität, was auf einen gewissen CT-Charakter hindeutet, doch sind weitere, laufende Berechnungen erforderlich, um die Natur des angeregten Zustands vollständig zu verstehen.

5. EXPERIMENTAL

5.1 Supporting Information Chapter 1

5.1.1 General experimental details

Unless otherwise noted, the following conditions apply. All syntheses were carried out using standard Schlenk and glovebox techniques under an argon atmosphere. The solvents used were dried using a solvent purification system (SPS) from Innovative Technology and all except CH₂Cl₂ (DCM) were degassed and stored over sodium-potassium-alloy. DCM was passed through alumina and stored over activated molecular sieves. Deuterated solvents (CD₂Cl₂ and C₆D₆) used for NMR spectroscopy were purchased from Cambridge Isotope Laboratories. C₆D₆ was dried over molecular sieves and stored under an argon atmosphere before use. *n*-Butyllithium (2.5 M solution in hexane) was purchased from Acros Organics and used as received. CoCp₂ was kindly provided by Prof. Dr. Udo Radius of our Institute. The compound 1-1-(4-methylphenyl)-1,2-dicarba-*clos*o-dodecarborane was prepared according to a literature procedure.^[1] All other starting materials were purchased from commercial sources and were used without further purification.

NMR: Spectra were recorded on a Bruker Avance 500 FT NMR spectrometer operating at ¹H: 500 MHz, ¹¹B{¹H}: 160 MHz, ¹³C{¹H}: 126 MHz. Chemical shifts (δ) are given in ppm and are referenced to external BF₃·Et₂O (¹¹B{¹H}). ¹H NMR spectra were referenced via residual proton resonances of CD₂Cl₂ (5.32 ppm) and C₆D₆ (7.16 ppm).^[2] ¹³C{¹H} spectra were referenced to CD₂Cl₂ (53.84 ppm) and C₆D₆ (128.06 ppm).^[2] GCMS analyses were performed on an Agilent Technologies GCMS system (GC 7890A, EI-MS 5975C). HRMS were recorded using a Thermo Scientific Exactive Plus Orbitrap MS system with either an Atmospheric Sample Analysis Probe (ASAP) or by Electro-Spray Ionization (ESI).

Single-crystal X-ray diffraction: Crystals suitable for single-crystal X-ray diffraction were selected, coated in perfluoropolyether oil or polybutyl oil, mounted on a polyimide microloop (MicroMounts from MiTeGen) and transferred to a stream of cold nitrogen (Oxford Cryostream 700 or 800, respectively). Due to the lack of transparency for some samples, the crystal choice was based on its shape. As these crystals were extremely unstable in air, they were rapidly mounted under an argon stream and cooled at 100 K using an Oxford Cryostream low-temperature device attached to the diffractometer. Diffraction data of **1.1** and {Na·(THF)₆}⁺**1.1**[−] were collected on a Bruker X8 Apex II 4-circle diffractometer with a CCD area detector, using Mo-K α radiation generated by a Nonius FR591 rotating anode and monochromated by multi-layer focusing mirrors.

Diffraction data of **1.1**[−] and CoCp₂⁺**1.1**[−] were collected on a Rigaku Oxford Diffraction XtaLAB Synergy diffractometer with a semiconductor HPA-detector (HyPix-6000) and multi-layer mirror monochromated Cu-K α radiation at 100 K.

Experimental

The images were processed and corrected for Lorentz-polarization effects and absorption (empirical scaling) as implemented in the Bruker software packages (**1.1**, $\{\text{Na}\cdot(\text{THF})_6\}^+\text{1.1}^-$) or using the CrysAlis^{Pro} software from Rigaku Oxford Diffraction (**1.1**⁻, $\text{CoCp}_2^+\text{1.1}^-$). The structures were solved using the intrinsic phasing method (SHELXT)^[3] and Fourier expansion technique. All non-hydrogen atoms were refined in anisotropic approximation, with all hydrogen atoms ‘riding’ in idealized positions, by full-matrix least squares against F^2 of all data, using SHELXL^[4] software and the SHELXLE^[5] graphical user interface. Due to strong disorder in the crystal structures of $\{\text{Na}\cdot(\text{THF})_6\}^+\text{1.1}^-$ and $\text{CoCp}_2^+\text{1.1}^-$, reflection intensities were very weak, especially for high-resolution data. Hence, the data:parameter ratio was very low resulting in a reduced quality of the diffraction data and structure refinements. The data collected on $\text{CoCp}_2^+\text{1.1}^-$ suffer from systematic errors in absorption correction and Co fluorescence scattering due to the choice of a very large plate-like crystal. Furthermore, the unit cell of $\text{CoCp}_2^+\text{1.1}^-$ contains disordered tetrahydrofuran solvent molecules, several of which have been treated as a diffuse contribution to the overall scattering without specific atom positions by using SQUEEZE/PLATON.^[6] This can introduce further systematic errors. Nevertheless, the crystal structures and, hence, molecular geometries could be solved from these data and crystal structures are included in the SI as a proof of conformation. Diamond^[7] software was used for graphical representation. Crystal data and experimental details are listed in Table 5.1.1; full structural information has been deposited with the Cambridge Crystallographic Data Centre. CCDC-2040247 (**1.1**), 2040248 (**1.1**⁻) and 2043596 ($\{\text{Na}\cdot(\text{THF})_6\}^+\text{1.1}^-$).

Photophysical measurements: All measurements were performed in standard quartz cuvettes (1 cm x 1 cm cross-section). UV-visible absorption spectra were recorded using an Agilent 8453 diode array UV-visible spectrophotometer.

Emission spectra were recorded using an Edinburgh Instruments FLSP920 spectrometer equipped with a double monochromator for both excitation and emission, operating in right-angle geometry mode, and all spectra were fully corrected for the spectral response of the instrument. All solutions used for photophysical measurements had a concentration lower than 2×10^{-5} M to minimize inner filter effects during fluorescence measurements.

Fluorescence quantum yields were measured using a calibrated integrating sphere (inner diameter: 150 mm) from Edinburgh Instruments combined with the FLSP920 spectrometer described above. For solution-state and solid-state measurements, the longest-wavelength absorption maximum of the compound in the respective solvent was chosen as the excitation wavelength.

Fluorescence lifetimes were recorded using the time-correlated single-photon counting (TCSPC) method using the same FLSP920 spectrometer described above. Solutions were excited with a picosecond pulsed diode laser at an emission maximum of 376.6 nm. The full width at half maximum (FWHM) of the laser pulses were ca. 72 ps, while the instrument response function (IRF) had a FWHM of ca. 1.0 ns, measured from the scatter of a Ludox solution at the excitation wavelength. Decays were recorded to at least 10000 counts in the peak channel with a record length of at least 1000 channels. The band pass of the monochromator was adjusted to give a signal count rate of <10 kHz. Iterative deconvolution of the IRF with one decay function and non-linear least-squares analysis were used to analyse the data. The quality of the fit was judged by the calculated value of the reduced χ^2 and visual inspection of the weighted residuals.

Experimental

Electrochemical measurements: All cyclic voltammetry experiments were conducted in an argon-filled glovebox using a Gamry Instruments Reference 600 potentiostat. A standard three-electrode cell configuration was employed using a platinum disk working electrode, a platinum wire counter electrode, and a silver wire reference electrode separated by a Vycor frit, serving as the reference electrode. The redox potentials are referenced to the ferrocene/ferrocenium ($[Fc/Fc^+]$) redox couple) as an internal standard. Tetra-*n*-butylammonium hexafluorophosphate ($[nBu_4N][PF_6]$) was employed as the supporting electrolyte.

EPR measurements: Measurements at X-band (9.85 GHz and 9.38 GHz) were carried out at room temperature and 240 K using a Bruker ELEXSYS E580 CW EPR spectrometer. CW EPR spectra were measured using 1 mW microwave power and 1 G field modulation at 100 kHz, with a conversion time of 20 ms.

Theoretical Studies: All calculations (DFT and TD-DFT) were carried out with the Gaussian 09 (9.E.01)^[8] program package and were performed on a parallel cluster system. GaussView (6.0.16) and multiwfn^[9] were used to visualize the results, to measure calculated structural parameters, and to plot orbital surfaces (isovalue: $\pm 0.030 [e \text{ } a_0^{-3}]^{1/2}$). The ground-state geometries were optimized using the B3LYP functional^[10] in combination with the 6-31+G(d) basis set.^[11,12] The D3 dispersion correction of Grimme and co-workers was used.^[13] The ultrafine integration grid and symmetry constraints were used for all molecules. Frequency calculations were performed on the optimized structures to confirm them to be local minima showing no negative (imaginary) frequencies. Based on these optimized structures, the lowest-energy vertical transitions (using the polarizable continuum model) were calculated (singlets, 25 states) by TD-DFT, using the Coulomb attenuated functional CAM-B3LYP^[14] as well as B3LYP. The CAM-B3LYP functional has been shown to more accurately describe CT systems in comparison to B3LYP.^[15] The optimized ground-state geometries were used as starting coordinates for TD-DFT geometry optimizations. The S_1 state of **1** were optimized using 10 excited states with the B3LYP functional in combination with the 6-31g* basis set and D3 dispersion correction and no symmetry constraints.

Experimental

5.1.2 Synthetic procedures

Synthesis of bis(1-(4-tolyl)-carboran-2-yl)-(4-tolyl)-borane (1.1)

The compound 1-(4-methylphenyl)-1,2-dicarba-*clos*o-dodecarborane (500 mg, 1.91 mmol) was dissolved in toluene (15 mL) and a 2.5 M *n*BuLi solution in hexane (0.40 mL, 1.04 mmol) was added dropwise at -78 °C. The reaction mixture was slowly warmed to room temperature and stirred at 80 °C overnight. Then, the reaction was cooled to -78 °C and dibromo(4-methylphenyl)borane (940 mg, 4.01 mmol) in toluene (5 mL) was added dropwise after which the reaction was slowly warmed to room temperature and stirred at room temperature for 4 d. The suspension was filtered, washed with cold toluene (5 mL), diethyl ether (10 mL), and hexane (10 mL). The crude product was recrystallized from toluene to give [(1-(4-MeC₆H₄)-*clos*o-1,2-C₂B₁₀H₉-2-)₂(4-MeC₆H₄)B] (**1**) (434 mg, 0.76 mmol) as a pale yellow solid in 40% yield. Traces of 1-(4-methylphenyl)-1,2-dicarba-*clos*o-dodecarborane and 4-methylphenyl-boronic acid can be observed in the ¹H, ¹¹B and ¹³C NMR spectra due to the instability of the compound in solution.

¹H NMR (500 MHz, C₆D₆, ppm): δ 6.73 (d, *J* = 8 Hz, 4H), 6.37 (d, *J* = 8 Hz, 4H), 6.18 (d, *J* = 8 Hz, 2H), 5.49 (d, *J* = 8 Hz, 2H), 4.5–2.0 (br, 20H), 1.95 (s, 3H), 1.90 ppm (s, 6H).

¹¹B NMR (160 MHz, C₆D₆, ppm): δ 71.5, 5.3, -2.4, -7.2, -9.6.

¹¹B{¹H} NMR (160 MHz, C₆D₆, ppm): δ 71.5, 5.3, -2.5, -7.2, -9.8.

¹³C{¹H} NMR (125 MHz, C₆D₆, ppm): δ 141.3, 139.6, 139.0, 131.3, 130.1, 129.7, 128.9, 126.4, 88.9, 81.4, 21.9, 21.3.

HR-MS (ASAP⁺) (*m/z*): calc. for [C₂₅H₄₁B₂₁]⁺ 568.53022; found 568.52916 [M+H]⁺.

Elem. Anal. Calc. (%) for C₂₅H₄₁B₂₁: C 52.81, H 7.27; found: C 52.90, H 7.36.

Preparation of {K[18]crown-6·(THF)₂}⁺**1**^{•-}

In an argon filled glove box, compound **1** (5 mg, 9 µmol) was dissolved in THF (1 mL) and 88 µL of a 0.1 M K[18]crown-6 naphthalenide stock solution in THF was added. A deep blue colour could be observed immediately. Dry hexane vapor was diffused at -30 °C into 1 mL GC vials containing the reaction solution. Dark blue crystalline solid formed after 1-2 weeks giving {K[18]crown-6·(THF)₂}⁺**1**^{•-} (8 mg, 7 µmol) in 84% yield.

Due to insufficient amounts of isolated compound, it was only characterized by single-crystal X-ray diffraction.

Experimental

Preparation of $\text{CoCp}_2^+\mathbf{1.1}^-$

In an argon filled glove box, compound **1.1** (5 mg, 9 μmol) and CoCp_2 (2 mg, 11 μmol) were dissolved in CH_2Cl_2 (1 mL) and the reaction turned deep blue immediately. Hexane (5 mL) was added and a solid precipitated at -30°C overnight which was washed with hexane and toluene several times giving $\text{CoCp}_2^+\mathbf{1.1}^-$ (6 mg, 8 μmol) as a dark blue solid in 90% yield.

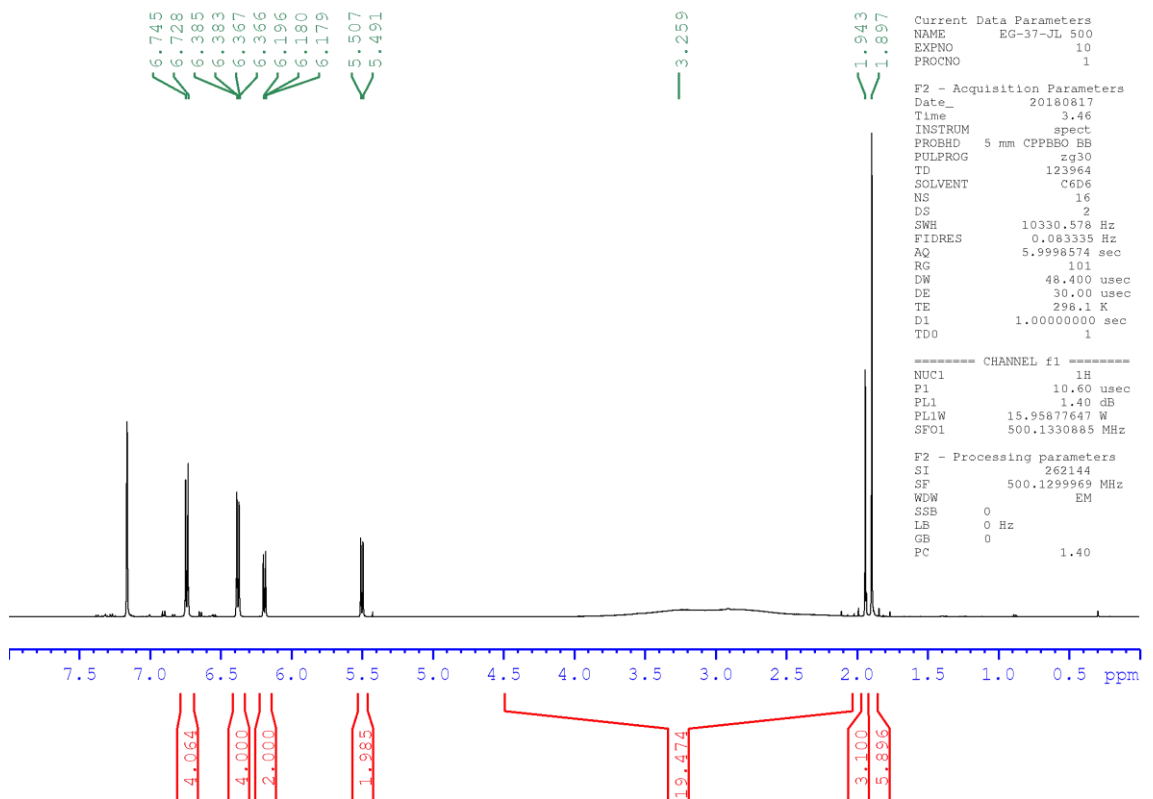
Due to insufficient amounts of isolated compound, it was only characterized by single-crystal X-ray diffraction.

Preparation of $\{\text{Na}\cdot(\text{THF})_6\}^+\mathbf{1.1}^-$

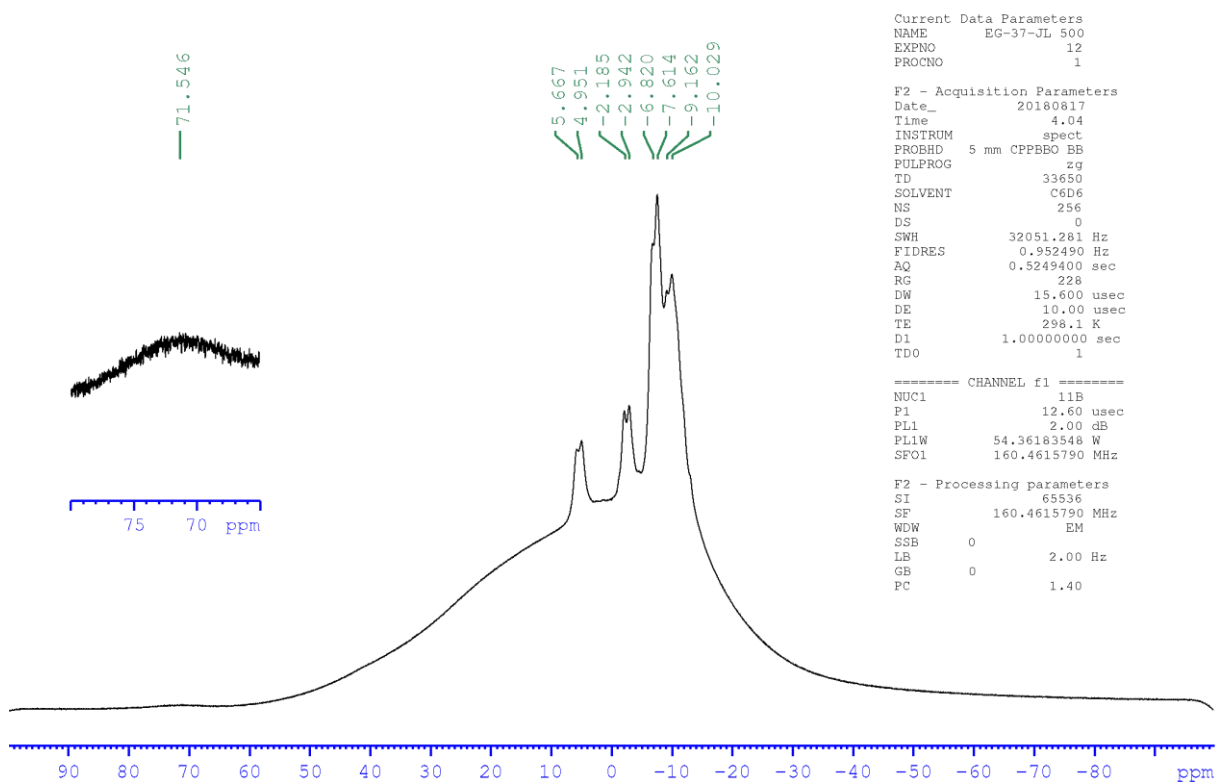
In an argon filled glove box, compound **1.1** (5 mg, 9 μmol) was dissolved in THF (1 mL) and a grain of cleanly cut sodium was added. The reaction turned deep blue immediately. From the filtered solution, crystallization was achieved by hexane diffusion at -30°C . Only a small amount of $\{\text{Na}\cdot(\text{THF})_6\}^+\mathbf{1.1}^-$ was obtained and used for single-crystal structure analysis.

Experimental

¹H NMR spectrum of 1.1 in C₆D₆

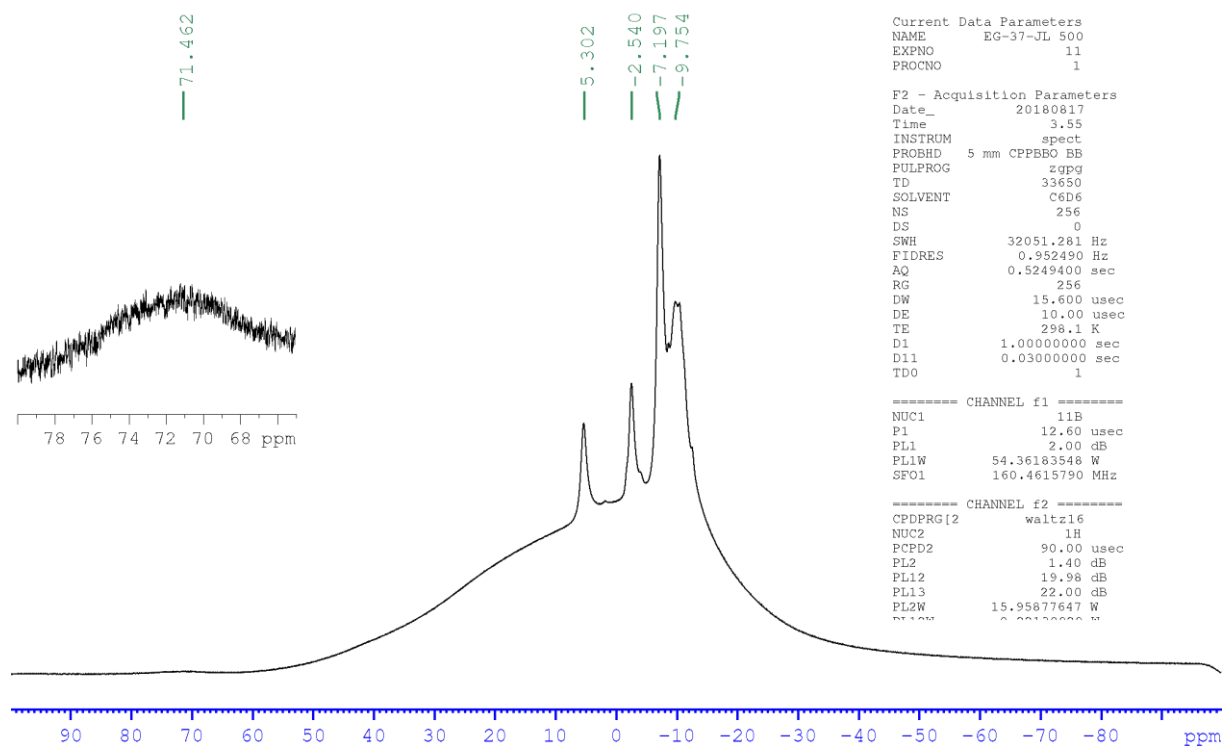


¹¹B NMR spectrum of 1.1 in C₆D₆

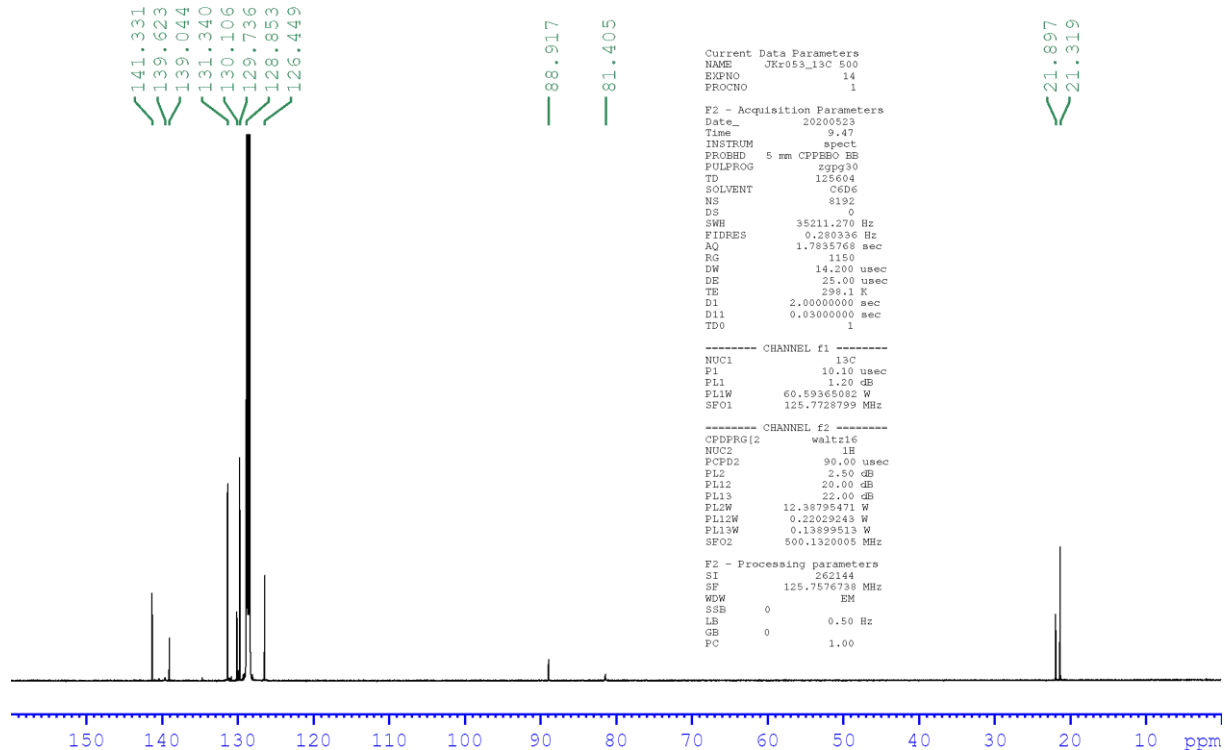


Experimental

$^{11}\text{B}\{\text{H}\}$ NMR spectrum of 1.1 in C_6D_6



$^{13}\text{C}\{\text{H}\}$ NMR spectrum of 1.1 in C_6D_6



5.1.3 EPR measurement

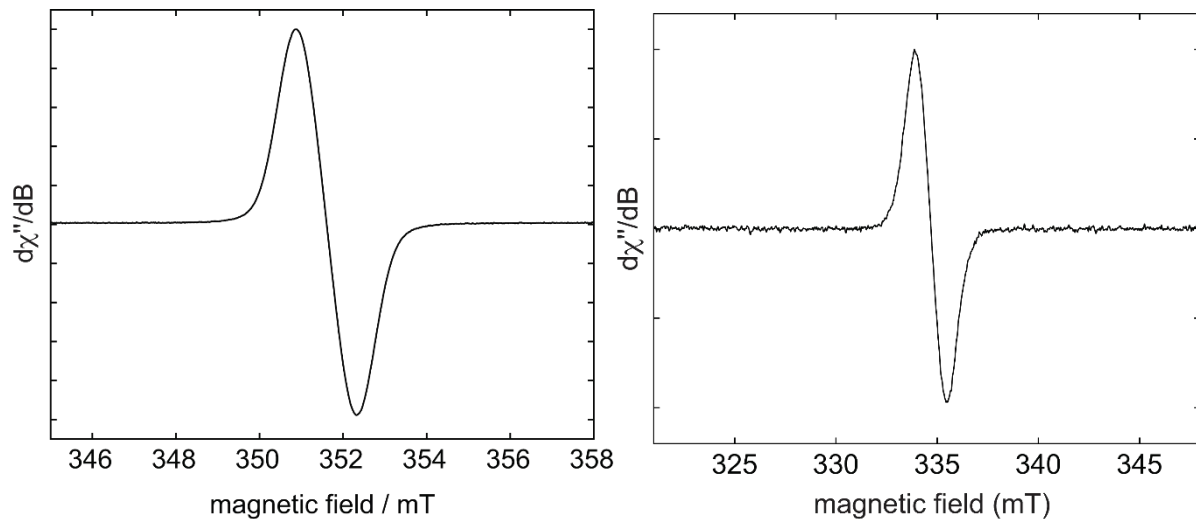


Figure 5.1.1. Left: Room temperature continuous-wave (CW) X-band (9.85 GHz) EPR spectrum of $\text{Na}^+ \mathbf{1.1}^{*-}$ in tetrahydrofuran. The isotropic g value is 2.0026 and the peak-to-peak linewidth is 1.4 mT. Right: The signal shape remains unchanged upon cooling to 240 K (9.38 GHz).

Experimental

5.1.4 Single-crystal X-ray diffraction

Table 5.1.1. Details on single-crystal X-ray diffraction data and structure refinements of **1.1**, **1.1⁻**, **CoCp₂⁺1.1⁻**, and **{Na·(THF)₆}⁺1.1⁻**.

Data	1.1	1.1⁻	CoCp₂⁺1.1⁻	{Na·(THF)₆}⁺1.1⁻
CCDC	2040247	2040248		2043596
Empirical formula	C ₂₅ H ₄₁ B ₂₁	C ₂₅ H ₄₁ B ₂₁ · C ₂₀ H ₄₀ KO ₈ · C ₄ H ₈ O	C ₂₅ H ₄₁ B ₂₁ · C ₁₀ H ₁₀ Co · 0.75(C ₄ H ₈ O) [+solvent]	C ₂₅ H ₄₁ B ₂₁ · 6(C ₄ H ₈ O)Na
ρ _{calc} /g·cm ⁻³	1.146	1.178	1.038	1.132
F(000)	1184	2316	3384	4376
Crystal size/mm ³	0.35×0.25×0.20	0.22×0.04×0.03	0.79×0.44×0.07	0.17×0.11×0.05
Crystal color, habit	colourless block	Blue block	blue plate	blue plate
μ/mm ⁻¹	0.055	1.138	2.768	0.071
M _r /g·mol ⁻¹	568.59	1088.31	3247.09 [+solvent]	1024.20
Temperature/K	100(2)	100(2)	100(2)	100(2)
Radiation, λ/Å	MoK _α , 0.71073	CuK _α , 1.54184	CuK _α , 1.54184	MoK _α , 0.71073
Crystal system	monoclinic	monoclinic	triclinic	Monoclinic
Space group	P2 ₁ /n	P2 ₁ /n	P $\bar{1}$	P2 ₁ /n
a/Å	10.777(6)	10.4239(2)	12.81360(10)	13.689(13)
b/Å	25.213(13)	37.4152(6)	29.3642(4)	46.23(4)
c/Å	12.356(7)	15.7574(3)	29.8382(3)	19.737(19)
α/°	90	90	69.5130(10)	90
β/°	101.036(8)	92.772(2)	81.3770(10)	105.82(2)
γ/°	90	90	84.9700(10)	90
Volume/Å ³	3295(3)	6138.39(19)	10390.5(2)	12017(20)
Z	4	4	2	8
2θ/°	3.23–53.47	4.724–155.044	5.244–136.50	2.776–50.246
Unique reflections	7001	12733	36295	21468
Parameters / restraints	438/0	842/361	2382 / 886	1597 / 690
GooF on F ²	1.026	1.035	1.554	0.998
R ₁ [I>=2σ(I)]	0.0480	0.0602	0.1214	0.1016
wR ² [all data]	0.1255	0.1690	0.3754	0.2766
Max./min. residual electron density/ e Å ⁻³	0.30 / -0.26	0.82 / -0.55	3.82 / -0.90	0.58 / -0.43

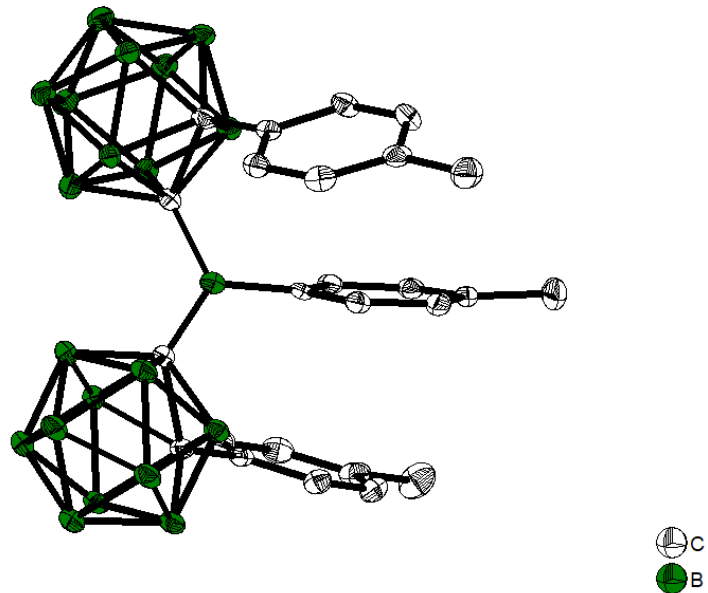


Figure 5.1.2. Solid state molecular structure of **1.1** from single-crystal X-ray diffraction at 100 K. Atomic displacement ellipsoids are drawn at the 50% probability level and hydrogen atoms are omitted for clarity.

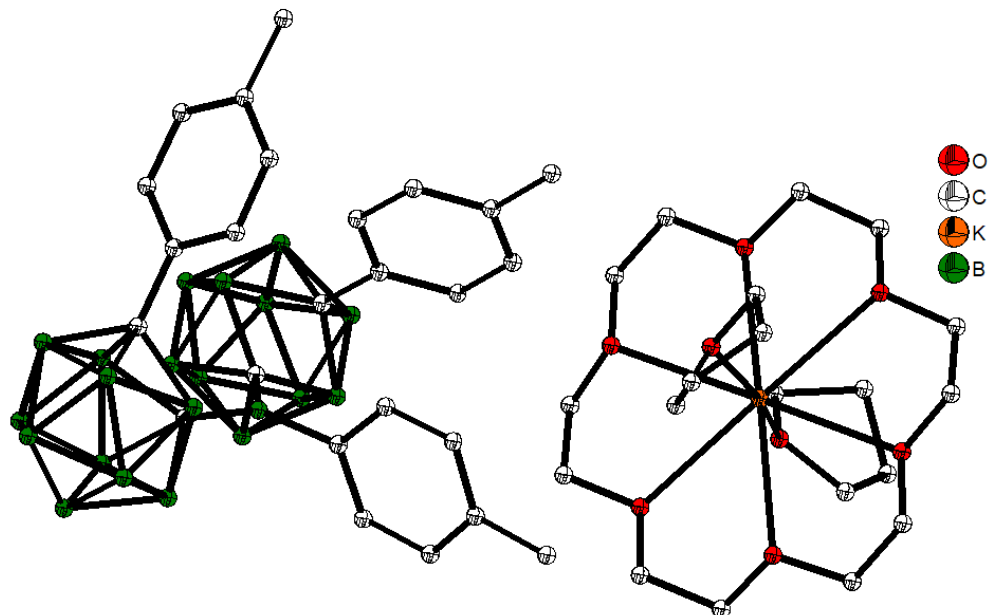


Figure 5.1.3. Solid state molecular structure of $\{\text{K}[18]\text{crown-6}\cdot(\text{THF})_2\}^+\text{1.1}^{--}$ from single-crystal X-ray diffraction at 100 K. Atomic displacement ellipsoids are drawn at the 50% probability level and solvent molecules and hydrogen atoms are omitted for clarity.

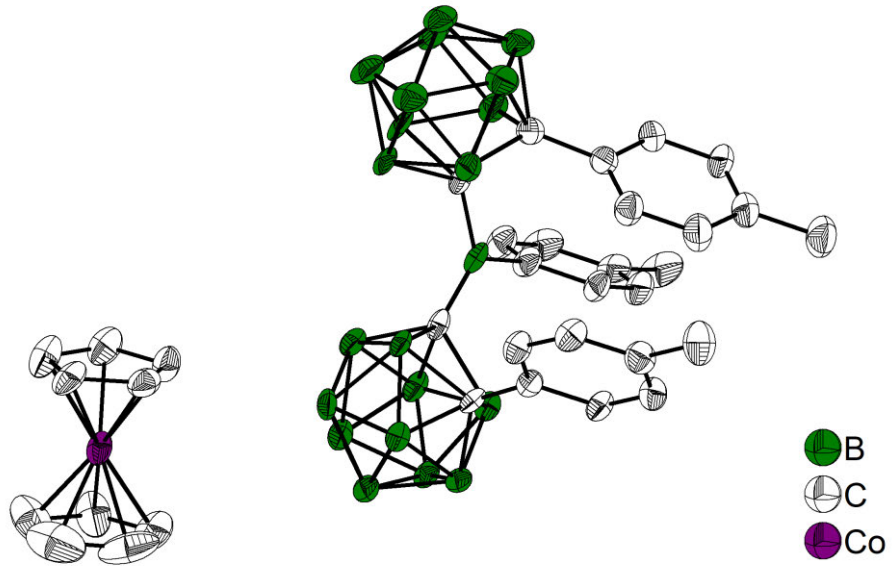


Figure 5.1.4. Solid state molecular structure of $\text{CoCp}_2^+ \cdot 1.1^-$ from single-crystal X-ray diffraction at 100 K. Atomic displacement ellipsoids are drawn at the 50% probability level and hydrogen atoms as well as solvent molecules are omitted for clarity. Only one of four symmetry-independent anions and cations each are shown.

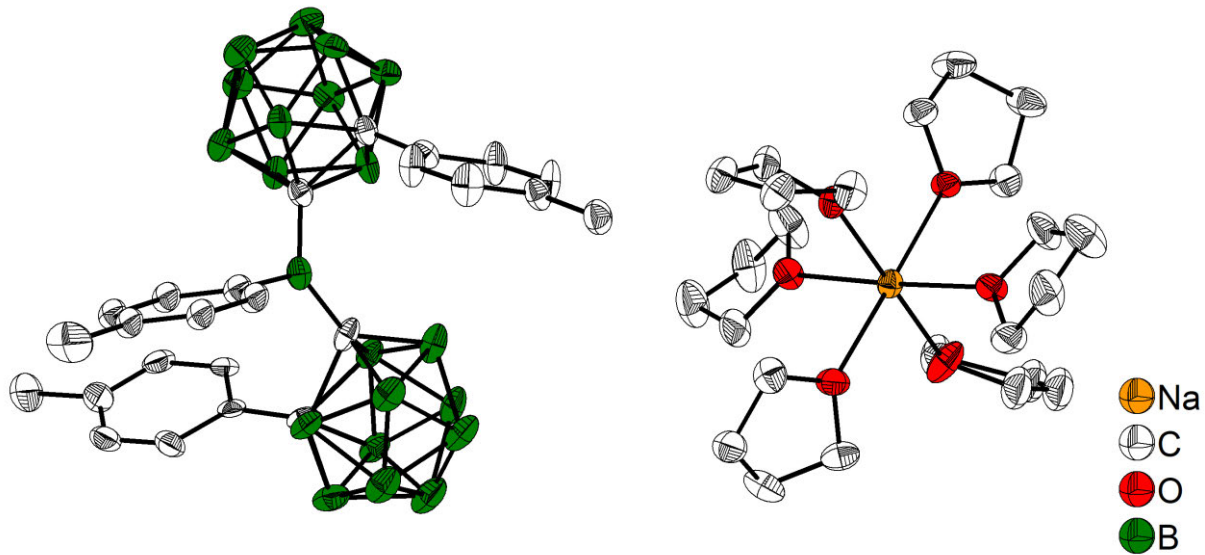


Figure 5.1.5. Solid state molecular structure of $\{\text{Na} \cdot (\text{THF})_6\}^+ \cdot 1.1^-$ from single-crystal X-ray diffraction at 100 K. Atomic displacement ellipsoids are drawn at the 50% probability level, and hydrogen atoms as well as the minor occupied parts of disordered THF and tolyl groups are omitted for clarity. Only one of two symmetry-independent anions and cations each are shown.

Experimental

Table 5.1.2. Selected bond lengths [Å] and angles [°] for **1.1** and $\{\text{K}[18]\text{crown-6}\cdot(\text{THF})_2\}^+\text{1.1}^-$ (abbreviated as **1.1**⁻ in the table), $\text{CoCp}_2^+\text{1.1}^-$, and $\{\text{Na}\cdot(\text{THF})_6\}^+\text{1.1}^-$ in the solid state at 100 K.

Compound	1.1	1.1 ⁻	$\text{CoCp}_2^+\text{1.1}^-$	$\{\text{Na}\cdot(\text{THF})_6\}^+\text{1.1}^-$
B1–C1	1.553(3)	1.575(3)	1.566(8) / 1.576(8) / 1.576(7) / 1.564(7)	1.580(8) / 1.604(10) and 1.610(10)
B1–C1a	1.608(3)	1.521(3)	1.536(7) / 1.527(7) / 1.525(8) / 1.532(8)	1.495(10) / 1.519(10)
B1–C1b	1.626(2)	1.616(3)	1.595(8) / 1.604(8) / 1.613(8) / 1.613(8)	1.625(10) / 1.610(10)
C1a–C2a	1.726(2)	2.311(3)	2.318(9) / 2.336(8) / 2.334(8) / 2.319(9)	2.335(8) / 2.339(8)
C1b–C2b	1.761(2)	1.732(3)	1.729(7) / 1.727(7) / 1.730(6) / 1.715(6)	1.739(8) / 1.742(8)
C2a–C3a	1.507(2)	1.477(3)	1.468(11) / 1.485(9) / 1.465(6) / 1.458(6)	1.477(9) / 1.476(7)
C2b–C3b	1.502(2)	1.504(3)	1.503(9) / 1.488(9) / 1.490(8) / 1.491(8)	1.502(7) / 1.504(7)
∠ C1–B1–C1a	118.4(1)	118.6(2)	119.4(5) / 119.0(5) / 119.3(5) / 118.9(4)	118.4(5) / 119.4(10) and 117.7(12)
∠ C1–B1–C1b	120.2(1)	118.6(2)	119.0(5) / 117.7(4) / 118.0(4) / 118.1(4)	116.1(5) / 115.9(10) and 118.0(12)
∠ C1a–B1–C1b	121.2(1)	122.2(2)	121.1(5) / 122.7(5) / 122.5(4) / 122.6(4)	125.4(5) / 124.3(5)
Sum ∠ C–B1–C	359.8(3)	359.7(6)	359.5(5) / 359.4(5) / 359.8(5) / 359.6(4)	359.9(5) / 359.6(10) and 360.0(12)
∠ C2a–C1a–B1–C1	-62.4(2)	94.4(2)	93.9(6) / -100.3(6) / 97.4(5) / -95.4(6)	-87.8(7) / 77.0(9)
∠ C2b–C1b–B1–C1	-44.0(2)	-54.9(3)	-56.8(7) / 61.2(6) / -60.1(6) / 58.4(6)	-93.6(6) / 104.6(9)

^a Compound $\text{CoCp}_2^+\text{1.1}^-$ contains 4 symmetry-independent molecules in the unit cell and values for all molecules are given here.

^b Compound $\{\text{Na}\cdot(\text{THF})_6\}^+\text{1.1}^-$ contains 2 symmetry-independent molecules in the unit cell and values for both molecules are given here. One molecule has a disordered tolyl group attached to the B1 atom and values for both parts are given here.

Experimental

5.1.5 Electrochemistry

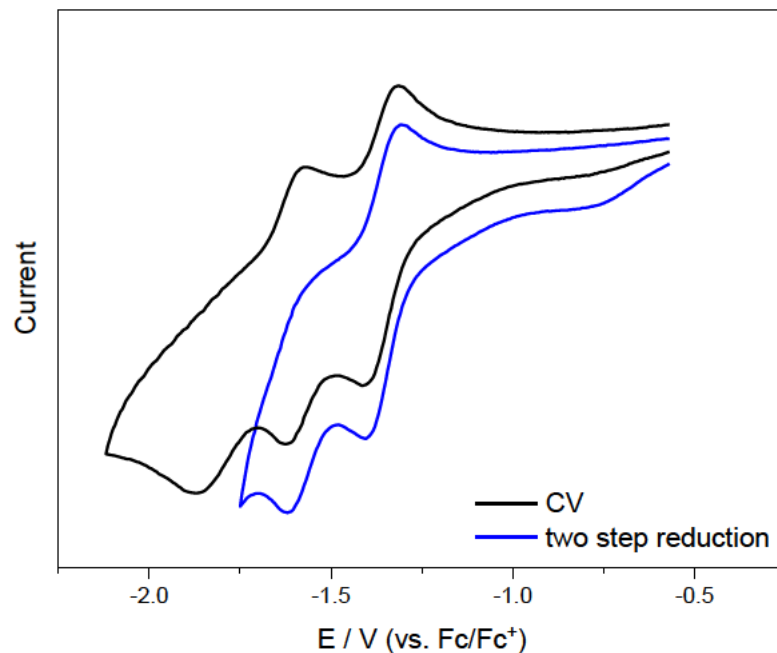


Figure 5.1.6. Cyclic voltammograms of the reversible ($E_{\text{red}} = -1.35 \text{ V}$) and irreversible redox events of **1.1**. In blue only two reduction events were achieved showing the irreversible nature of the second reduction. The cyclic voltammograms were measured in CH_2Cl_2 with $[n\text{Bu}_4\text{N}][\text{PF}_6]$ as the electrolyte with a scan rate of 250 mVs^{-1} . All measurements are referenced to the Fc/Fc^+ ion couple.

Experimental

5.1.6 Photophysical properties

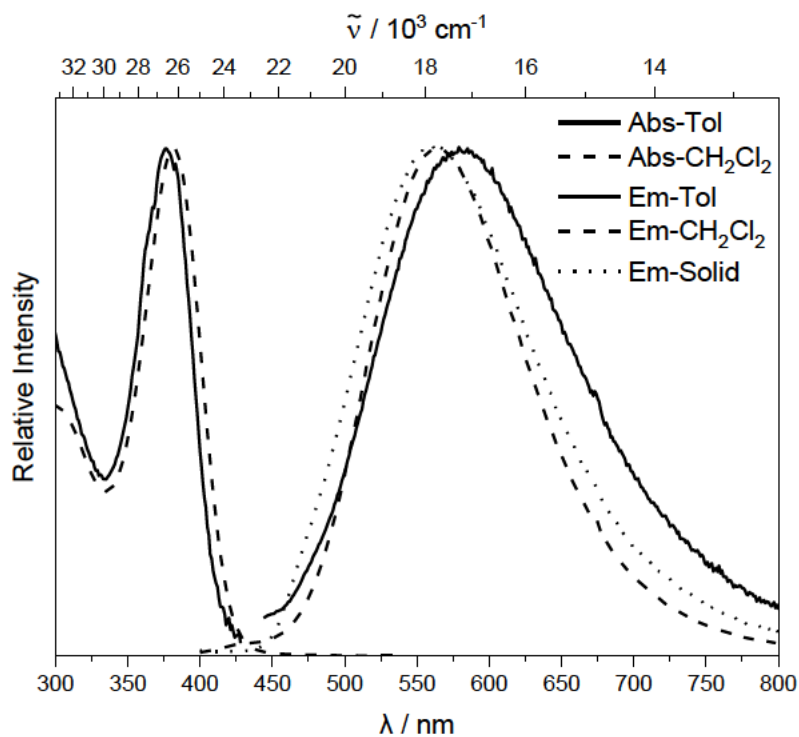


Figure 5.1.7. Absorption (<450 nm) and emission (>450 nm, excited at the lowest energy absorption maximum) spectra of 1.1 in toluene (solid line), CH_2Cl_2 (dashed line) and in the solid state (dotted line).

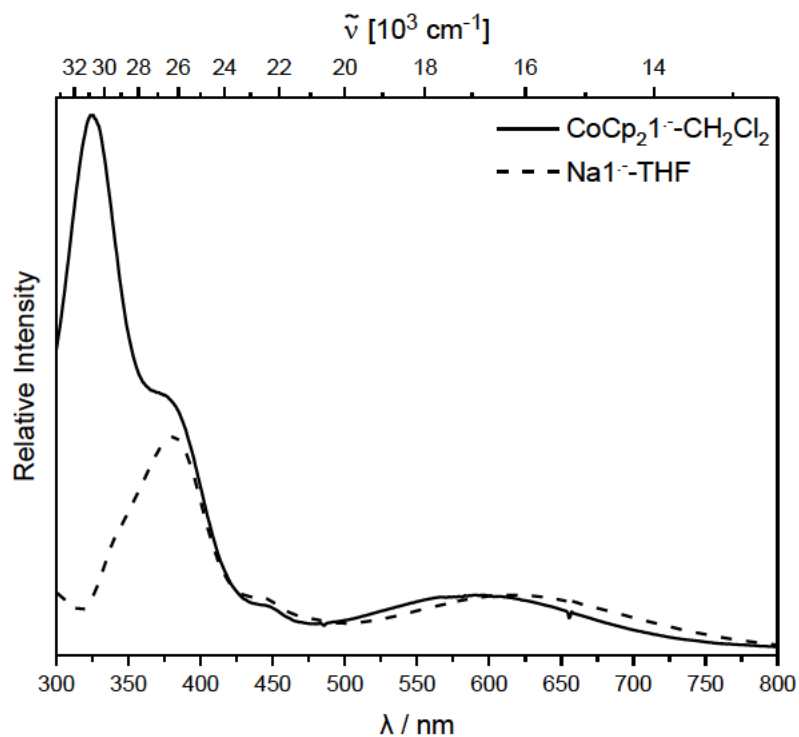


Figure 5.1.8. Absorption spectra of $\text{CoCp}_2^{+}\cdot\mathbf{1}\cdot\mathbf{1}^{-}$ (solid line) in CH_2Cl_2 and $\{\text{K}[18]\text{crown-6}\cdot(\text{THF})_2\}^{+}\cdot\mathbf{1}\cdot\mathbf{1}^{-}$ in THF (dashed line).

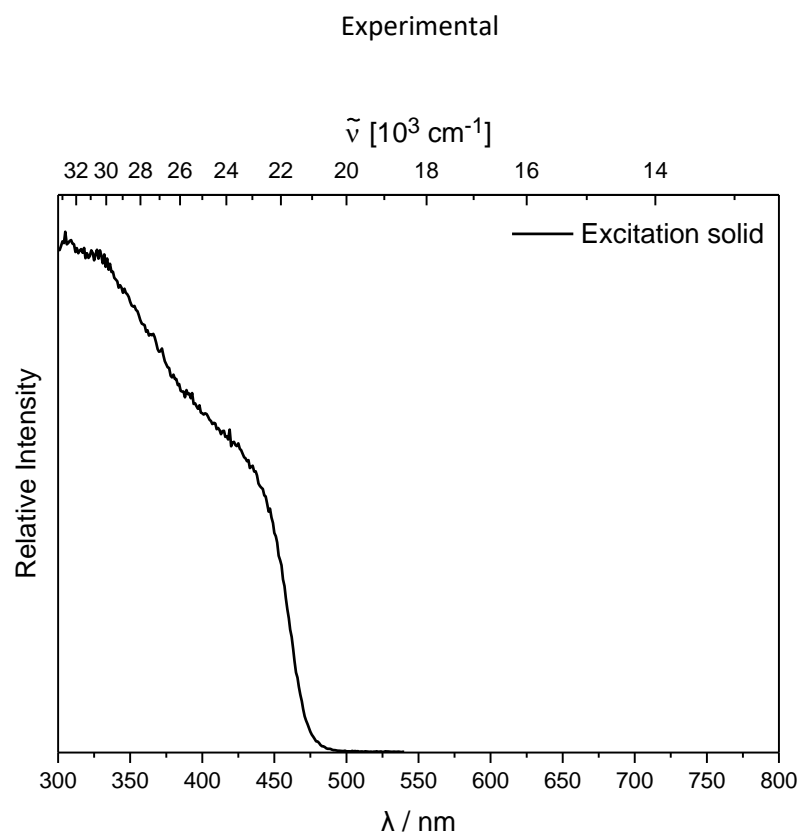


Figure 5.1.9. Excitation spectrum of **1.1** in the solid state.

Experimental

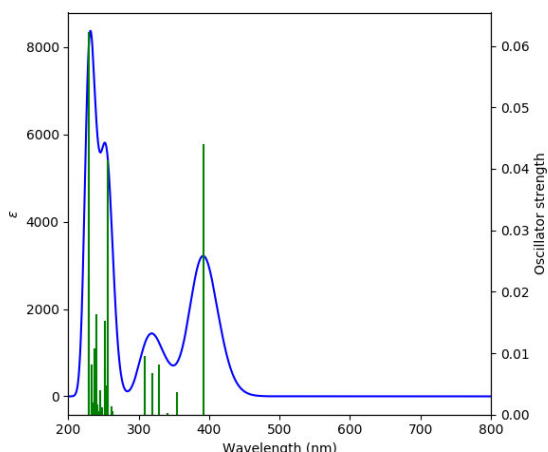
5.1.7 TD-DFT calculations

1.1

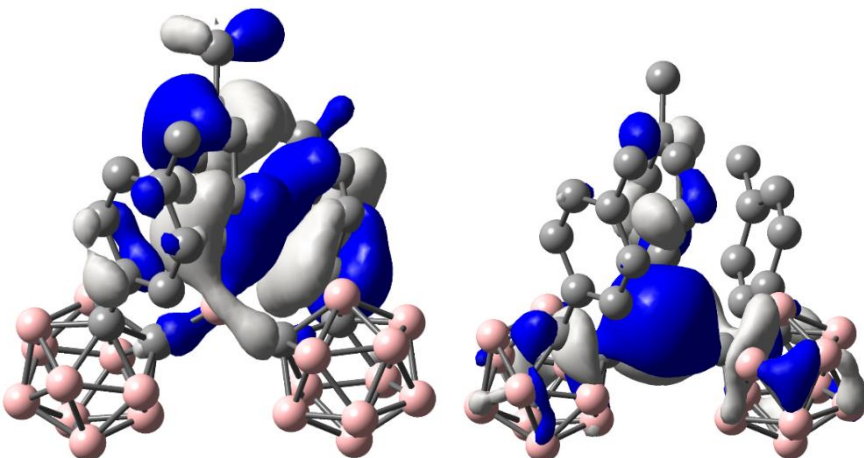
Table 5.1.3. Lowest energy singlet electronic transition of **1.1** (TD-DFT B3LYP/6-31G*, gas phase).

FC-S _n	E[eV](E[nm])	f	Contribution > 10%	Λ
S ₁	3.16 (392)	0.044	HOMO->LUMO (98%)	0.42
S ₂	3.50 (354)	0.0036	H-1->LUMO (98%)	0.30
S ₃	3.64 (340)	0.0002	H-2->LUMO (99%)	0.28
S ₄	3.76 (329)	0.0082	H-4->LUMO (16%) H-3->LUMO (82%)	0.31
S ₅	3.89 (319)	0.0067	H-4->LUMO (83%) H-3->LUMO (16%)	0.34

Simulated absorption spectrum at the B3LYP/6-31G* level of theory.



Orbitals relevant to the S₁←S₀ transition (B3LYP/6-31G*)



HOMO: -6.64

LUMO: -2.75

Experimental

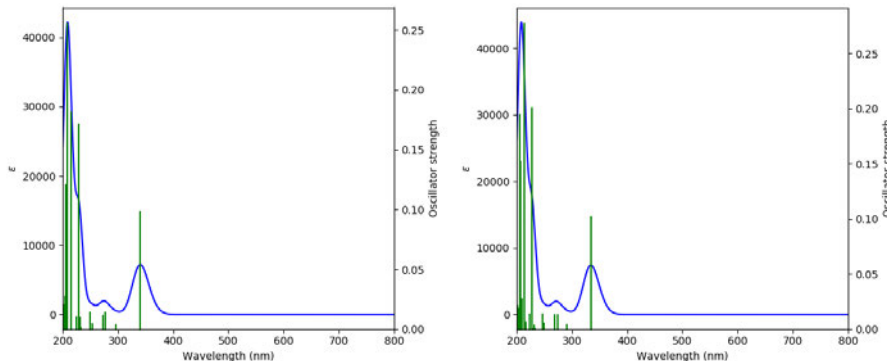
1.1

Table 5.1.4. Lowest energy singlet electronic transition of **1.1** (TD-DFT CAM-B3LYP/6-31G*, toluene).

FC-S _n	E[eV] (E[nm])	f	Contribution > 10%	Λ
S ₁	3.71 (334)	0.102	HOMO → LUMO (86%)	0.42
S ₂	4.27 (290)	0.004	H-2 → LUMO (12%) H-1 → LUMO (76%)	0.33
S ₃	4.53 (274)	0.013	H-2 → LUMO (82%) H-1 → LUMO (13%)	0.32
S ₄	4.61 (269)	0.014	H-4 → LUMO (11%) H-3 → LUMO (73%)	0.36
S ₅	4.96 (250)	0.006	H-4 → LUMO (76%) H-3 → LUMO (10%)	0.30

Table 5.1.5. Lowest energy singlet electronic transition of **1.1** (TD-DFT CAM-B3LYP/6-31G*, CH₂Cl₂).

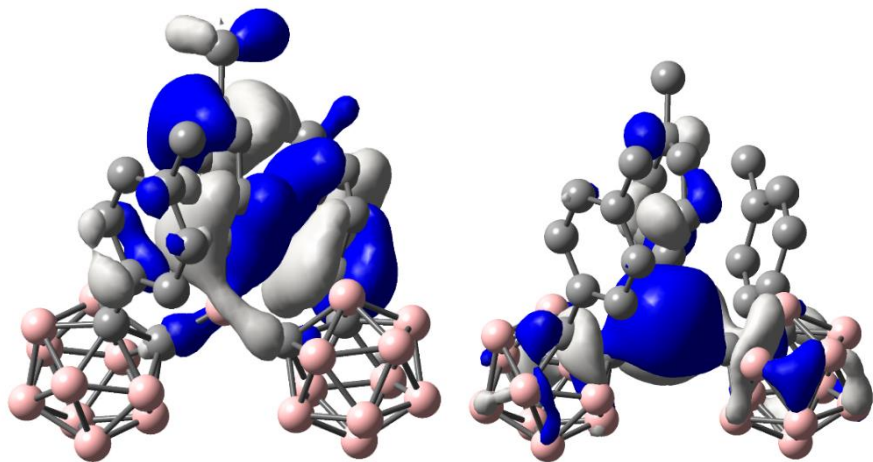
FC-S _n	E[eV] (E[nm])	F	Contribution > 10%	Λ
S ₁	3.64 (340)	0.099	HOMO → LUMO (86%)	0.41
S ₂	4.19 (296)	0.004	H-1 → LUMO (84%)	0.32
S ₃	4.48 (277)	0.015	H-2 → LUMO (88%)	0.30
S ₄	4.55 (272)	0.012	H-4 → LUMO (12%) H-3 → LUMO (73%)	0.35
S ₅	4.89 (253)	0.005	H-4 → LUMO (76%) H-3 → LUMO (13%)	0.30



Simulated absorption spectrum at the CAM-B3LYP/6-31G* level of theory (left toluene, right CH₂Cl₂).

Experimental

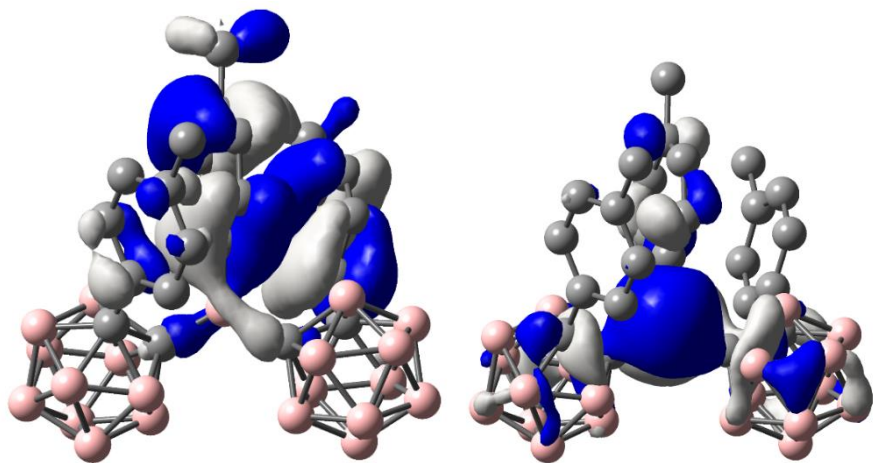
Orbitals relevant to the $S_1 \leftarrow S_0$ transition (CAM-B3LYP/6-31G*, toluene)



HOMO: -7.92

LUMO: -1.56

Orbitals relevant to the $S_1 \leftarrow S_0$ transition (CAM-B3LYP/6-31G*, CH₂Cl₂)



HOMO: -7.84

LUMO: -1.57

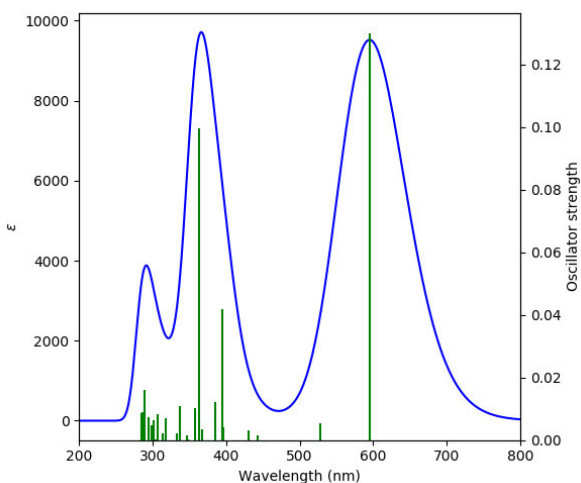
Experimental

1.1^{•-}

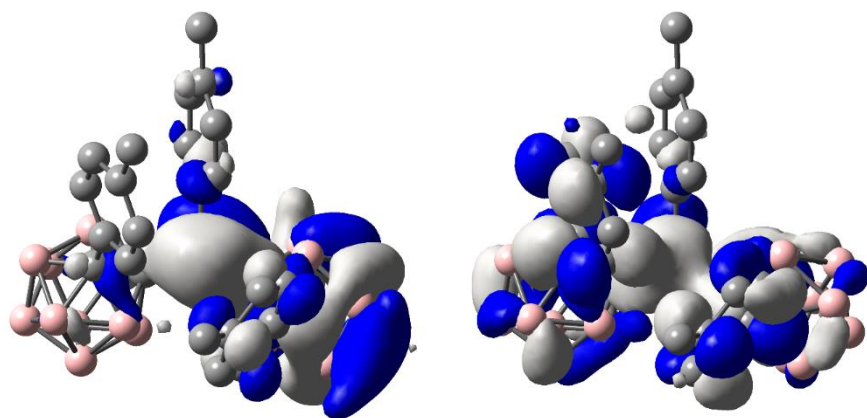
Table 5.1.6. Lowest energy singlet electronic transition of **1.1^{•-}** (B3LYP/6-31G*, gas phase).

FC-S _n	E[eV] (E[nm])	f	Contribution > 10%	Δ
S ₁	2.08 (596)	0.1301	HOMO α \rightarrow LUMO α (92%)	0.68
S ₂	2.35 (528)	0.0054	HOMO α \rightarrow L+1 α (93%)	0.54
S ₃	2.79 (443)	0.0014	HOMO α \rightarrow L+2 α (71%)	0.50
			HOMO α \rightarrow L+3 α (27%)	
S ₄	2.88 (430)	0.003	HOMO α \rightarrow L+2 α (27%)	0.68
			HOMO α \rightarrow L+3 α (71%)	
S ₅	3.13 (396)	0.0042	HOMO α \rightarrow L+4 α (35%)	0.54
			HOMO β \rightarrow LUMO β (46%)	

Simulated absorption spectrum at B3LYP/6-31G* level of theory.



Orbitals relevant to the S₁ \leftarrow S₀ transition (B3LYP/6-31G*)

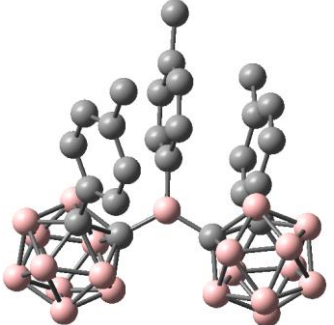


HOMO α : -1.53

LUMO α : 1.25

Experimental

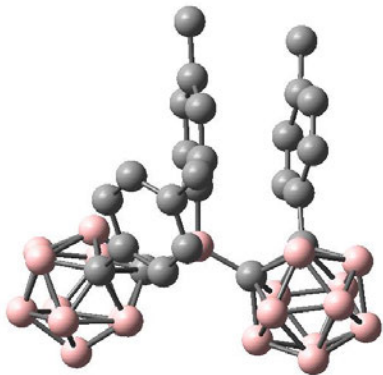
Theoretical calculations: Cartesian coordinates

1.1 DFT B3LYP/6-31G*, gas phase, S ₀  Point group: C1 Total energy: -941,162.143 kcal mol ⁻¹ Dipole moment: 9.5768 D Imaginary frequencies: 0	C 3.99097800 0.14364000 -2.20763100 H 4.18036300 -0.03794000 -3.26223400 C 4.46614200 1.31597500 -1.61320500 C 5.18961300 2.36574500 -2.41679200 H 6.04705700 2.77035500 -1.86823800 H 4.52361700 3.20894400 -2.64336100 H 5.55094400 1.96580400 -3.36883900 C 4.22495800 1.50131900 -0.24611000 H 4.59320900 2.39746800 0.24644900 C 3.51154100 0.56721800 0.49233800 H 3.33360200 0.74424700 1.54514100 B -0.22645900 -0.51973900 -0.16136500 B -2.07209200 0.46360100 -2.09639700 H -1.55051100 1.51007700 -2.01472900 B -3.82398300 0.28724800 -2.15987900 H -4.48090300 1.27089800 -2.12550200 B -4.25815800 -1.11470800 -1.17076600 H -5.20501400 -1.08464400 -0.46138100 B -2.76484300 -1.80516400 -0.51750800 H -2.69327200 -2.22487000 0.57609500 B -1.32126900 -0.96183900 -2.82575100 H -0.23318000 -0.86381000 -3.28657600 B -1.77728100 -2.37626300 -1.87036400 H -1.00437400 -3.24687700 -1.70307500 B -3.53735300 -2.55588600 -1.91386500 H -4.04326000 -3.62268700 -1.80240700 B -4.18540000 -1.25857800 -2.94349300 H -5.17554100 -1.39042600 -3.58407900 B -2.81394800 -0.25982000 -3.50463100 H -2.79622400 0.32171400 -4.53877500 B -2.64164900 -2.02799700 -3.36660400 H -2.50093300 -2.72975900 -4.31293700 B 1.37244300 -2.84896800 -0.10403500 H 1.32404800 -2.85371400 -1.28138400 B -0.00291500 -3.25855200 0.93422800 H -1.00508800 -3.60424000 0.43468000 B 0.01265300 -2.12483500 2.28417000 H -0.97783400 -1.64306200 2.71674700 B 1.43862200 -1.08429200 2.09869700 H 1.43952700 0.05702700 2.36819700 B 1.45230900 -4.24777500 0.98676500 H 1.45264200 -5.34630800 0.53995300 B 0.60792500 -3.79267900 2.49435800 H -0.01094700 -4.57389200 3.13818000 B 1.49209000 -2.43024200 3.22636800 H 1.51923600 -2.22010500 4.39391100 B 2.89175300 -2.08879900 2.20561400 H 3.89934500 -1.56924900 2.54419800 B 2.85979200 -3.18877800 0.81656300 H 3.84502300 -3.42609400 0.20573700 B 2.37694400 -3.76636100 2.42987000 H 3.06044100 -4.52670000 3.03221200
---	---

Experimental

1.1(S₁)

DFT B3LYP/6-31G*, gas phase, S₁



Point group: C1

Total energy: -940,356.149 kcal mol⁻¹

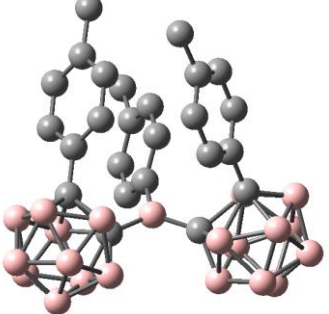
Dipole moment: 17.7779 D

Imaginary frequencies: 0

C 0.45644255 0.83132640 -0.47167087
 C 1.20514537 1.37313004 -1.56384542
 H 1.35675199 0.75599538 -2.43843505
 C 1.69911730 2.64595285 -1.52641958
 H 2.26144484 3.04268464 -2.36501346
 C 1.48169848 3.46782512 -0.39644601
 C 2.02217494 4.85697037 -0.37195224
 H 2.06855936 5.25984816 0.64151902
 H 1.37257563 5.51587572 -0.96307672
 H 3.01645233 4.90260497 -0.82555405
 C 0.71199861 2.97343764 0.67858885
 H 0.52134681 3.61376900 1.53310793
 C 0.18961207 1.71002781 0.63453647
 H -0.42542680 1.34887444 1.44891329
 C -1.42972112 -0.69135959 -1.36645761
 C -3.25228352 0.15586011 -0.54459854
 C -3.15696073 0.77686215 0.79829808
 C -3.00219470 0.01243350 1.95504566
 H -3.02543086 -1.06608610 1.88903523
 C -2.81163018 0.61687188 3.19212915
 H -2.67879719 -0.00809097 4.07083293
 C -2.79068850 2.00344142 3.32409149
 C -2.61628929 2.65483474 4.66978183
 H -3.58487973 2.81150700 5.15813739
 H -2.13570219 3.63366771 4.58280961
 H -2.01178212 2.03555857 5.33822049
 C -2.97370481 2.76844488 2.16944448
 H -2.97654935 3.85296512 2.24251997
 C -3.14921268 2.17078030 0.93222785
 H -3.27251635 2.79000465 0.05166733
 C 0.52123885 -1.80302605 0.29856303
 C 2.19984536 -1.72734932 0.51078000
 C 3.01555384 -0.58077647 -0.01957547
 C 3.56878685 -0.62035677 -1.30731183
 H 3.34653391 -1.45419011 -1.96047968

C 4.40860779 0.38759632 -1.74946906
 H 4.82188112 0.33269462 -2.75228456
 C 4.73449053 1.46835107 -0.92819156
 C 5.66297451 2.55016488 -1.40486033
 H 5.50866256 3.48236129 -0.85421546
 H 5.52937302 2.75206086 -2.47134633
 H 6.70869924 2.25661058 -1.25983449
 C 4.20007363 1.49415282 0.36184903
 H 4.45415874 2.31280246 1.02909603
 C 3.36869184 0.48414767 0.81483865
 H 2.99299016 0.51908928 1.82877260
 B -0.16084262 -0.61473728 -0.52924476
 B -2.22194083 0.82296122 -1.72724843
 H -1.64730031 1.82991596 -1.46848519
 B -4.02604547 0.84410492 -1.80855045
 H -4.62166161 1.84911310 -1.60397689
 B -4.47842106 -0.74376524 -1.15803274
 H -5.41080964 -0.93801479 -0.45168470
 B -2.87855174 -1.48913289 -0.76316220
 H -2.76902912 -2.20154569 0.17106060
 B -1.59320653 -0.29731411 -2.96208727
 H -0.59127160 -0.06264201 -3.55553828
 B -2.03411625 -1.89041317 -2.31078294
 H -1.37784687 -2.86611262 -2.43313442
 B -3.79300523 -1.96913851 -2.22282240
 H -4.32777149 -3.02353176 -2.32879021
 B -4.46675881 -0.46518908 -2.91448281
 H -5.48630593 -0.42530249 -3.52224979
 B -3.07879511 0.58951477 -3.27684950
 H -3.09237786 1.40967740 -4.13622378
 B -3.00752392 -1.15581945 -3.59782762
 H -2.97663813 -1.61462018 -4.69317448
 B 1.53694110 -2.86836045 -0.57827385
 H 1.64179954 -2.68486923 -1.73952711
 B 0.05429303 -3.43976296 0.17695884
 H -0.86024039 -3.70594799 -0.51187422
 B -0.16294551 -2.55358580 1.67652569
 H -1.22387411 -2.18355769 2.03132841
 B 1.18527723 -1.44788806 1.84921490
 H 1.07125038 -0.34740090 2.25888871
 B 1.53704350 -4.39309699 0.29855679
 H 1.65962886 -5.41248586 -0.29443569
 B 0.47774733 -4.19797474 1.71180981
 H -0.17588658 -5.08997805 2.14042713
 B 1.17894133 -2.94795076 2.75807500
 H 1.04111649 -2.91937876 3.93618504
 B 2.66751950 -2.39631488 2.00212011
 H 3.59769157 -1.89628619 2.53724433
 B 2.88894528 -3.28189448 0.48908693
 H 3.96733114 -3.37430836 0.00877841
 B 2.23140060 -4.10266855 1.90912485
 H 2.87146964 -4.91966124 2.48399420

Experimental

1.1°- DFT B3LYP/6-31G*, gas phase, S ₀  Point group: C1 Total energy: -941211.546 kcal mol ⁻¹ Dipole moment: 14.4146 D Imaginary frequencies: 0	C 0.56625700 -0.46292700 1.82098000 C 0.99346600 0.87420900 1.74532800 H 0.60445300 1.51382700 0.96232000 C 1.93170700 1.39456200 2.63021300 H 2.24687100 2.43148300 2.52630200 C 2.48174400 0.60546400 3.64663200 C 2.04060900 -0.71652700 3.75584000 H 2.43393800 -1.34796200 4.55050500 C 1.10506300 -1.23738100 2.86138900 H 0.78377900 -2.26871400 2.98122500 C 3.53588900 1.16001100 4.57380400 H 4.52726700 1.16143800 4.09891100 H 3.61514500 0.56665000 5.49125100 H 3.31575000 2.19557300 4.85925500 C -1.95741100 -0.66138200 0.95302800 C -2.81528200 1.22284400 -0.01199500 B -2.33517300 0.95321300 1.60466100 H -1.45155900 1.59649200 2.05139500 B -3.06118300 -0.42339300 -0.40085200 H -2.72901300 -0.79497500 -1.47000700 B -3.86776500 1.81374100 1.09641000 H -3.95883400 2.99772000 1.17282600 B -4.37948200 0.84346000 -0.31363400 H -4.86208800 1.29034200 -1.30501300 B -3.30691800 -1.59386500 0.96806200 H -3.15166200 -2.76436500 0.85701600 B -2.78253500 -0.61361500 2.37567900 H -2.20923900 -1.02788500 3.33109500 B -3.88525300 0.76178600 2.50792200 H -4.08205700 1.23184500 3.58481500 B -4.70718900 -0.79490800 0.25048900 H -5.51074800 -1.45974300 -0.32471800 B -4.51728800 -0.83695500 2.02927100 H -5.18628300 -1.51841800 2.74227600 B -5.16454500 0.60811600 1.26504500 H -6.29196900 0.95608800 1.43423000 C -1.96626500 2.05080000 -0.88892200 C -1.88780000 1.80535700 -2.27118200 H -2.47055100 0.99706300 -2.69672100 C -1.07973900 2.58212200 -3.09465800 H -1.04025500 2.36435800 -4.16002100 C -0.31661200 3.63848000 -2.57892500 C -0.40412600 3.89203100 -1.20555700 H 0.17045900 4.71040100 -0.77632400 C -1.20762600 3.11501500 -0.37497800 H -1.25839800 3.33463000 0.68530000 C 0.58849200 4.45084300 -3.47248200 H 0.11103200 4.67203100 -4.43415600 H 1.52139900 3.91405900 -3.69449200 H 0.86229000 5.40244100 -3.00407000
---	--

5.1.8 References

- [1] A. Toppino, A. R. Genady, M. E. El-Zaria, J. Reeve, F. Mostofian, J. Kent, J. F. Valliant, *Inorg. Chem.* **2013**, *52*, 8743–8749.
- [2] G. R. Fulmer, A. J. M. Miller, N. H. Sherden, H. E. Gottlieb, A. Nudelman, B. M. Stoltz, J. E. Bercaw, K. I. Goldberg, *Organometallics* **2010**, *29*, 2176–2179.
- [3] G. M. Sheldrick, *Acta Crystallogr. Sect. A* **2015**, *71*, 3–8.
- [4] G. M. Sheldrick, *Acta Crystallogr. Sect. A* **2008**, *64*, 112–122.
- [5] C. B. Hübschle, G. M. Sheldrick, B. Dittrich, *J. Appl. Cryst.* **2011**, *44*, 1281–1284.
- [6] A. Spek, *Acta Crystallogr. C* **2015**, *71*, 9–18.
- [7] K. Brandenburg, H. Putz, Diamond Version 4.2.0. Crystal and Molecular Structure Visualization, Crystal Impact, Bonn (Germany), **2016**.
- [8] Gaussian 09, Revision 9.E.01, M. J. Frisch, G. W. Trucks, H. B. Schlegel, G. E. Scuseria, M. A. Robb, J. R. Cheeseman, G. Scalmani, V. Barone, G. A. Petersson, H. Nakatsuji, X. Li, M. Caricato, A. V. Marenich, J. Bloino, B. G. Janesko, R. Gomperts, B. Mennucci, H. P. Hratchian, J. V. Ortiz, A. F. Izmaylov, J. L. Sonnenberg, D. Williams-Young, F. Ding, F. Lipparini, F. Egidi, J. Goings, B. Peng, A. Petrone, T. Henderson, D. Ranasinghe, V. G. Zakrzewski, J. Gao, N. Rega, G. Zheng, W. Liang, M. Hada, M. Ehara, K. Toyota, R. Fukuda, J. Hasegawa, M. Ishida, T. Nakajima, Y. Honda, O. Kitao, H. Nakai, T. Vreven, K. Throssell, J. A. Montgomery, Jr., J. E. Peralta, F. Ogliaro, M. J. Bearpark, J. J. Heyd, E. N. Brothers, K. N. Kudin, V. N. Staroverov, T. A. Keith, R. Kobayashi, J. Normand, K. Raghavachari, A. P. Rendell, J. C. Burant, S. S. Iyengar, J. Tomasi, M. Cossi, J. M. Millam, M. Klene, C. Adamo, R. Cammi, J. W. Ochterski, R. L. Martin, K. Morokuma, O. Farkas, J. B. Foresman, and D. J. Fox, Gaussian, Inc., Wallingford CT, **2016**.
- [9] T. Lu, F. Chen, *J. Comput. Chem.* **2012**, *33*, 580–592.
- [10] Lee, Yang, Parr, *Phys. Rev. B* **1988**, *37*, 785–789.
- [11] G. A. Petersson, M. A. Al-Laham, *J. Chem. Phys.* **1991**, *94*, 6081–6090.
- [12] G. A. Petersson, A. Bennett, T. G. Tensfeldt, M. A. Al-Laham, W. A. Shirley, J. Mantzaris, *J. Chem. Phys.* **1988**, *89*, 2193–2218.
- [13] S. Grimme, *Chem. Eur. J.* **2004**, *10*, 3423–3429.
- [14] T. Yanai, D. P. Tew, N. C. Handy, *Chem. Phys. Lett.* **2004**, *393*, 51–57.
- [15] M. J. G. Peach, P. Benfield, T. Helgaker, D. J. Tozer, *J. Chem. Phys.* **2008**, *128*, 044118.

Experimental

5.2 Supporting Information Chapter 2

5.2.1 General experimental details

Unless otherwise noted, the following conditions apply. All syntheses were carried out using standard Schlenk and glovebox techniques under an argon atmosphere. The solvents used were dried using either a solvent purification system (SPS) from Innovative Technology or were distilled and degassed from appropriate drying agents and stored under argon. Deuterated solvents (CD_2Cl_2 and C_6D_6) used for NMR spectroscopy were purchased from Cambridge Isotope Laboratories. C_6D_6 and CD_2Cl_2 were dried over molecular sieves, degassed by three freeze-pump-thaw cycles and stored under an argon atmosphere prior to use. *n*-Butyllithium (2.5 M solution in hexane) was purchased from Acros Organics and used as received. The compounds 9-bromo-9-borafluorene^[1] and 1,2-bis(dichloroboryl)benzene^[2] were prepared according to literature procedures. All other starting materials were purchased from commercial sources and were used without further purification.

NMR Spectra were recorded on a Bruker Avance 500 FT NMR spectrometer (operating at ^1H : 500 MHz, ^{11}B : 160 MHz, $^{13}\text{C}\{^1\text{H}\}$: 126 MHz. Chemical shifts (δ) are given in ppm and $^{11}\text{B}\{^1\text{H}\}$ NMR spectra are referenced to external $\text{BF}_3\cdot\text{Et}_2\text{O}$. ^1H NMR spectra were referenced via residual proton resonances of CD_2Cl_2 (5.32 ppm) and C_6D_6 (7.16 ppm). $^{13}\text{C}\{^1\text{H}\}$ spectra were referenced to CD_2Cl_2 (53.84 ppm) and C_6D_6 (128.06 ppm).

HRMS were recorded using a Thermo Scientific Exactive Plus Orbitrap MS system by Liquid Injection Field Desorption Ionization (LIFDI).

Single-crystal X-ray diffraction: Crystals suitable for single-crystal X-ray diffraction were selected, coated in perfluoropolyether oil or polybutyl oil, mounted on a polyimide microloop (MicroMounts from MiTeGen) and transferred to a stream of cold nitrogen (Oxford Cryostream 700 or 800, respectively). Diffraction data were collected on a Bruker X8 Apex II 4-circle diffractometer with a CCD area detector, using Mo-K α radiation generated by a Nonius FR591 rotating anode and monochromated by graphite (**2.3a**) or by multi-layer focusing mirrors (**2.2b**). Diffraction data were collected on a Rigaku Oxford Diffraction XtaLAB Synergy diffractometer with a semiconductor HPA-detector (HyPix-6000 or HyPix-Arc-150) and multi-layer mirror monochromated Cu-K α radiation generated by a PhotonJet (**2.3a**·THF) or a PhotonJet-R (**2.3b** and **2.5**) source. Data were collected at 100 K or 173 K (**2.5**). The images were processed and corrected for Lorentz-polarization effects and absorption (empirical scaling) as implemented in the Bruker software packages (**2.2b** and **2.3a**) or using the CrysAlis^{Pro} software from Rigaku Oxford Diffraction (**2.3b**, **2.3a**·THF and **2.5**). The structures were solved using the intrinsic phasing method (SHELXT)^[3] and Fourier expansion technique. All non-hydrogen atoms were refined in anisotropic approximation, with all hydrogen atoms ‘riding’ in idealized positions, by full-matrix least squares against F^2 of all data, using SHELXL^[4] software and the SHELXE^[5] graphical user interface. In the case of **2.3a** disordered solvent was masked using

Experimental

SQUEEZE/PLATON.^[6] **2.3b** and **2.3a·THF** were refined as two-component twins, both with twin fractions of 48%. Diamond software was used for graphical representation.^[7] Crystal data and experimental details are listed in Table 5.1.1. Full structural information has been deposited with the Cambridge Crystallographic Data Centre. CCDC-2174245 (**2.2b**), 2174247 (**2.3a**), 2174246 (**2.3b**), 2174248 (**2.3a·THF**), and 2174249 (**2.5**).

Photophysical measurements: All measurements were performed in standard quartz cuvettes (1 cm x 1 cm cross-section). UV-visible absorption spectra were recorded using an Perkin Elmer Lambda 465 UV-visible spectrophotometer. **Emission spectra** were recorded using an Edinburgh Instruments FLSP920 spectrophotometer equipped with a double monochromator for both excitation and emission, operating in right-angle geometry mode, and all spectra were fully corrected for the spectral response of the instrument. **Fluorescence quantum yields** were measured using a calibrated integrating sphere (inner diameter: 150 mm) from Edinburgh Instruments combined with the FLSP920 spectrophotometer described above. For solution-state and solid-state measurements, the longest-wavelength absorption maximum of the compound in the respective solvent was chosen as the excitation wavelength. **Fluorescence lifetimes** were recorded using the time-correlated single-photon counting (TCSPC) method using the same FLSP920 spectrometer described above. Solutions were excited with a picosecond pulsed diode laser at 376.6 nm. The full width at half maximum (FWHM) of the laser pulses were ca. 70–200 ps, while the instrument response function (IRF) had a FWHM of ca. 1.0 ns, measured from the scatter of a Ludox solution at the excitation wavelength. Decays were recorded to at least 10000 counts in the peak channel with a record length of at least 1000 channels. The band pass of the monochromator was adjusted to give a signal count rate of <10 kHz. Iterative deconvolution of the IRF with one decay function and non-linear least-squares analysis were used to analyze the data. The quality of the fit was judged by the calculated value of the reduced χ^2 and visual inspection of the weighted residuals.

Experimental

Computational methods

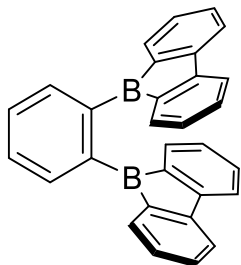
All molecular geometries were fully optimized via DFT calculations at the B3LYP-D(BJ), wB97X-D^[8] and M062X^[9-11]/6-31G(d,p)^[12-13] level of theory. Frequency calculations at the same level of theory were performed to confirm that all stationary points are local minima (no imaginary frequencies) or transition states (one imaginary frequency) and to provide free energies at 298.15K. Transition states were located using the Berny algorithm and further confirmed by calculations of intrinsic reaction coordinates (IRC)^[14] showing that the transition states indeed connect the two relevant minima. All DFT calculations were performed with the Gaussian 09 (D.01) program.^[15]

All calculations regarding the photophysical experiments of **2.2a**, **2.2b**, **2.3a** and **2.3b** (DFT and TD-DFT) were carried out with the Gaussian 09 (9.E.01)^[16] program package and were performed on a parallel cluster system. GaussView (6.0.16) and multiwfn^[17] were used to visualize the results, to measure calculated structural parameters, and to plot orbital surfaces (isovalue: $\pm 0.030 [e a_0^{-3}]^{1/2}$). The ground-state geometries were optimized using the B3LYP functional^[18] in combination with the 6-31+G(d,p) basis set.^[19-20] The orbital overlap parameter was calculated with $\Lambda = \frac{\sum_{i,a} c_{i,a}^2 \langle | \varphi_a | | \varphi_i | \rangle}{\sum_{i,a} c_{i,a}^2}$, resulting in $0 \leq \Lambda \leq 1$, where $\Lambda = 0$ corresponds to no overlap and $\Lambda = 1$ corresponds to complete overlap.^[21] The ultrafine integration grid and symmetry constraints were used for all molecules. Frequency calculations were performed on the optimized structures to confirm them to be local minima showing no negative (imaginary) frequencies. Based on these optimized structures, the lowest-energy vertical transitions (using the polarizable continuum model) were calculated (singlets, 25 states) by TD-DFT, using the Coulomb attenuated functional CAM-B3LYP^[22] as well as B3LYP. The CAM-B3LYP functional has been shown to more accurately describe CT systems in comparison to B3LYP.^[21] The optimized ground-state geometries were used as starting coordinates for TD-DFT geometry optimizations.

Experimental

5.2.2 Synthetic procedures

Bis(bis-9-borafluorenyl)benzene (2.2b)



Via syringe, a solution of 1,2-bis(dichloroboryl)benzene **2.4** (119 mg, 495 μmol , 1.0 eq.) in 10 mL toluene was slowly added to a solution of dimethyldibenzostannole (300 mg, 990 μmol , 2.0 eq.) in 10 mL toluene at -78°C in a Schlenk tube. The solution was stirred and allowed to warm to room temperature overnight. After removal of all volatiles including Me_2SnCl_2 *in vacuo*, the residue was washed with hexane (3 x 20 mL) to yield a yellow solid **2.2b** (158 mg, 393 μmol , 79%).

$^1\text{H NMR}$ (500.1 MHz, CD_2Cl_2): δ = 8.03 (m, 2H, CH_{Ar}), 7.70 (m, 2H, CH_{Ar}), 7.47 (m, 4H, CH), 7.29 (m, 4H, CH), 7.23 (m, 4H, CH), 6.95 (m, 4H, CH) ppm.

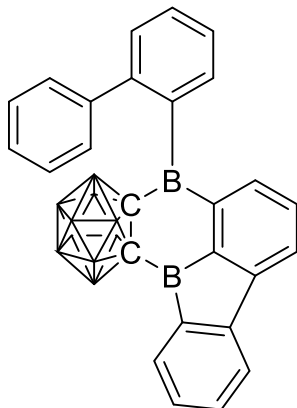
$^{11}\text{B NMR}$ (160.5 MHz, CD_2Cl_2): δ = 67.0 (br) ppm.

$^{13}\text{C}\{^1\text{H}\} \text{NMR}$ (125.8 MHz, CD_2Cl_2): δ = 154.03 ($C_{\text{q},\text{Ar}}$), 145.03 ($C_{\text{q},\text{Ar}}$), 143.78 ($C_{\text{q},\text{Ar}}$), 134.81 (CH_{Ar}), 134.43 (CH_{Ar}), 134.16 (CH_{Ar}), 130.70 (CH_{Ar}), 128.42 (CH_{Ar}), 120.06 (CH_{Ar}) ppm.

HRMS LIFDI calc. for $[\text{C}_{30}\text{H}_{20}\text{B}_2]^+$ = [M]⁺: 402.1746, found 402.1744.

Experimental

3-([1,1'-biphenyl]-2-yl)-3*H*-1,2-(1,2-*ortho*-carboranyl)-3,10*b*-diborafluoranthene (2.3a**)**



Ortho-carborane (200 mg, 1.39 mmol, 1.0 eq.) was dissolved in toluene (5 mL) and a 2.5 M *n*BuLi solution in hexane (1.16 mL, 2.91 mmol, 2.1 eq.) was added dropwise at -78 °C. The reaction mixture was slowly warmed to room temperature and stirred at 80 °C overnight to obtain the dilithiated species **1** *in situ*. Then 9-bromo-9-borafluorene (707 mg, 2.91 mmol, 2.1 eq.) in toluene (5 mL) was added dropwise at -78 °C after which the reaction was slowly warmed to room temperature and stirred for 4 d. The suspension was filtered, the solid was washed with toluene (5 mL) and all volatiles were removed from the filtrate *in vacuo*. The crude product was recrystallized from toluene by hexane diffusion at -30 °C to give **2.3b** as orange crystals (85.0 mg, 182 μmol, 13%).

¹H NMR (500.1 MHz, CD₂Cl₂): δ = 7.65 (m, 1H, CH_{Ar}), 7.59 (m, 1H, CH_{Ar}), 7.56 (m, 1H, CH_{Ar}), 7.42 (m, 3H, CH_{Ar}), 7.36 (m, 1H, CH_{Ar}), 7.31 (m, 6H, CH_{Ar}), 7.25 (m, 1H, CH_{Ar}), 7.18 (m, 1H, CH_{Ar}), 7.16 (m, 1H, CH_{Ar}), 3.18–1.53 (br, 10H, BH) ppm.

¹H{¹¹B} NMR (500.1 MHz, CD₂Cl₂): δ = 7.65 (m, 1H, CH_{Ar}), 7.59 (m, 1H, CH_{Ar}), 7.56 (m, 1H, CH_{Ar}), 7.42 (m, 3H, CH_{Ar}), 7.36 (m, 1H, CH_{Ar}), 7.31 (m, 6H, CH_{Ar}), 7.25 (m, 1H, CH_{Ar}), 7.18 (m, 1H, CH_{Ar}), 7.16 (m, 1H, CH_{Ar}), 2.61(s, 1H, BH), 2.45–2.34 (m, 5H, BH), 2.27 (s, 1H, BH), 2.21(s, 1H, BH), 2.05(s, 1H, BH), 1.55(s, 1H, BH) ppm.

¹¹B NMR (160.5 MHz, CD₂Cl₂): δ = 66.1, 3.2, -4.4, -8.8 ppm.

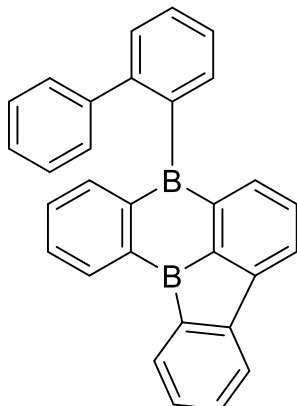
¹¹B{¹H} NMR (160.5 MHz, CD₂Cl₂): δ = 66.1, 2.6, 2.2, -5.0, -5.7, -9.6 ppm.

¹³C{¹H} NMR (125.8 MHz, CD₂Cl₂): δ = 155.8 (C_{q,Ar}), 152.9 (C_{q,Ar}), 143.9 (C_{q,Ar}), 143.8 (C_{q,Ar}), 138.6 (CH_{Ar}), 137.1 (CH_{Ar}), 136.4 (CH_{Ar}), 136.2 (CH_{Ar}), 129.9 (CH_{Ar}), 129.7 (CH_{Ar}), 129.6 (CH_{Ar}), 126.5 (CH_{Ar}), 129.1 (CH_{Ar}), 129.0 (CH_{Ar}), 128.1 (CH_{Ar}), 126.1 (CH_{Ar}), 125.7 (CH_{Ar}), 121.7 (CH_{Ar}) ppm.

HRMS LIFDI calc. for [C₂₆H₂₆B₁₂]⁺ = [M]⁺: 468.3219, found 468.3218.

Experimental

5-([1,1'-biphenyl]-2-yl)-5H-benzo[4,5]borolo[3,2,1-de]boranthrene (**2.3b**)



Compound **2.2b** (37.0 mg, 92.0 μmol) was heated for 3 d at 120 °C in toluene. Removal of all volatiles *in vacuo* led to the isolation of **2.3b** as an orange solid (34.0 mg, 84.5 μmol , 92%).

$^1\text{H NMR}$ (500.1 MHz, CD_2Cl_2): δ = 8.33 (m, 1H, CH_{Ar}), 8.02 (m, 1H, CH_{Ar}), 7.73 (m, 1H, CH_{Ar}), 7.67 (m, 1H, CH_{Ar}), 7.58 (m, 1H, CH_{Ar}), 7.55 (m, 1H, CH_{Ar}) 7.48 (m, 3H, CH_{Ar}), 7.42 (m, 1H, CH_{Ar}), 7.39 (m, 1H, CH_{Ar}), 7.35 (m, 3H, CH_{Ar}), 7.20 (m, 1H, CH_{Ar}), 7.13 (m, 4H, CH_{Ar}), 6.98 (m, 1H, CH_{Ar}) ppm.

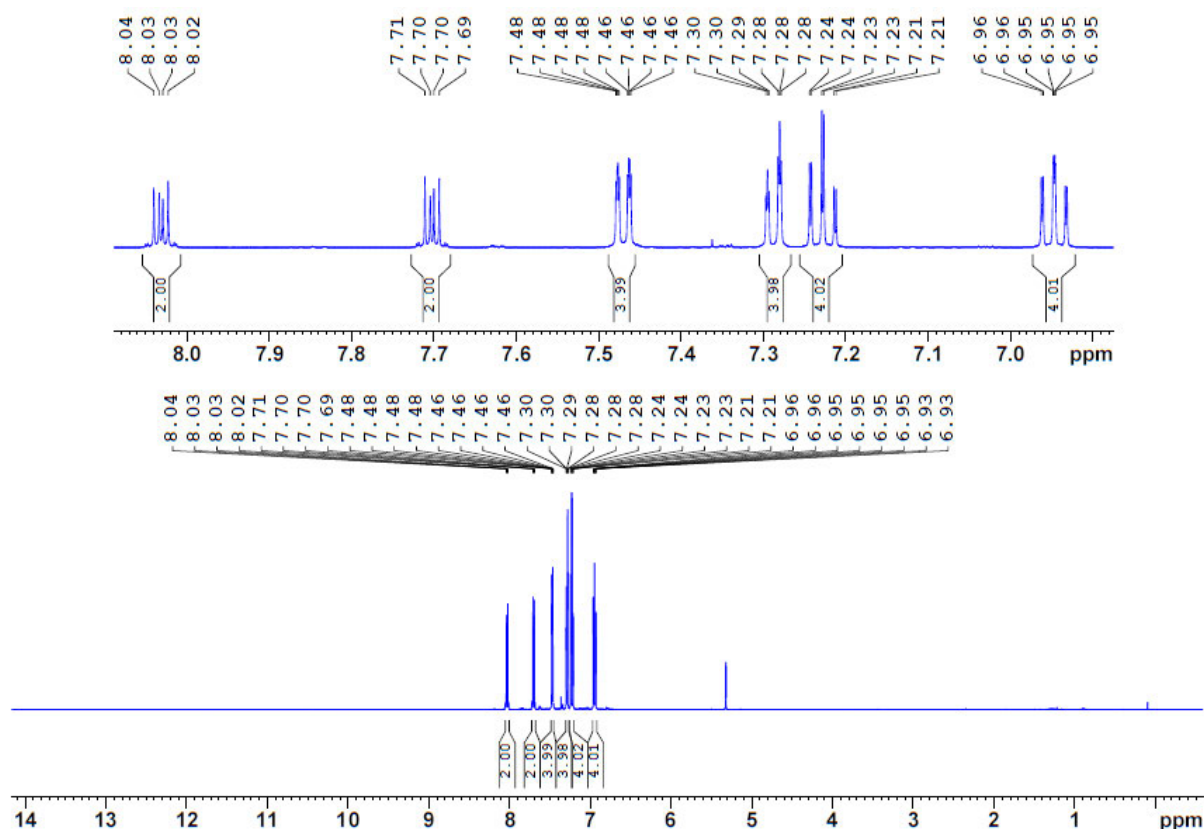
$^{11}\text{B NMR}$ (160.5 MHz, CD_2Cl_2): δ = 63.9 (br) ppm.

$^{13}\text{C}\{^1\text{H}\} \text{NMR}$ (125.8 MHz, CD_2Cl_2): δ = 156.80 ($C_{\text{q},\text{Ar}}$), 153.26 ($C_{\text{q},\text{Ar}}$), 150.80 ($C_{\text{q},\text{Ar}}$), 149.68 ($C_{\text{q},\text{Ar}}$), 145.62 ($C_{\text{q},\text{Ar}}$), 144.32 ($C_{\text{q},\text{Ar}}$), 144.11 ($C_{\text{q},\text{Ar}}$), 143.36 ($C_{\text{q},\text{Ar}}$), 141.99 ($C_{\text{q},\text{Ar}}$), 141.12 (CH_{Ar}), 137.49 (CH_{Ar}), 135.79 (CH_{Ar}), 135.60 (CH_{Ar}), 134.72 (CH_{Ar}), 133.97 (CH_{Ar}), 133.95 (CH_{Ar}), 132.18 (CH_{Ar}), 131.51 (CH_{Ar}), 129.08 (CH_{Ar}), 128.96 (CH_{Ar}), 128.93 (CH_{Ar}), 128.50 (CH_{Ar}), 128.44 (CH_{Ar}), 127.52 (CH_{Ar}), 126.46 (CH_{Ar}), 123.40 (CH_{Ar}), 121.14 (CH_{Ar}), ppm.

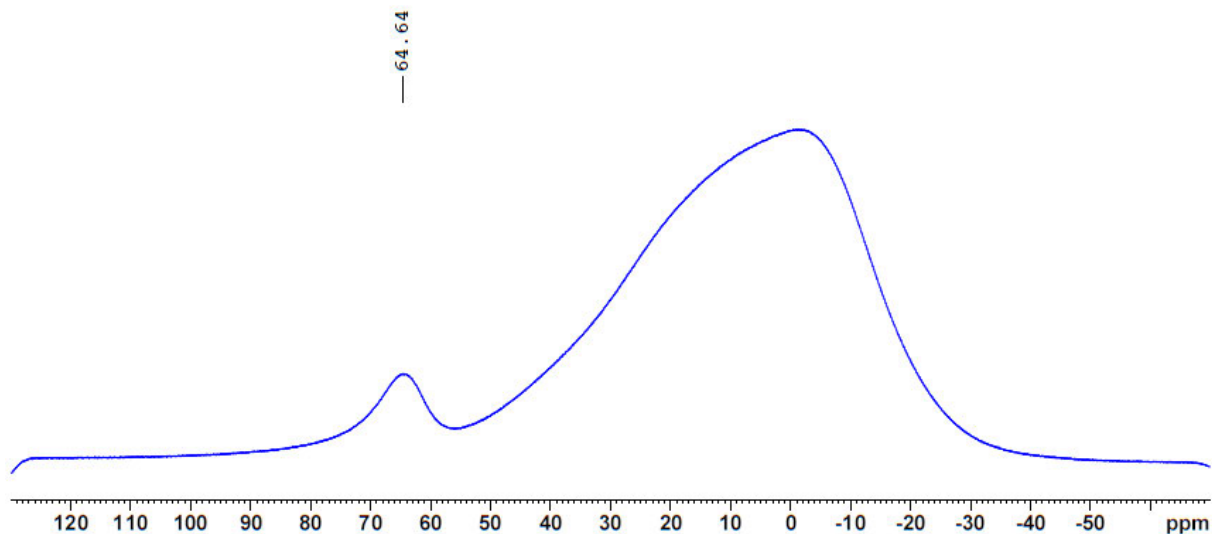
HRMS LIFDI calc. for $[\text{C}_{30}\text{H}_{20}\text{B}_2]^+$ = [M]⁺: 402.1746, found 402.1743.

Experimental

¹H NMR spectrum of 2.2b in CD₂Cl₂

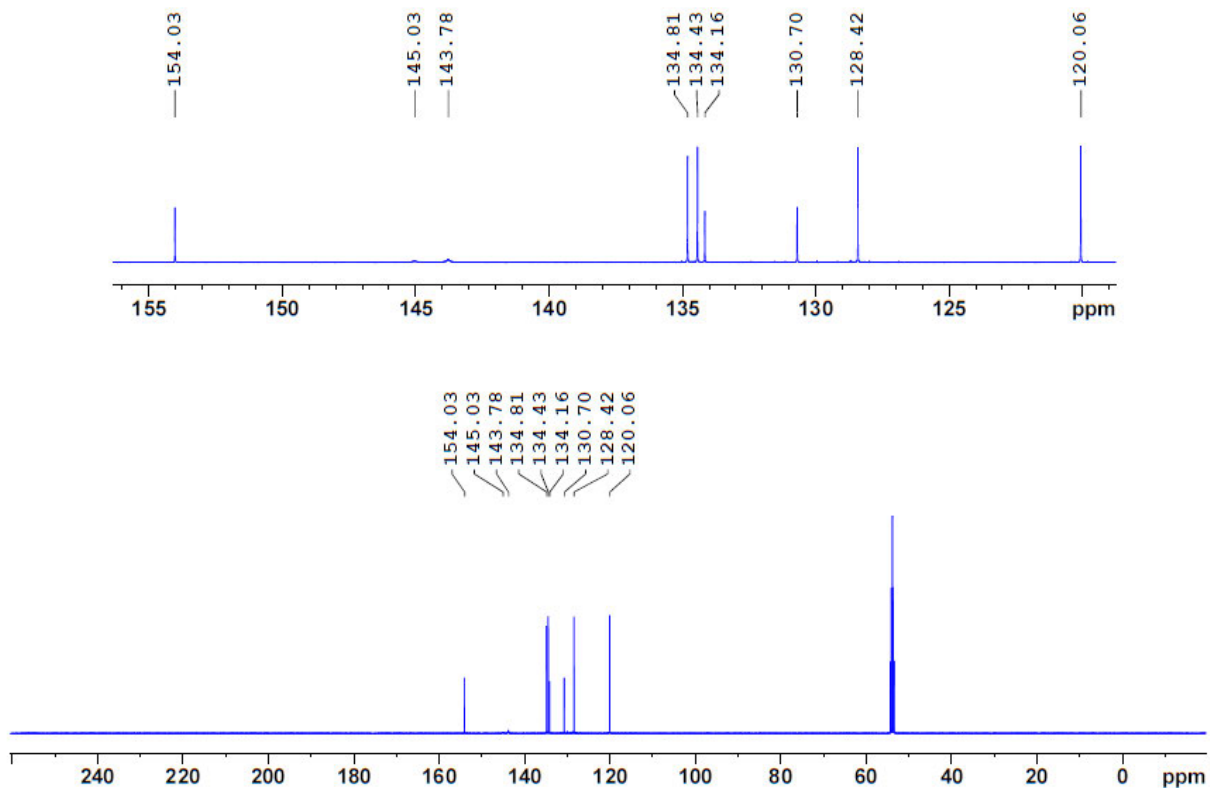


¹¹B NMR spectrum of 2.2b in CD₂Cl₂



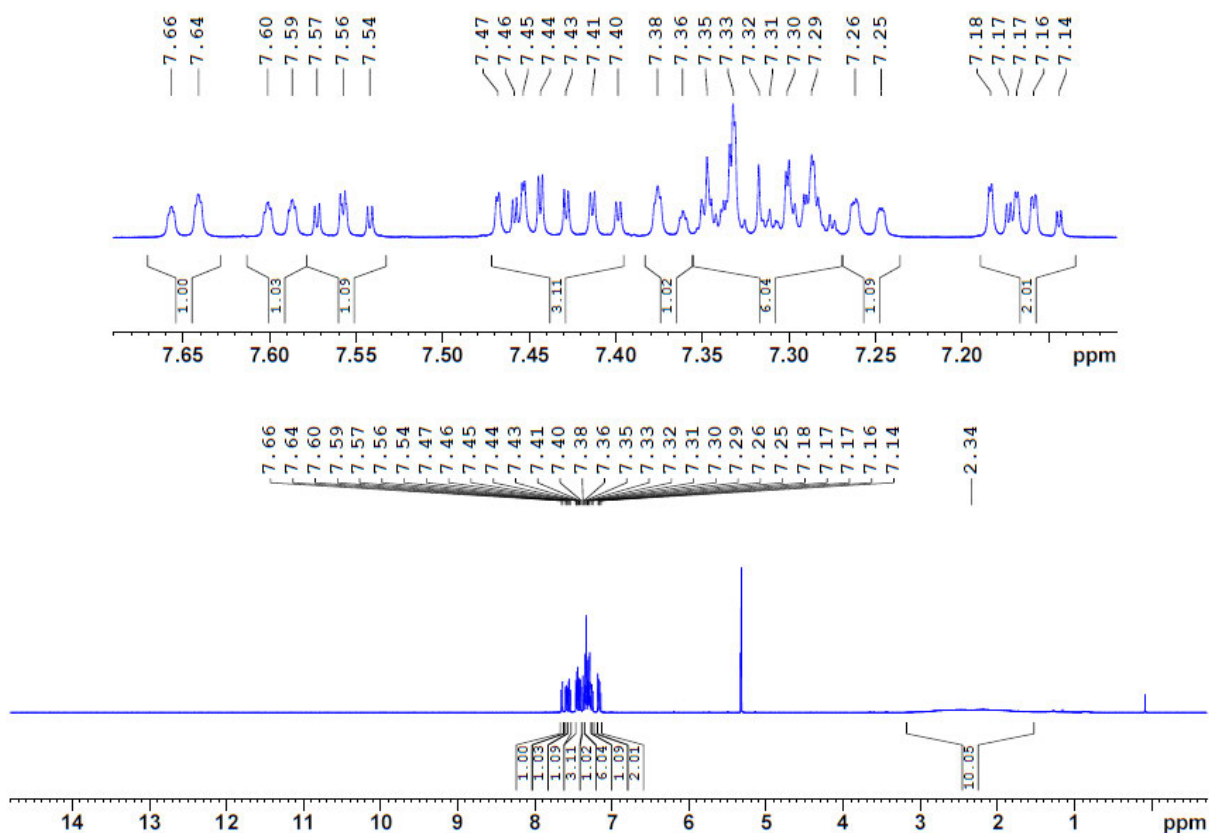
Experimental

$^{13}\text{C}\{^1\text{H}\}$ NMR spectrum of 2.2b in CD_2Cl_2

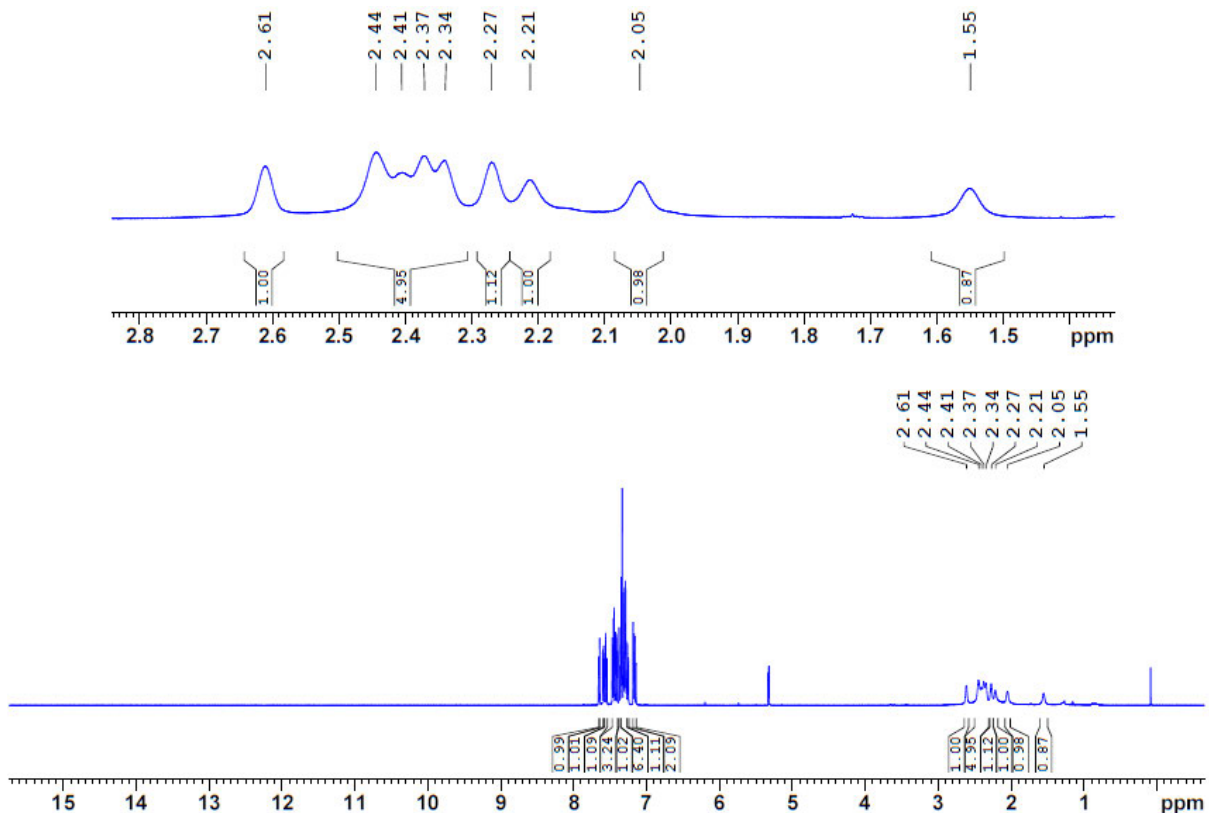


Experimental

^1H NMR spectrum of 2.3a in CD_2Cl_2

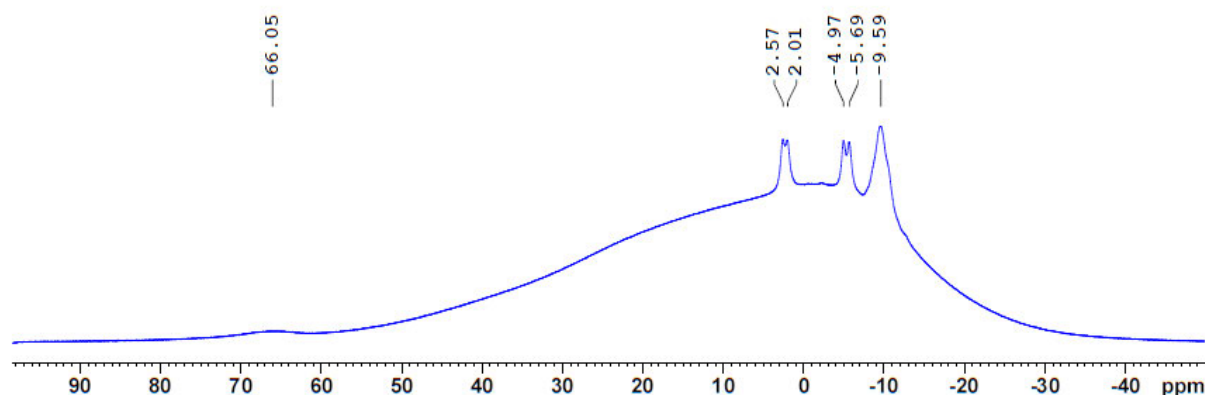


$^1\text{H} \{^{11}\text{B}\}$ NMR spectrum of 2.3a in CD_2Cl_2

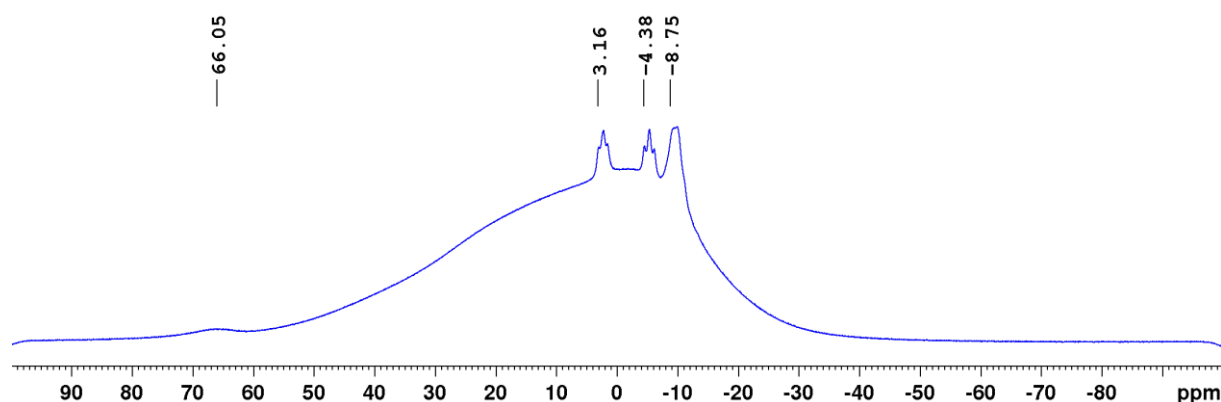


Experimental

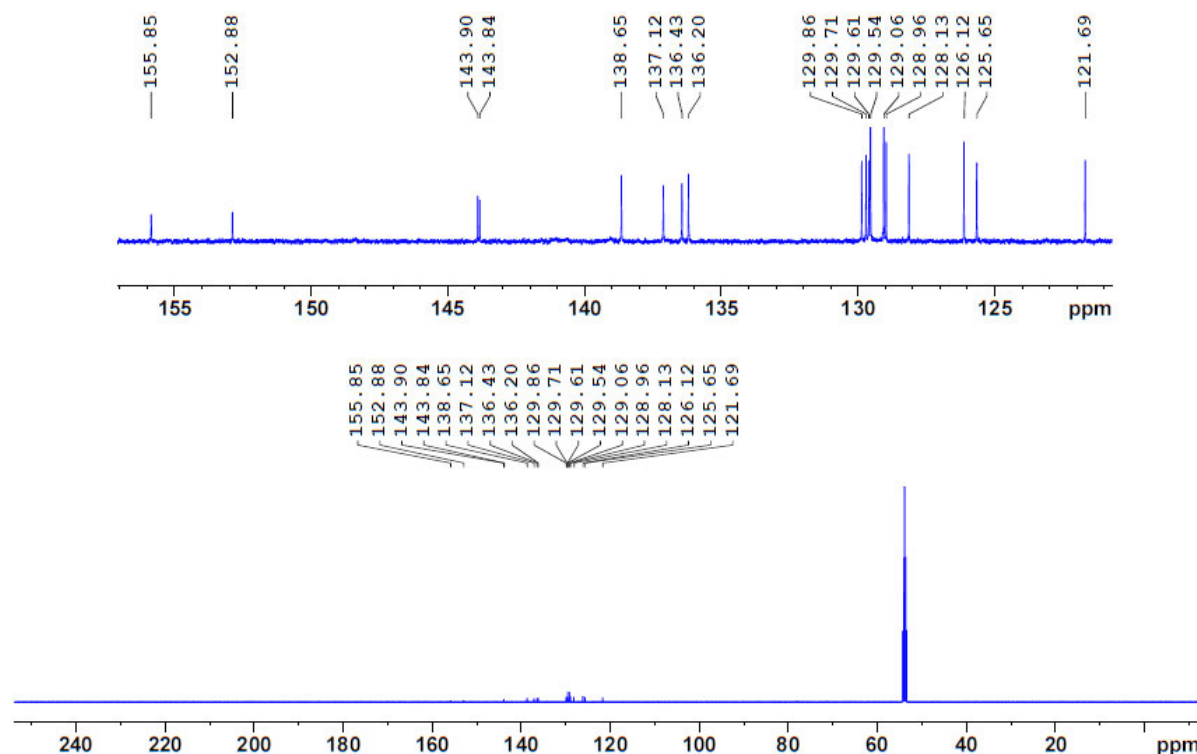
^{11}B NMR spectrum of 2.3a in CD_2Cl_2



$^{11}\text{B}\{\text{H}\}$ NMR spectrum of 2.3a in CD_2Cl_2

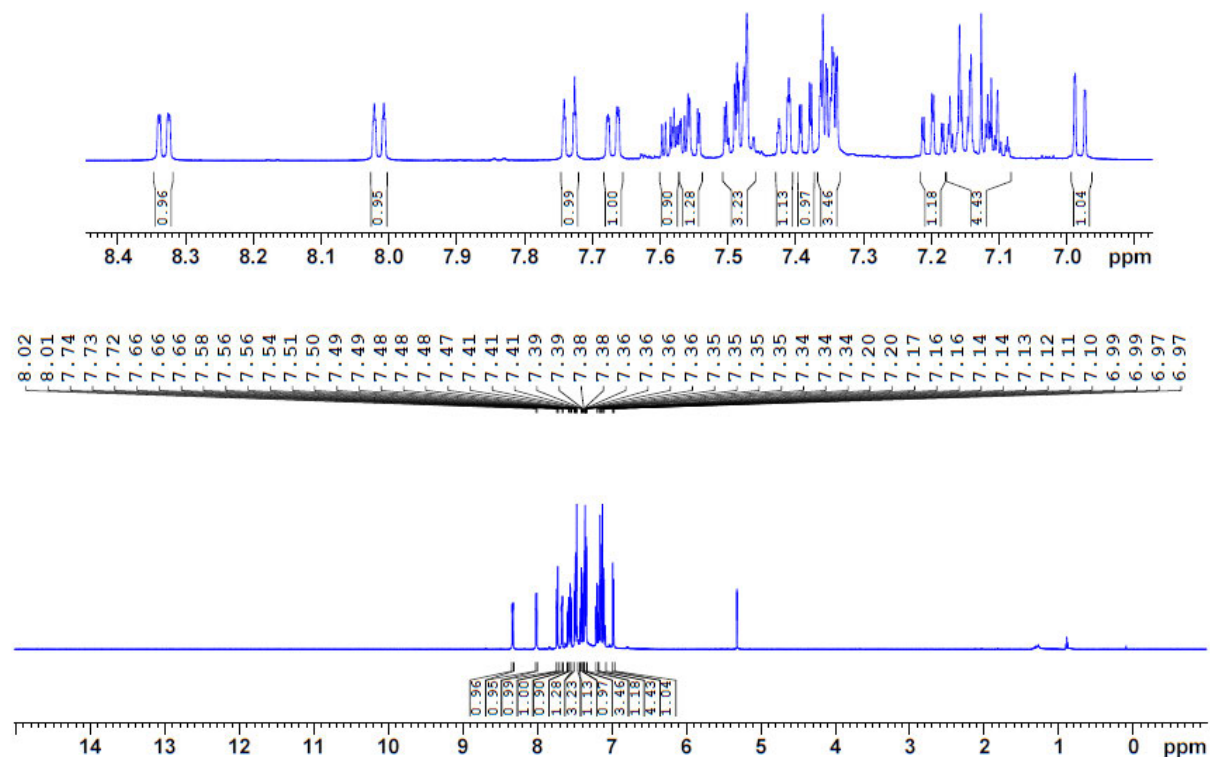


$^{13}\text{C}\{\text{H}\}$ NMR spectrum of 2.3a in CD_2Cl_2

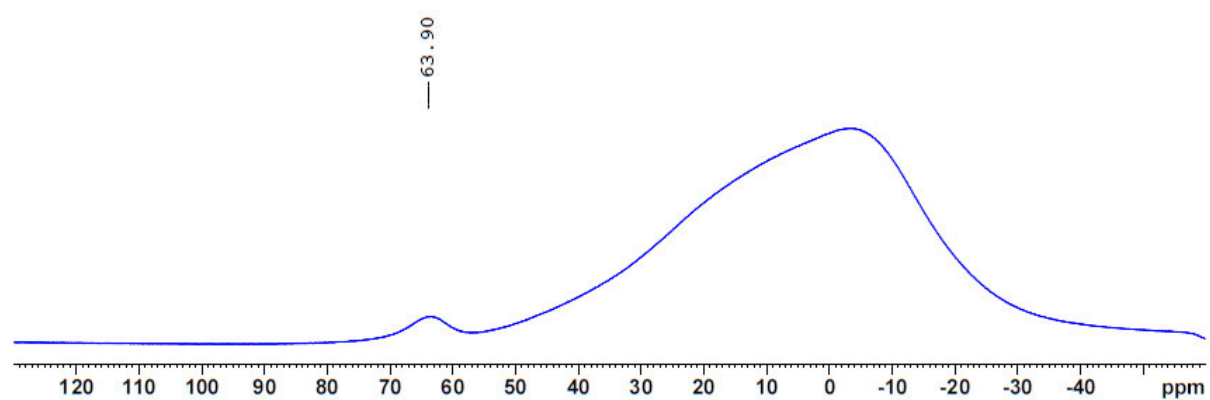


Experimental

¹H NMR spectrum of 2.3b in CD₂Cl₂

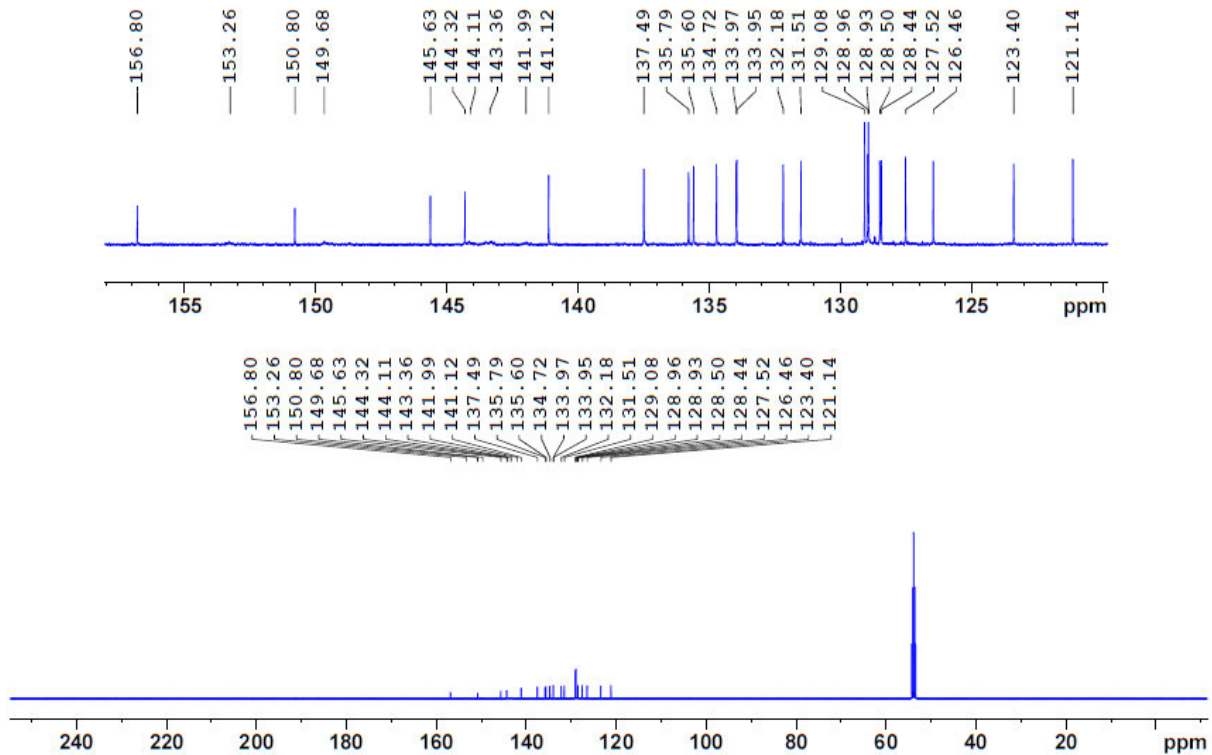


¹¹B NMR spectrum of 2.3b in CD₂Cl₂



¹³C{¹H} NMR spectrum of 2.3b in CD₂Cl₂

Experimental



Experimental

5.2.3 Single-crystal X-ray diffraction

Table 5.1.1. Single-crystal X-ray diffraction data and structure refinements of **2.2b**, **2.3a**, **2.3b**, **2.3a·THF**, and **2.5**.

	2.2b	2.3a	2.3b	2.3a·THF	2.5
CCDC	2174245	2174247	2174246	2174248	2174249
Empirical formula	C ₃₀ H ₂₀ B ₂	C ₂₆ H ₂₆ B ₁₂	C ₃₀ H ₂₀ B ₂ [+solvent]	2(C ₃₀ H ₃₄ B ₁₂ O), C ₇ H ₈	C ₃₈ H ₅₀ B ₁₂ Br ₂ LiO ₃ , C ₁₆ H ₃₂ LiO ₄
$\rho_{\text{calc}}/\text{g}\cdot\text{cm}^{-3}$	1.260	1.213	1.065	1.207	1.132
F(000)	840	968	1680	614	2392
Crystal size/mm ³	0.22×0.20× 0.16	0.68×0.32×0.27	0.15×0.04× 0.02	0.31×0.18×0.13	0.24×0.13×0.12
Crystal colour, habit	yellow block	orange block	orange block	colourless block	yellow block
μ/mm^{-1}	0.070	0.062	0.445	0.476	2.082
M _r /g·mol ⁻¹	402.08	468.19	402.08	1172.71	1146.60
Temperature/K	100(2)	100(2)	100(2)	100(2)	173.01(10)
Radiation, $\lambda/\text{\AA}$	MoK _α , 0.71073	MoK _α , 0.71073	CuK _α , 1.54184	CuK _α , 1.54184	CuK _α , 1.54184
Crystal system	monoclinic	monoclinic	monoclinic	triclinic	orthorhombic
Space group	P2 ₁ /n	P2 ₁ /c	P2 ₁	P̄1	P2 ₁ 2 ₁ 2 ₁
a/Å	10.040(3)	11.6705(5)	9.81472(6)	10.0646(3)	10.14540(10)
b/Å	14.612(6)	11.4351(5)	30.3107(2)	11.5240(4)	15.55010(10)
c/Å	14.451(4)	19.4944(8)	16.86116(12)	15.6916(5)	37.9243(2)
$\alpha/^\circ$	90	90	90	105.086(3)	90
$\beta/^\circ$	90.177(9)	99.7240(10)	90.0056(6)	98.763(3)	90
$\gamma/^\circ$	90	90	90	108.320(3)	90
Volume/Å ³	2120.0(12)	2564.21(19)	5016.04(6)	1612.85(9)	5983.02(8)
Z	4	4	8	4	4
2θ/°	3.96–53.46	3.54–52.08	5.24–150.63	6.03–153.86	4.66–151.03
Unique reflections	4510	5057	20250	12402	12305
Parameters / restraints	289/0	383/0	1154/1	463/122	919/624
GooF on F^2	1.076	1.032	1.039	1.046	1.020
R ₁ [$ I \geq 2\sigma(I)$]	0.0443	0.0432	0.0575	0.0654	0.0519
wR ₂ [all data]	0.1072	0.1134	0.1629	0.1955	0.1512
Max./min. res. electron density/e Å ⁻³	0.33 / -0.26	0.30 / -0.26	0.39 / -0.28	0.30 / -0.35	0.65 / -0.60

Experimental

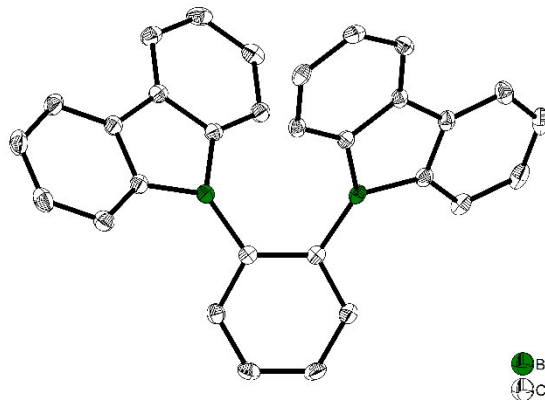


Figure 5.1.1. Solid state molecular structure of **2.2b** from single-crystal X-ray diffraction at 100 K. Atomic displacement ellipsoids are drawn at the 50% probability level and hydrogen atoms are omitted for clarity.

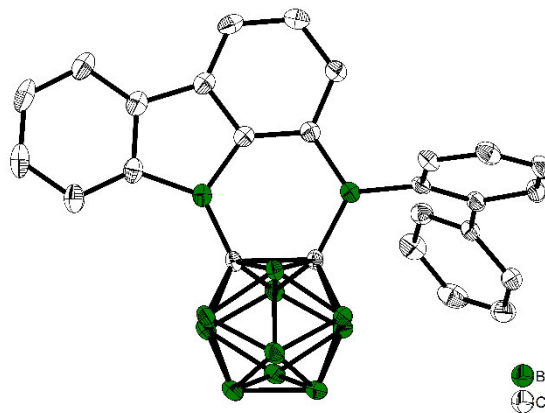


Figure 5.1.2 Solid state molecular structure of **2.3a** from single-crystal X-ray diffraction at 100 K. Atomic displacement ellipsoids are drawn at the 50% probability level and hydrogen atoms are omitted for clarity.

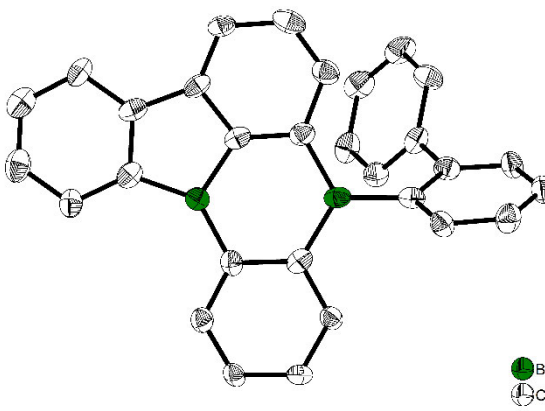


Figure 5.1.3. Solid state molecular structure of **2.3b** from single-crystal X-ray diffraction at 100 K. Atomic displacement ellipsoids are drawn at the 50% probability level and hydrogen atoms and solvent molecules are omitted for clarity. Only one of four symmetry-independent molecules is shown.

Experimental

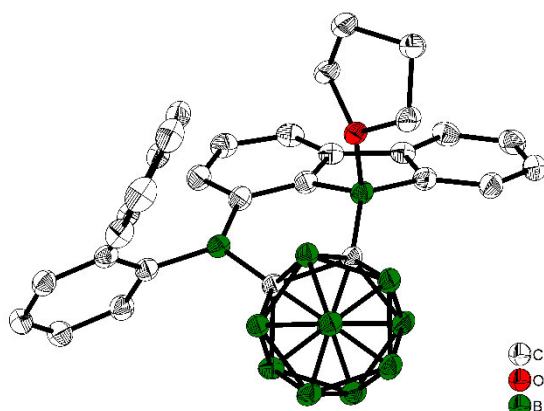


Figure 5.1.4. Solid state molecular structure of **2.3a·THF** from single-crystal X-ray diffraction at 100 K. Atomic displacement ellipsoids are drawn at the 50% probability level and solvent molecules and hydrogen atoms are omitted for clarity.

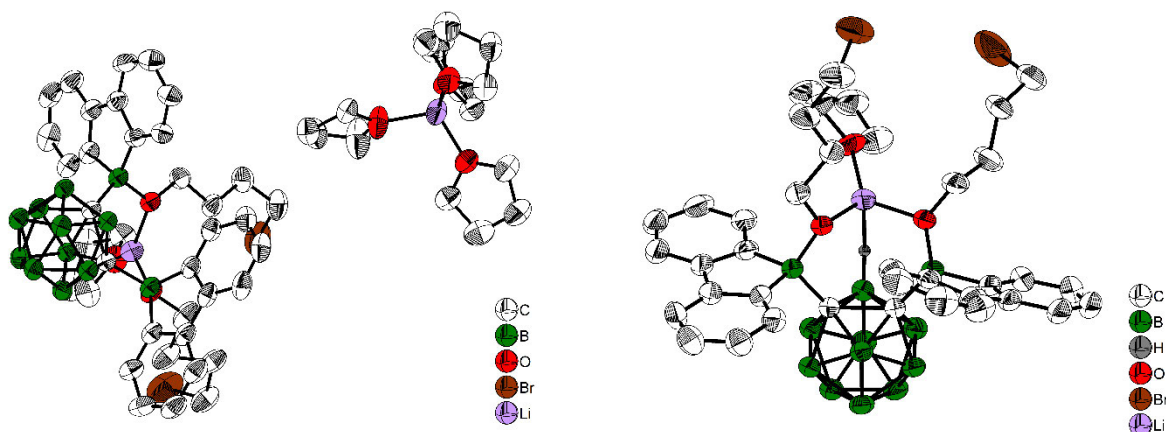
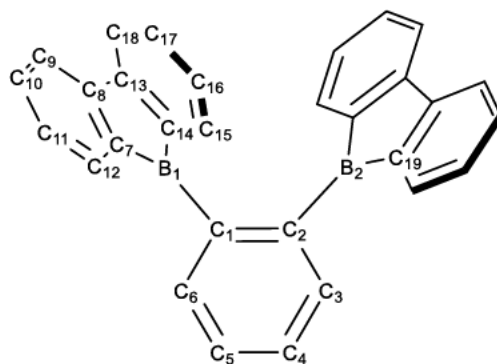


Figure 5.1.5. Solid state molecular structure of **2.5** from single-crystal X-ray diffraction at 100 K, on the left with the lithium counterion and on the right from a different angle. Atomic displacement ellipsoids are drawn at the 50% probability level, and hydrogen atoms and the minor occupied components of disordered THF and alkyl groups are omitted for clarity. Only one of two symmetry-independent anions and cations are shown.

Experimental

5.2.4 Geometry tables



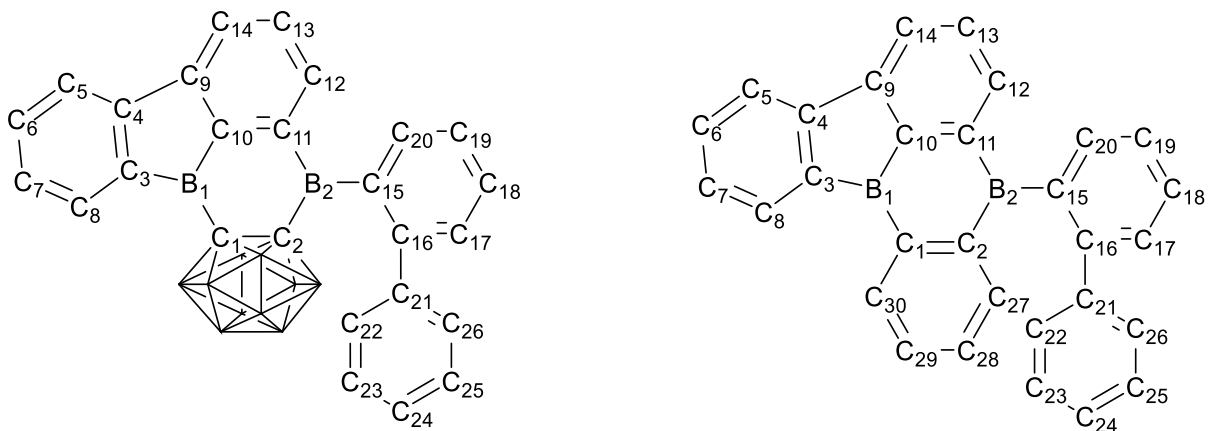
Scheme 5.1.1. Atom labeling in compound **2.2b**.

Table 5.1.2. Selected bond lengths [\AA], distances [\AA], and angles [$^\circ$] in the crystal and calculated at the B3LYP-d3bj and ω B97X-D level of theory (starting molecule).

	2.2a calc. B3LYP-d3bj	2.2a calc. ω B97X-D	2.2b crystal	2.2b calc. B3LYP-d3bj	2.2b calc. ω B97X-D
C ₁ –C ₂	1.674	1.674	1.426(2)	1.426	1.420
C ₁ –C ₆ / C ₂ –C ₃	–	–	1.402(2) / 1.405(2)	1.404	1.402
C ₅ –C ₆ / C ₃ –C ₄	–	–	1.388(2) / 1.389(2)	1.396	1.393
C ₄ –C ₅	–	–	1.386(2)	1.395	1.393
B ₁ –C ₁ ^a	1.591	1.600	1.554(2) / 1.551(2)	1.550	1.556
B ₁ –C ₁₄ ^a	1.566	1.570	1.571(2) / 1.571(2)	1.564	1.568
B ₁ –C ₇ ^a	1.562	1.566	1.568(2) / 1.571(2)	1.565	1.570
B ₁ –B ₂	3.025	3.054	3.186(2)	3.005	3.083
B ₂ –C ₁₅ ^a	3.428	3.487	3.252(2) / 3.354(2)	3.153	3.231
C ₁₄ –C ₁₃ ^a	1.426	1.418	1.417(2) / 1.415(2)	1.421	1.414
C ₇ –C ₈ ^a	1.421	1.413	1.416(2) / 1.419(2)	1.422	1.413
C ₈ –C ₁₃ ^a	1.480	1.483	1.487(2) / 1.489(2)	1.485	1.489
C ₁ –B ₁ –C ₁₄ ^a	129.0	128.8	128.1(1) / 128.5(1)	126.7	127.9
C ₁₄ –B ₁ –C ₇ ^a	105.1	105.0	103.9(1) / 103.7(1)	104.2	103.9
C ₇ –B ₁ –C ₁ ^a	125.1	125.1	127.5(1) / 127.5(1)	128.9	128.2
Σ C–B ₁ –C ^a	359.2	358.9	359.5(3) / 359.8(3)	359.8	359.8
C ₂ –C ₁ –B ₁ , C ₁ –C ₂ –B ₂	115.0	115.6	124.9(1) / 123.6(1)	120.4	122.1
B ₁ –C ₁ –C ₂ –B ₂	5.8	6.3	13.2(2)	8.5	9.4
C ₂ –C ₁ –B ₁ –C ₁₄ ^a	58.8	59.5	43.6(2) / 39.2(2)	43.3	43.5
C ₁₅ –C ₁₄ –B ₁ –C ₁ ^a	11.2	12.8	4.7(2) / 2.7(2)	8.1	2.6

^a Values are given for both borafluorene moieties of B1 and B2, respectively, for the crystal of **2.2b**.

Experimental



Scheme 5.1.2. Atom labeling in compounds **2.3a** and **2.3b**.

Table 5.1.3. Selected bond lengths [\AA], distances [\AA], and angles [$^\circ$] in the crystals and calculated structures of **2.3a** and **2.3b** at the B3LYP-d3bj and ω B97X-D level of theory.

	2.3a crystal	2.3a B3LYP-d3bj	2.3a ω B97X-D	2.3b crystal ^a	2.3b B3LYP-d3bj	2.3b ω B97X-D	2.3a -THF crystal
C ₁ -C ₂	1.718(2)	1.712	1.693	1.460(8), 1.409(7), 1.425(7), 1.425(7)	1.435	1.429	1.717(2)
C ₂ -C ₂₇	-	-	-	1.399(7), 1.401(7), 1.423(7), 1.402(7)	1.402	1.399	-
C ₂₇ -C ₂₈	-	-	-	1.393(7), 1.389(8), 1.380(8), 1.396(7)	1.397	1.394	-
C ₂₈ -C ₂₉	-	-	-	1.403(7), 1.360(9), 1.403(9), 1.390(8)	1.394	1.390	-
C ₂₉ -C ₃₀	-	-	-	1.364(8), 1.402(9), 1.417(8), 1.376(8)	1.396	1.393	-
C ₃₀ -C ₁	-	-	-	1.379(7), 1.407(8), 1.384(8), 1.391(8)	1.403	1.398	-
B ₁ -C ₁	1.551(2)	1.549	1.555	1.555(8), 1.548(8), 1.565(8), 1.554(8)	1.541	1.547	1.624(3)
B ₁ -C ₃	1.546(2)	1.549	1.551	1.545(9), 1.591(9), 1.553(9), 1.604(9)	1.570	1.574	1.622(2)
B ₁ -C ₁₀	1.538(2)	1.541	1.544	1.567(9), 1.554(9), 1.561(9), 1.533(9)	1.549	1.553	1.595(3)
B ₂ -C ₂	1.607(2)	1.599	1.604	1.587(9), 1.597(8), 1.570(8), 1.573(8)	1.583	1.588	1.603(3)

Experimental

B ₂ —C ₁₁	1.557(2)	1.557	1.562	1.558(8), 1.577(8), 1.557(8), 1.564(8)	1.563	1.567	1.541(2)
B ₂ —C ₁₅	1.572(2)	1.562	1.568	1.593(8), 1.577(8), 1.556(9), 1.604(8)	1.567	1.574	1.572(2)
C ₃ —C ₄	1.424(2)	1.430	1.422	1.401(9), 1.431(9), 1.457(9), 1.423(8)	1.432	1.424	1.419(3)
C ₉ —C ₁₀	1.406(2)	1.410	1.403	1.415(9), 1.421(9), 1.414(8), 1.396(8)	1.405	1.399	1.399(2)
C ₄ —C ₉	1.492(2)	1.492	1.495	1.470(10), 1.450(10), 1.440(10), 1.545(8)	1.491	1.493	1.485(2)
B ₁ —C ₁ —C ₂	114.4(1)	114.2	114.3	116.6(5), 117.9(5), 117.5(4), 116.9(5)	117.3	117.2	114.0(1)
B ₂ —C ₂ —C ₁	118.5(1)	118.5	118.8	122.3(5), 122.9(4), 124.0(5), 122.3(5)	122.7	122.7	119.6(1)
C ₁ —B ₁ —C ₁₀ C ₁₀ —B ₁ —C ₃ C ₃ —B ₁ —C ₁	/ 119.5(1) / 105.5(1) / 135.0(1)	/ 120.0 / 105.2 / 134.8	/ 119.9 / 105.1 / 134.9	/ 118.4(5) / 104.0(5) / 137.6(5), / 117.5(5) / 103.8(5) / 138.7(5), / 116.9(5) / 102.4(5) / 140.6(5), / 118.8(5) / 103.7(5) / 137.5(5)	/ 118.5 / 103.5 / 138.0	/ 118.5 / 103.3 / 138.2	/ 112.1(1) / 100.0(1) / 123.9(1)
ΣC—B ₁ —C	360.0	360.0	359.9	360.0	360.0	360.0	336.0
C ₂ —B ₂ —C ₁₅ C ₁₅ —B ₂ —C ₁₁ C ₁₅ —B ₂ —C ₂	/ 119.6(1) / 120.0(1) / 119.2(1)	/ 120.1 / 119.6 / 119.7	/ 119.9 / 119.9 / 119.6	/ 120.6(5) / 119.3(5) / 120.1(5), / 117.8(5) / 120.9(5) / 121.3(5), / 119.1(5) / 119.2(5) / 121.7(5), / 120.2(5) / 119.5(5) / 120.3(5)	/ 120.9 / 119.9 / 119.2	/ 120.9 / 119.8 / 119.2	/ 118.3(1) / 122.2(2) / 118.1(1)
ΣC—B ₂ —C	358.8	359.4	359.4	360.0	360.0	359.9	358.6
B ₁ —C ₁ —C ₂ —B ₂	2.6(2)	5.5	3.6	3.3(8), 3.3(7), 1.9(7), 3.4(7)	2.2	2.7	0.9(2)
C ₂ —B ₂ —C ₁₅ —C ₁₆	82.4(1)	76.2	79.4	58.2(6), 60.2(6), 60.7(6), 58.2(6)	61.1	63.3	78.6(2)
C ₂ —C ₁ —B ₁ —C ₃	176.1(1)	176.6	177.9	175.4(6),	179.4	179.5	142.5(2)

Experimental

				176.7(6), 176.0(7), 176.1(6)			
C ₁ –C ₂ –B ₂ –C ₁₅	159.7(2)	166.3	170.4	178.0(5), 178.1(5), 177.1(5), 179.4(5)	175.3	176.1	176.0(1)
C ₁₅ –C ₁₆ –C ₂₁ –C ₂₆	140.8(2)	141.6	136.6	126.0(6), 128.6(6), 128.9(6), 126.0(6)	136.7	133.4	133.3(2)

^a Four symmetry-independent molecules are present in the crystal structure of **2.3b**. Values are given for all four molecules.

Table 5.1.4. Selected bond lengths [Å], distances (B–B, B–C₁₅ [Å]), and angles [°] of the calculated transition state structures at the ωB97X-D level of theory.

	2.2a-2.3a	2.2b-2.3b
C ₁ –C ₁ *	1.689	1.422
B ₁ –B ₁	3.229	3.101
B ₁ –C ₁	1.551	1.534
B ₁ –C ₃	1.551	1.577
B ₁ –C ₁₀	1.548	1.554
B ₁ –C ₂	1.638	1.610
B ₁ –C ₁₅	1.596	1.597
B ₁ –C ₂₂	1.723	1.733
B ₁ –C ₁₁	1.771	1.750
B ₁ –C ₁ –C ₂	114.6	118.1
B ₂ –C ₂ –C ₁	123.0	126.4
B ₁ –C ₁ –C ₂ –B ₂	2.6	4.7
C ₂ –C ₁ –B ₁ –C ₃	175.0	172.6
C ₁₅ –C ₁₆ –C ₂₁ –C ₂₂	176.2	176.6

Experimental

5.2.5 Photophysical data

2.2b

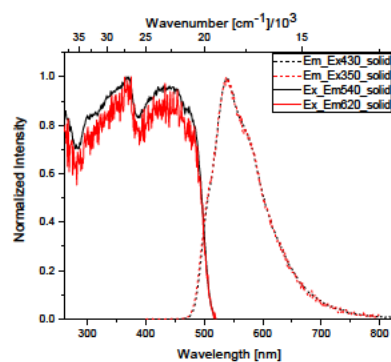


Figure 5.1.6. Excitation (solid) and emission (dashed) spectra of **2.2b** in the solid state.

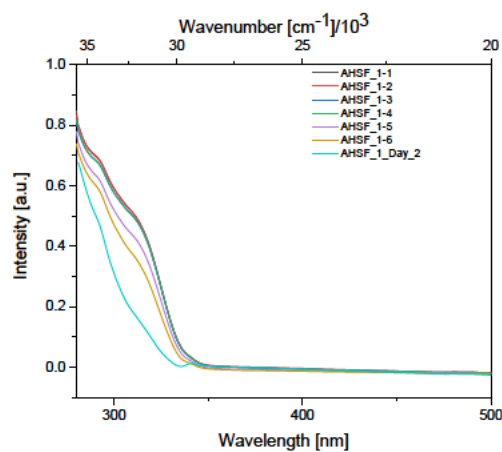


Figure 5.1.7. Absorption spectra of compound **2.2b** in toluene over time.

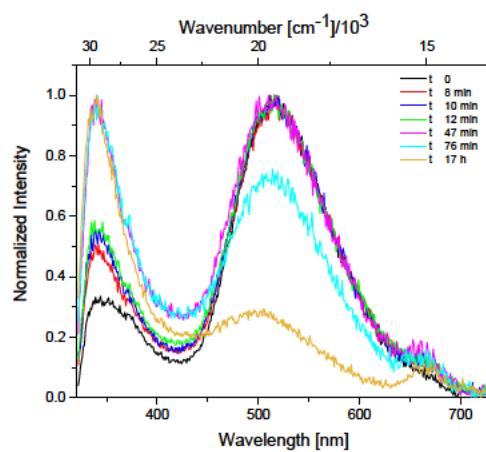


Figure 5.1.8. Normalized emission spectra of compound **2.2b** in toluene over time.

Experimental

2.3a

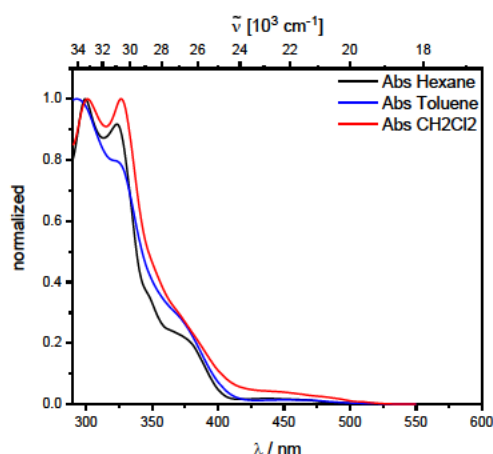


Figure 5.1.9. Absorption spectra of 2.3a in hexane (black), toluene (blue) and CH₂Cl₂ (red).

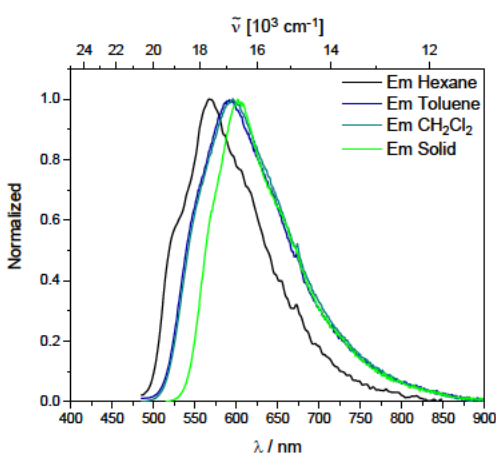


Figure 5.1.10. Emission spectra of 2.3a in hexane (black), toluene (blue), CH₂Cl₂ (turquoise) and in the solid state (green).

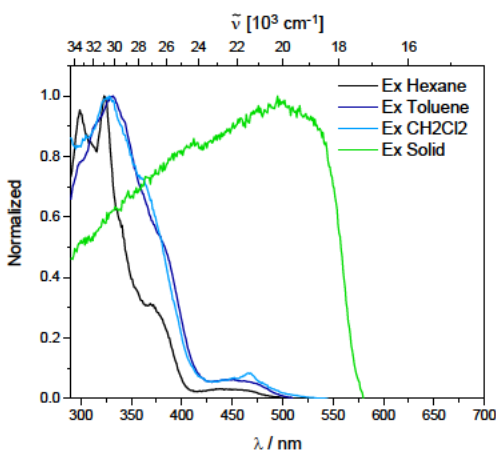


Figure 5.1.11. Excitation spectra of 2.3a in hexane (black), toluene (blue), CH₂Cl₂ (turquoise) and in the solid state (green).

Experimental

2.3b

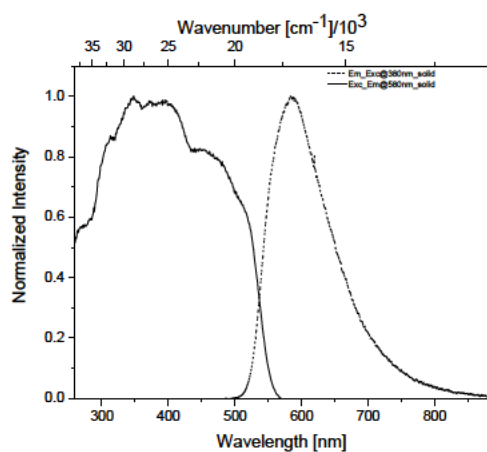


Figure 5.1.12. Excitation (solid) and emission (dashed) spectra of 2.3b in the solid state.

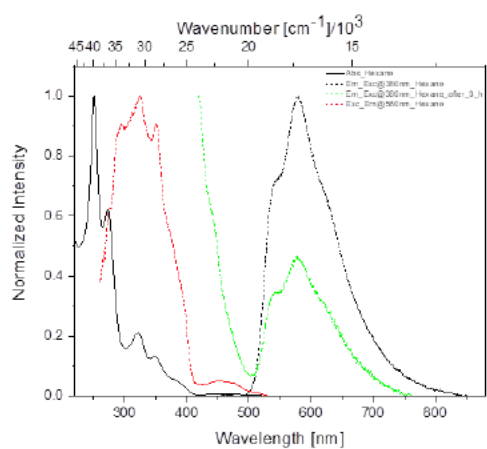


Figure 5.1.13. Absorption (black, solid), emission (black, dashed) and excitation (red, dashed) spectra of 2.3b in hexane initially and after 3 h (green, dashed).

5.2.6 Cyclic voltammetry

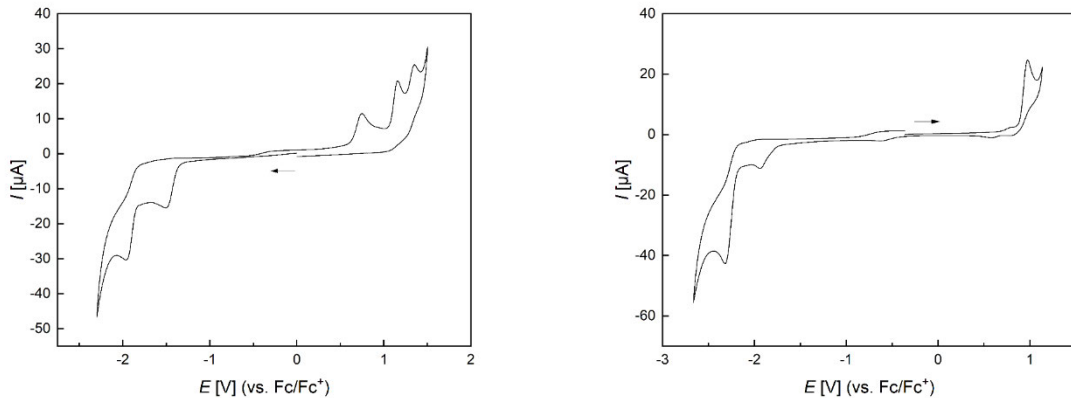


Figure 5.1.14. Cyclic voltammograms of **2.2b** measured in CH_2Cl_2 with $[\text{nBu}_4\text{N}][\text{PF}_6]$ as the electrolyte with a scan rate of 250 mVs^{-1} . All measurements are referenced to the Fc/Fc^+ ion couple.

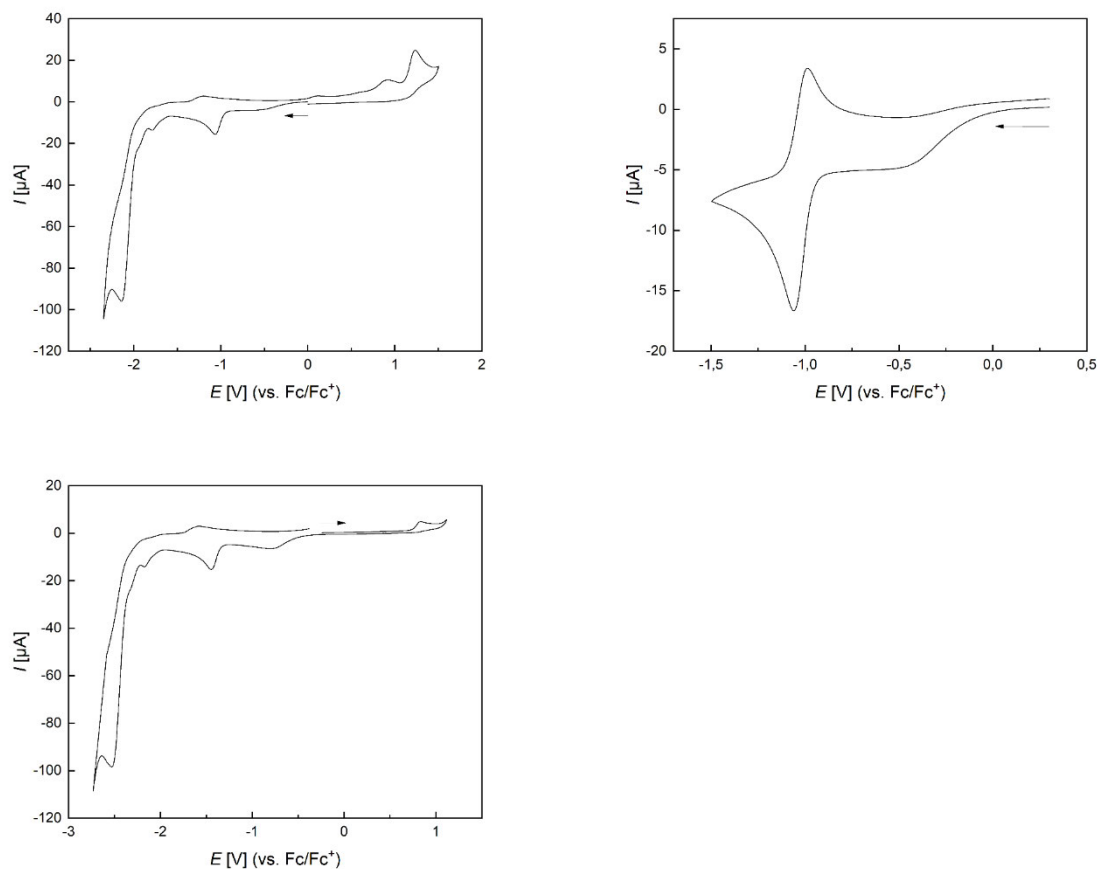


Figure 5.1.15. Cyclic voltammograms of **2.3a** measured in CH_2Cl_2 with $[\text{nBu}_4\text{N}][\text{PF}_6]$ as the electrolyte with a scan rate of 250 mVs^{-1} . All measurements are referenced to the Fc/Fc^+ ion couple.

Experimental

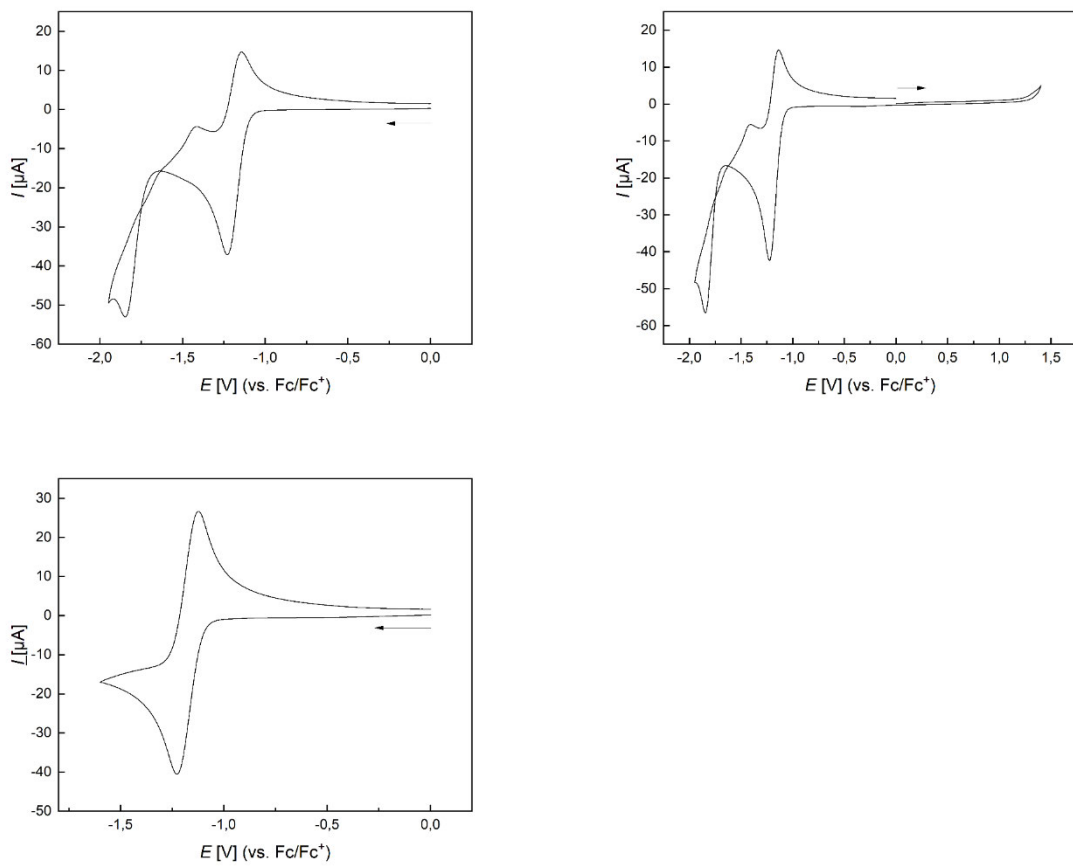


Figure 5.1.16. Cyclic voltammograms of **2.3b** measured in CH_2Cl_2 with $[\text{nBu}_4\text{N}][\text{PF}_6]$ as the electrolyte with a scan rate of 250 mVs^{-1} . All measurements are referenced to the Fc/Fc^+ ion couple.

Table 5.1.5. Reduction and oxidation potentials of **2.2b**, **2.3a** and **2.3b**.

compound	1 st reduction	2 nd reduction	1 st oxidation
2.2b	$E_{pc} = -1.50 \text{ V}$	$E_{pc} = -1.96 \text{ V}$	$E_{pa} = 0.98 \text{ V}$
2.3a	$E_{1/2}^a = -1.03 \text{ V}$	$E_{pc} = -2.14 \text{ V}$	$E_{pa} = 0.84 \text{ V}$
2.3b	$E_{1/2} = -1.17 \text{ V}$	$E_{pc} = -1.85 \text{ V}$	

[a] partially reversible.

5.2.7 DFT and TD-DFT results

Experimental

64 M062X_2.3a (E = -1304.39502822 a.u.)				52 M062X_2.2b (E = -1204.509805 a.u.)			
H	-0.247664000	1.206098000	1.836781000	C	2.067705000	-1.333805000	1.333483000
B	-0.474233000	1.325253000	-1.982113000	B	-1.480458000	0.838310000	-0.467083000
C	-4.024259000	-1.229137000	0.407632000	B	1.480458000	0.838242000	0.466672000
C	-0.385690000	-1.667725000	-0.118726000	C	-3.880835000	1.090549000	0.780815000
B	0.743728000	-0.643482000	-0.469964000	H	-3.668830000	2.069722000	1.204696000
H	-0.774805000	0.448397000	-2.718164000	C	2.937324000	0.455194000	0.017885000
H	-2.657528000	2.644387000	-2.006354000	C	5.105068000	0.464650000	-1.046108000
B	-2.214437000	0.238233000	-0.119020000	H	5.848036000	0.958299000	-1.664308000
C	2.111577000	-1.850692000	-2.191904000	C	5.370104000	-0.795912000	-0.520886000
H	1.165526000	-1.973492000	-2.715520000	H	6.320912000	-1.276035000	-0.732393000
C	-1.220843000	1.389605000	-0.448705000	C	4.425801000	-1.458971000	0.272168000
B	-1.375890000	2.934602000	0.207296000	H	4.643742000	-2.447427000	0.667077000
H	-0.028559000	3.387521000	-3.451227000	C	3.219352000	-0.831133000	0.535232000
C	-1.689838000	-1.206490000	0.030900000	C	1.021143000	-0.383950000	1.338606000
B	1.183880000	1.894463000	-1.717123000	C	1.945793000	-2.537411000	2.007885000
H	1.963567000	4.320016000	-1.312826000	H	2.747397000	-3.270879000	2.001455000
H	-0.972805000	5.123273000	-1.104078000	C	0.760145000	-2.799215000	2.705100000
C	0.391335000	0.922182000	-0.562573000	H	0.649485000	-3.740637000	3.234901000
B	-0.150843000	1.788563000	0.812039000	C	-0.273768000	-1.868921000	2.733310000
C	-0.175148000	-3.051901000	0.055107000	H	-1.182442000	-2.087666000	3.284576000
H	0.823602000	-3.466300000	-0.055052000	C	-0.140168000	-0.652616000	2.054155000
H	0.544447000	4.193540000	1.397836000	H	-0.948360000	0.075669000	2.091405000
B	-0.050509000	3.007077000	-2.330489000	C	-2.937256000	0.455296000	-0.018026000
H	2.386320000	1.900670000	0.562422000	C	-5.104807000	0.464858000	1.046339000
B	-0.598563000	4.008626000	-0.961893000	H	-5.847701000	0.958606000	1.664549000
C	-1.240897000	-3.891256000	0.367524000	C	-5.369853000	-0.795843000	0.521460000
H	-1.059333000	-4.953222000	0.502206000	H	-6.320591000	-1.275981000	0.733249000
B	-1.578863000	2.645794000	-1.518341000	C	-4.425652000	-1.459025000	-0.271617000
C	-2.550980000	-3.402167000	0.509829000	H	-4.643603000	-2.447588000	-0.666249000
H	-3.359888000	-4.087154000	0.749009000	C	-3.219291000	-0.831165000	-0.535034000
B	0.280328000	3.474887000	0.494934000	C	-2.067743000	-1.333923000	-1.333380000
H	2.042812000	1.386228000	-2.350651000	C	-1.945910000	-2.537593000	-2.007689000
C	-2.773702000	-2.045040000	0.335717000	H	-2.747488000	-3.271088000	-2.001038000
B	1.385509000	2.179934000	0.007695000	C	-0.760389000	-2.799419000	-2.705105000
H	-2.315386000	3.133376000	0.899600000	H	-0.649812000	-3.740874000	-3.234866000
C	-3.745623000	0.140153000	0.139290000	C	0.273481000	-1.869083000	-2.733626000
B	1.099575000	3.542902000	-1.083954000	H	1.182053000	-2.087862000	-3.285047000
C	-5.311783000	-1.648905000	0.687106000	C	0.139949000	-0.652701000	-2.054603000
H	-5.531295000	-2.692379000	0.894094000	H	0.948111000	0.075609000	-2.092033000
C	-6.341464000	-0.697538000	0.700556000	C	-1.021232000	-0.384014000	-1.338851000
H	-7.356367000	-1.014970000	0.919811000	H	3.669012000	2.069364000	-1.205118000
C	-6.084782000	0.643602000	0.438646000	C	3.880998000	1.090306000	-0.780964000
H	-6.898176000	1.361297000	0.454802000	C	1.354787000	3.369438000	0.298231000
C	-4.780657000	1.066707000	0.156151000	C	0.692500000	2.141997000	0.157228000
H	-4.579288000	2.114882000	-0.048220000	C	-0.692536000	2.142054000	-0.157605000
C	2.131691000	-1.188304000	-0.953924000	C	-1.354773000	3.369531000	-0.298352000
C	3.276819000	-2.335463000	-2.776249000	C	-0.678942000	4.579300000	-0.150709000
H	3.236080000	-2.826178000	-3.743215000	C	0.679006000	4.579258000	0.150818000
C	4.488557000	-2.198725000	-2.104738000	H	2.413921000	3.376429000	0.545841000
H	5.402747000	-2.589333000	-2.540069000	H	-2.413918000	3.376612000	-0.545905000
C	4.523245000	-1.581291000	-0.860931000	H	-1.210775000	5.518331000	-0.269463000
H	5.461069000	-1.513776000	-0.317216000	H	1.210848000	5.518260000	0.269764000
C	3.360044000	-1.069438000	-0.275622000				
C	3.426195000	-0.426606000	1.058499000				
C	4.494953000	0.416238000	1.386987000				
H	5.282514000	0.583526000	0.658432000				
C	4.518396000	1.090666000	2.601152000				
H	5.342206000	1.759171000	2.829741000				
C	3.475352000	0.932181000	3.512285000				
H	3.487539000	1.470954000	4.453890000				
C	2.421768000	0.075346000	3.209774000				
H	1.615097000	-0.069181000	3.921353000				
C	2.402963000	-0.606815000	1.996016000				
H	1.595766000	-1.306740000	1.788480000				

Experimental

64 wB97XD_2.3a (E = -1304.502156 a.u.)	52 wB97XD_2.2b (E = -1204.612990 a.u.)
H -0.127483000 1.114217000 1.830602000	C 1.932513000 -1.341403000 1.355123000
B -0.534850000 1.462531000 -1.976628000	B -1.442675000 0.874441000 -0.543661000
C -3.950859000 -1.309275000 0.300669000	B 1.442348000 0.873712000 0.543440000
C -0.326823000 -1.648966000 -0.376622000	C -3.862693000 1.069906000 0.667450000
B 0.787474000 -0.579518000 -0.611548000	H -3.692783000 2.069309000 1.060832000
H -0.860463000 0.632036000 -2.757458000	C 2.888605000 0.448968000 0.105474000
H -2.732807000 2.766358000 -1.820027000	C 5.061191000 0.403607000 -0.945680000
B -2.175101000 0.224435000 -0.129999000	H 5.828174000 0.886426000 -1.543230000
C 2.358694000 -1.517804000 -2.338804000	C 5.269478000 -0.883330000 -0.460587000
H 1.479725000 -1.576722000 -2.977014000	H 6.201123000 -1.395731000 -0.682167000
C -1.216998000 1.418214000 -0.402918000	C 4.292761000 -1.531278000 0.305066000
B -1.351009000 2.923026000 0.356277000	H 4.467454000 -2.540318000 0.667753000
H -0.169808000 3.621605000 -3.332344000	C 3.112283000 -0.863193000 0.583422000
C -1.629788000 -1.219480000 -0.143451000	C 0.931835000 -0.344533000 1.388287000
B 1.134944000 2.030834000 -1.747005000	C 1.742949000 -2.563919000 1.976214000
H 1.912384000 4.443593000 -1.227492000	H 2.506088000 -3.336397000 1.946340000
H -1.023725000 5.200096000 -0.836742000	C 0.536704000 -2.796821000 2.647976000
C 0.403408000 0.977537000 -0.616668000	H 0.373606000 -3.754034000 3.134434000
B -0.086262000 1.756080000 0.837246000	C -0.450685000 -1.819369000 2.705241000
C -0.100983000 -3.040574000 -0.356424000	H -1.378573000 -2.016026000 3.232704000
H 0.897770000 -3.430690000 -0.531709000	C -0.249026000 -0.584837000 2.080170000
H 0.616487000 4.133212000 1.538994000	H -1.022501000 0.177107000 2.131209000
B -0.139189000 3.167179000 -2.235218000	C -2.888807000 0.449527000 -0.105481000
H 2.441089000 1.903402000 0.471277000	C -5.060998000 0.403621000 0.946470000
B -0.633901000 4.078905000 -0.779890000	H -5.827843000 0.886218000 1.544378000
C -1.150300000 -3.920188000 -0.109884000	C -5.269201000 -0.883317000 0.461342000
H -0.957430000 -4.988675000 -0.096739000	H -6.200659000 -1.395923000 0.683237000
B -1.631657000 2.741959000 -1.378381000	C -4.292634000 -1.530993000 -0.304735000
C -2.458012000 -3.462441000 0.123027000	H -4.467246000 -2.540031000 -0.667464000
H -3.253846000 -4.177852000 0.310655000	C -3.112399000 -0.862639000 -0.583472000
B 0.317043000 3.465038000 0.603603000	C -1.932779000 -1.340613000 -1.355541000
H 1.973278000 1.576694000 -2.450121000	C -1.743161000 -2.563061000 -1.976736000
C -2.695736000 -2.097768000 0.103979000	H -2.506170000 -3.335663000 -1.946752000
B 1.411611000 2.212177000 -0.015429000	C -0.537013000 -2.795737000 -2.648756000
H -2.260717000 3.073904000 1.103432000	H -0.373860000 -3.752914000 -3.135268000
C -3.691277000 0.081991000 0.166000000	C 0.450219000 -1.818139000 -2.706183000
B 1.065119000 3.639799000 -1.007395000	H 1.378026000 -2.014655000 -3.233841000
C -5.226151000 -1.766990000 0.574638000	C 0.248512000 -0.583670000 -2.080998000
H -5.433445000 -2.827721000 0.681487000	H 1.021856000 0.178402000 -2.132117000
C -6.260451000 -0.831306000 0.716539000	C -0.932246000 -0.343598000 -1.388857000
H -7.266281000 -1.179740000 0.931030000	H 3.692642000 2.069019000 -1.060399000
C -6.021099000 0.531714000 0.585129000	C 3.862645000 1.069619000 -0.667046000
H -6.837695000 1.237377000 0.697514000	C 1.331900000 3.414835000 0.385746000
C -4.729529000 0.993139000 0.308323000	C 0.680570000 2.187332000 0.203070000
H -4.539268000 2.057403000 0.203448000	C -0.680548000 2.187801000 -0.203115000
C 2.229488000 -1.031031000 -1.029445000	C -1.331259000 3.415688000 -0.385149000
C 3.592020000 -1.904798000 -2.850490000	C -0.667051000 4.624771000 -0.193684000
H 3.669028000 -2.262403000 -3.872290000	C 0.668324000 4.624344000 0.194833000
C 4.721616000 -1.839198000 -2.040762000	H 2.373651000 3.424116000 0.697909000
H 5.687743000 -2.152250000 -2.423853000	H -2.373030000 3.425692000 -0.697223000
C 4.607567000 -1.388831000 -0.731504000	H -1.190238000 5.563990000 -0.346051000
H 5.483156000 -1.371625000 -0.088956000	H 1.191963000 5.563242000 0.347625000
C 3.374727000 -0.980121000 -0.212557000	
C 3.282075000 -0.511324000 1.193375000	
C 4.241937000 0.363561000 1.716639000	
H 5.061925000 0.692340000 1.085272000	
C 4.118410000 0.864097000 3.006242000	
H 4.858822000 1.561394000 3.385300000	
C 3.035524000 0.494643000 3.802146000	
H 2.932060000 0.897915000 4.804275000	
C 2.089858000 -0.394086000 3.303815000	
H 1.251327000 -0.702089000 3.920538000	
C 2.216956000 -0.899265000 2.012472000	
H 1.491423000 -1.622690000 1.651968000	

Experimental

52 wB97XD_TS1-2.2b/2.3b (E = -1204.558240 a.u.)	52 wB97XD_2.3b (E = -1204.614720 a.u.)
C -3.784105000 -1.019414000 0.227679000	C -3.958707000 -0.693975000 0.299040000
C -0.107061000 -1.211044000 0.178587000	C -0.401778000 -1.593150000 -0.124292000
B 1.028634000 0.062209000 -0.210383000	B 0.770918000 -0.672476000 -0.607882000
B -2.022785000 0.599729000 -0.088230000	B -1.995690000 0.470444000 -0.485136000
C 2.209730000 -1.118985000 -2.328961000	C 2.537532000 -2.305671000 -1.480571000
H 1.287694000 -1.115080000 -2.904152000	H 1.735662000 -2.760190000 -2.057995000
C -1.435475000 -0.813611000 0.182665000	C -1.653777000 -0.988686000 -0.078714000
C 0.185328000 -2.581193000 0.307235000	C -0.320014000 -2.924255000 0.326792000
H 1.217894000 -2.918498000 0.320805000	H 0.635608000 -3.442122000 0.330589000
C -0.852061000 -3.500755000 0.410120000	C -1.461796000 -3.585585000 0.776025000
H -0.619454000 -4.557429000 0.501129000	H -1.381261000 -4.613764000 1.117172000
C -2.196155000 -3.094838000 0.399685000	C -2.715437000 -2.954702000 0.809039000
H -2.984076000 -3.838847000 0.477606000	H -3.584041000 -3.498079000 1.171729000
C -2.482042000 -1.743559000 0.283094000	C -2.804823000 -1.638170000 0.379143000
C -3.578105000 0.373525000 0.037343000	C -3.541254000 0.571518000 -0.202443000
C -5.057959000 -1.550900000 0.340985000	C -5.279625000 -0.930425000 0.637685000
H -5.209821000 -2.617297000 0.482203000	H -5.594800000 -1.897437000 1.019785000
C -6.157835000 -0.688991000 0.277585000	C -6.214778000 0.099272000 0.480187000
H -7.161235000 -1.093693000 0.370794000	H -7.254518000 -0.076986000 0.739522000
C -5.978042000 0.678148000 0.100369000	C -5.827751000 1.342055000 -0.006897000
H -6.841048000 1.335338000 0.057176000	H -6.565570000 2.129697000 -0.123601000
C -4.689239000 1.207553000 -0.022978000	C -4.490798000 1.576562000 -0.346787000
H -4.566736000 2.278140000 -0.160830000	H -4.204736000 2.553313000 -0.727374000
C 2.227950000 -0.584305000 -1.042980000	C 2.243455000 -1.228078000 -0.632306000
C 3.372166000 -1.654920000 -2.878883000	C 3.833041000 -2.793704000 -1.618347000
H 3.358718000 -2.063166000 -3.885092000	H 4.035278000 -3.618424000 -2.294792000
C 4.557606000 -1.674406000 -2.141275000	C 4.865352000 -2.222277000 -0.880552000
H 5.456828000 -2.099362000 -2.576891000	H 5.877787000 -2.603796000 -0.970860000
C 4.592892000 -1.156272000 -0.850861000	C 4.593525000 -1.172977000 -0.010013000
H 5.516425000 -1.180630000 -0.278838000	H 5.391232000 -0.748715000 0.593515000
C 3.428630000 -0.611976000 -0.309637000	C 3.296070000 -0.669714000 0.122853000
C 3.250223000 -0.008576000 1.021234000	C 3.021987000 0.440527000 1.071065000
C 4.218396000 0.271202000 1.982833000	C 3.837111000 1.576808000 1.100417000
H 5.257914000 0.005412000 1.814227000	H 4.686214000 1.638885000 0.425458000
C 3.846816000 0.916032000 3.160745000	C 3.545916000 2.637321000 1.950992000
H 4.600646000 1.136157000 3.910540000	H 4.181234000 3.517856000 1.950982000
C 2.522385000 1.292102000 3.385037000	C 2.434967000 2.579089000 2.789380000
H 2.251667000 1.800282000 4.304943000	H 2.204162000 3.409742000 3.448829000
C 1.550446000 1.016333000 2.426081000	C 1.622845000 1.449292000 2.777111000
H 0.514680000 1.302254000 2.591310000	H 0.759731000 1.390519000 3.432743000
C 1.912153000 0.366212000 1.249624000	C 1.918016000 0.386791000 1.929120000
H 0.801901000 -0.531815000 0.950221000	H 1.293764000 -0.503138000 1.945386000
C -1.552132000 2.989171000 -0.946336000	C -1.068308000 2.675297000 -1.489449000
C -1.082986000 1.721212000 -0.550663000	C -0.862100000 1.368858000 -1.035192000
C 0.306251000 1.433886000 -0.644068000	C 0.445179000 0.796820000 -1.114564000
C 1.157897000 2.439551000 -1.123653000	C 1.468189000 1.569456000 -1.674547000
C 0.671944000 3.681975000 -1.509144000	C 1.240569000 2.868109000 -2.127618000
C -0.692003000 3.965828000 -1.419423000	C -0.027683000 3.427674000 -2.029841000
H -2.616006000 3.201013000 -0.884606000	H -2.060043000 3.114256000 -1.423735000
H 2.223901000 2.241118000 -1.203227000	H 2.466875000 1.151186000 -1.759891000
H 1.358722000 4.435437000 -1.884793000	H 2.057368000 3.442174000 -2.555126000
H -1.071532000 4.937065000 -1.721701000	H -0.206820000 4.440698000 -2.377553000

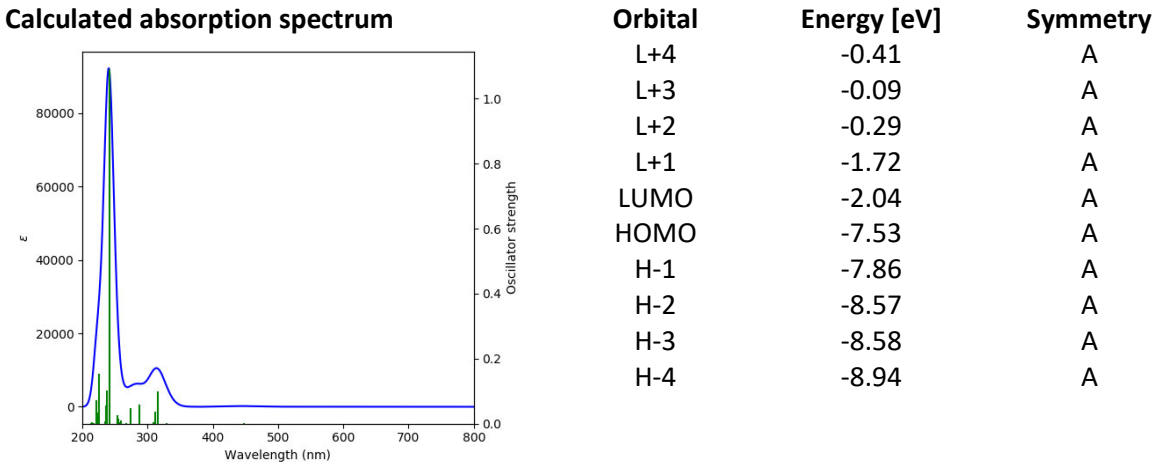
Experimental

52 B3LYP(D3bj)_TS1- 2.2b/2.3b (E = -1205.095101 a.u.)	52 B3LYP(D3bj) _2.3b (E = -1205.154418 a.u.)
C -3.799739000 -1.007244000 0.246068000	C -3.952661000 -0.700893000 0.290209000
C -0.118978000 -1.231184000 0.177492000	C -0.394073000 -1.619271000 -0.135573000
B 1.022846000 0.027051000 -0.219990000	B 0.782374000 -0.702322000 -0.601000000
B -2.021200000 0.591618000 -0.100551000	B -1.980916000 0.450522000 -0.500079000
C 2.236836000 -1.196115000 -2.292591000	C 2.566158000 -2.355076000 -1.400508000
H 1.319806000 -1.218916000 -2.875378000	H 1.775108000 -2.832425000 -1.973389000
C -1.447089000 -0.819804000 0.185484000	C -1.647586000 -1.007048000 -0.094472000
C 0.164015000 -2.606064000 0.323647000	C -0.320872000 -2.955418000 0.316764000
H 1.192836000 -2.952842000 0.333374000	H 0.632458000 -3.475971000 0.327252000
C -0.884504000 -3.516441000 0.446326000	C -1.470873000 -3.614361000 0.759274000
H -0.660315000 -4.574552000 0.546909000	H -1.397739000 -4.644400000 1.097566000
C -2.229303000 -3.098235000 0.440959000	C -2.725436000 -2.975870000 0.790223000
H -3.022736000 -3.834699000 0.535194000	H -3.597396000 -3.516800000 1.148963000
C -2.507259000 -1.742697000 0.307223000	C -2.808107000 -1.653570000 0.363597000
C -3.574913000 0.387666000 0.032213000	C -3.519783000 0.568439000 -0.210927000
C -5.084409000 -1.519515000 0.368152000	C -5.277804000 -0.920130000 0.637237000
H -5.250514000 -2.581971000 0.524026000	H -5.603978000 -1.884879000 1.016109000
C -6.176032000 -0.642132000 0.291345000	C -6.202104000 0.126946000 0.493804000
H -7.185138000 -1.032116000 0.389480000	H -7.241660000 -0.036167000 0.763836000
C -5.978227000 0.723520000 0.092442000	C -5.800671000 1.371047000 0.011205000
H -6.833333000 1.390681000 0.038422000	H -6.527649000 2.170985000 -0.092362000
C -4.679156000 1.235087000 -0.039843000	C -4.459936000 1.589005000 -0.339871000
H -4.543490000 2.302028000 -0.193816000	H -4.162291000 2.565131000 -0.713350000
C 2.237088000 -0.627335000 -1.018795000	C 2.251044000 -1.249791000 -0.590024000
C 3.413633000 -1.730599000 -2.823618000	C 3.870987000 -2.833959000 -1.511309000
H 3.413026000 -2.160698000 -3.821140000	H 4.088223000 -3.678690000 -2.158440000
C 4.597047000 -1.715756000 -2.076146000	C 4.893157000 -2.226227000 -0.781019000
H 5.505693000 -2.138103000 -2.495339000	H 5.910717000 -2.599805000 -0.848323000
C 4.616147000 -1.163740000 -0.795910000	C 4.602043000 -1.150225000 0.054661000
H 5.535293000 -1.160411000 -0.216468000	H 5.388818000 -0.701359000 0.653990000
C 3.438762000 -0.619860000 -0.272964000	C 3.294658000 -0.655223000 0.160979000
C 3.248866000 0.019644000 1.035960000	C 2.995760000 0.475725000 1.070381000
C 4.215459000 0.345511000 1.991532000	C 3.832597000 1.600491000 1.126262000
H 5.257262000 0.082929000 1.831905000	H 4.719880000 1.633395000 0.501082000
C 3.836635000 1.030627000 3.147919000	C 3.509927000 2.689126000 1.933403000
H 4.588650000 1.285746000 3.888938000	H 4.160864000 3.558405000 1.950486000
C 2.504883000 1.403420000 3.358797000	C 2.345465000 2.672947000 2.704597000
H 2.228639000 1.944110000 4.258775000	H 2.091331000 3.525104000 3.327550000
C 1.532362000 1.080566000 2.408902000	C 1.512706000 1.554535000 2.670215000
H 0.494510000 1.363904000 2.564124000	H 0.609977000 1.526456000 3.272979000
C 1.902236000 0.391448000 1.255466000	C 1.839635000 0.463671000 1.866741000
H 0.790761000 -0.532393000 0.961680000	H 1.202928000 -0.415932000 1.871280000
C -1.537220000 2.961543000 -1.003286000	C -1.048929000 2.642142000 -1.524275000
C -1.077173000 1.693018000 -0.584524000	C -0.848248000 1.335848000 -1.053910000
C 0.315284000 1.391476000 -0.682508000	C 0.464462000 0.759697000 -1.118493000
C 1.173185000 2.380847000 -1.190690000	C 1.493612000 1.529437000 -1.679939000
C 0.694661000 3.622959000 -1.598723000	C 1.270347000 2.827180000 -2.147204000
C -0.6696668000 3.922321000 -1.502998000	C -0.002240000 3.390331000 -2.065500000
H -2.598636000 3.183300000 -0.939892000	H -0.2041755000 3.080081000 -1.471761000
H 2.235802000 2.169142000 -1.272949000	H 2.492107000 1.110572000 -1.750498000
H 1.384547000 4.362145000 -1.997455000	H 2.091320000 3.397710000 -2.572605000
H -1.041470000 4.891762000 -1.821668000	H -0.177958000 4.400576000 -2.424157000

Experimental

Cartesian coordinates of optimized structures of 2.2a, 2.2b, 2.3a and 2.3b for the TD-DFT calculations, orbital energies, and transitions

TD-DFT calculations 2.2a:



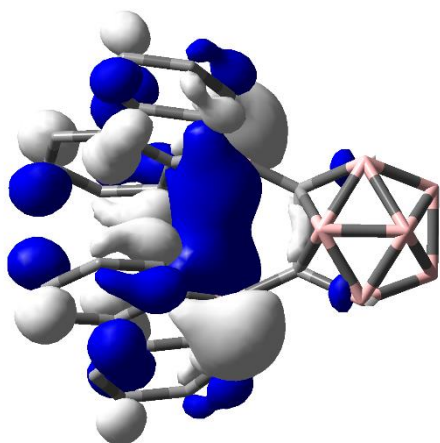
TD-DFT CAMB3LYP/6-31+G(d, p), gas phase

Table 5.1.6: Lowest energy singlet electronic transition of **2.2a** (TD-DFT CAM-B3LYP/6-31+G(d, p), gas phase).

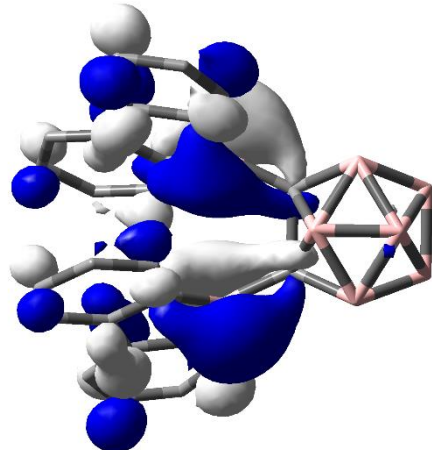
State	E [eV]	λ [nm]	f	Symmetry	Major contributions	Λ
1	2.77	448.08	0.0026	Singlet-A	H-1→L+1 (22%), HOMO→LUMO (75%)	0.60
2	2.88	430.84	0.0002	Singlet-A	H-1→LUMO (51%), HOMO→L+1 (46%)	0.60
3	3.77	329.00	0.0019	Singlet-A	H-2→LUMO (12%), H-1→LUMO (35%), HOMO→L+1 (45%)	0.60
4	3.93	315.36	0.1006	Singlet-A	H-3→LUMO (14%), H-1→L+1 (54%), HOMO→LUMO (20%)	0.60
5	3.97	312.18	0.0363	Singlet-A	H-3→LUMO (54%), H-1→L+1 (21%)	0.61
6	4.02	308.27	0.0042	Singlet-A	H-3→L+1 (17%), H-2→LUMO (50%), H-1→LUMO (11%)	0.62
7	4.31	287.89	0.0582	Singlet-A	H-4→LUMO (50%), H-3→LUMO (11%), H-2→L+1 (22%)	0.63
8	4.53	273.71	0.0468	Singlet-A	H-5→LUMO (13%), H-4→L+1 (21%), H-3→L+1 (44%), H-2→LUMO (10%)	0.62
9	4.65	266.87	0.0024	Singlet-A	H-5→LUMO (44%), H-3→L+1 (25%), H-2→LUMO (10%)	0.65
10	4.78	259.22	0.0104	Singlet-A	H-5→L+1 (20%), H-4→LUMO (14%), H-3→LUMO (13%), H-2→L+1 (32%)	0.63
11	4.85	255.87	0.0047	Singlet-A	H-15→LUMO (17%), H-14→L+1 (17%), H-12→LUMO (22%), H-7→LUMO (11%)	0.44
12	4.85	255.67	0.016	Singlet-A	H-14→LUMO (22%), H-12→L+1 (11%), H-9→LUMO (10%), HOMO→L+2 (14%)	0.50
13	4.90	253.02	0.0265	Singlet-A	H-1→L+3 (10%), HOMO→L+2 (52%)	0.68
14	5.15	240.97	1.0913	Singlet-A	H-2→L+1 (18%), H-1→L+2 (26%), HOMO→L+3 (46%)	0.71
15	5.21	237.82	0.1028	Singlet-A	H-8→LUMO (16%), H-5→L+1 (13%), H-4→LUMO (20%)	0.63
16	5.24	236.69	0.0552	Singlet-A	H-6→LUMO (12%), H-5→LUMO (12%), H-4→L+1 (50%)	0.68
17	5.29	234.50	0.0072	Singlet-A	H-10→LUMO (30%)	0.45
18	5.30	233.89	0.0003	Singlet-A	H-16→LUMO (10%), H-11→LUMO (14%), H-10→L+1 (17%), H-9→LUMO (20%)	0.44
19	5.49	225.84	0.1545	Singlet-A	H-6→LUMO (59%)	0.71
20	5.52	224.63	0.0341	Singlet-A	H-8→LUMO (20%), H-6→L+1 (24%), H-5→L+1 (36%)	0.68
21	5.53	224.13	0.0296	Singlet-A	H-1→L+2 (44%), HOMO→L+3 (33%)	0.71
22	5.59	221.98	0.0722	Singlet-A	H-3→L+2 (18%), H-1→L+3 (39%), HOMO→L+2 (12%)	0.68
23	5.71	216.98	0.0023	Singlet-A	H-4→L+2 (12%), H-1→L+3 (13%), HOMO→L+9 (10%)	0.64
24	5.78	214.34	0.0021	Singlet-A	H-3→L+3 (17%), H-2→L+2 (16%), HOMO→L+6 (11%)	0.59
25	5.79	214.05	0.0034	Singlet-A	H-7→LUMO (71%)	0.34

Experimental

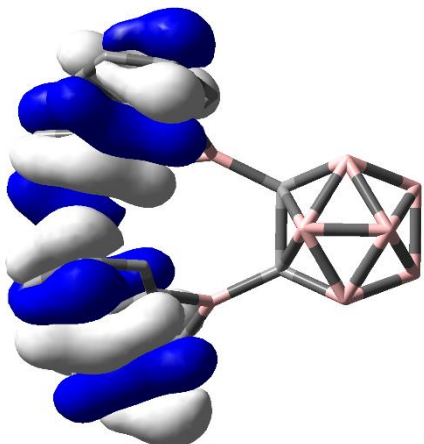
Orbitals relevant to the $S_1 \leftarrow S_0$ and $S_2 \leftarrow S_0$ transitions



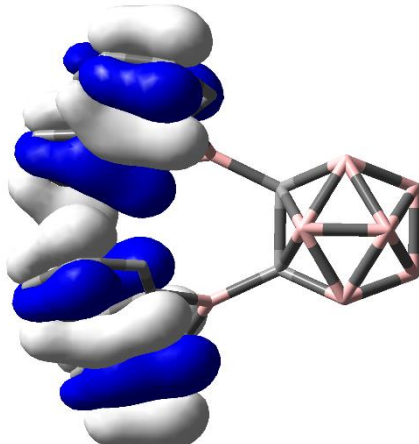
LUMO: -2.04 eV



LUMO+1: -1.72 eV



HOMO: -7.53 eV



HOMO-1: -7.86 eV

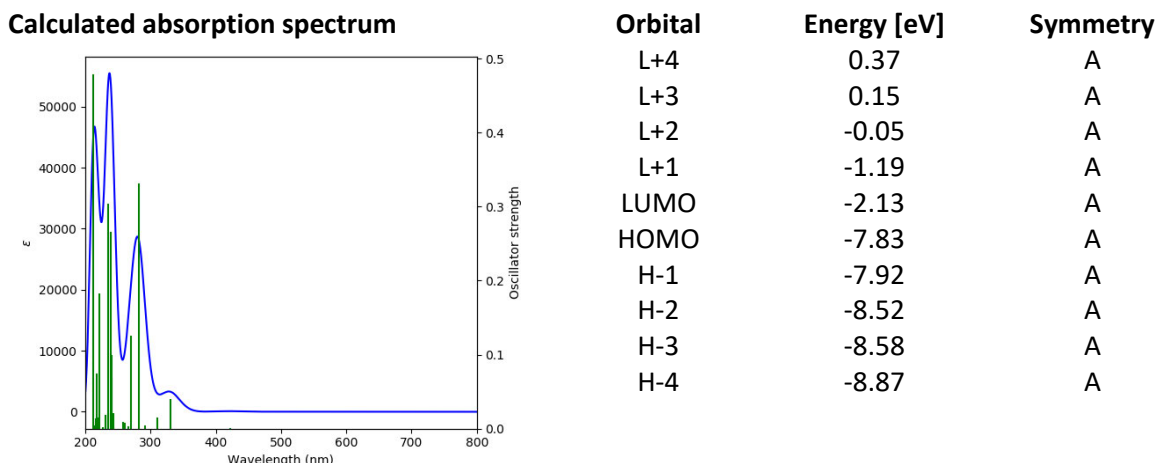
Isovalue= 0.03

Experimental

H	1.67283600	-1.59448300	-1.73728900
B	2.39100200	0.96788900	1.05534700
C	-1.86961000	-1.27415200	1.45252200
B	0.47775900	1.18248700	-0.95459200
H	1.67353600	1.59337700	1.73714400
H	3.09116100	-0.81109500	2.74327500
B	0.47710700	-1.18289000	0.95444800
C	0.46092200	3.72384700	0.03663700
H	1.51649800	3.76663000	0.27480700
C	1.91379900	-0.62775600	0.55460600
B	3.26922600	-1.65564400	0.30781500
H	4.72219000	1.65807500	1.83973700
C	-0.08688500	-2.59046100	0.57024500
B	3.27007100	1.65374100	-0.30788300
H	5.68768900	1.13862100	-1.03602400
H	5.68707000	-1.14173900	1.03606200
C	1.91414200	0.62654000	-0.55474200
B	2.39056300	-0.96935200	-1.05545900
C	-0.35909300	-4.81983800	-0.34863200
H	0.07130700	-5.70032800	-0.81544200
H	4.721444000	-1.66070900	-1.83974000
B	4.14515900	0.96649100	1.06989900
H	3.09169400	0.80928200	-2.74335500
B	4.69642100	-0.65964800	0.59946200
C	-1.72503400	-4.77973000	-0.06381300
H	-2.35331500	-5.63012300	-0.31252000
B	3.24461500	-0.47061000	1.62112100
C	-2.29640400	-3.64805300	0.53775400
H	-3.36271200	-3.62134200	0.74174300
B	4.14472200	-0.96883500	-1.06992900
H	3.14537200	2.80001300	-0.55591500
C	-1.47930900	-2.57037500	0.85220300
B	3.24492400	0.46872000	-1.62119400
H	3.14395100	-2.80184800	0.55585000
C	-0.73747400	-0.41836000	1.58792600
B	4.69677800	0.65702800	-0.59946900
C	-3.13914000	-0.86262500	1.82926600
H	-3.99803100	-1.51529100	1.70471400
C	-3.30623400	0.42239000	2.37019000
H	-4.29712100	0.75693600	2.66335600
C	-2.21097700	1.26752900	2.53479000
H	-2.34637500	2.25962100	2.95313700
C	-0.93033400	0.84771500	2.14757200
H	-0.10179600	1.52895700	2.27820800
C	-0.08531200	2.59037300	-0.57024900
C	-0.35598300	4.81983900	0.34885300
H	0.07503600	5.70001900	0.81567800
C	-1.72199100	4.78060700	0.06423000
H	-2.34970300	5.63137400	0.31309600
C	-2.29415800	3.64933900	-0.53735300
H	-3.36050900	3.62332100	-0.74121100
C	-1.47778300	2.57117500	-0.85200700
C	-1.86895700	1.27526900	-1.45243700
C	-3.13878700	0.86460700	-1.82911300
H	-3.99725100	1.51779700	-1.70437000
C	-3.30675000	-0.42020500	-2.37024500
H	-4.29787800	-0.75407500	-2.66336900
C	-2.21203700	-1.26598800	-2.53513700
H	-2.34810100	-2.25791400	-2.95366000
C	-0.93108700	-0.84704400	-2.14799000
H	-0.10300700	-1.52878200	-2.27887500
C	-0.73736100	0.41879500	-1.58810100
H	1.51405500	-3.76781100	-0.27494300
C	0.45854400	-3.72433200	-0.03662900

Experimental

TD-DFT calculations 2.3a:



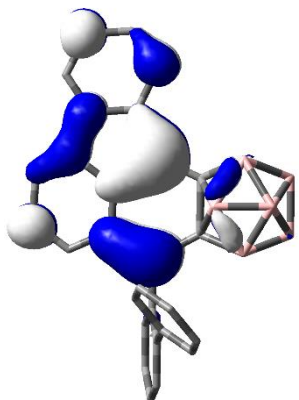
TD-DFT CAMB3LYP/6-31+G(d, p), gas phase

Table 5.1.7: Lowest energy singlet electronic transition of **2.3a** (TD-DFT CAM-B3LYP/6-31+G(d, p), gas phase).

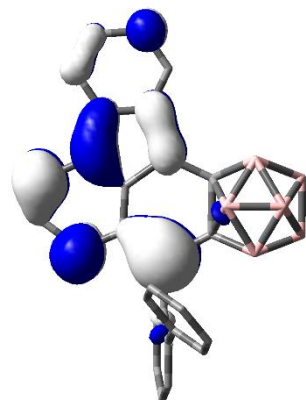
State	E [eV]	λ [nm]	f	Symmetry	Major contributions	Λ
1	2.93	422.45	0.0014	Singlet-A	H-1→LUMO (85%)	0.55
2	3.74	331.07	0.0403	Singlet-A	HOMO→LUMO (64%), HOMO→L+1 (13%)	0.29
3	3.99	310.81	0.0153	Singlet-A	H-4→LUMO (39%), H-1→L+1 (39%)	0.65
4	4.25	291.41	0.004	Singlet-A	H-2→LUMO (59%), H-2→L+1 (13%), HOMO→LUMO (12%)	0.23
5	4.39	282.10	0.3311	Singlet-A	H-4→LUMO (39%), H-1→L+1 (33%)	0.65
6	4.61	269.21	0.1259	Singlet-A	H-6→LUMO (63%), H-3→LUMO (11%)	0.65
7	4.67	265.75	0.0038	Singlet-A	H-15→LUMO (12%), H-11→LUMO (25%), H-7→LUMO (14%), HOMO→L+1 (17%)	0.38
8	4.76	260.51	0.0084	Singlet-A	H-3→LUMO (62%)	0.28
9	4.81	257.75	0.0091	Singlet-A	HOMO→L+1 (46%)	0.36
10	5.09	243.52	0.0208	Singlet-A	H-5→LUMO (16%), H-2→L+2 (11%), HOMO→L+5 (18%)	0.47
11	5.12	242.11	0.0008	Singlet-A	H-14→LUMO (21%), H-13→LUMO (29%)	0.42
12	5.15	240.63	0.0688	Singlet-A	H-5→LUMO (13%), H-2→L+2 (10%)	0.46
13	5.17	239.65	0.0991	Singlet-A	H-6→L+1 (14%), H-4→L+1 (13%)	0.56
14	5.20	238.29	0.2662	Singlet-A	H-5→LUMO (10%), HOMO→L+2 (57%)	0.68
15	5.28	235.03	0.0206	Singlet-A	H-9→LUMO (15%), H-8→LUMO (22%)	0.50
16	5.28	234.80	0.3035	Singlet-A	H-6→LUMO (12%), H-4→L+1 (38%)	0.61
17	5.37	230.98	0.0188	Singlet-A	H-9→LUMO (13%), H-5→LUMO (28%), H-3→L+2 (11%)	0.39
18	5.39	230.19	0.0023	Singlet-A	H-2→LUMO (13%), H-2→L+1 (44%)	0.29
19	5.46	227.26	0.0021	Singlet-A	H-11→LUMO (24%), H-7→LUMO (50%)	0.35
20	5.62	220.79	0.1826	Singlet-A	H-10→LUMO (16%), H-9→LUMO (15%), H-1→L+3 (26%)	0.56
21	5.67	218.63	0.0146	Singlet-A	H-15→LUMO (37%), H-9→LUMO (13%)	0.48
22	5.69	217.86	0.011	Singlet-A	H-10→LUMO (46%), H-8→LUMO (15%), H-3→L+1 (14%)	0.50
23	5.70	217.35	0.0744	Singlet-A	H-10→LUMO (20%), H-3→L+1 (49%)	0.36
24	5.75	215.55	0.0142	Singlet-A	H-12→LUMO (79%)	0.42
25	5.81	213.56	0.0047	Singlet-A	H-14→LUMO (23%), H-13→LUMO (38%)	0.38

Experimental

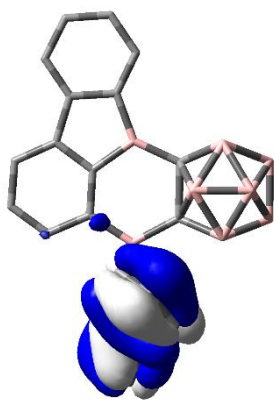
Orbitals relevant to the $S_1 \leftarrow S_0$ and $S_2 \leftarrow S_0$ transitions



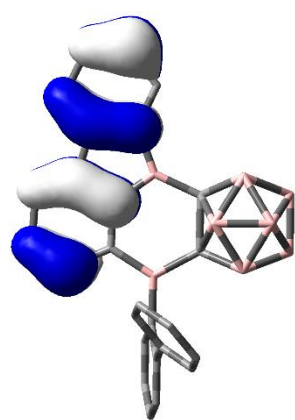
LUMO: -2.13 eV



LUMO+1: -1.19 eV



HOMO: -7.83 eV



HOMO-1: -7.92 eV

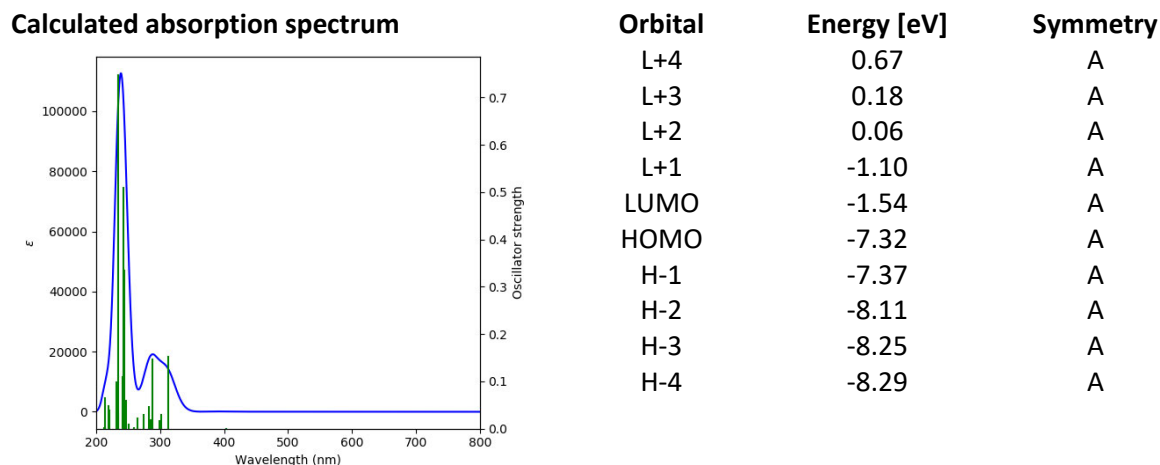
Isovalue= 0.03

Experimental

H	-0.11437800	1.00249100	1.90953000
B	-0.66272300	1.70243700	-1.83068800
C	-3.94761000	-1.40795800	0.21882800
C	-0.31763500	-1.55962400	-0.55747600
B	0.77129200	-0.44580200	-0.69711300
H	-0.99693100	0.95728500	-2.68533400
H	-2.87763800	2.94547900	-1.48300900
B	-2.22158200	0.23059900	-0.07412900
C	2.36030800	-1.11549000	-2.52665200
H	1.47682400	-1.10399400	-3.16134200
C	-1.30477100	1.48123600	-0.24723600
B	-1.43151900	2.91268700	0.66071900
H	-0.38941200	3.99032900	-2.98385800
C	-1.63424000	-1.19017600	-0.25562200
B	1.00646300	2.29015700	-1.60384400
H	1.75081900	4.65951800	-0.87036500
H	-1.18719000	5.30375200	-0.31109700
C	0.34311000	1.09949000	-0.55994900
B	-0.12464600	1.72832300	0.97855400
C	-0.05962400	-2.94633100	-0.69729900
H	0.94301300	-3.29059800	-0.93364200
H	0.55371400	4.04042900	1.89621900
B	-0.31197800	3.43530900	-1.93861800
H	2.38989500	1.97381700	0.55092900
B	-0.77361700	4.19382500	-0.37950100
C	-1.08415600	-3.88041500	-0.53543800
H	-0.86341700	-4.93831500	-0.64812700
B	-1.76706600	2.89584600	-1.07576900
C	-2.40167900	-3.48515800	-0.22775500
H	-3.17552100	-4.23910700	-0.10877100
B	0.23788500	3.46281900	0.90991500
H	1.82589900	1.93845900	-2.37892000
C	-2.67523700	-2.12821700	-0.08796600
B	1.33994100	2.30494500	0.12986400
H	-2.31116500	2.97699800	1.45061100
C	-3.73055000	0.00507400	0.23887600
B	0.92918500	3.81988200	-0.70463000
C	-5.20787700	-1.93710000	0.46170900
H	-5.38151100	-3.00971200	0.44737900
C	-6.27409500	-1.05939500	0.73076200
H	-7.26338500	-1.46553000	0.92242500
C	-6.07860400	0.32204200	0.75395400
H	-6.91402000	0.98335100	0.96296500
C	-4.80371200	0.85646300	0.50677800
H	-4.65702700	1.93255400	0.52511000
C	2.23206500	-0.81651300	-1.15402000
C	3.59598900	-1.40005300	-3.10850100
H	3.65963900	-1.60986700	-4.17223600
C	4.74161600	-1.41624500	-2.31134800
H	5.71043700	-1.64713600	-2.74476700
C	4.63442400	-1.15611500	-0.94639400
H	5.52058800	-1.21100600	-0.32090200
C	3.39702800	-0.85659300	-0.34784400
C	3.35372900	-0.63108600	1.12467200
C	4.32654900	0.16512400	1.75712700
H	5.08720700	0.65507300	1.15651200
C	4.30370600	0.36637000	3.13688100
H	5.05664700	0.99776400	3.59997700
C	3.30870600	-0.22738700	3.92031500
H	3.28978100	-0.06838400	4.99443600
C	2.34118300	-1.02648500	3.30907500
H	1.57023400	-1.50417700	3.90707100
C	2.36604100	-1.22850400	1.92636000
H	1.63072900	-1.88633000	1.47437100

Experimental

TD-DFT calculations 2.2b:



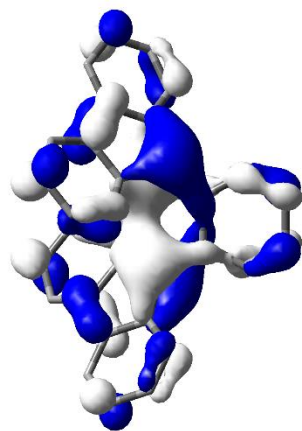
TD-DFT CAMB3LYP/6-31+G(d, p), gas phase

Table 5.1.8: Lowest energy singlet electronic transition of **2.2b** (TD-DFT CAM-B3LYP/6-31+G(d, p), gas phase).

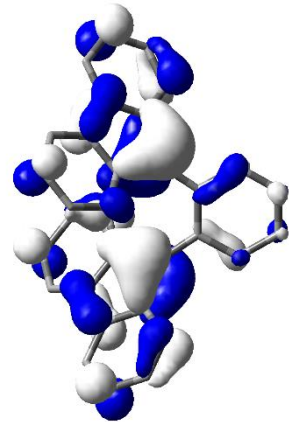
State	E [eV]	λ [nm]	f	Symmetry	Major contributions	Λ
1	3.07	403.46	0.0016	Singlet-A	H-1→L+1 (30%), HOMO→LUMO (66%)	0.61
2	3.10	400.57	0.0001	Singlet-A	H-1→LUMO (62%), HOMO→L+1 (35%)	0.61
3	3.97	312.68	0.1529	Singlet-A	H-2→LUMO (83%)	0.61
4	4.11	301.61	0.0315	Singlet-A	H-4→L+1 (10%), H-3→LUMO (46%), H-1→L+1 (14%)	0.66
5	4.15	298.63	0.0173	Singlet-A	H-4→LUMO (45%), H-3→L+1 (17%), HOMO→L+2 (11%)	0.68
6	4.31	287.37	0.1489	Singlet-A	H-5→LUMO (67%)	0.56
7	4.34	285.63	0.0197	Singlet-A	H-1→LUMO (34%), HOMO→L+1 (52%)	0.62
8	4.39	282.70	0.0481	Singlet-A	H-1→L+1 (51%), HOMO→LUMO (29%)	0.63
9	4.53	273.78	0.0319	Singlet-A	H-2→L+1 (70%)	0.56
10	4.68	265.18	0.0236	Singlet-A	H-7→L+1 (12%), H-6→LUMO (50%)	0.72
11	4.79	258.88	0.0038	Singlet-A	H-7→LUMO (41%), H-6→L+1 (25%)	0.75
12	4.95	250.37	0.0103	Singlet-A	H-10→LUMO (19%), H-5→L+1 (42%), H-4→L+1 (17%)	0.56
13	5.03	246.43	0.0616	Singlet-A	H-4→LUMO (28%), H-1→L+3 (21%), HOMO→L+2 (28%)	0.69
14	5.08	243.91	0.3361	Singlet-A	H-10→LUMO (39%), H-3→LUMO (12%), H-1→L+2 (12%), HOMO→L+3 (11%)	0.60
15	5.10	242.93	0.5115	Singlet-A	H-10→LUMO (17%), H-5→L+1 (15%), H-3→LUMO (17%), H-1→L+2 (17%), HOMO→L+3 (15%)	0.64
16	5.14	241.28	0.1113	Singlet-A	H-3→L+1 (46%), HOMO→L+2 (15%)	0.69
17	5.29	234.49	0.0401	Singlet-A	H-12→LUMO (36%), H-11→L+1 (24%), H-4→L+1 (11%)	0.60
18	5.30	233.92	0.0296	Singlet-A	H-13→LUMO (20%), H-12→L+1 (13%), H-11→LUMO (29%), H-10→L+1 (23%)	0.53
19	5.30	233.91	0.7495	Singlet-A	H-5→L+1 (20%), H-4→L+1 (31%)	0.66
20	5.36	231.29	0.0998	Singlet-A	H-13→LUMO (19%), H-11→LUMO (14%), H-10→L+1 (20%), H-3→L+1 (13%)	0.58
21	5.62	220.63	0.0395	Singlet-A	H-12→LUMO (11%), H-9→LUMO (26%), H-8→L+1 (11%), H-6→LUMO (19%)	0.69
22	5.64	219.69	0.0496	Singlet-A	H-11→LUMO (11%), H-9→L+1 (10%), H-8→LUMO (35%)	0.70
23	5.78	214.32	0.0665	Singlet-A	H-6→L+1 (13%), H-5→LUMO (11%), H-2→L+5 (22%)	0.64
24	5.80	213.68	0.0049	Singlet-A	H-7→LUMO (13%), H-4→L+3 (13%), H-3→L+2 (21%)	0.69
25	5.82	212.99	0.0029	Singlet-A	H-9→LUMO (23%), H-7→L+1 (11%), H-6→LUMO (17%)	0.73

Experimental

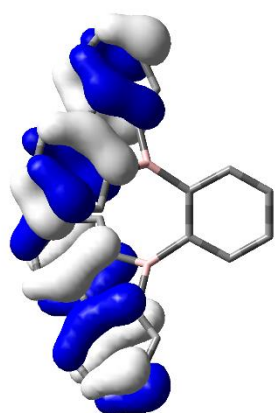
Orbitals relevant to the $S_1 \leftarrow S_0$ and $S_2 \leftarrow S_0$ transitions



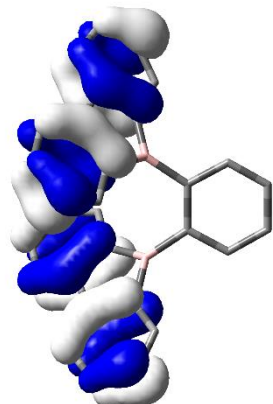
LUMO: -1.54 eV



LUMO+1: -1.10 eV



HOMO: -7.32 eV



HOMO-1: -7.37 eV

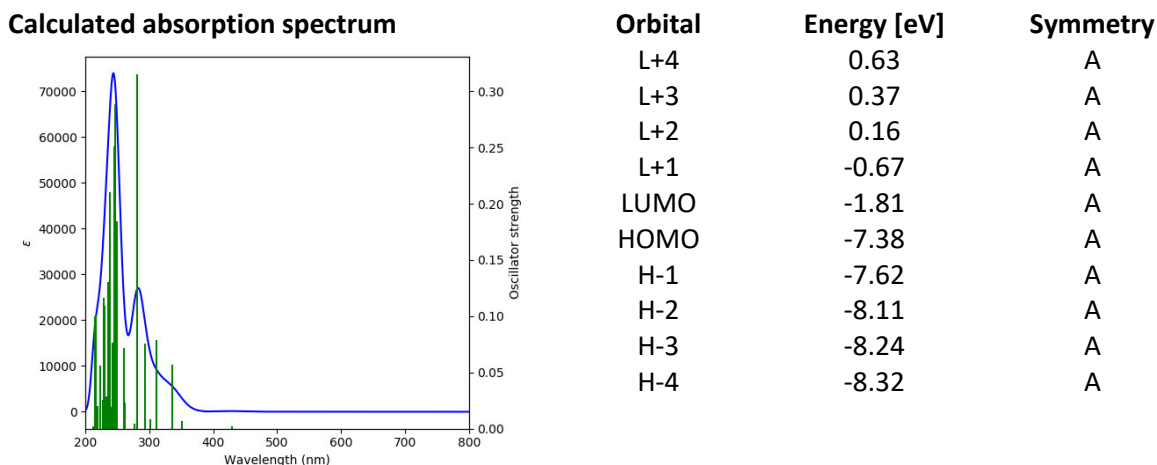
Isovalue= 0.03

Experimental

B	1.54656300	0.77025200	-0.41969800
B	-1.54649400	0.77027300	0.41962900
C	-1.22882400	-0.41785100	1.39776300
C	-0.15304600	-0.69239100	2.24415100
H	0.69777000	-0.01752600	2.28951800
C	-0.16236500	-1.84501700	3.04618100
H	0.67868800	-2.06119900	3.69850700
C	-1.25508500	-2.71284300	3.00801500
H	-1.25856500	-3.60242600	3.63212200
C	-2.35713800	-2.44647100	2.17736100
H	-3.20419500	-3.12743600	2.16910000
C	-2.34039000	-1.30543500	1.38302600
C	-3.38749800	-0.80584900	0.45080200
C	-4.61142600	-1.38151300	0.12620200
H	-4.92710300	-2.32250700	0.56901800
C	-5.44732500	-0.72855500	-0.79564200
H	-6.40550100	-1.17066700	-1.05515500
C	-5.05932000	0.47661400	-1.38447400
H	-5.71512600	0.96594600	-2.09892000
C	-3.82090500	1.05130700	-1.05464000
H	-3.52004100	1.98444400	-1.52519700
C	-2.97966100	0.42513200	-0.13307000
C	-0.70297100	2.04896900	0.13047400
C	-1.36575600	3.28918200	0.24157500
H	-2.43360800	3.30368800	0.44478800
C	-0.68642300	4.50447900	0.12372100
H	-1.22717400	5.44185300	0.22205500
C	0.68647100	4.50451100	-0.12366600
H	1.22719200	5.44191100	-0.22192300
C	1.36584400	3.28924800	-0.24161700
H	2.43369300	3.30380400	-0.44485100
C	0.70311400	2.04900900	-0.13060800
C	1.22879800	-0.41793300	-1.39772400
C	0.15298000	-0.69248400	-2.24405800
H	-0.69779500	-0.01757000	-2.28946400
C	0.16219900	-1.84518900	-3.04597500
H	-0.67888700	-2.06138000	-3.69825500
C	1.25486400	-2.71308100	-3.00775600
H	1.25826700	-3.60272700	-3.63177500
C	2.35696100	-2.44669800	-2.17716500
H	3.20397400	-3.12771800	-2.16886300
C	2.34030800	-1.30558700	-1.38293700
C	3.38748500	-0.80597000	-0.45080500
C	4.61140900	-1.38165300	-0.12623000
H	4.92701900	-2.32270400	-0.56897200
C	5.44739400	-0.72863800	0.79549700
H	6.40556600	-1.17076700	1.05499700
C	5.05947800	0.47660600	1.38423300
H	5.71534900	0.96598300	2.09858900
C	3.82106600	1.05132000	1.05442100
H	3.52026600	1.98450800	1.52491500
C	2.97973900	0.42509200	0.13296200

Experimental

TD-DFT calculations 2.3b:



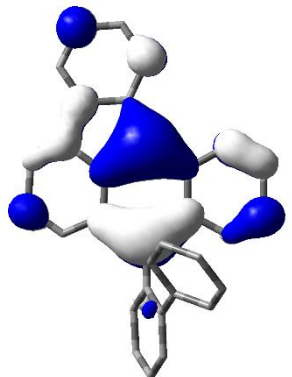
TD-DFT CAMB3LYP/6-31+G(d, p), gas phase

Table 5.1.9: Lowest energy singlet electronic transition of **2.3b** (TD-DFT CAM-B3LYP/6-31+G(d, p), gas phase).

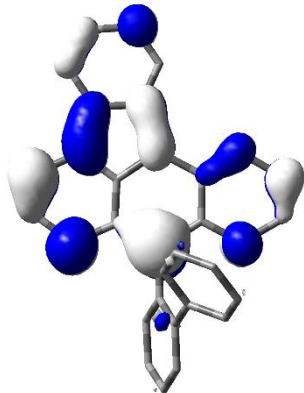
State	E [eV]	λ [nm]	f	Symmetry	Major contributions	Λ
1	2.89	429.67	0.0022	Singlet-A	HOMO \rightarrow LUMO (91%)	0.51
2	3.54	350.44	0.0066	Singlet-A	H-2 \rightarrow LUMO (89%)	0.60
3	3.70	335.18	0.0571	Singlet-A	H-3 \rightarrow LUMO (16%), H-1 \rightarrow LUMO (62%)	0.34
4	3.98	311.74	0.0791	Singlet-A	H-4 \rightarrow LUMO (56%), HOMO \rightarrow L+1 (23%)	0.60
5	4.11	301.52	0.008	Singlet-A	H-9 \rightarrow LUMO (28%), H-3 \rightarrow LUMO (26%), H-1 \rightarrow LUMO (14%)	0.50
6	4.23	293.04	0.0753	Singlet-A	H-6 \rightarrow LUMO (24%), H-3 \rightarrow LUMO (13%), HOMO \rightarrow L+1 (23%)	0.54
7	4.41	281.31	0.3153	Singlet-A	H-6 \rightarrow LUMO (25%), H-4 \rightarrow LUMO (17%), HOMO \rightarrow L+1 (24%)	0.62
8	4.49	276.13	0.0047	Singlet-A	H-9 \rightarrow LUMO (29%), H-3 \rightarrow LUMO (22%)	0.53
9	4.74	261.55	0.0231	Singlet-A	H-11 \rightarrow LUMO (46%), H-5 \rightarrow LUMO (27%)	0.47
10	4.77	260.19	0.0716	Singlet-A	H-11 \rightarrow LUMO (30%), H-5 \rightarrow LUMO (41%)	0.43
11	4.96	249.72	0.1841	Singlet-A	H-8 \rightarrow LUMO (16%), H-2 \rightarrow L+1 (10%), H-1 \rightarrow L+1 (18%), HOMO \rightarrow L+1 (11%)	0.55
12	5.03	246.61	0.2885	Singlet-A	H-2 \rightarrow L+1 (45%), H-1 \rightarrow L+1 (23%)	0.50
13	5.05	245.74	0.2508	Singlet-A	H-12 \rightarrow LUMO (10%), H-8 \rightarrow LUMO (14%), H-1 \rightarrow L+1 (17%)	0.55
14	5.10	243.01	0.0764	Singlet-A	H-12 \rightarrow LUMO (20%), H-7 \rightarrow LUMO (12%), H-3 \rightarrow L+2 (10%), H-1 \rightarrow L+5 (12%)	0.53
15	5.16	240.19	0.019	Singlet-A	H-12 \rightarrow LUMO (37%), H-1 \rightarrow L+5 (10%)	0.51
16	5.21	238.12	0.2103	Singlet-A	H-1 \rightarrow L+2 (48%)	0.67
17	5.26	235.51	0.1306	Singlet-A	H-3 \rightarrow L+2 (12%), H-1 \rightarrow L+2 (26%)	0.760
18	5.31	233.29	0.0288	Singlet-A	H-10 \rightarrow LUMO (23%), H-9 \rightarrow LUMO (14%), H-8 \rightarrow LUMO (29%)	0.67
19	5.38	230.27	0.1095	Singlet-A	H-7 \rightarrow LUMO (16%), H-6 \rightarrow LUMO (13%), H-4 \rightarrow L+1 (17%)	0.56
20	5.43	228.32	0.1167	Singlet-A	H-9 \rightarrow L+1 (12%), H-7 \rightarrow LUMO (27%), H-3 \rightarrow L+1 (12%)	0.47
21	5.46	227.00	0.0253	Singlet-A	H-13 \rightarrow LUMO (16%), H-9 \rightarrow L+1 (12%), H-1 \rightarrow L+1 (11%)	0.51
22	5.55	223.40	0.056	Singlet-A	H-4 \rightarrow L+1 (36%), HOMO \rightarrow L+3 (23%)	0.58
23	5.66	219.15	0.0198	Singlet-A	H-13 \rightarrow LUMO (36%), H-3 \rightarrow L+1 (36%)	0.42
24	5.73	216.23	0.1017	Singlet-A	H-6 \rightarrow L+1 (40%), H-5 \rightarrow L+1 (12%)	0.59
25	5.77	214.90	0.0996	Singlet-A	H-10 \rightarrow LUMO (11%), H-8 \rightarrow L+1 (10%), HOMO \rightarrow L+3 (11%), HOMO \rightarrow L+12 (14%)	0.64

Experimental

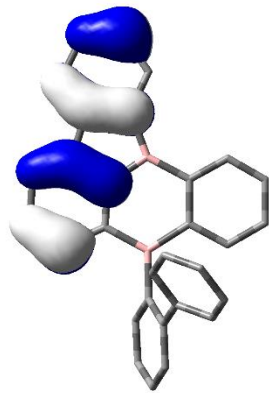
Orbitals relevant to the $S_1 \leftarrow S_0$ and $S_2 \leftarrow S_0$ transitions



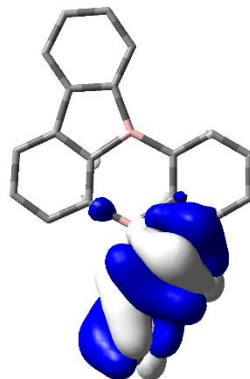
LUMO: -1.81 eV



LUMO+1: -0.67 eV



HOMO: -7.38 eV



HOMO-1: -7.62 eV

Isovalue= 0.03

Experimental

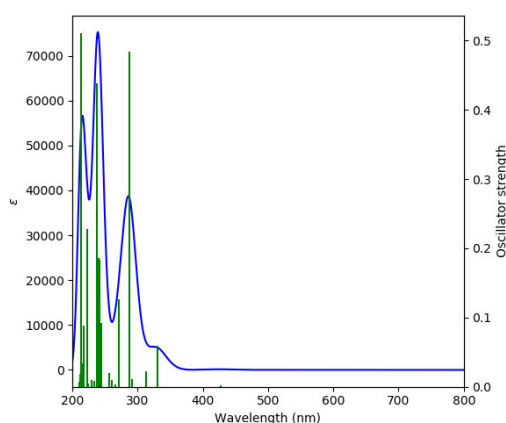
C	4.01006900	0.68943100	0.36383000
C	0.43005200	1.52432700	-0.11335700
B	-0.72385700	0.59121100	-0.62791500
B	2.07660800	-0.50699000	-0.46751900
C	-2.42304500	2.16556000	-1.68631600
H	-1.58168500	2.55512800	-2.25524300
C	1.69948800	0.94017200	-0.05059200
C	0.32325100	2.86154600	0.33657100
H	-0.63747700	3.36955700	0.32423400
C	1.45075300	3.54495100	0.80503200
H	1.34787400	4.57312300	1.14219000
C	2.71901500	2.93337800	0.85787100
H	3.57148600	3.49494100	1.23237100
C	2.83832900	1.61316500	0.42747400
C	3.61951900	-0.58611600	-0.15761500
C	5.32570300	0.94015000	0.73557400
H	5.62167500	1.90858600	1.13050600
C	6.28265100	-0.07982200	0.59657600
H	7.31294900	0.10909800	0.88568100
C	5.92283400	-1.33020600	0.09283600
H	6.67255900	-2.10962700	-0.00831600
C	4.59264400	-1.58016200	-0.28289800
H	4.33068700	-2.56049800	-0.67231200
C	-2.19730000	1.14785000	-0.73612400
C	-3.69872200	2.67110800	-1.94304400
H	-3.83693100	3.44418000	-2.69375600
C	-4.78977800	2.18316900	-1.22083000
H	-5.78660100	2.57807500	-1.39582500
C	-4.59084600	1.19922100	-0.25299100
H	-5.43396400	0.85026700	0.33672200
C	-3.31256700	0.67067100	0.00095000
C	-3.15444000	-0.35827900	1.06633300
C	-4.06195200	-1.42723200	1.17941700
H	-4.87238300	-1.51724400	0.46154200
C	-3.91702800	-2.39027000	2.17887500
H	-4.62354200	-3.21351900	2.23877300
C	-2.86164800	-2.30496500	3.09225100
H	-2.74799700	-3.05520400	3.86932900
C	-1.95637400	-1.24578000	2.99744000
H	-1.13822800	-1.16167600	3.70713800
C	-2.10379200	-0.28187900	1.99735400
H	-1.41305600	0.55524000	1.95850200
C	1.20746100	-2.71651800	-1.52831800
C	0.96756400	-1.41801900	-1.04798300
C	-0.36214800	-0.87388400	-1.12798300
C	-1.36286800	-1.67178400	-1.70884200
C	-1.09920700	-2.96147600	-2.18536800
C	0.18806400	-3.48987800	-2.09209700
H	2.21008000	-3.13093600	-1.46776500
H	-2.37211100	-1.28086800	-1.79502800
H	-1.89946500	-3.54926900	-2.62715700
H	0.39830400	-4.49103400	-2.45857400

Experimental

CAM-B3LYP-Hexane

TD-DFT calculations 2.3a:

Calculated absorption spectrum



Orbital	Energy [eV]	Symmetry
L+4	0.42	A
L+3	0.20	A
L+2	-0.04	A
L+1	-1.15	A
LUMO	-2.10	A
HOMO	-7.81	A
H-1	-7.87	A
H-2	-8.51	A
H-3	-8.57	A
H-4	-8.81	A

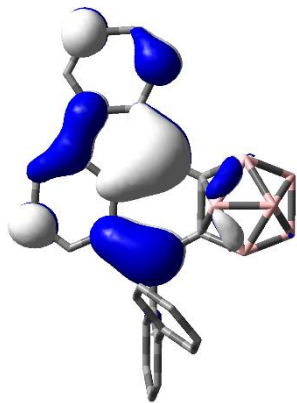
TD-DFT CAMB3LYP/6-31+G(d, p), n-Hexane

Table 5.1.10: Lowest energy singlet electronic transition of **2.3a** (TD-DFT CAM-B3LYP/6-31+G(d, p), n-hexane).

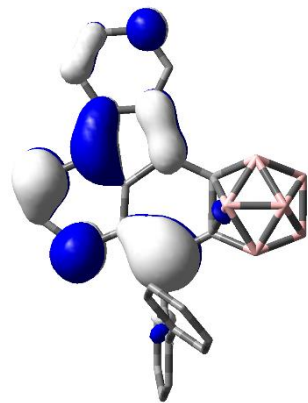
State	E [eV]	λ [nm]	f	Symmetry	Major contributions	Λ
1	2.90	427.41	0.0021	Singlet-A	H-1 \rightarrow LUMO (68%), HOMO \rightarrow LUMO (25%)	0.51
2	3.75	330.81	0.059	Singlet-A	H-1 \rightarrow LUMO (16%), HOMO \rightarrow LUMO (52%), HOMO \rightarrow L+1 (12%)	0.41
3	3.97	312.24	0.0231	Singlet-A	H-4 \rightarrow LUMO (40%), H-1 \rightarrow L+1 (33%)	0.62
4	4.26	291.15	0.0106	Singlet-A	H-2 \rightarrow LUMO (59%), H-2 \rightarrow L+1 (13%), HOMO \rightarrow LUMO (10%)	0.25
5	4.32	286.97	0.4836	Singlet-A	H-4 \rightarrow LUMO (39%), H-1 \rightarrow L+1 (30%), HOMO \rightarrow L+1 (10%)	0.63
6	4.57	271.09	0.1269	Singlet-A	H-6 \rightarrow LUMO (69%)	0.68
7	4.67	265.29	0.0036	Singlet-A	H-15 \rightarrow LUMO (10%), H-11 \rightarrow LUMO (24%), H-8 \rightarrow LUMO (24%), HOMO \rightarrow L+1 (12%)	0.42
8	4.77	259.90	0.0097	Singlet-A	H-3 \rightarrow LUMO (66%)	0.29
9	4.83	256.73	0.02	Singlet-A	H-1 \rightarrow L+1 (10%), HOMO \rightarrow L+1 (41%)	0.47
10	5.09	243.65	0.0928	Singlet-A	H-5 \rightarrow LUMO (11%), H-2 \rightarrow L+2 (10%), HOMO \rightarrow L+2 (19%), HOMO \rightarrow L+5 (12%)	0.53
11	5.12	242.17	0.1836	Singlet-A	H-7 \rightarrow LUMO (29%), H-6 \rightarrow L+1 (21%), H-4 \rightarrow L+1 (14%)	0.65
12	5.13	241.49	0.0104	Singlet-A	H-14 \rightarrow LUMO (17%), H-13 \rightarrow LUMO (34%)	0.42
13	5.16	240.37	0.1856	Singlet-A	H-2 \rightarrow L+2 (11%), HOMO \rightarrow L+2 (20%)	0.61
14	5.17	239.72	0.1557	Singlet-A	H-5 \rightarrow LUMO (28%), HOMO \rightarrow L+2 (21%)	0.47
15	5.23	236.85	0.4388	Singlet-A	H-7 \rightarrow LUMO (13%), H-6 \rightarrow LUMO (11%), H-4 \rightarrow L+1 (35%)	0.62
16	5.31	233.54	0.0083	Singlet-A	H-9 \rightarrow LUMO (24%), H-5 \rightarrow LUMO (19%)	0.34
17	5.39	230.01	0.0096	Singlet-A	H-9 \rightarrow LUMO (16%), H-5 \rightarrow LUMO (22%), H-3 \rightarrow L+2 (11%)	0.37
18	5.41	228.97	0.0015	Singlet-A	H-9 \rightarrow LUMO (19%), H-2 \rightarrow LUMO (10%), H-2 \rightarrow L+1 (35%)	0.30
19	5.54	223.80	0.005	Singlet-A	H-11 \rightarrow LUMO (33%), H-8 \rightarrow LUMO (34%)	0.41
20	5.56	222.95	0.2281	Singlet-A	H-7 \rightarrow LUMO (39%), H-1 \rightarrow L+3 (22%)	0.65
21	5.71	217.06	0.0881	Singlet-A	H-3 \rightarrow L+1 (58%)	0.31
22	5.74	216.09	0.0345	Singlet-A	H-15 \rightarrow LUMO (34%), H-9 \rightarrow LUMO (24%)	0.43
23	5.80	213.86	0.0415	Singlet-A	H-10 \rightarrow LUMO (85%)	0.40
24	5.80	213.66	0.5111	Singlet-A	H-6 \rightarrow L+1 (36%), H-4 \rightarrow L+1 (10%)	0.60
25	5.85	212.11	0.019	Singlet-A	H-12 \rightarrow LUMO (82%)	0.33

Experimental

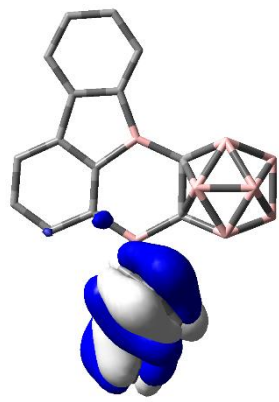
Orbitals relevant to the $S_1 \leftarrow S_0$ and $S_2 \leftarrow S_0$ transitions



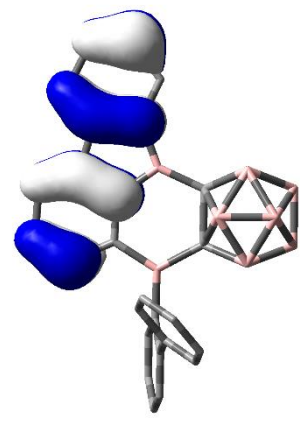
LUMO: -2.10 eV



LUMO+1: -1.15 eV



HOMO: -7.81 eV



HOMO-1: -7.87 eV

Isovalue= 0.03

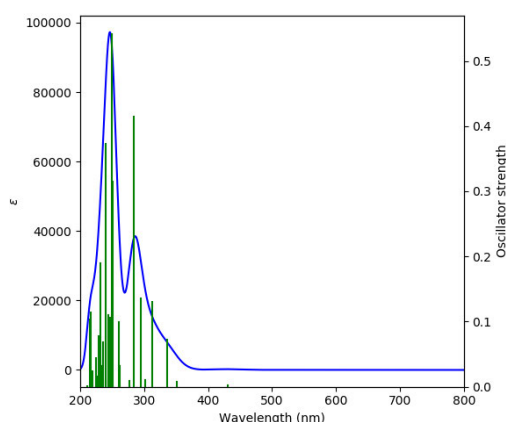
Experimental

H	-0.11437800	1.00249100	1.90953000
B	-0.66272300	1.70243700	-1.83068800
C	-3.94761000	-1.40795800	0.21882800
C	-0.31763500	-1.55962400	-0.55747600
B	0.77129200	-0.44580200	-0.69711300
H	-0.99693100	0.95728500	-2.68533400
H	-2.87763800	2.94547900	-1.48300900
B	-2.22158200	0.23059900	-0.07412900
C	2.36030800	-1.11549000	-2.52665200
H	1.47682400	-1.10399400	-3.16134200
C	-1.30477100	1.48123600	-0.24723600
B	-1.43151900	2.91268700	0.66071900
H	-0.38941200	3.99032900	-2.98385800
C	-1.63424000	-1.19017600	-0.25562200
B	1.00646300	2.29015700	-1.60384400
H	1.75081900	4.65951800	-0.87036500
H	-1.18719000	5.30375200	-0.31109700
C	0.34311000	1.09949000	-0.55994900
B	-0.12464600	1.72832300	0.97855400
C	-0.05962400	-2.94633100	-0.69729900
H	0.94301300	-3.29059800	-0.93364200
H	0.55371400	4.04042900	1.89621900
B	-0.31197800	3.43530900	-1.93861800
H	2.38989500	1.97381700	0.55092900
B	-0.77361700	4.19382500	-0.37950100
C	-1.08415600	-3.88041500	-0.53543800
H	-0.86341700	-4.93831500	-0.64812700
B	-1.76706600	2.89584600	-1.07576900
C	-2.40167900	-3.48515800	-0.22775500
H	-3.17552100	-4.23910700	-0.10877100
B	0.23788500	3.46281900	0.90991500
H	1.82589900	1.93845900	-2.37892000
C	-2.67523700	-2.12821700	-0.08796600
B	1.33994100	2.30494500	0.12986400
H	-2.31116500	2.97699800	1.45061100
C	-3.73055000	0.00507400	0.23887600
B	0.92918500	3.81988200	-0.70463000
C	-5.20787700	-1.93710000	0.46170900
H	-5.38151100	-3.00971200	0.44737900
C	-6.27409500	-1.05939500	0.73076200
H	-7.26338500	-1.46553000	0.92242500
C	-6.07860400	0.32204200	0.75395400
H	-6.91402000	0.98335100	0.96296500
C	-4.80371200	0.85646300	0.50677800
H	-4.65702700	1.93255400	0.52511000
C	2.23206500	-0.81651300	-1.15402000
C	3.59598900	-1.40005300	-3.10850100
H	3.65963900	-1.60986700	-4.17223600
C	4.74161600	-1.41624500	-2.31134800
H	5.71043700	-1.64713600	-2.74476700
C	4.63442400	-1.15611500	-0.94639400
H	5.52058800	-1.21100600	-0.32090200
C	3.39702800	-0.85659300	-0.34784400
C	3.35372900	-0.63108600	1.12467200
C	4.32654900	0.16512400	1.75712700
H	5.08720700	0.65507300	1.15651200
C	4.30370600	0.36637000	3.13688100
H	5.05664700	0.99776400	3.59997700
C	3.30870600	-0.22738700	3.92031500
H	3.28978100	-0.06838400	4.99443600
C	2.34118300	-1.02648500	3.30907500
H	1.57023400	-1.50417700	3.90707100
C	2.36604100	-1.22850400	1.92636000
H	1.63072900	-1.88633000	1.47437100

Experimental

TD-DFT calculations 2.3b:

Calculated absorption spectrum



Orbital	Energy [eV]	Symmetry
L+4	0.63	A
L+3	0.34	A
L+2	0.13	A
L+1	-0.70	A
LUMO	-1.84	A
HOMO	-7.41	A
H-1	-7.65	A
H-2	-8.15	A
H-3	-8.27	A
H-4	-8.35	A

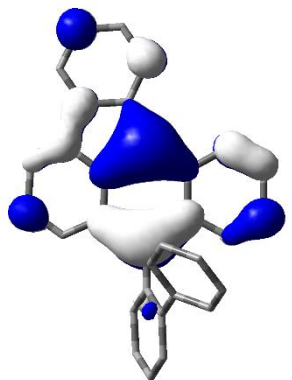
TD-DFT CAMB3LYP/6-31+G(d, p), n-Hexane

Table 5.1.11: Lowest energy singlet electronic transition of **2.3b** (TD-DFT CAM-B3LYP/6-31+G(d, p), n-Hexane).

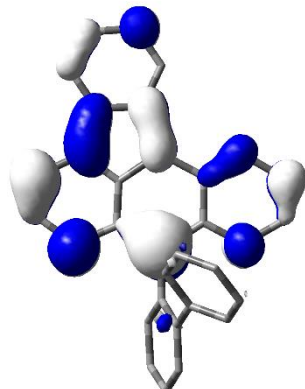
State	E [eV]	λ [nm]	f	Symmetry	Major contributions	Λ
1	2.88	430.44	0.0031	Singlet-A	HOMO \rightarrow LUMO (91%)	0.51
2	3.53	350.79	0.0091	Singlet-A	H-2 \rightarrow LUMO (89%)	0.60
3	3.69	335.95	0.0738	Singlet-A	H-3 \rightarrow LUMO (16%), H-1 \rightarrow LUMO (62%)	0.34
4	3.96	313.04	0.1311	Singlet-A	H-4 \rightarrow LUMO (61%), HOMO \rightarrow L+1 (19%)	0.60
5	4.11	301.89	0.0114	Singlet-A	H-9 \rightarrow LUMO (30%), H-3 \rightarrow LUMO (25%), H-1 \rightarrow LUMO (13%)	0.50
6	4.21	294.42	0.1364	Singlet-A	H-6 \rightarrow LUMO (17%), H-3 \rightarrow LUMO (12%), HOMO \rightarrow L+1 (31%)	0.54
7	4.37	283.97	0.4162	Singlet-A	H-6 \rightarrow LUMO (32%), H-4 \rightarrow LUMO (14%), HOMO \rightarrow L+1 (21%)	0.62
8	4.48	276.50	0.0099	Singlet-A	H-9 \rightarrow LUMO (30%), H-3 \rightarrow LUMO (22%)	0.53
9	4.73	261.88	0.0332	Singlet-A	H-11 \rightarrow LUMO (43%), H-5 \rightarrow LUMO (28%)	0.47
10	4.76	260.65	0.1	Singlet-A	H-11 \rightarrow LUMO (33%), H-5 \rightarrow LUMO (38%)	0.45
11	4.93	251.34	0.3167	Singlet-A	H-8 \rightarrow LUMO (13%), H-2 \rightarrow L+1 (31%), HOMO \rightarrow L+1 (11%)	0.59
12	4.98	249.08	0.5429	Singlet-A	H-8 \rightarrow LUMO (10%), H-2 \rightarrow L+1 (39%), H-1 \rightarrow L+1 (12%)	0.55
13	5.03	246.34	0.1075	Singlet-A	H-1 \rightarrow L+1 (39%)	0.46
14	5.09	243.47	0.1119	Singlet-A	H-12 \rightarrow LUMO (24%), H-7 \rightarrow LUMO (10%), H-1 \rightarrow L+5 (10%)	0.54
15	5.16	240.42	0.0123	Singlet-A	H-12 \rightarrow LUMO (34%), H-1 \rightarrow L+5 (11%)	0.51
16	5.16	240.04	0.3739	Singlet-A	H-1 \rightarrow L+2 (62%)	0.72
17	5.25	236.02	0.0694	Singlet-A	H-5 \rightarrow L+2 (10%), H-3 \rightarrow L+2 (15%)	0.53
18	5.29	234.53	0.0334	Singlet-A	H-10 \rightarrow LUMO (25%), H-9 \rightarrow LUMO (12%), H-8 \rightarrow LUMO (31%)	0.70
19	5.37	231.05	0.1904	Singlet-A	H-6 \rightarrow LUMO (12%), H-4 \rightarrow L+1 (22%), HOMO \rightarrow L+3 (11%)	0.60
20	5.42	228.71	0.0785	Singlet-A	H-9 \rightarrow L+1 (12%), H-7 \rightarrow LUMO (40%), H-3 \rightarrow L+1 (11%)	0.43
21	5.46	227.27	0.0174	Singlet-A	H-13 \rightarrow LUMO (18%), H-9 \rightarrow L+1 (14%), H-1 \rightarrow L+1 (11%)	0.51
22	5.52	224.48	0.0452	Singlet-A	H-10 \rightarrow LUMO (11%), H-4 \rightarrow L+1 (39%), HOMO \rightarrow L+3 (24%)	0.58
23	5.65	219.41	0.0255	Singlet-A	H-13 \rightarrow LUMO (32%), H-3 \rightarrow L+1 (37%)	0.41
24	5.71	217.24	0.1148	Singlet-A	H-13 \rightarrow LUMO (12%), H-6 \rightarrow L+1 (43%), H-5 \rightarrow L+1 (12%)	0.60
25	5.76	215.40	0.1041	Singlet-A	H-10 \rightarrow LUMO (13%), H-8 \rightarrow L+1 (11%), HOMO \rightarrow L+11 (16%)	64

Experimental

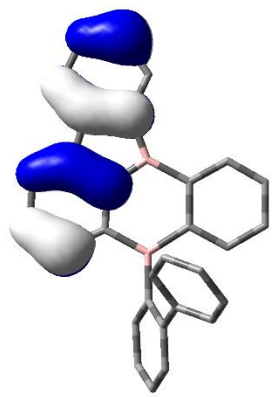
Orbitals relevant to the $S_1 \leftarrow S_0$ and $S_2 \leftarrow S_0$ transitions



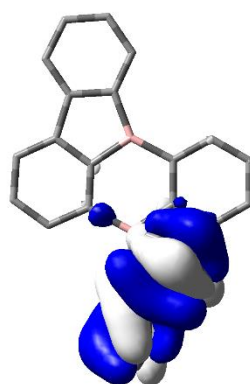
LUMO: -1.84 eV



LUMO+1: -0.70eV



HOMO: -7.41 eV



HOMO-1: -7.65 eV

Isovalue= 0.03

Experimental

C	4.01006900	0.68943100	0.36383000
C	0.43005200	1.52432700	-0.11335700
B	-0.72385700	0.59121100	-0.62791500
B	2.07660800	-0.50699000	-0.46751900
C	-2.42304500	2.16556000	-1.68631600
H	-1.58168500	2.55512800	-2.25524300
C	1.69948800	0.94017200	-0.05059200
C	0.32325100	2.86154600	0.33657100
H	-0.63747700	3.36955700	0.32423400
C	1.45075300	3.54495100	0.80503200
H	1.34787400	4.57312300	1.14219000
C	2.71901500	2.93337800	0.85787100
H	3.57148600	3.49494100	1.23237100
C	2.83832900	1.61316500	0.42747400
C	3.61951900	-0.58611600	-0.15761500
C	5.32570300	0.94015000	0.73557400
H	5.62167500	1.90858600	1.13050600
C	6.28265100	-0.07982200	0.59657600
H	7.31294900	0.10909800	0.88568100
C	5.92283400	-1.33020600	0.09283600
H	6.67255900	-2.10962700	-0.00831600
C	4.59264400	-1.58016200	-0.28289800
H	4.33068700	-2.56049800	-0.67231200
C	-2.19730000	1.14785000	-0.73612400
C	-3.69872200	2.67110800	-1.94304400
H	-3.83693100	3.44418000	-2.69375600
C	-4.78977800	2.18316900	-1.22083000
H	-5.78660100	2.57807500	-1.39582500
C	-4.59084600	1.19922100	-0.25299100
H	-5.43396400	0.85026700	0.33672200
C	-3.31256700	0.67067100	0.00095000
C	-3.15444000	-0.35827900	1.06633300
C	-4.06195200	-1.42723200	1.17941700
H	-4.87238300	-1.51724400	0.46154200
C	-3.91702800	-2.39027000	2.17887500
H	-4.62354200	-3.21351900	2.23877300
C	-2.86164800	-2.30496500	3.09225100
H	-2.74799700	-3.05520400	3.86932900
C	-1.95637400	-1.24578000	2.99744000
H	-1.13822800	-1.16167600	3.70713800
C	-2.10379200	-0.28187900	1.99735400
H	-1.41305600	0.55524000	1.95850200
C	1.20746100	-2.71651800	-1.52831800
C	0.96756400	-1.41801900	-1.04798300
C	-0.36214800	-0.87388400	-1.12798300
C	-1.36286800	-1.67178400	-1.70884200
C	-1.09920700	-2.96147600	-2.18536800
C	0.18806400	-3.48987800	-2.09209700
H	2.21008000	-3.13093600	-1.46776500
H	-2.37211100	-1.28086800	-1.79502800
H	-1.89946500	-3.54926900	-2.62715700
H	0.39830400	-4.49103400	-2.45857400

5.2.8 References

- [1] C. J. Berger, G. He, C. Merten, R. McDonald, M. J. Ferguson, E. Rivard, *Inorg. Chem.* **2014**, *53*, 1475–1486.
- [2] D. Kaufmann, *Chem. Ber.* **1987**, *120*, 901–905.
- [3] G. M. Sheldrick, *Acta Crystallogr.* **2015**, *A71*, 3–8.
- [4] G. M. Sheldrick, *Acta Crystallogr.* **2008**, *A64*, 112–122.
- [5] C. B. Hubschle, G. M. Sheldrick, B. Dittrich, *J. Appl. Crystallogr.* **2011**, *44*, 1281–1284.
- [6] A. L. Spek, *Acta Crystallogr.* **2015**, *C71*, 9–18.
- [7] H. P. K. Brandenburg, Diamond Version 4.2.0. Crystal and Molecular Structure Visualizatuib, Crystal Impact, Bonn (Germany), **2016**.
- [8] J.-D. Chai, M. Head-Gordon, *Physical Chemistry Chemical Physics* **2008**, *10*, 6615–6620.
- [9] Y. Zhao, D. G. Truhlar, *Theor. Chem. Acc.* **2007**, *120*, 215–241.
- [10] Y. Zhao, D. G. Truhlar, *J. Chem. Theory. Comput.* **2008**, *4*, 1849–1868.
- [11] N. Mardirossian, M. Head-Gordon, *J. Chem. Theory. Comput.* **2016**, *12*, 4303–4325.
- [12] W. J. Hehre, R. Ditchfield, J. A. Pople, *The Journal of Chemical Physics* **1972**, *56*, 2257–2261.
- [13] P. C. Hariharan, J. A. Pople, *Theoretica chimica acta* **1973**, *28*, 213–222.
- [14] K. Fukui, *Accounts of Chemical Research* **1981**, *14*, 363–368.
- [15] M. J. Frisch, G. W. Trucks, H. B. Schlegel, G. E. Scuseria, M. A. Robb, J. R. Cheeseman, G. Scalmani, V. Barone, B. Mennucci, G. A. Petersson, H. Nakatsuji, M. Caricato, X. Li, H. P. Hratchian, A. F. Izmaylov, J. Bloino, G. Zheng, J. L. Sonnenberg, M. Hada, M. Ehara, K. Toyota, R. Fukuda, J. Hasegawa, M. Ishida, T. Nakajima, Y. Honda, O. Kitao, H. Nakai, T. Vreven, J. A. Montgomery, Jr.; , J. E. Peralta, F. Ogliaro, M. Bearpark, J. J. Heyd, E. Brothers, K. N. Kudin, V. N. Staroverov, R. Kobayashi, J. Normand, K. Raghavachari, A. Rendell, J. C. Burant, S. S. Iyengar, J. Tomasi, M. Cossi, N. Rega, J. M. Millam, M. Klene, J. E. Knox, J. B. Cross, V. Bakken, C. Adamo, J. Jaramillo, R. Gomperts, R. E. Stratmann, O. Yazyev, A. J. Austin, R. Cammi, C. Pomelli, J. W. Ochterski, R. L. Martin, K. Morokuma, V. G. Zakrzewski, G. A. Voth, P. Salvador, J. J. Dannenberg, S. Dapprich, A. D. Daniels, Ö. Farkas, J. B. Foresman, J. V. Ortiz, J. Cioslowski, D. J. Fox, in *Gaussian 09, Revision D.01*, Gaussian, Inc., Wallingford CT, **2009**.
- [16] M. J. Frisch, G. W. Trucks, H. B. Schlegel, G. E. Scuseria, M. A. Robb, J. R. Cheeseman, G. Scalmani, V. Barone, B. Mennucci, G. A. Petersson, H. Nakatsuji, M. Caricato, X. Li, H. P. Hratchian, A. F. Izmaylov, J. Bloino, G. Zheng, J. L. Sonnenberg, M. Hada, M. Ehara, K. Toyota, R. Fukuda, J. Hasegawa, M. Ishida, T. Nakajima, Y. Honda, O. Kitao, H. Nakai, T. Vreven, J. A. Montgomery, Jr.; , J. E. Peralta, F. Ogliaro, M. Bearpark, J. J. Heyd, E. Brothers, K. N. Kudin, V. N. Staroverov, R. Kobayashi, J. Normand, K. Raghavachari, A. Rendell, J. C. Burant, S. S. Iyengar, J. Tomasi, M. Cossi, N. Rega, J. M. Millam, M. Klene, J. E. Knox, J. B. Cross, V. Bakken, C. Adamo, J. Jaramillo, R. Gomperts, R. E. Stratmann, O. Yazyev, A. J. Austin, R. Cammi, C. Pomelli, J. W. Ochterski, R. L. Martin, K. Morokuma, V. G. Zakrzewski, G. A. Voth, P. Salvador, J. J. Dannenberg, S. Dapprich, A. D. Daniels, Ö. Farkas, J. B. Foresman, J. V. Ortiz, J. Cioslowski, D. J. Fox, in *Gaussian 09, Revision 9.E.01*, Gaussian, Inc., Wallingford CT, **2016**.
- [17] T. Lu, F. Chen, *J. Comput. Chem.* **2012**, *33*, 580–592.
- [18] C. Lee, W. Yang, R. G. Parr, *Phys. Rev. Br* **1988**, *37*, 785–789.
- [19] G. A. Petersson, M. A. Al-Laham, *J. Chem. Phys.* **1991**, *94*, 6081–6090.
- [20] G. A. Petersson, A. Bennett, T. G. Tensfeldt, M. A. Al-Laham, W. A. Shirley, J. Mantzaris, *J. Chem. Phys.* **1988**, *89*, 2193–2218.
- [21] M. J. Peach, P. Benfield, T. Helgaker, D. J. Tozer, *J. Chem. Phys.* **2008**, *128*, 044118.
- [22] T. Yanai, D. P. Tew, N. C. Handy, *Chem. Phys. Lett.* **2004**, *393*, 51–57.

Experimental

5.3 Supporting Information Chapter 3

5.3.1 General experimental details

The solvents used were dried using either a solvent purification system (SPS) from Innovative Technology or were distilled and degassed from appropriate drying agents and stored under argon. All other starting materials were purchased from commercial sources and used as received. Compound **3.1** was prepared according to literature procedure.^[1] All other starting materials were purchased from commercial sources and were used without further purification.

NMR Spectra were recorded either on a Bruker Avance 500 FT NMR spectrometer (operating at ^1H : 500 MHz, ^{11}B : 160 MHz, $^{13}\text{C}[^1\text{H}]$: 126 MHz or a or Bruker Avance III HD 300 spectrometer (operating at ^1H , 300 MHz; ^{13}C , 75 MHz; ^{11}B , 96 MHz). Chemical shifts (δ) are given in ppm and are referenced to external $\text{BF}_3 \cdot \text{Et}_2\text{O}$ ($^{11}\text{B}[^1\text{H}]$) ^1H NMR spectra were referenced via residual proton resonances of CD_2Cl_2 (5.32 ppm) and C_6D_6 (7.16 ppm). $^{13}\text{C}[^1\text{H}]$ spectra were referenced to CD_2Cl_2 (53.84 ppm) and C_6D_6 (128.06 ppm).

HRMS were recorded using a Thermo Scientific Exactive Plus Orbitrap MS system with either an Atmospheric Sample Analysis Probe (ASAP) or by Electrospray Ionization (ESI).

Elemental analyses were performed on an Elementar vario MICRO cube elemental analyzer.

Single-crystal X-ray diffraction: Crystals suitable for single-crystal X-ray diffraction were selected, coated in perfluoropolyether oil or polybutyl oil, mounted on a polyimide microloop (MicroMounts from MiTeGen) and transferred to a stream of cold nitrogen (Oxford Cryostream 800). Diffraction data were collected on a Rigaku Oxford Diffraction XtaLAB Synergy diffractometer with a semiconductor HPA-detector (HyPix-6000) and multi-layer mirror monochromated Cu-K α radiation generated by a PhotonJet source. Data were collected at 100 K or 173 K (**3.2**). The images were processed and corrected for Lorentz-polarization effects and absorption (empirical scaling) using the CrysAlis^{Pro} software from Rigaku Oxford Diffraction. The structures were solved using the intrinsic phasing method (SHELXT)^[2] and Fourier expansion technique. All non-hydrogen atoms were refined in anisotropic approximation, with hydrogen atoms ‘riding’ in idealized positions, by full-matrix least squares against F^2 of all data, using SHELXL^[3] software and the SHELXLE^[4] graphical user interface. However, hydrogen atoms bonded to boron in compound **3.6** were refined freely. The crystal structure of **3.5** is a superstructure of body-centered $I2/a$ space group symmetry with the same unit cell and was refined in subgroup $P2_1/c$ due to the presence of weak but distinct reflections violating the body-centering. Because I -lattice violating reflections are weak, and disorder is also present, the data:parameter ratio is below 10 and refinement residual values are relatively high. Diamond software

Experimental

was used for graphical representation.^[5] Crystal data and experimental details are listed in Table 5.3.1. Full structural information has been deposited with the Cambridge Crystallographic Data Centre. CCDC-2183060 (**3.2**), 2183061 (**3.4**), 2183062 (**3.5**), and 2183063 (**3.6**).

Photophysical measurements: All measurements were performed in standard quartz cuvettes (1 cm x 1 cm cross-section). UV-visible absorption spectra were recorded using a Perkin Elmer Lambda 450 UV-visible spectrophotometer. **Emission spectra** were recorded using an Edinburgh Instruments FLSP920 spectrophotometer equipped with a double monochromator for both excitation and emission, operating in right-angle geometry mode, and all spectra were fully corrected for the spectral response of the instrument. **Fluorescence quantum yields** were measured using a calibrated integrating sphere (inner diameter: 150 mm) from Edinburgh Instruments combined with the FLSP920 spectrophotometer described above. For solution-state and solid-state measurements, the longest-wavelength absorption maximum of the compound in the respective solvent was chosen as the excitation wavelength. **Fluorescence lifetimes** were recorded using the time-correlated single-photon counting (TCSPC) method using the same FLSP920 spectrometer described above. Solutions were excited with a picosecond pulsed diode laser at emission maxima of 376.6 nm. The full width at half maximum (FWHM) of the laser pulses were ca. 70–200 ps, while the instrument response function (IRF) had a FWHM of ca. 1.0 ns, measured from the scatter of a Ludox solution at the excitation wavelength. Decays were recorded to at least 10000 counts in the peak channel with a record length of at least 1000 channels. The band pass of the monochromator was adjusted to give a signal count rate of <10 kHz. Iterative deconvolution of the IRF with one decay function and non-linear least-squares analysis were used to analyze the data. The quality of the fit was judged by the calculated value of the reduced χ^2 and visual inspection of the weighted residuals.

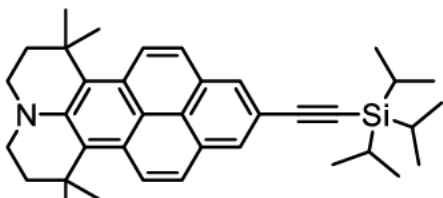
Experimental

Computational methods

All calculations (DFT and TD-DFT) were carried out with the program package Gaussian 09^[6] and were performed on a parallel cluster system. GaussView 6.0.16 was used to visualize the results, to measure calculated structural parameters, and to plot orbital surfaces (isovalue: $\pm 0.030 [e a_0^{-3}]^{1/2}$). The ground-state geometries were optimized using the B3LYP functional^[7] in combination with the 6-31+G(d) basis set.^[8-9] The optimized geometries were confirmed to be local minima by performing frequency calculations and obtaining only positive (real) frequencies. Based on these optimized structures, the lowest-energy gas-phase vertical transitions were calculated (singlets, 25 states) by TD-DFT, using the Coulomb attenuated functional CAM-B3LYP^[10] in combination with the 6-31G(d,p) basis set. The CAM-B3LYP functional has been shown to be effective for both pyrene and CT systems, hence its selection here.^[11-12] No symmetry constraints were used throughout. Lambda values were generated using the multiwfn program.^[13]

5.3.2 Synthetic procedures

Synthesis of 3.2



3.2

In an argon-filled glove box 3.1 (800 mg, 1.67 mmol) cesium carbonate (1.09 g, 3.34 mmol) and Pd(dba)₂ (96.0 mg, 167 μ mol) were added in a Schlenk tube. The solids were suspended in degassed methanol (46 mL). In a separate Schlenk tube, (iodoethynyl)triisopropylsilane (567 mg, 1.84 mmol) was degassed by using freeze-pump-thaw and added to the reaction mixture. The tube was sealed and stirred at room temperature for 20 h and monitored *via* TLC (silica, hexane/ethyl acetate, 9:1) and GC/MS. The reaction mixture was passed through a silica plug and washed with EtOAc (100 mL) and the solvent was removed under reduced pressure. The crude product was passed through a silica plug (eluent: hexane/ EtOAc 9:1 (400 mL)) and the solvent was removed under reduced pressure. The obtained solid was washed with acetone (3 x 1 mL) under argon and dried in vacuo to give 3.2 as a yellow solid (401 mg, 751 μ mol, 45%).

¹H NMR (500 MHz, CD₂Cl₂, ppm): δ 8.54 (d, *J* = 10 Hz, 2H), 8.06 (s, 2H), 7.81 (d, *J* = 10 Hz, 2H), 3.31 (m, 4H), 2.01 (m, 4H), 1.80 (s, 12H), 1.21 (s, 21H).

¹³C {¹H} NMR (125 MHz, CD₂Cl₂, ppm): δ 143.6, 129.4, 129.2, 127.8, 127.1, 126.3, 125.4, 124.9, 119.6, 118.7, 108.5, 90.2, 47.9, 43.6, 34.6, 32.1, 18.9, 11.9.

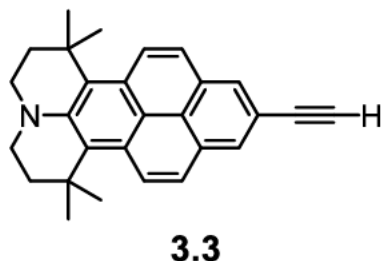
¹⁵N, ¹H HMBC (300 MHz, CD₂Cl₂, ppm): δ -304.1.

HR-MS (ASAP⁺) (*m/z*): calc. for [C₃₇H₄₈NSi]⁺ 534.35505; found 534.3541 [M+H]⁺.

Elem. Anal. Calc. (%) for C₃₇H₄₇NSi: C 83.24; H 8.87; N 2.62; found: C 83.05; H 9.15; N 2.49.

Experimental

Synthesis of 3.3



3.3

In a round bottom flask 3.2 (910 mg, 1.70 mmol) was dissolved in THF (90 mL). A solution of tetra-n-butylammonium fluoride in THF (8.50 mL, 8.50 mmol, 1 M) was added dropwise and the mixture was stirred at room temperature for 1 h. The reaction was monitored with TLC (alumina, hexane/ethyl acetate, 9:1). After completion, water was added (25 mL) and THF was removed under reduced pressure. The resulting light-yellow precipitate was filtered over a glass frit. The solid was dissolved with CH₂Cl₂ and the newly obtained solution was filtered over a silica plug with CH₂Cl₂ (200 mL) as the eluent. All volatile components were removed under reduced pressure to give Product 3.3 as a light-yellow solid (530 mg, 1.04 mmol, 82%).

¹H NMR (500 MHz, CD₂Cl₂, ppm): δ 8.55 (d, *J* = 10 Hz, 2H), 8.07 (s, 2H), 7.82 (d, *J* = 10 Hz, 2H), 3.31 (m, 4H), 3.24 (s, 1H), 2.01 (m, 4H), 1.79 (s, 12H).

¹³C{¹H} NMR (125 MHz, CD₂Cl₂, ppm): δ 143.6, 129.4, 129.2, 127.8, 127.2, 126.4, 125.6, 124.8, 119.5, 117.1, 84.9, 76.9, 47.8, 43.5, 34.5, 32.1.

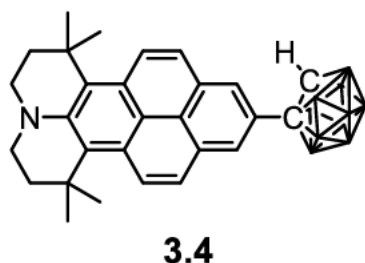
¹⁵N, ¹H HMBC (300 MHz, CD₂Cl₂, ppm): δ -304.0.

HR-MS (ASAP⁺) (*m/z*): calc. for [C₂₈H₂₈N]⁺ 378.22163; found 378.2208 [M+H]⁺.

Elem. Anal. Calc. (%) for C₂₈H₂₇N: C 89.08; H 7.21; N 3.71; found: C 88.79; H 7.60; N 3.85.

Experimental

Synthesis of 3.4



In a Young's tap tube, **3.3** (117 mg, 236 µmol), silver(I)acetate (4 mg, 24.0 µmol) and $B_{10}H_{12}(SMe_2)_2$ (86.4 mg, 354 µmol) were evacuated three times. After flushing with argon, toluene was added, and the mixture was stirred at 80 °C for 2 d. In an argon filled glovebox, the mixture was filtered through an alumina plug with toluene as the eluent. All volatile components were removed under reduced pressure. The resulting solid was purified by vapor diffusion of pentane into a concentrated solution in toluene at –30 °C. The precipitate from two fractions was washed with hexane and dried in vacuum for 2 d. Product **3.4** was obtained as an orange yellow solid (42 mg, 85 µmol, 36 %).

1H NMR (500 MHz, C_6D_6 , ppm): δ 8.59 (d, J = 10 Hz, 2H), 7.91 (s, 2H), 7.67 (d, J = 10 Hz, 2H), 3.17 (s, 1H), 2.91 (m, 4H), 1.77 (m, 4H), 1.68 (s, 12H).

$^{13}C\{^1H\}$ NMR (125 MHz, C_6D_6 , ppm): δ 143.7, 129.7, 129.5, 128.8, 127.6, 126.6, 126.3, 125.3, 123.5, 120.0, 77.9, 61.2, 47.6, 43.5, 34.4, 32.1.

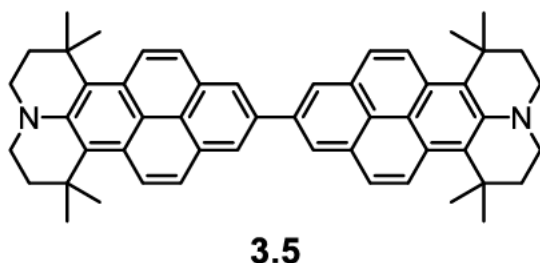
^{15}N , 1H HMBC (300 MHz, C_6D_6 , ppm): δ –304.6.

$^{11}B\{^1H\}$ NMR (160 MHz, C_6D_6 , ppm): δ 1.6, –3.9, –8.6, –10.2, –10.9, –12.3.

HR-MS (ASAP⁺) (*m/z*): calc. for $[C_{28}H_{38}B_{10}N]^+$ 496.4007; found 496.3998 [M+H]⁺.

Experimental

Synthesis of 3.5



3.5

Compound 3.5 was obtained as a side product in the synthesis of 3.2 due the presence of a small amount of air acting as the oxidant. The crude product was purified *via* column chromatography (silica, ethyl acetate, gradient) and the solvent was removed under reduced pressure and dried in *vacuo* to give 3.5 as a yellow solid (38 mg, 54 µmol, 3%).

¹H NMR (300 MHz, C₆D₆, ppm): δ 8.67 (d, J = 10 Hz, 4H), 8.60 (s, 4H), 8.04 (d, J = 10 Hz, 4H), 2.98 (m, 8H), 1.86 (m, 8H), 1.77 (s, 24H).

¹³C{¹H} NMR (125 MHz, C₆D₆, ppm): δ 143.2, 137.9, 130.4, 129.7, 126.7, 126.2, 126.1, 125.6, 124.8, 121.2, 47.8, 44.0, 34.5, 32.3.

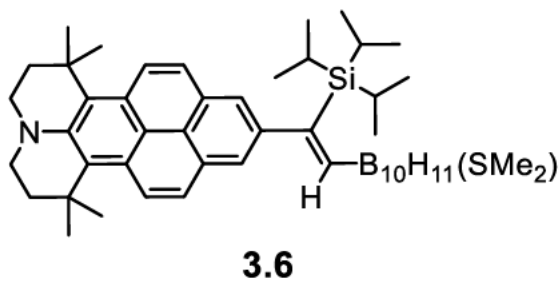
¹⁵N, ¹H HMBC (300 MHz, C₆D₆, ppm): δ -306.4.

HR-MS (ASAP⁺) (*m/z*): calc. for [C₅₂H₅₃N₂]⁺ 705.42033; found 705.4189 [M+H]⁺.

Elem. Anal. Calc. (%) for C₅₂H₅₂N₂: C 88.59; H 7.43; N 3.97; **found:** C 87.16; H 7.52; N 3.35.

Experimental

Synthesis of 3.6



3.6

In a Young's tap tube, **3.2** (200 mg, 529 µmol), silver(I) acetate (8.8 mg, 53 µmol) and $B_{10}H_{12}(SMe_2)_2$ (194 mg, 795 µmol) were evacuated three times. After flushing with argon, toluene (5 mL) was added, and the mixture was stirred at 100 °C for 2 d. In an argon filled glovebox, the mixture was filtered through an alumina plug with toluene as the eluent. All volatile components were removed under reduced pressure. Column chromatography (silica, hexane/ethyl acetate, gradient) of the residue yielded **3.6** as a yellow solid (236 mg, 330 µmol, 62%).

1H NMR (500 MHz, C_6D_6 , ppm): δ 8.60 (d, J = 10 Hz, 2H), 8.05 (s, 2H), 7.91 (d, J = 10 Hz, 2H), 7.47 (s, 1H), 2.93 (m, 4H), 1.81 (m, 4H), 1.70 (d, J = 2.75 Hz, 12H), 1.58 (s, 3H), 1.40 (s, 3H), 1.22 (m, 9H), 1.02 (m, 12H).

$^{13}C\{^1H\}$ NMR (125 MHz, C_6D_6 , ppm): δ 153.8, 149.8, 147.5, 143.0, 129.5, 129.4, 126.8, 126.1, 125.7, 124.6, 124.0, 121.1, 47.7, 43.9, 34.4, 32.2, 32.2, 25.6, 22.9, 19.9, 19.4, 14.5, 12.2.

$^{15}N, ^1H$ HMBC (300 MHz, C_6D_6 , ppm): δ -306.3.

^{11}B NMR (160 MHz, C_6D_6 , ppm): δ 29.7, 3.5, 3.0, -1.7, -4.0, -4.5, -6.7, -10.5, -23.5, -24.4, -41.0, -41.6.

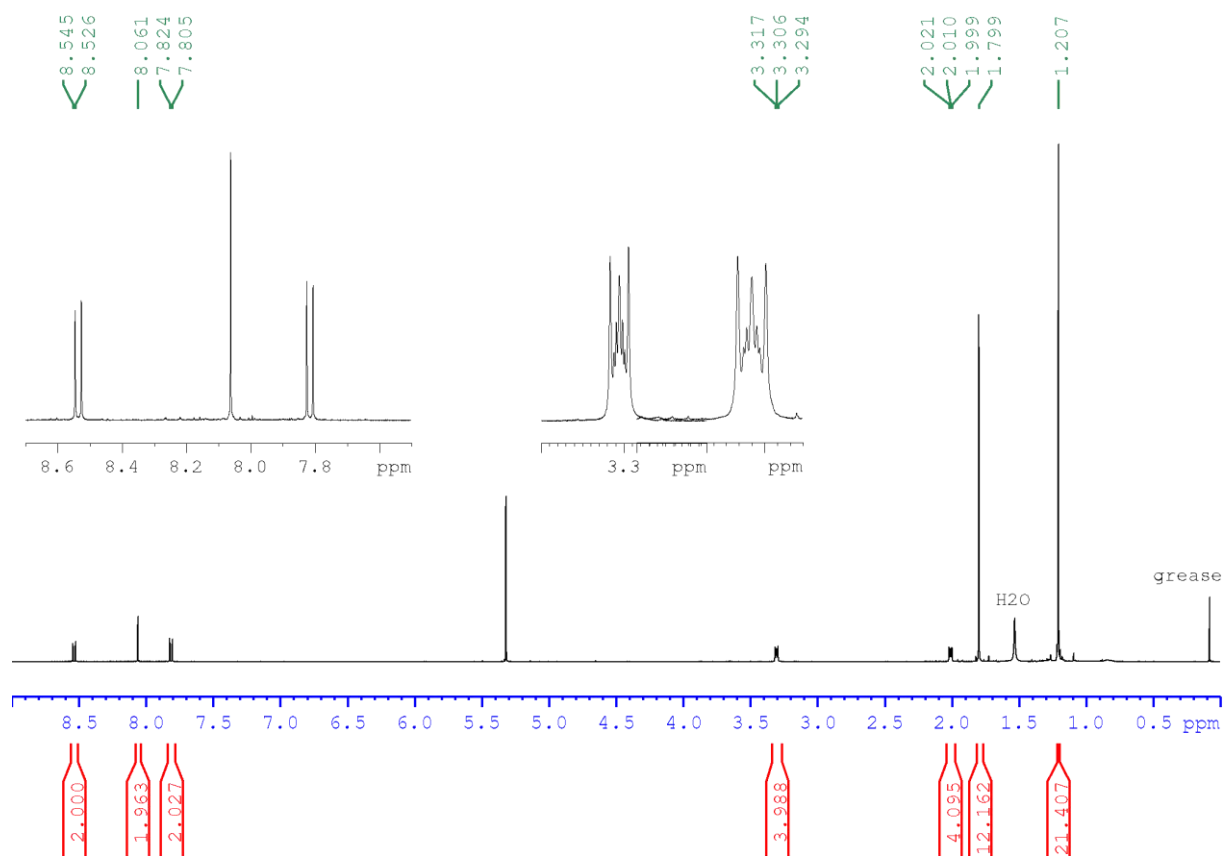
$^{11}B\{^1H\}$ NMR (160 MHz, C_6D_6 , ppm): δ 29.1, 3.3, -1.7, -4.3, -6.9, -10.6, -24.0, -41.3.

HR-MS (APCI $^+$) (m/z): calc. for $[C_{39}H_{66}B_{10}NSSi]^+$ 717.5697; found $[M+H]^+$ 717.5629.

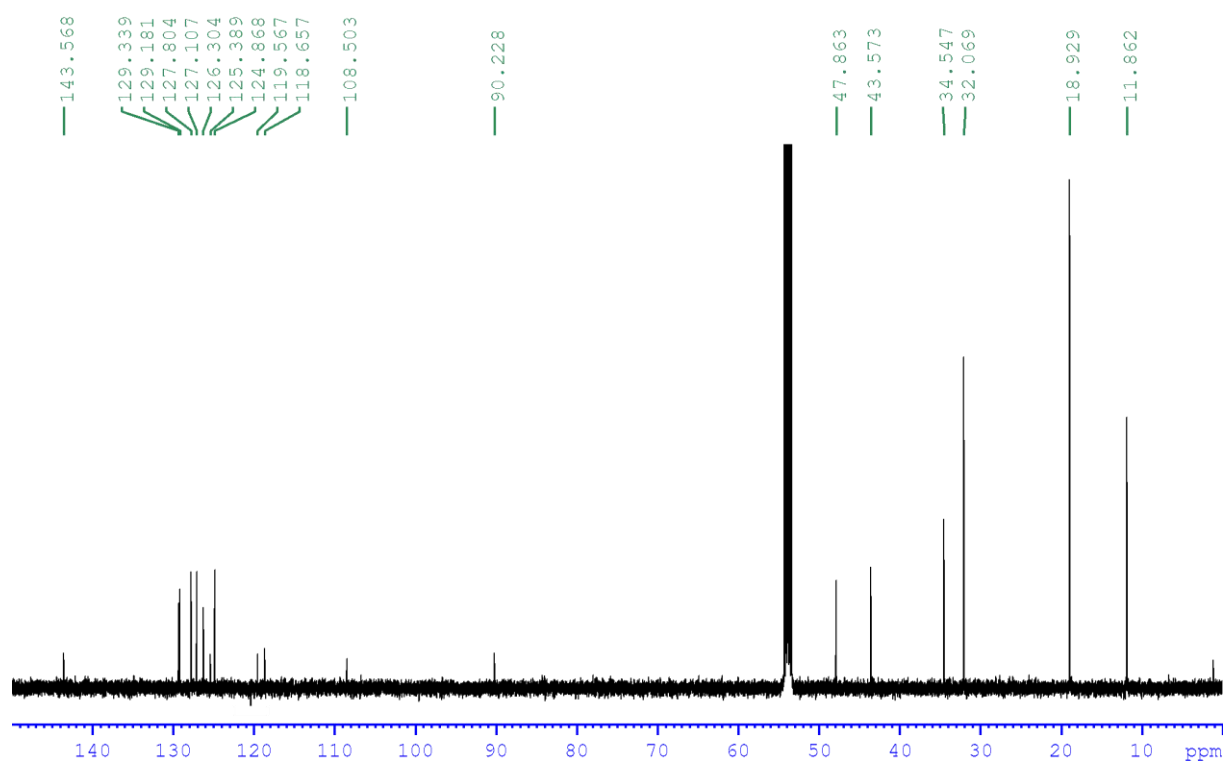
Elem. Anal. Calc. (%) for $C_{39}H_{65}B_{10}NSSi$: C 65.40; H 9.15; N 1.96; found: C 65.29; H 9.26; N 1.74.

Experimental

^1H NMR spectrum of 3.2 in CD_2Cl_2

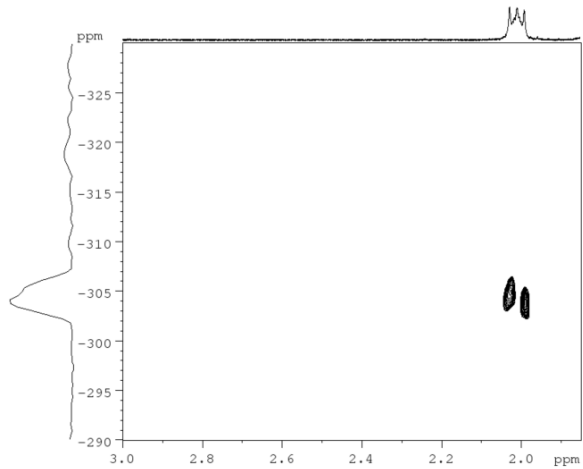


$^{13}\text{C}\{^1\text{H}\}$ NMR spectrum of 2 in CD_2Cl_2



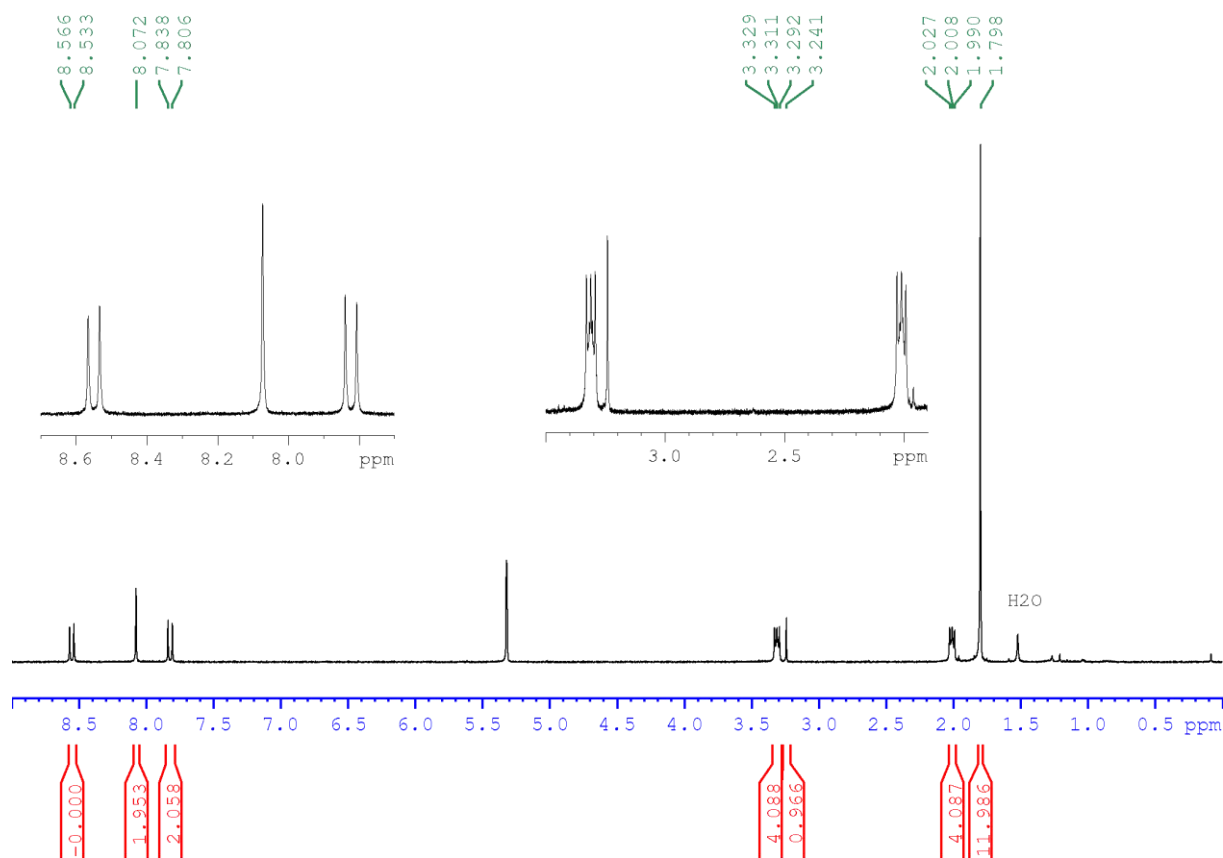
Experimental

$^{15}\text{N}, ^1\text{H}$ HMBC NMR spectrum of 3.2 in CD_2Cl_2

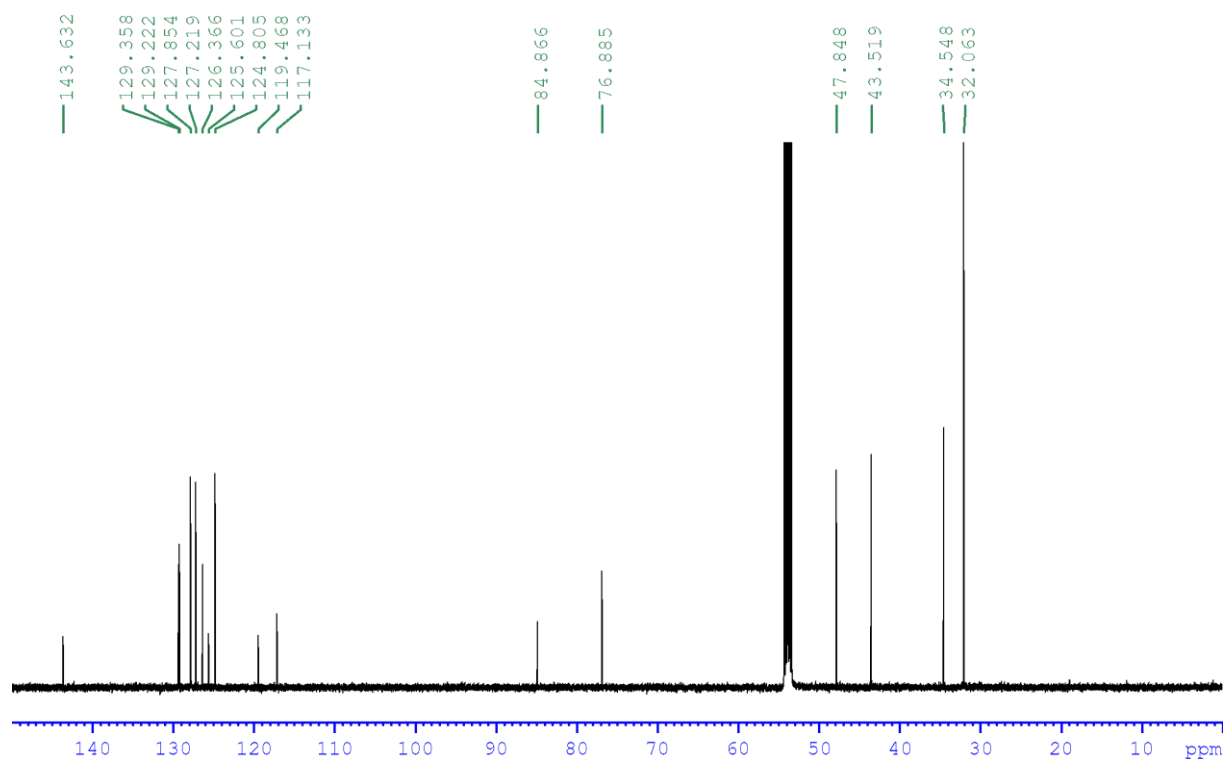


Experimental

^1H NMR spectrum of 3.3 in CD_2Cl_2

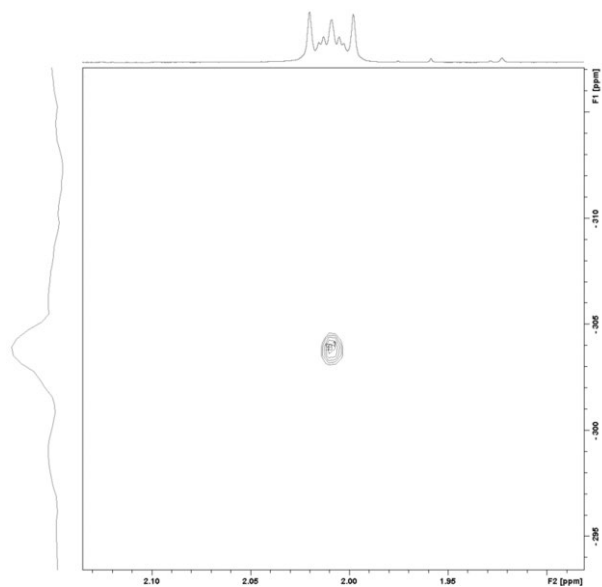


$^{13}\text{C}\{^1\text{H}\}$ NMR spectrum of 3.3 in CD_2Cl_2



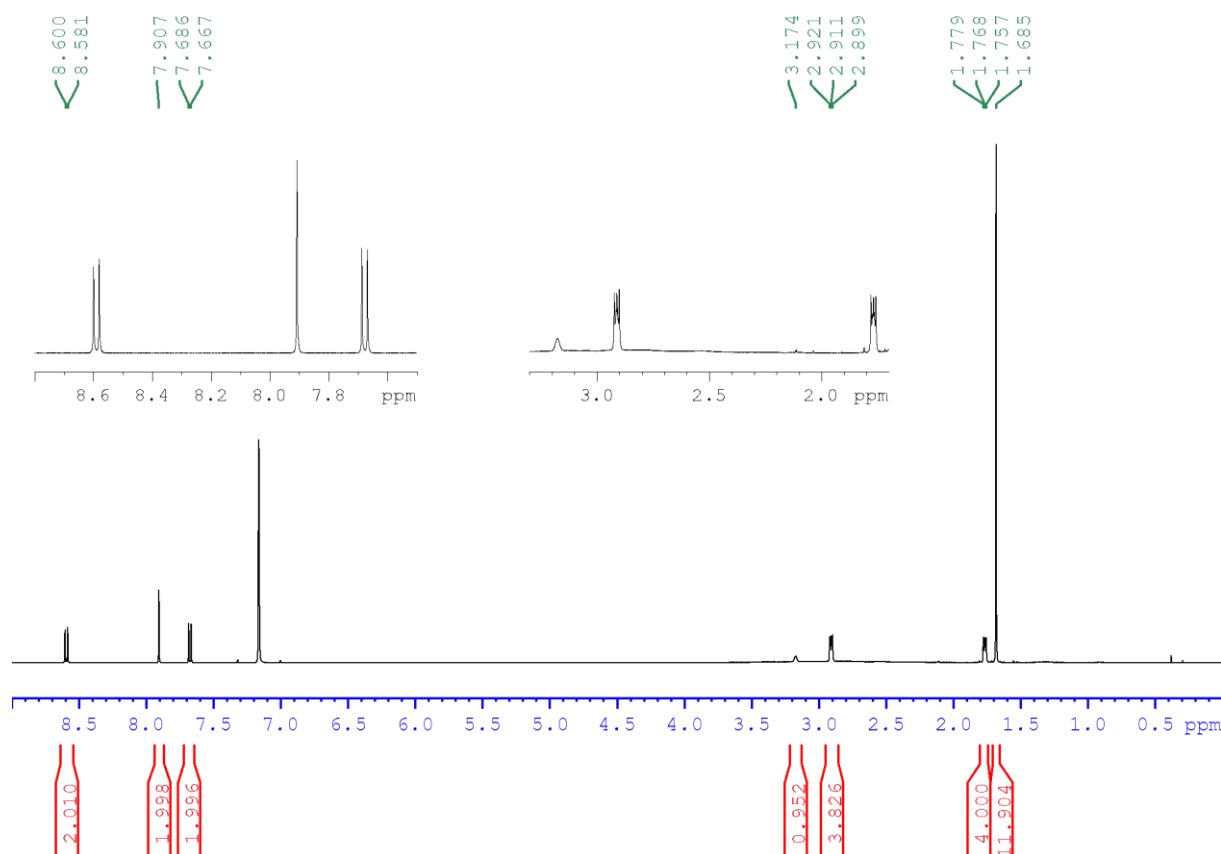
Experimental

^{15}N , ^1H HMBC NMR spectrum of 3.3 in CD_2Cl_2

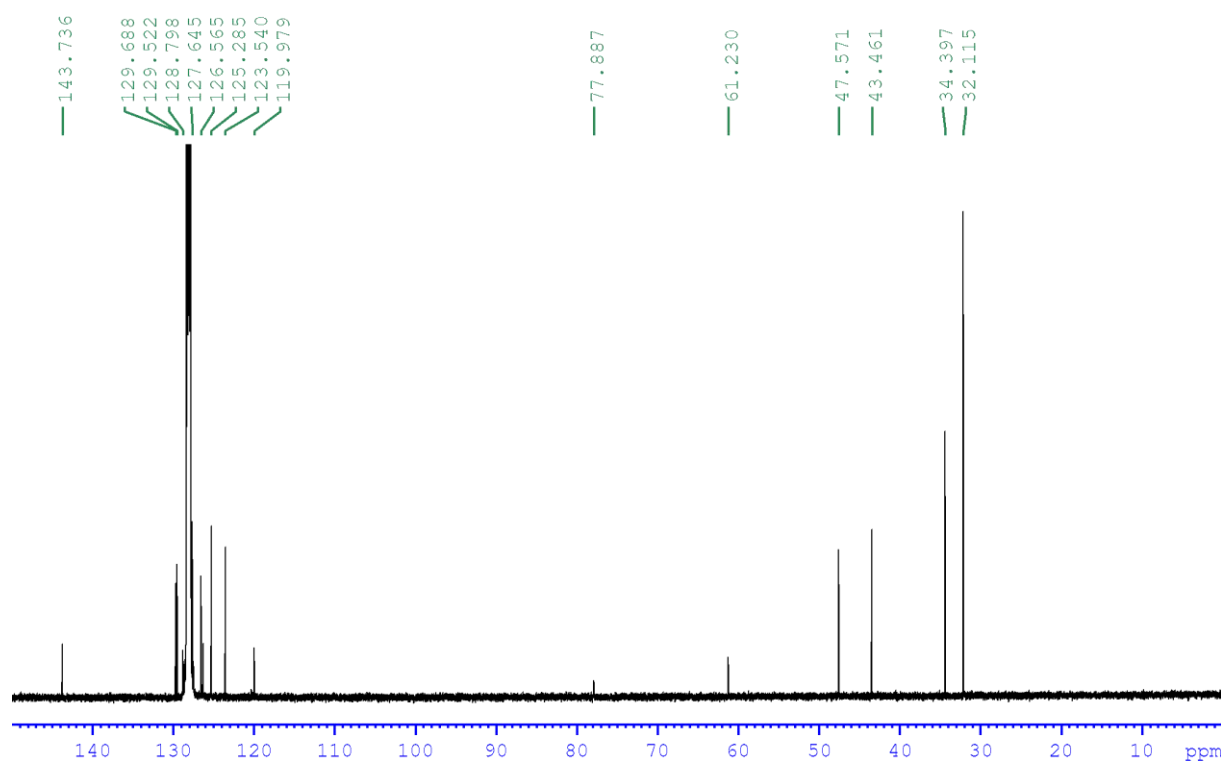


Experimental

^1H NMR spectrum of 3.4 in C_6D_6

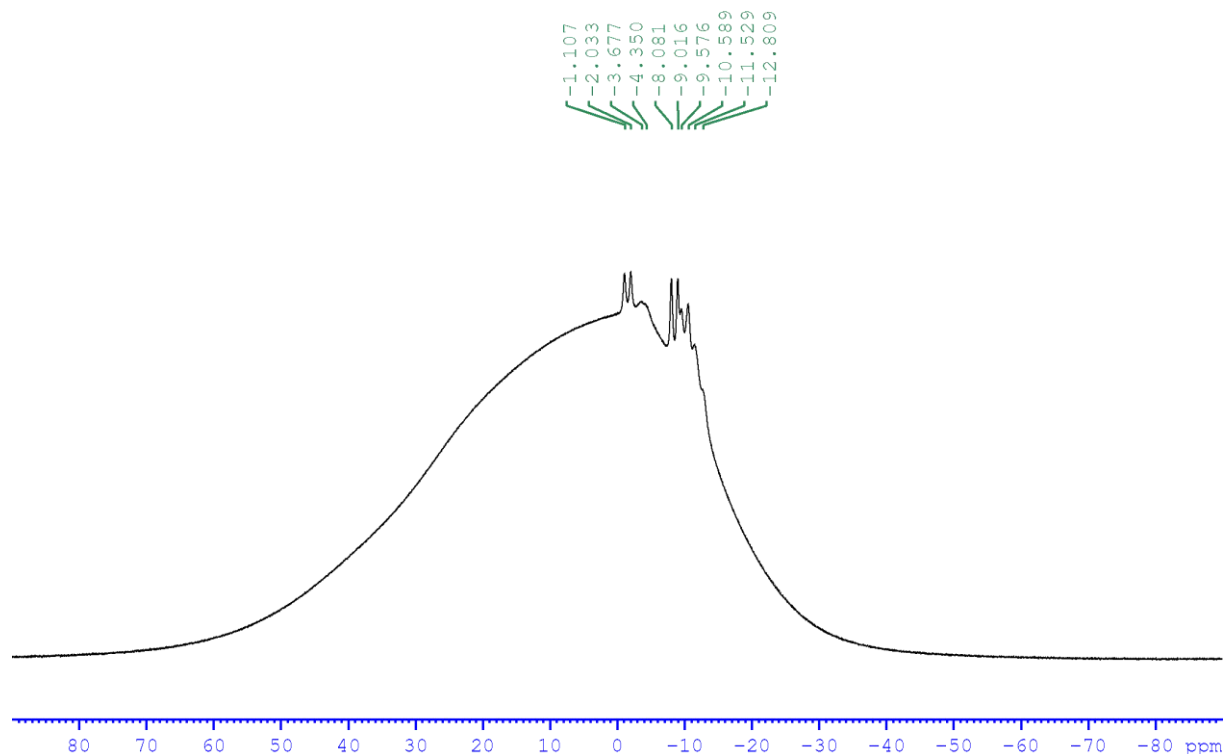


$^{13}\text{C}\{^1\text{H}\}$ NMR spectrum of 4 in CD_2Cl_2

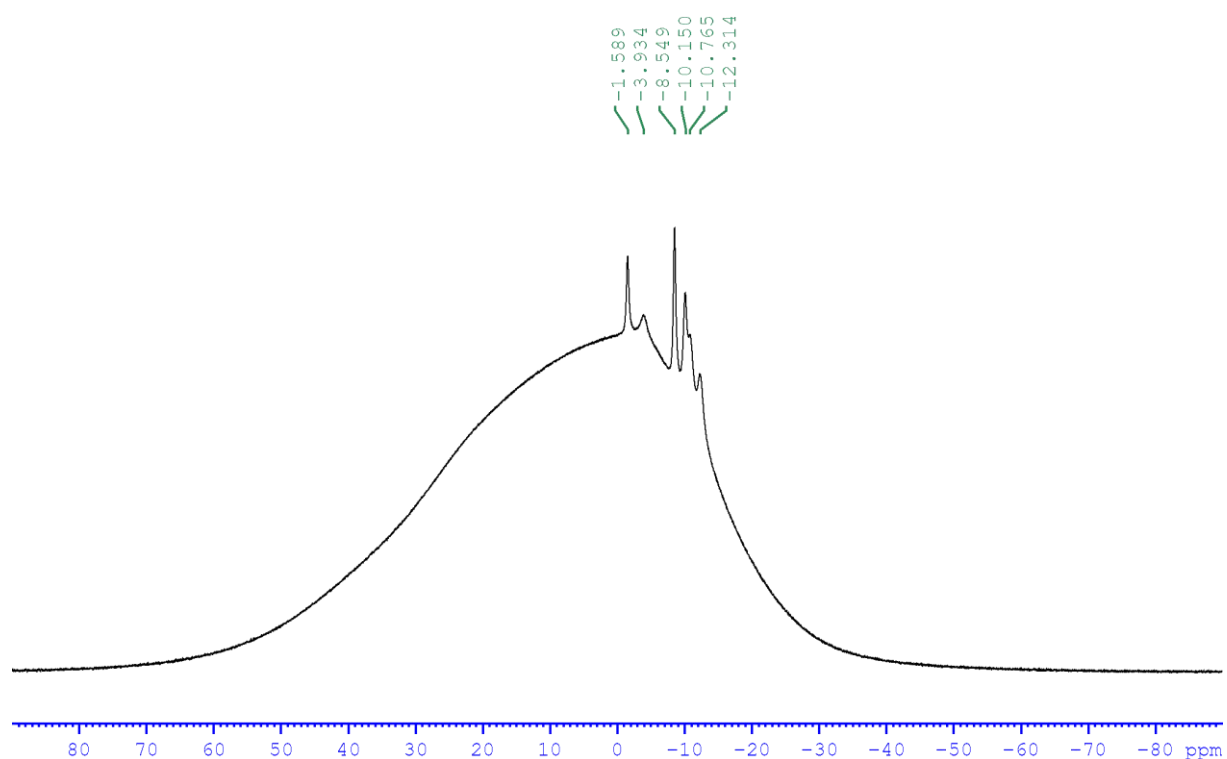


Experimental

^{11}B NMR spectrum of 3.4 in C_6D_6

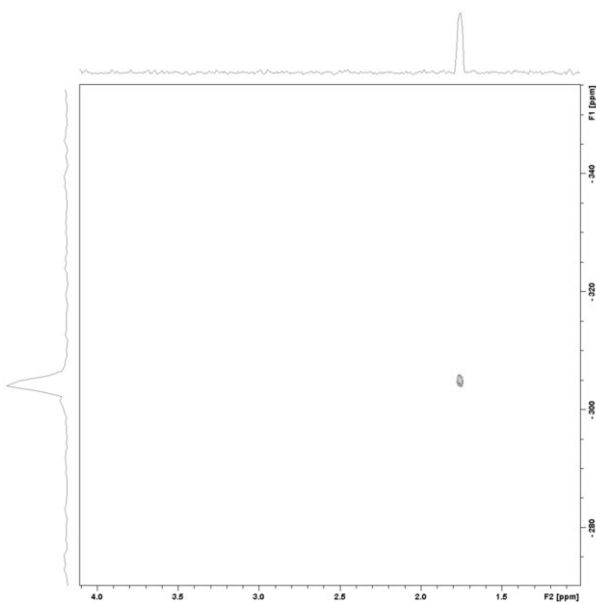


$^{11}\text{B}\{\text{H}\}$ NMR spectrum of 3.4 in C_6D_6



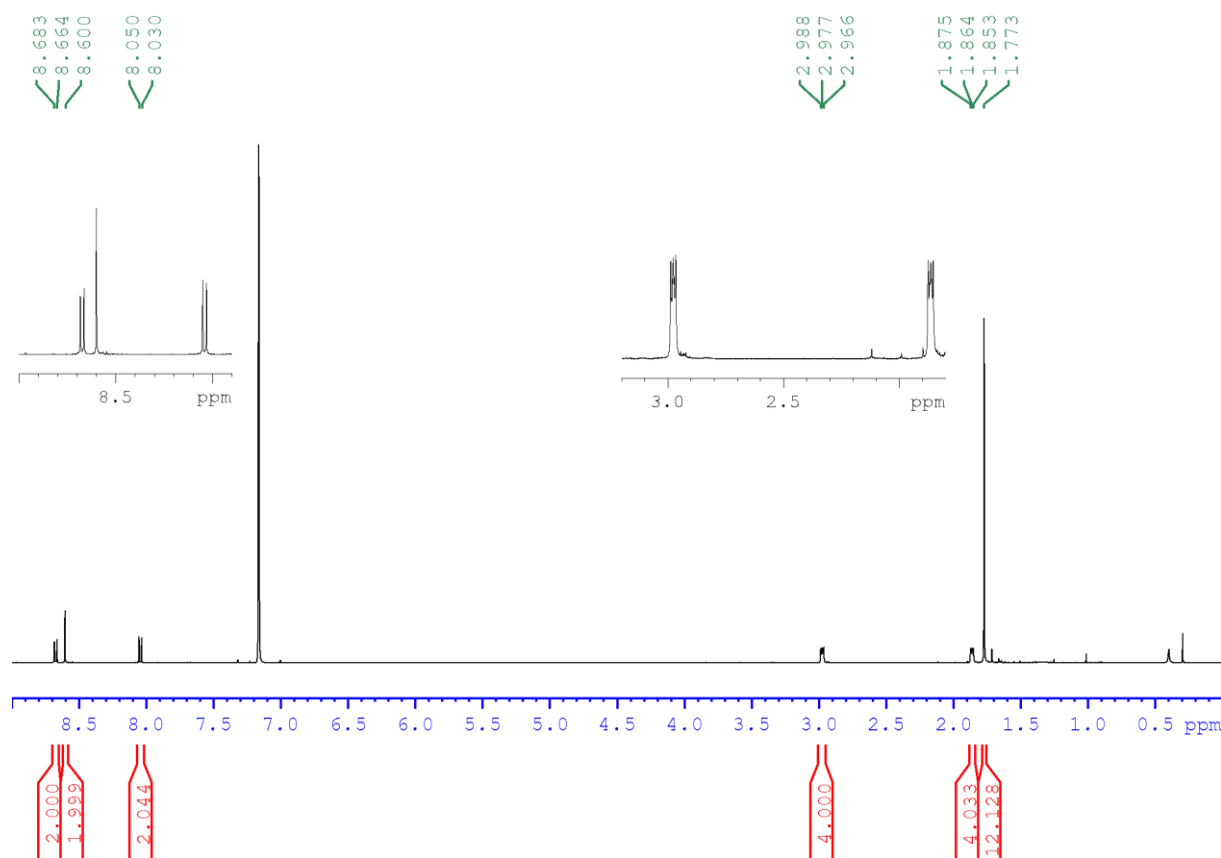
Experimental

$^{15}\text{N}, ^1\text{H}$ HMBC NMR spectrum of 3.4 in C_6D_6

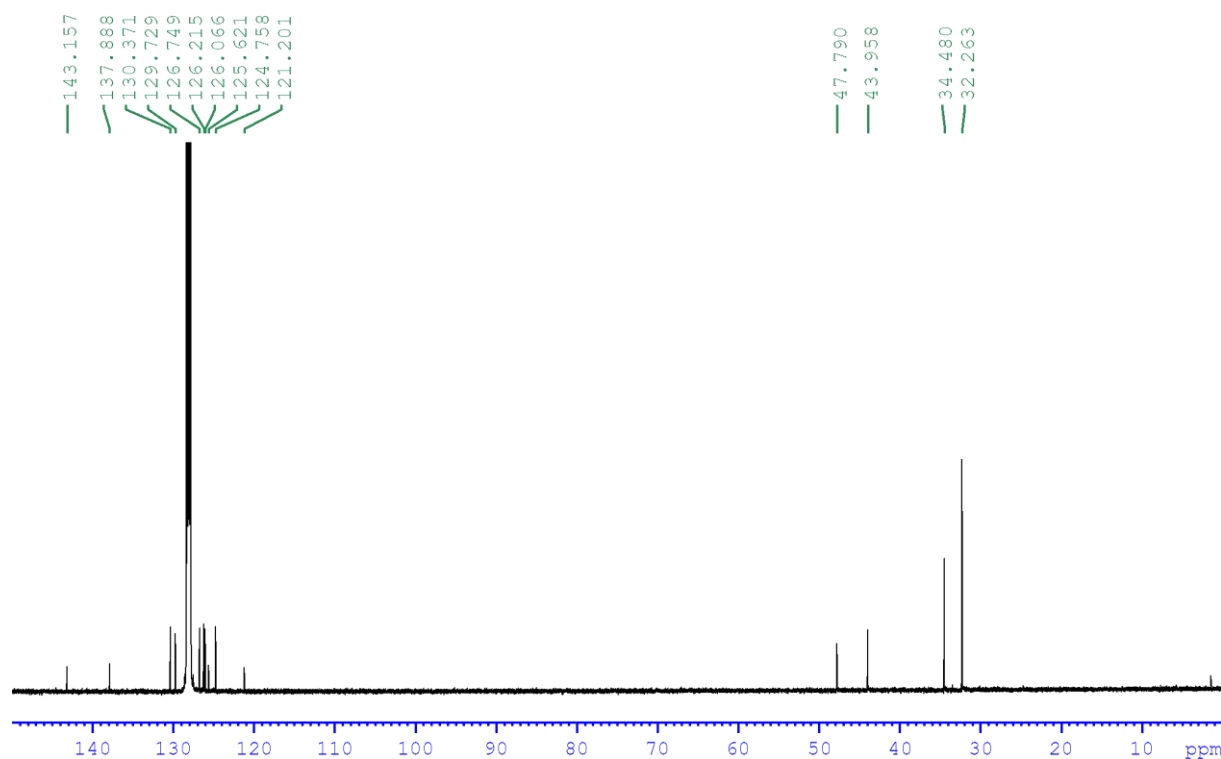


Experimental

¹H NMR spectrum of 3.5 in C₆D₆

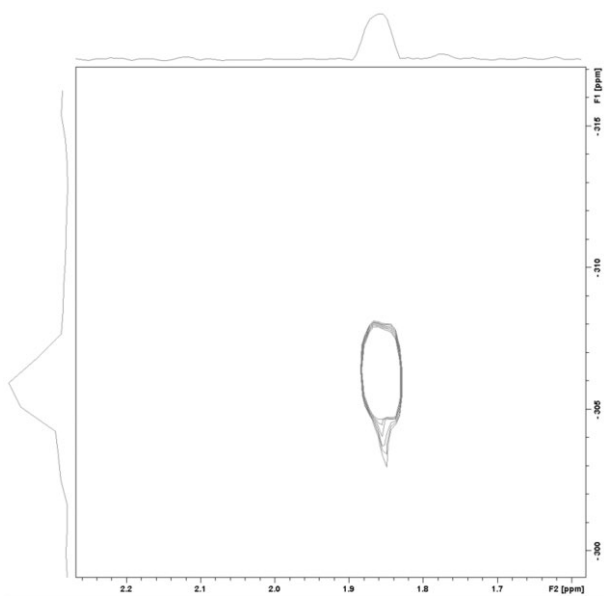


¹³C{¹H} NMR spectrum of 3.5 in C₆D₆



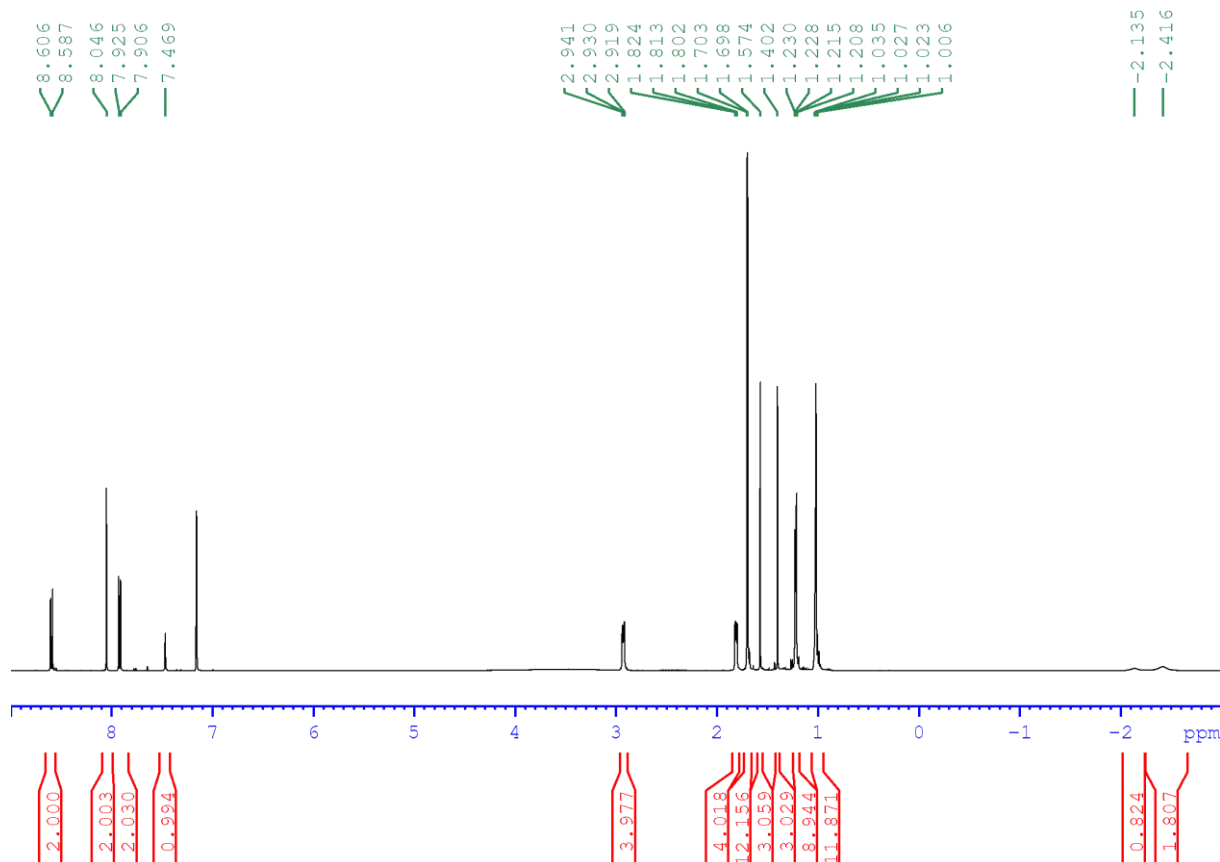
Experimental

$^{15}\text{N}, ^1\text{H}$ HMBC NMR spectrum of 3.5 in C_6D_6

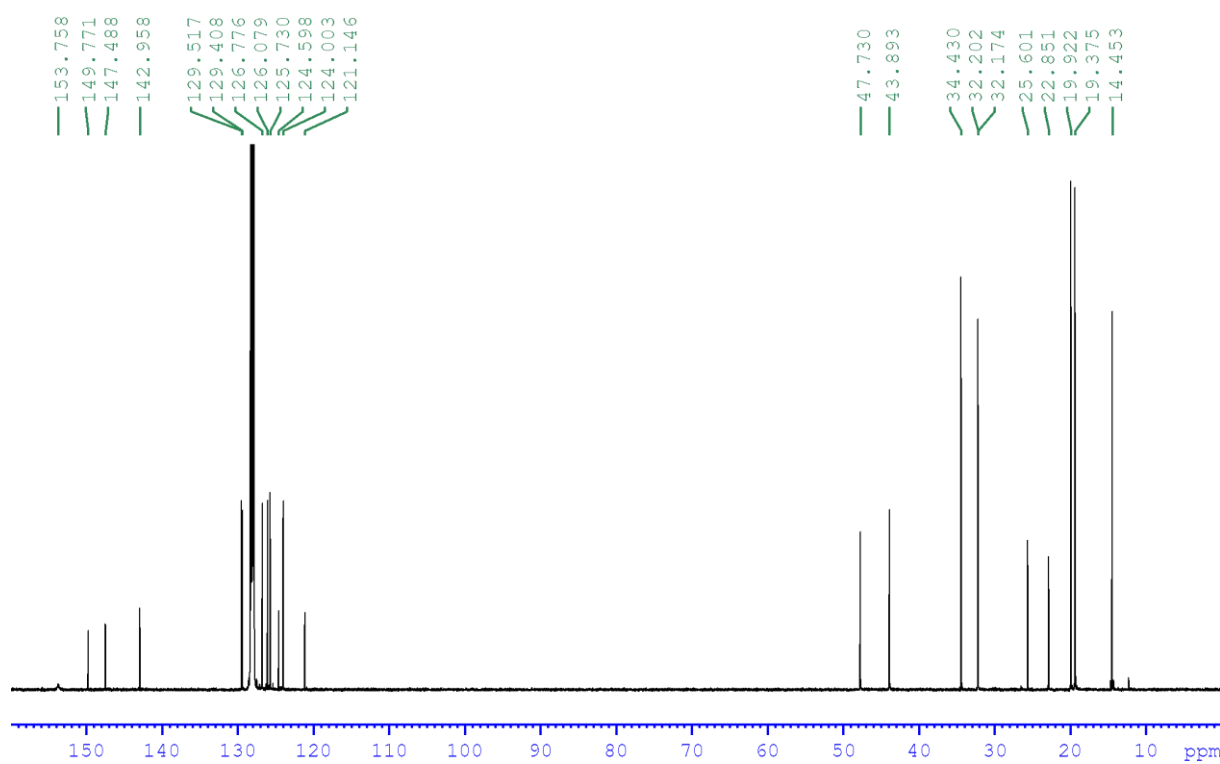


Experimental

^1H NMR spectrum of 3.6 in C_6D_6

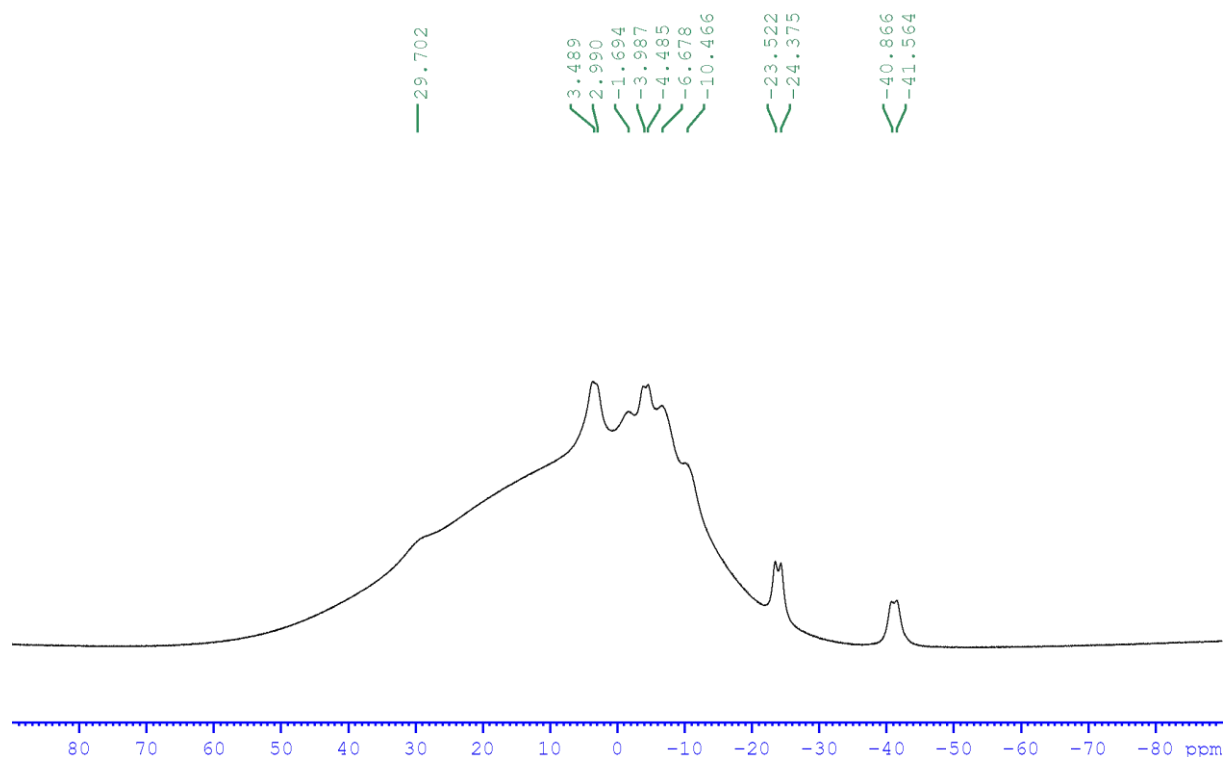


$^{13}\text{C}\{^1\text{H}\}$ NMR spectrum of 3.6 in CD_2Cl_2

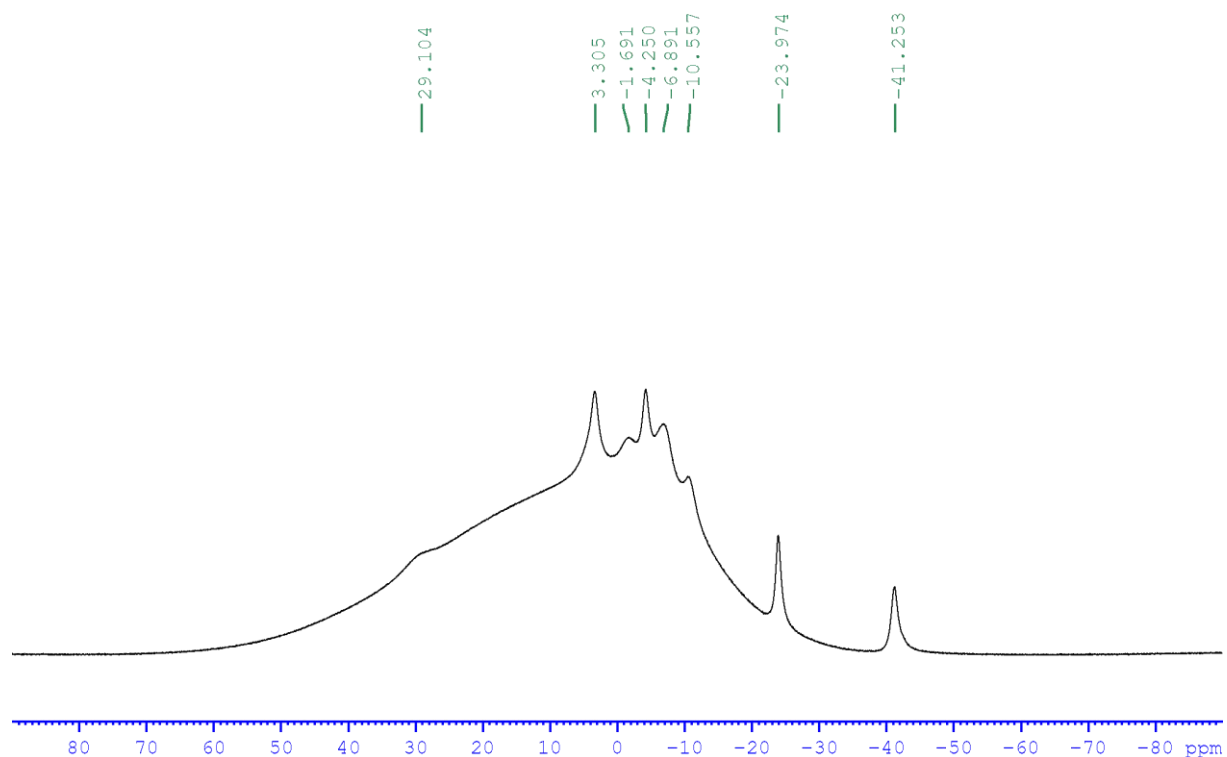


Experimental

^{11}B NMR spectrum of 3.6 in C_6D_6

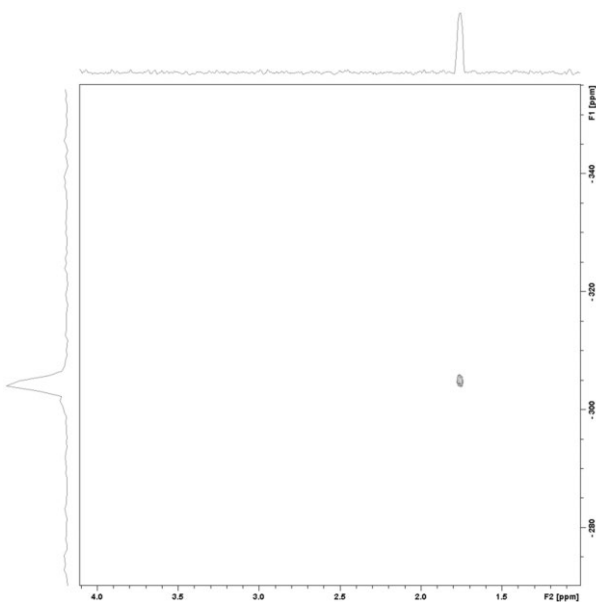


$^{11}\text{B}\{^1\text{H}\}$ NMR spectrum of 3.6 in C_6D_6



Experimental

$^{15}\text{N}, ^1\text{H}$ HMBC NMR spectrum of 3.6 in C_6D_6



Experimental

5.3.3 Single-crystal X-ray diffraction

Table 5.3.1. Single-crystal X-ray diffraction data and structure refinements of **3.2**, **3.4**, **3.5** and **3.6**.

	3.2	3.4	3.5	3.6
CCDC	2183060	2183061	2183062	2183063
Empirical formula	C ₃₇ H ₄₇ NSi	C ₂₈ H ₃₇ B ₁₀ N	C ₅₂ H ₅₂ N ₂ · 2(C ₇ H ₈)	C ₃₉ H ₆₅ B ₁₀ NSSi · 0.389(C ₇ H ₈) · 0.611(C ₅ H ₁₂)
$\rho_{\text{calc}}/\text{g} \cdot \text{cm}^{-3}$	1.139	1.227	1.211	1.091
$F(000)$	1160	524	1912	862
Crystal size/mm ³	0.162×0.228×0.281	0.029×0.121×0.198	0.18×0.22×0.30	0.031×0.084×0.160
Crystal colour, habit	yellow block	yellow plate	yellow block	yellow plate
μ/mm^{-1}	0.835	0.466	0.519	1.041
$M_r/\text{g} \cdot \text{mol}^{-1}$	533.84	495.68	889.22	796.09
Temperature/K	173(2)	100(2)	100(2)	100(2)
Radiation, $\lambda/\text{\AA}$	Cu K_α 1.54184	Cu K_α 1.54184	CuK α 1.54184	CuK α 1.54184
Crystal system	monoclinic	monoclinic	monoclinic	monoclinic
Space group	$P2_1/n$	$P2_1/m$	$P2_1/c$	$P2_1$
$a/\text{\AA}$	10.45970(10)	7.01033(14)	25.3070(4)	9.8790(2)
$b/\text{\AA}$	15.04800(10)	16.0301(4)	9.29050(10)	16.7509(3)
$c/\text{\AA}$	20.32480(10)	12.1588(3)	21.3388(3)	14.6886(2)
$\alpha/^\circ$	90	90	90	90
$\beta/^\circ$	103.2340(10)	100.889(2)	103.644(2)	94.7480(10)
$\gamma/^\circ$	90	90	90	90
Volume/ \AA^3	3114.12(3)	1341.77(5)	4875.48(12)	2422.36(7)
Z	4	2	4	2
2 Θ range/°	4.47–155.41	7.404–148.994	7.19–149.00	5.28–160.70
Reflections collected	78380	14166	52384	51486
Unique reflections	6621	2833	9905	10423
Parameters / restraints	362 / 0	192 / 0	1000 / 1368	637 / 43
GoodF on F^2	1.044	1.048	1.063	1.089
R_1 [$ I \geq 2\sigma(I)$]	0.0409	0.0447	0.1028	0.0605
wR_2 [all data]	0.1161	0.1292	0.3173	0.1692
Max./min. res. electron density / e \AA^{-3}	0.21/–0.27	0.27/–0.28	0.61/–0.62	0.78/–0.49

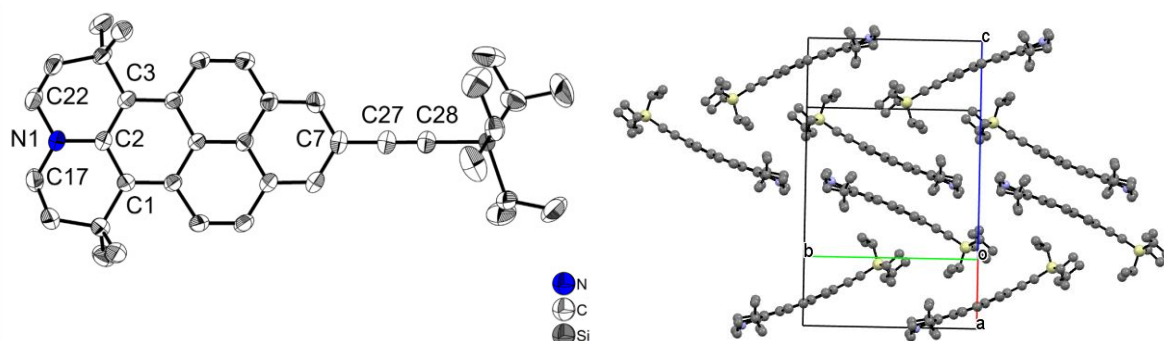


Figure 5.3.1. Left: Solid state molecular structure of **3.2** from single-crystal X-ray diffraction at 173 K. Atomic displacement ellipsoids are drawn at the 50% probability level. Hydrogen atoms are omitted for clarity. Right: Sandwich herringbone structure of **3.2**.

Experimental

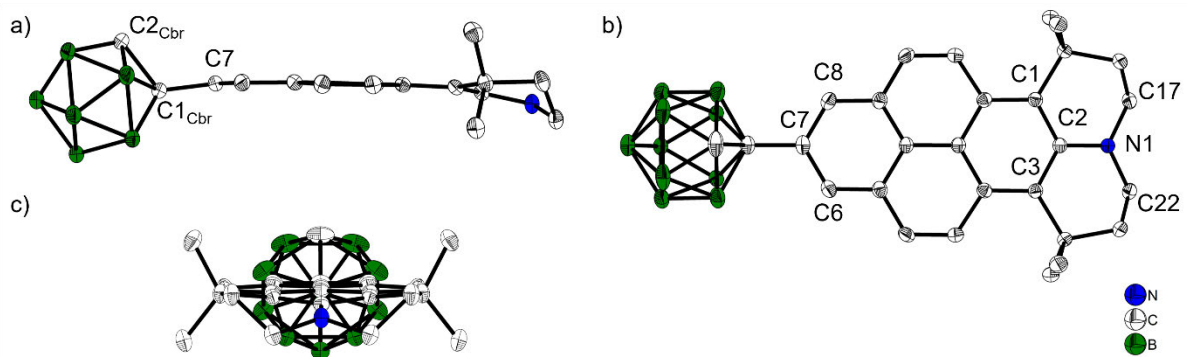


Figure 5.3.2. Solid state molecular structure of **3.4** from single-crystal X-ray diffraction at 100 K. Atomic displacement ellipsoids are drawn at the 50% probability level. Hydrogen atoms are omitted for clarity.

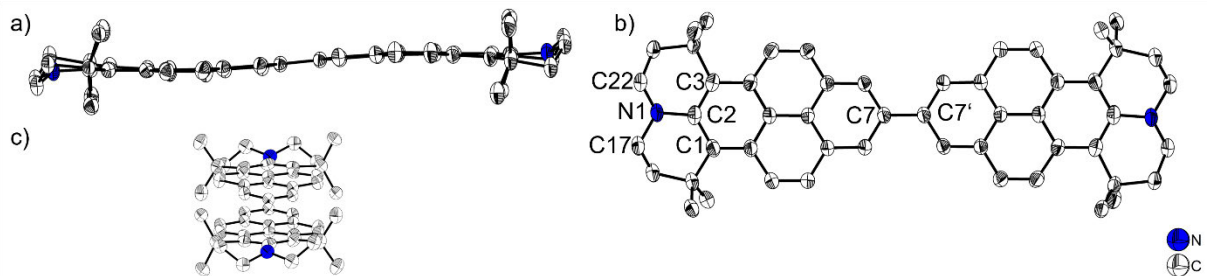


Figure 5.3.3. Solid state molecular structure of **3.5** from single-crystal X-ray diffraction at 100 K. Atomic displacement ellipsoids are drawn at the 50% probability level. Hydrogen atoms and solvent molecules are omitted for clarity.

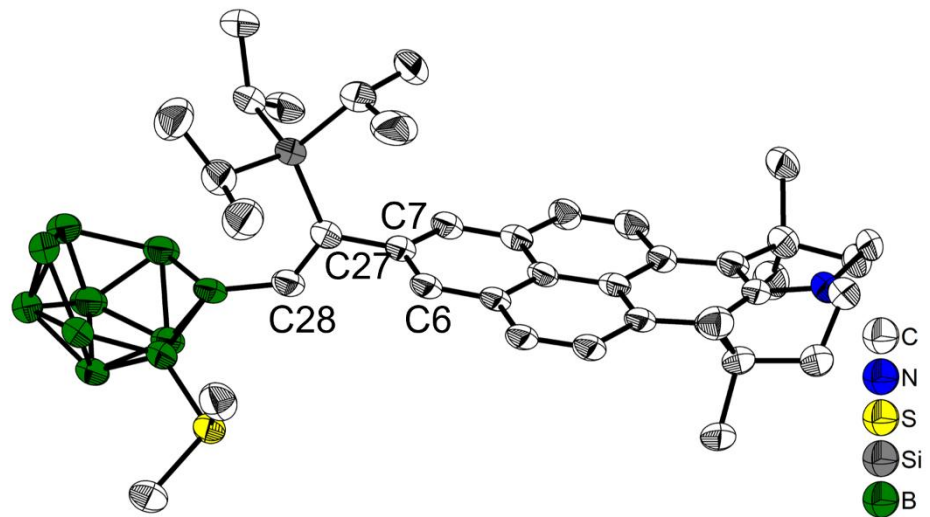


Figure 5.3.4. Solid state molecular structure of **3.6** from single-crystal X-ray diffraction at 100 K. Atomic displacement ellipsoids are drawn at the 50% probability level. Hydrogen atoms and solvent molecules are omitted for clarity.

Experimental

5.3.4 Photophysical data

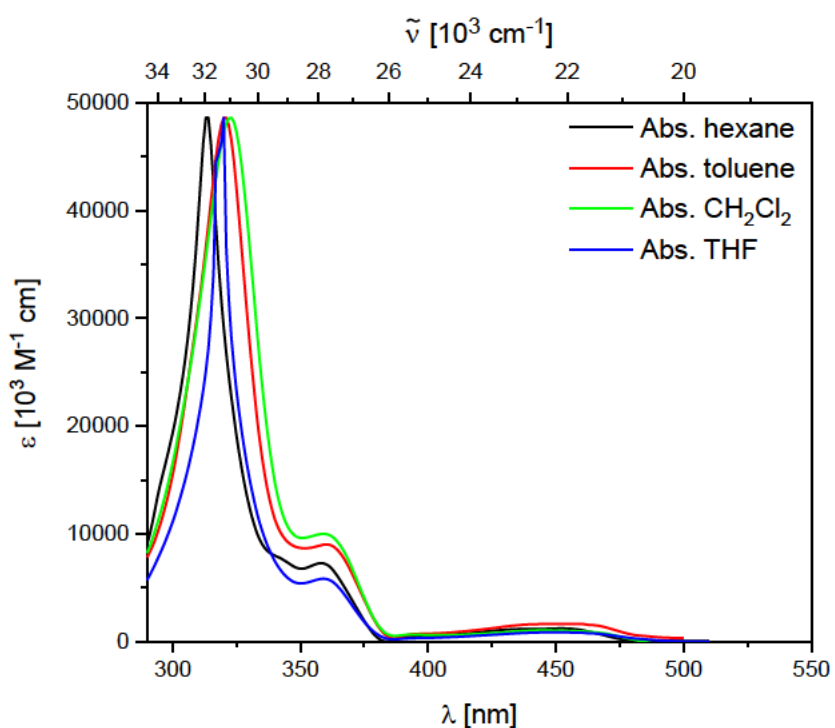


Figure 5.3.5. Absorption spectra of 3.4 in hexane (black), toluene (red), CH₂Cl₂ (green), and THF (blue).

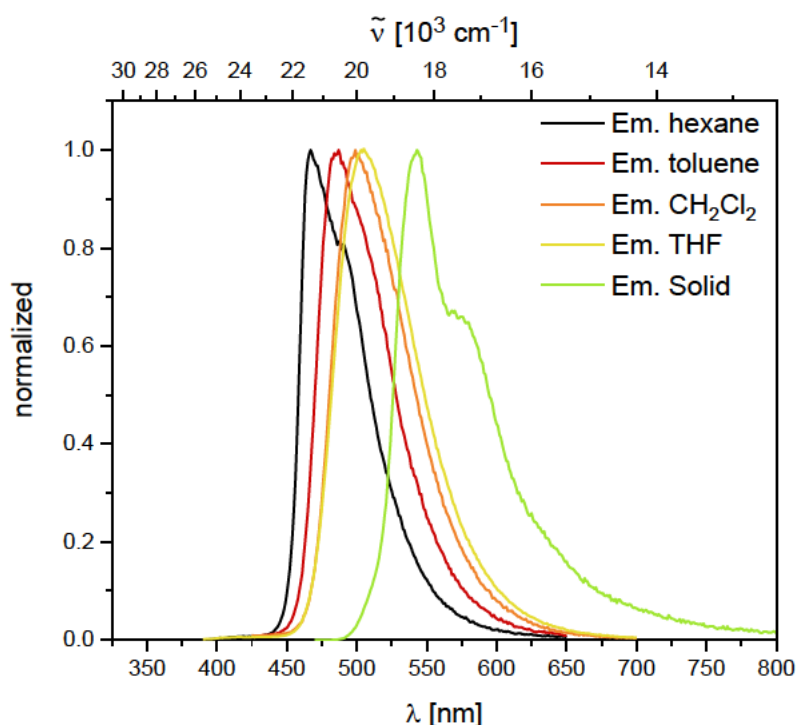


Figure 5.3.6. Emission spectra of 3.4 in hexane (black), toluene (red), CH₂Cl₂ (orange), THF (yellow), and in the solid state (green).

Experimental

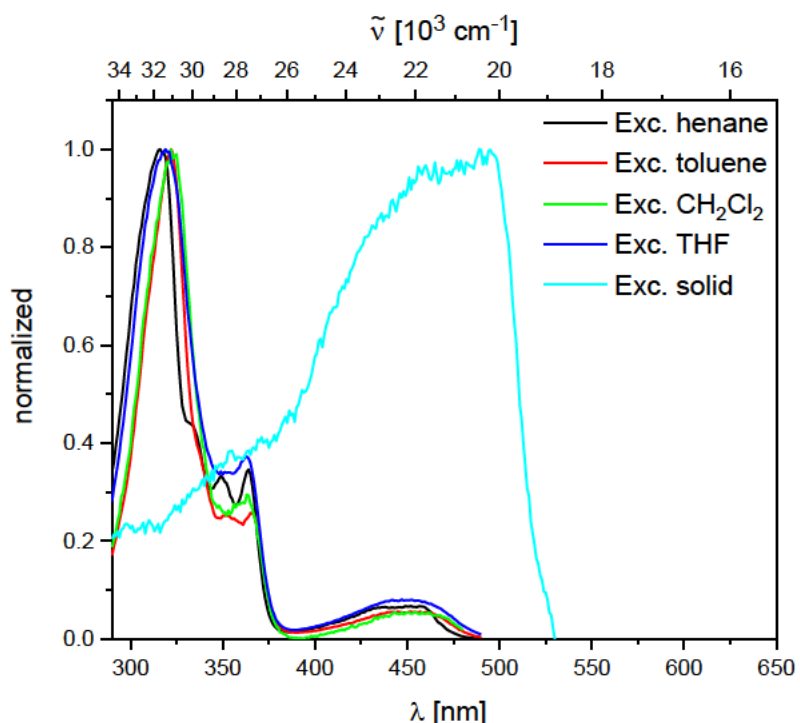


Figure 5.3.7. Excitation spectra of 3.4 in hexane (black), toluene (red), CH_2Cl_2 (green), THF (blue), and in the solid state (turquoise).

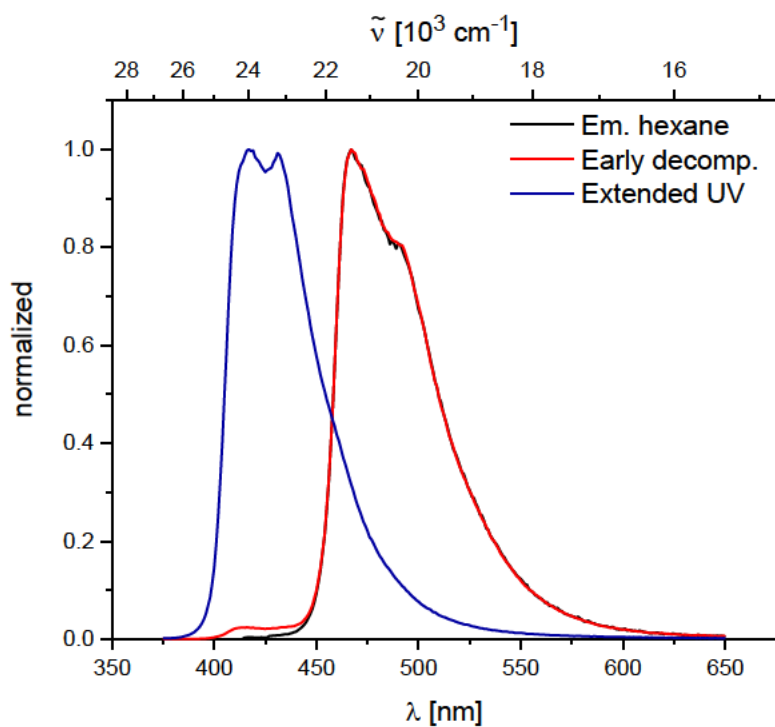


Figure 5.3.8. Decomposition visible in the emission spectrum of 3.4 in a hexane solution at the start (black), after an hour (red), and after complete decomposition (blue).

Experimental

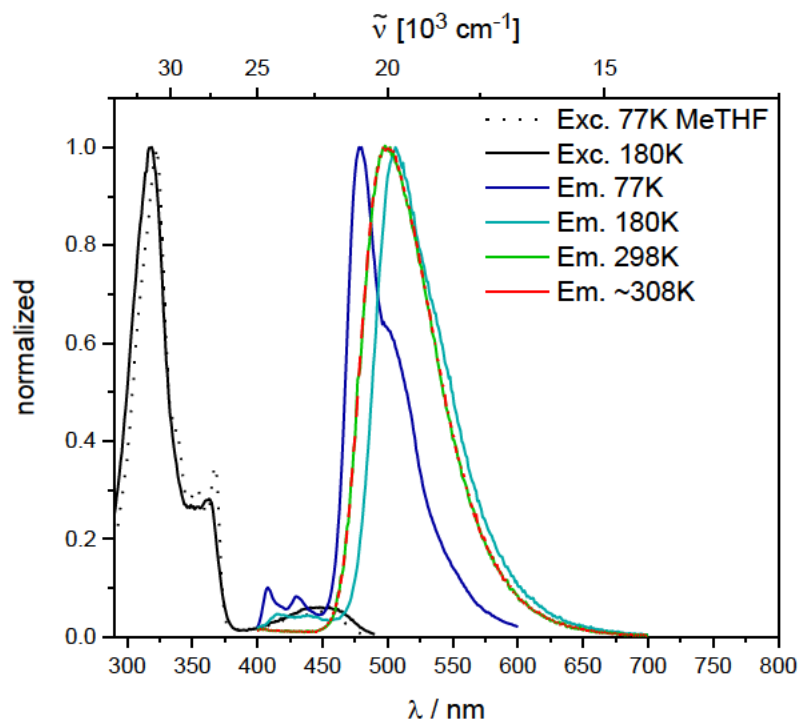
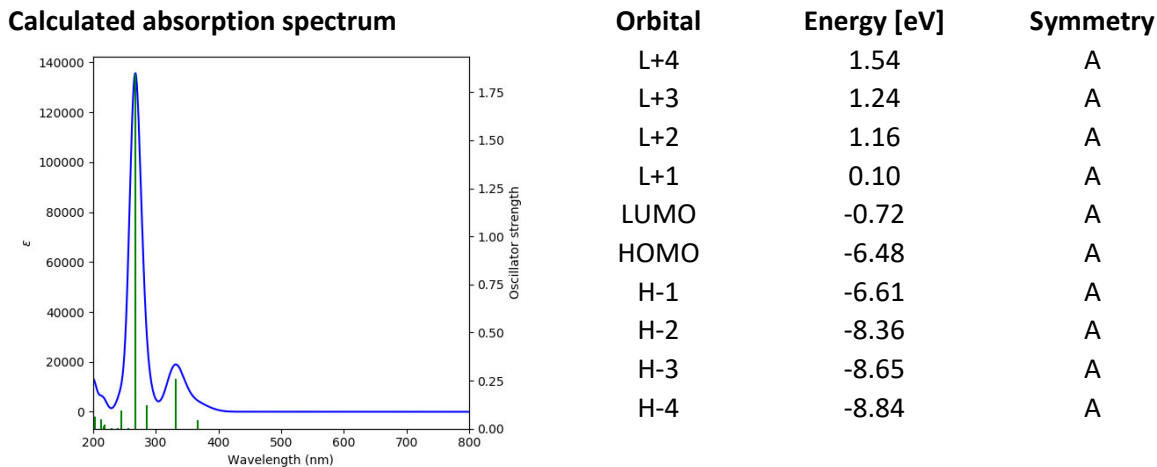


Figure 5.3.9. Temperature-dependent emission spectra of 3.4 in 2-methyltetrahydrofuran. Decomposition becomes visible over time.

5.3.5 DFT and TD-DFT results

TD-DFT calculations of 3.4:



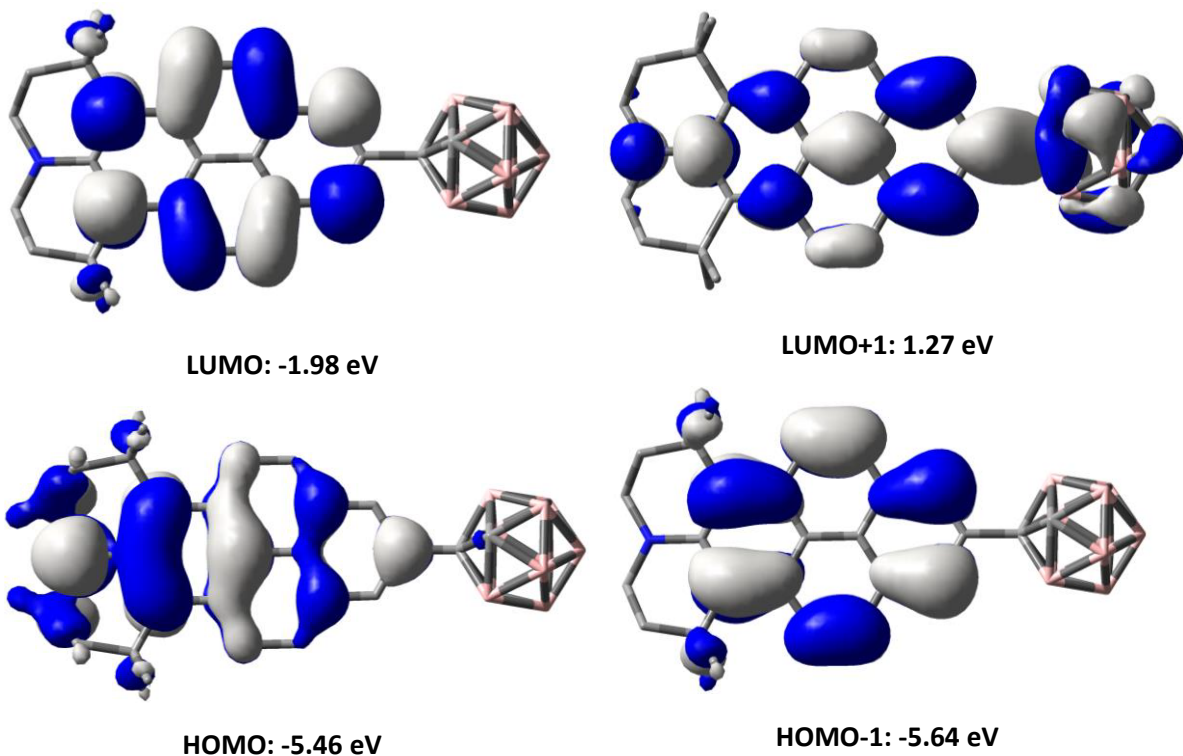
TD-DFT CAM-B3LYP/6-31G(d,p), gas phase

Table 5.3.2. Lowest energy singlet electronic transition of 3.4 (TD-DFT CAM-B3LYP/6-31G(d, p), gas phase).

State	E [eV]	λ [nm]	f	Symmetry	Major contributions	Λ
1	3.37	367.56	0.0427	Singlet-A	H-1->L+1 (12%), HOMO->LUMO (83%)	0.58
2	3.74	331.61	0.2587	Singlet-A	H-1->LUMO (81%), HOMO->L+1 (16%)	0.84
3	4.35	285.07	0.1239	Singlet-A	H-2->LUMO (11%), H-1->L+1 (70%), HOMO->LUMO (11%)	0.60
4	4.64	267.20	1.8442	Singlet-A	H-1->LUMO (18%), HOMO->L+1 (74%)	0.64
5	4.85	255.75	0.0027	Singlet-A	H-3->LUMO (10%), H-2->LUMO (48%), H-1->L+2 (38%)	0.61
6	5.05	245.66	0.0949	Singlet-A	H-2->LUMO (26%), H-1->L+2 (51%)	0.59
7	5.19	239.00	0.0041	Singlet-A	HOMO->L+2 (83%)	
8	5.39	230.16	0.0026	Singlet-A	H-3->LUMO (50%), HOMO->L+4 (25%)	
9	5.68	218.14	0.0208	Singlet-A	H-4->LUMO (15%), H-2->L+1 (22%), H-1->L+4 (37%)	
10	5.72	216.82	0.014	Singlet-A	H-4->LUMO (67%), H-1->L+4 (15%)	
11	5.81	213.39	0.0494	Singlet-A	H-3->LUMO (32%), H-2->LUMO (13%), HOMO->L+4 (26%)	
12	6.13	202.25	0.0621	Singlet-A	H-2->L+1 (57%), H-1->L+4 (18%)	
13	6.20	199.88	0.0581	Singlet-A	H-6->LUMO (24%), H-3->L+1 (21%), HOMO->L+5 (17%)	
14	6.22	199.42	0.0214	Singlet-A	H-4->L+1 (12%), H-1->L+3 (50%), HOMO->L+4 (10%)	
15	6.24	198.78	0.0235	Singlet-A	H-6->LUMO (42%), HOMO->L+5 (10%)	
16	6.28	197.37	0.0055	Singlet-A	H-4->L+1 (18%), H-1->L+3 (37%), H-1->L+5 (20%)	
17	6.38	194.24	0.018	Singlet-A	HOMO->L+3 (73%)	
18	6.57	188.59	0.103	Singlet-A	H-3->L+1 (33%), H-1->L+5 (10%), HOMO->L+5 (17%)	
19	6.59	188.23	0.0587	Singlet-A	H-4->L+1 (23%), H-1->L+5 (34%)	
20	6.65	186.39	0.0005	Singlet-A	H-19->LUMO (11%), H-11->LUMO (71%)	
21	6.88	180.16	0.6613	Singlet-A	H-2->L+2 (49%), H-1->L+6 (13%)	
22	6.91	179.54	0.1575	Singlet-A	H-4->L+2 (22%), H-2->L+2 (13%), H-1->L+6 (33%)	
23	6.91	179.42	0.0114	Singlet-A	H-4->L+2 (23%), H-2->L+4 (12%), H-1->L+6 (39%)	
24	7.01	176.94	0.0701	Singlet-A	HOMO->L+6 (46%)	
25	7.02	176.71	0.0042	Singlet-A	H-10->LUMO (66%)	

Experimental

Orbitals relevant to the $S_1 \leftarrow S_0$ and $S_2 \leftarrow S_0$ transitions B3LYP/6-31G(d,p)



Experimental

Cartesian coordinates of the optimized structures of 3.4.

B	-6.89095100	0.57433700	1.40446700	H	2.86381400	3.63499000	-1.38806300
B	-5.44493600	1.15958900	-1.01038000	H	4.42344900	3.06230200	-1.94179100
B	-6.91199200	1.54149200	-0.08517200	H	3.77987700	2.66986100	2.32795100
B	-6.98622500	0.40628800	-1.46247400	H	4.36710600	4.18533500	1.61918800
B	-5.49279000	-0.55902800	-1.46191000	H	2.66679300	3.74040300	1.48086500
C	-4.60900000	-0.01967700	-0.10007500	H	4.39352700	-4.46340400	-0.88541500
B	-5.39321700	1.26776400	0.75881200	H	2.91188700	-3.63358200	-1.38716300
C	-5.47421100	-0.35259900	1.27989900	H	4.46469100	-3.04165300	-1.93984000
B	-6.93888000	-1.14115900	0.95662800	H	3.81299000	-2.65525100	2.32914400
B	-7.88170000	0.04358300	0.03176100	H	2.71418200	-3.74019600	1.48167400
B	-6.99506900	-1.25655600	-0.81662100	H	4.41998600	-4.16342200	1.62140400
B	-5.47535200	-1.51274100	0.02948600				
C	-3.10408900	-0.03844500	-0.05235100				
C	-2.39685900	1.16822400	-0.04766300				
C	-0.99649200	1.19483600	-0.03130700				
C	-0.25020700	-0.01942700	-0.01991800				
C	-0.98082800	-1.24260500	-0.03124700				
C	-2.38289900	-1.23554200	-0.05206900				
C	-0.26932200	2.42428500	-0.02601600				
C	1.08949300	2.43715700	0.00330300				
C	1.89294100	1.23376000	0.02102300				
C	1.18274000	-0.01017600	-0.00017200				
C	1.90896400	-1.24472000	0.02130700				
C	1.12113900	-2.45811200	0.00328400				
C	-0.23791100	-2.46237500	-0.02651500				
C	3.30885400	1.25248300	0.02888700				
C	4.01240600	0.00808200	-0.05333000				
C	3.32517200	-1.24511400	0.02937000				
C	4.07523500	2.59462200	0.16832300				
C	5.59135000	2.34856000	0.31358500				
C	6.05660100	1.24442400	-0.60395800				
N	5.40224400	0.01713500	-0.19866400				
C	6.07264800	-1.20188400	-0.60260600				
C	5.62141700	-2.31125700	0.31566400				
C	4.10871900	-2.57712200	0.16967700				
C	3.90049200	3.49500500	-1.08264000				
C	3.68073500	3.34251900	1.46888000				
C	3.94645200	-3.48038800	-1.08089500				
C	3.72303100	-3.32948000	1.47029400				
H	-7.23039400	0.92066900	2.48491100				
H	-4.79371300	1.91654400	-1.64441100				
H	-7.38592700	2.62905800	-0.10935100				
H	-7.51977600	0.69086600	-2.48380500				
H	-4.86394900	-0.94775500	-2.38586600				
H	-4.71054300	2.00770700	1.37324500				
H	-4.86827600	-0.59524900	2.14386700				
H	-7.31185100	-1.95369000	1.73326500				
H	-9.06659200	0.06016400	0.09534500				
H	-7.52869700	-2.16815900	-1.35705100				
H	-4.87482900	-2.51243100	0.19538200				
H	-2.92905100	2.11237500	-0.06493500				
H	-2.89761900	-2.18793500	-0.07866500				
H	-0.82178600	3.36046500	-0.05024900				
H	1.56857400	3.40004600	-0.00738500				
H	1.61238700	-3.41488200	-0.00763400				
H	-0.77791800	-3.40586400	-0.05179200				
H	5.83100000	2.05232400	1.34201400				
H	6.12556100	3.28362200	0.10743700				
H	7.13702600	1.09490800	-0.51253200				
H	5.84907200	1.48153900	-1.66273000				
H	5.86862200	-1.44260600	-1.66125100				
H	7.15100600	-1.03827200	-0.51091700				
H	6.16790200	-3.23943900	0.11057700				
H	5.85659800	-2.01106700	1.34397900				
H	4.33529300	4.48369400	-0.88814000				

Experimental

Cartesian coordinates of the optimized structures of 3.VI.

C	-2.35386100	0.09710300	-0.05597300	
C	-3.16684600	-1.12336800	0.69351900	
B	-3.16039100	0.40800400	1.46075000	
B	-3.26198000	1.54673300	0.10368500	
B	-3.25799600	0.62681100	-1.42141800	
B	-3.16361500	-1.09940300	-1.02420200	
B	-4.61530400	-0.61538500	1.42539600	
B	-4.71810200	1.11199500	1.02736900	
B	-4.78575400	1.24988000	-0.75691900	
B	-4.71965300	-0.39539300	-1.45239600	
B	-4.61100500	-1.54280600	-0.09583400	
B	-5.62736600	-0.09242300	0.06181300	
H	-2.46780600	0.54937800	2.40792300	
H	-2.54513800	-1.87483700	1.16350300	
H	-2.68701500	2.57729200	0.18448500	
H	-2.64205000	1.02199200	-2.35290600	
H	-2.48581300	-1.88056000	-1.59438500	
H	-4.93584100	-1.14406300	2.43669200	
H	-5.23356800	1.89207200	1.75937700	
H	-5.35697300	2.14158000	-1.29514900	
H	-5.23671700	-0.69552200	-2.47836400	
H	-4.93182600	-2.68396700	-0.09324800	
H	-6.81074500	-0.17834700	0.11374100	
C	-0.84072600	0.05909300	-0.03838000	
C	-0.14942600	-1.15948400	-0.03588600	
C	-0.11420200	1.25566200	-0.03438600	
C	1.25338800	-1.20574000	-0.01855600	
H	-0.68790000	-2.10176100	-0.06743200	
C	1.28944100	1.25697200	-0.02408900	
H	-0.63438700	2.20655100	-0.04066100	
C	1.99080800	0.01509900	-0.01212400	
C	1.97894800	-2.44877000	-0.01332300	
C	2.05121900	2.47822200	-0.02028000	
C	3.41658100	-0.00612900	0.00168800	
C	3.34217700	-2.46995200	0.00106600	
H	1.41547400	-3.37902800	-0.02187300	
C	3.41445400	2.45908000	-0.00521700	
H	1.51438600	3.42381600	-0.02959500	
C	4.11183800	-1.25398500	0.00984700	
C	4.14796000	1.22094000	0.00633600	
H	3.87469100	-3.41828700	0.00506800	
H	3.97484000	3.39121000	-0.00230200	
C	5.51707200	-1.24979100	0.02397200	
C	5.55253400	1.17517000	0.02053000	
C	6.22593500	-0.04739400	0.02953000	
H	6.05142100	-2.19702800	0.03003100	
H	6.11443100	2.10632800	0.02394200	
H	7.31259200	-0.06325400	0.04026600	

Experimental

Cartesian coordinates of two of the optimized structures of the radical anion of 3.4 at C1-C2 bond lengths 1.669 and 2.389 Å.

1.669	2.389
B -6.91180000 1.22496000 0.91089000	B -7.22233500 0.89220300 1.19897900
B -5.56706500 0.43720900 -1.50486200	B -5.45767400 0.90524200 -1.21969900
B -7.04413100 1.18545400 -0.86019300	B -6.95549700 1.43277400 -0.46130700
B -7.05618000 -0.524413100 -1.35666100	B -6.95487100 -0.00046200 -1.54461800
B -5.49164000 -1.23252200 -0.90950400	B -5.45744900 -0.90600500 -1.21907100
C -4.61473700 0.01719700 -0.14521800	C -4.52766900 -0.00000200 -0.25001000
B -5.48738600 1.51230300 -0.10667200	B -5.47803100 1.21484300 0.60507300
C -5.43525100 0.46911700 1.23686800	C -5.94805000 0.00045700 1.67164600
B -6.84197400 -0.44248400 1.50159400	B -7.22231400 -0.89162200 1.19950400
B -7.89039400 -0.03236400 0.13408900	B -7.99134000 -0.00018200 -0.12729800
B -6.91955700 -1.53217800 0.10712100	B -6.95529500 -1.43314900 -0.46041900
B -5.36373300 -1.18607200 0.85798600	B -5.47775800 -1.21434800 0.60602900
C -3.11255500 0.04362200 -0.12398900	C -3.07561800 0.00009900 -0.20361400
C -2.41253300 1.25041000 -0.11651100	C -2.34306600 1.20154200 -0.17655300
C -0.98921800 1.26207300 -0.08212400	C -0.94687400 1.21780400 -0.12444500
C -0.25693300 0.03223000 -0.05959800	C -0.20384000 0.00011700 -0.09565100
C -0.99965500 -1.19397000 -0.08108600	C -0.94699500 -1.21756000 -0.12483700
C -2.42152800 -1.16724900 -0.10693000	C -2.34311800 -1.20134800 -0.17708400
C -0.25386500 2.45972800 -0.07271500	C -0.20632100 2.43798300 -0.10050700
C 1.12665600 2.46111700 -0.03112400	C 1.15098600 2.44653100 -0.03905400
C 1.91319100 1.26833200 0.00641800	C 1.94653100 1.23942700 -0.00092900
C 1.18173900 0.02543000 -0.01914900	C 1.22702700 0.00007200 -0.03965900
C 1.88840900 -1.22576200 0.00646100	C 1.94641600 -1.23932500 -0.00096700
C 1.10312200 -2.41001300 -0.02939100	C 1.15088500 -2.44640900 -0.03902400
C -0.27499900 -2.39983300 -0.07068800	C -0.20640800 -2.43780800 -0.10076300
C 3.36422600 1.24917500 0.04102400	C 3.36382100 1.24450100 0.04401900
C 4.02328000 -0.01182700 -0.00739000	C 4.05774300 0.00002100 -0.00584700
C 3.31847500 -1.24346900 0.04041000	C 3.36375000 -1.24436300 0.04441400
C 4.16547900 2.56938500 0.17240600	C 4.13209700 2.58390100 0.18855900
C 5.67570200 2.29363800 0.32148100	C 5.64560300 2.33939900 0.35778100
C 6.10586100 1.14791000 -0.55974900	C 6.11599500 1.21524200 -0.53161900
N 5.44147700 -0.04585900 -0.09154800	N 5.46839300 -0.00009800 -0.08898200
C 6.04899500 -1.27239500 -0.55941300	C 6.11578100 -1.21558700 -0.53159800
C 5.56505000 -2.39740600 0.32275500	C 5.64542800 -2.33975100 0.35785700
C 4.04427400 -2.59668000 0.17101500	C 4.13189100 -2.58395500 0.18874200
C 4.01875800 3.46313700 -0.109027000	C 3.97755500 3.47372800 -1.07129400
C 3.78821400 3.34447900 1.46348500	C 3.71562500 3.33959800 1.47567300
C 3.85027200 -3.48031800 -1.08934400	C 3.97723000 -3.47369100 -1.07121100
C 3.62081300 -3.35244600 1.45583900	C 3.71539700 -3.33960700 1.47584100
H -7.26116100 2.10151200 1.62552000	H -7.76167100 1.58365700 2.00336900
H -4.99643400 0.74559000 -2.49180000	H -4.88669500 1.60179900 -1.99729000
H -7.60645300 2.04569800 -1.45253300	H -7.40907800 2.47868200 -0.80610700
H -7.63518400 -0.89713600 -2.32316100	H -7.42086700 -0.00085100 -2.64129300
H -4.88644300 -2.04950000 -1.50799600	H -4.88651500 -1.60312000 -1.99627000
H -4.90057800 2.52885100 -0.05815400	H -4.88811900 2.15393400 1.03629400
H -4.78740500 0.78750900 2.04199600	H -5.57048600 0.00046800 2.68554900
H -7.14158400 -0.69403100 2.61881400	H -7.76158000 -1.58247400 2.00447700
H -9.07169300 -0.04331200 0.24788100	H -9.17605100 -0.000051200 -0.25345300
H -7.39396600 -2.61572000 0.19672300	H -7.40879500 -2.47921400 -0.80487200
H -4.66725500 -1.87637300 1.50781500	H -4.88774000 -2.15326100 1.03748500
H -2.92824900 2.20017600 -0.15282300	H -2.88032400 2.14367700 -0.19758200
H -2.95469000 -2.10975700 -0.11881400	H -2.88018900 -2.14356900 -0.19903700
H -0.79050600 3.40575800 -0.10246400	H -0.75283900 3.37679600 -0.13652200
H 1.60277800 3.42278500 -0.04104200	H 1.63505500 3.40737900 -0.03769300
H 1.58205500 -3.37771600 -0.03759400	H 1.63478400 -3.40735200 -0.03739100
H -0.81903500 -3.34146300 -0.09805800	H -0.75301500 -3.37657600 -0.13657800
H 5.90968400 2.01561600 1.35527100	H 5.87018700 2.05693400 1.39211200
H 6.23545200 3.20824100 0.08927700	H 6.18490200 3.26944500 0.14475900
H 7.18740100 0.98456400 -0.48457900	H 7.19809500 1.07355600 -0.43883900
H 5.88536300 1.35857200 -1.62319600	H 5.90893600 1.43271900 -1.59549900
H 5.81834200 -1.47259700 -1.62294600	H 5.90833900 -1.43306500 -1.59539200
H 7.13725200 -1.16110700 -0.48452900	H 7.19792200 -1.07408000 -0.43915100
H 6.07967500 -3.33828000 0.09131400	H 6.18458500 -3.26990100 0.14482200
H 5.81158100 -2.13151400 1.35678100	H 5.87016800 -2.05729700 1.39215100
H 4.42935900 4.46385600 -0.90119000	H 4.40406900 4.46617700 -0.88176300
H 2.98964600 3.57185000 -1.42337800	H 2.94578000 3.60123800 -1.39257000
H 4.57535200 3.02558300 -1.92498900	H 4.51719200 3.03271600 -1.91460800
H 3.94429400 2.69517200 2.33066100	H 3.83882800 2.68158500 2.34112100
H 4.43942600 4.22166800 1.57293700	H 4.37003400 4.20860200 1.61478400
H 2.75724500 3.68455400 1.49783000	H 2.68696800 3.69281100 1.48083600
H 4.20616100 -4.50176900 -0.90026000	H 4.40371000 -4.46617500 -0.88176000
H 2.81341300 -3.53203100 -1.41995700	H 2.94545500 -3.60110300 -1.39252800
H 4.42888700 -3.07392700 -1.92467000	H 4.51693800 -3.03263200 -1.91445300
H 3.80610300 -2.71482400 2.32574000	H 3.83879900 -2.68156500 2.34123100
H 2.56957300 -3.63636900 1.47991200	H 2.68670300 -3.69265500 1.48099100
H 4.22311300 -4.26364900 1.56672900	H 4.36976000 -4.20865700 1.61486600

5.3.6 References

- [1] J. Merz, J. Fink, A. Friedrich, I. Krummenacher, H. H. Al Mamari, S. Lorenzen, M. Haehnel, A. Eichhorn, M. Moos, M. Holzapfel, H. Braunschweig, C. Lambert, A. Steffen, L. Ji, T. B. Marder, *Chem. Eur. J.* **2017**, *23*, 13164–13180.
- [2] G. M. Sheldrick, *Acta Crystallogr.* **2015**, *A71*, 3–8.
- [3] G. M. Sheldrick, *Acta Crystallogr.* **2008**, *A64*, 112–122.
- [4] C. B. Hubschle, G. M. Sheldrick, B. Dittrich, *J. Appl. Crystallogr.* **2011**, *44*, 1281–1284.
- [5] H. P. K. Brandenburg, Diamond Version 4.2.0. Crystal and Molecular Structure Visualizatuib, Crystal Impact, Bonn (Germany), **2016**.
- [6] M. J. Frisch, G. W. Trucks, H. B. Schlegel, G. E. Scuseria, M. A. Robb, J. R. Cheeseman, G. Scalmani, V. Barone, B. Mennucci, G. A. Petersson, H. Nakatsuji, M. Caricato, X. Li, H. P. Hratchian, A. F. Izmaylov, J. Bloino, G. Zheng, J. L. Sonnenberg, M. Hada, M. Ehara, K. Toyota, R. Fukuda, J. Hasegawa, M. Ishida, T. Nakajima, Y. Honda, O. Kitao, H. Nakai, T. Vreven, J. A. Montgomery, Jr.; , J. E. Peralta, F. Ogliaro, M. Bearpark, J. J. Heyd, E. Brothers, K. N. Kudin, V. N. Staroverov, R. Kobayashi, J. Normand, K. Raghavachari, A. Rendell, J. C. Burant, S. S. Iyengar, J. Tomasi, M. Cossi, N. Rega, J. M. Millam, M. Klene, J. E. Knox, J. B. Cross, V. Bakken, C. Adamo, J. Jaramillo, R. Gomperts, R. E. Stratmann, O. Yazyev, A. J. Austin, R. Cammi, C. Pomelli, J. W. Ochterski, R. L. Martin, K. Morokuma, V. G. Zakrzewski, G. A. Voth, P. Salvador, J. J. Dannenberg, S. Dapprich, A. D. Daniels, Ö. Farkas, J. B. Foresman, J. V. Ortiz, J. Cioslowski, D. J. Fox, in *Gaussian 09, Revision 9.E.01*, Gaussian, Inc., Wallingford CT, **2016**.
- [7] C. Lee, W. Yang, R. G. Parr, *Phys. Rev. Br* **1988**, *37*, 785–789.
- [8] G. A. Petersson, M. A. Al-Laham, *J. Chem. Phys.* **1991**, *94*, 6081–6090.
- [9] G. A. Petersson, A. Bennett, T. G. Tensfeldt, M. A. Al-Laham, W. A. Shirley, J. Mantzaris, *J. Chem. Phys.* **1988**, *89*, 2193–2218.
- [10] T. Yanai, D. P. Tew, N. C. Handy, *Chem. Phys. Lett.* **2004**, *393*, 51–57.
- [11] M. J. Peach, P. Benfield, T. Helgaker, D. J. Tozer, *J. Chem. Phys.* **2008**, *128*, 044118.
- [12] A. G. Crawford, A. D. Dwyer, Z. Liu, A. Steffen, A. Beeby, L.-O. Pålsson, D. J. Tozer, T. B. Marder, *J. Am. Chem. Soc.* **2011**, *133*, 13349–13362.
- [13] T. Lu, F. Chen, *J. Comput. Chem.* **2012**, *33*, 580–592.

